

Alma Mater Studiorum – Università di Bologna

DOTTORATO DI RICERCA IN
Scienze Farmacologiche e Tossicologiche, dello Sviluppo e del
Movimento Umano

Ciclo XXX

Settore Concorsuale: 05/F1 BIOLOGIA APPLICATA

Settore Scientifico Disciplinare: BIO/13 BIOLOGIA APPLICATA

EFFECTS OF OXIDATIVE AND FREE RADICAL STRESS
ON CELL MEMBRANE: POTENTIAL MARKERS AND
THERAPEUTIC/NUTRACEUTICAL STRATEGIES

Presentata da: Dott.ssa Giorgia Giacometti

Coordinatore Dottorato

Chiar.ma Prof.ssa Patrizia Hrelia

Supervisore

Prof.ssa Marina Marini

Co-Supervisore

Dott.ssa Carla Ferreri

Esame finale anno 2018

Table of Contents

List of Abbreviations.....	4
Abstract.....	7
Chapter 1: Introduction.....	10
1.1. Cell membrane	10
1.2. Lipid geometry	14
1.3. Effect of radical stress on lipids	16
1.3.1.Lipid peroxidation.....	18
1.3.2.Cis-trans isomerization.....	20
1.4. Exogenous sources of trans fatty acids.....	22
1.4.1.Partial Hydrogenation	22
1.4.2.Deodorization.....	24
1.4.3.Frying	24
1.4.4.Microbial biohydrogenation	25
1.5. Effects of trans fatty acids	25
1.6. Lipid signalling	27
1.7. Lipidomics for lipid biomarker discovery	29
1.8. Thesis Goals and Objectives.....	31
1.9. References.....	32
Chapter 2: Analytical Methodologies.....	38
2.1. Lipid analyses	38
2.2. Lipid extraction.....	39
2.3. Thin Layer Chromatography (TLC).....	39
2.3.1.Silver-ion thin layer chromatography (Ag-TLC).....	41
2.4. Gas Chromatography (GC).....	42
2.5. References.....	45
Chapter 3: Autism Spectrum Disorder	46
3.1. Introduction.....	46
3.2. Autism Spectrum Disorder (ASD)	47
3.3. Lipidomics for ASD biomarkers	48
3.4. Hyperspectral dark-field microscopy (HDFM).....	50
3.5. Experimental part	52
3.5.1. Erythrocyte membrane fatty acid analysis	52
3.5.2. HDFM analysis	54
3.5.2.1. HDFM analysis of RBCs.....	54
3.5.2.2. HDFM analysis of phospholipids.....	55
3.5.2.3. HDFM analysis of Protoporphyrin IX.....	55
3.5.3. Statistical analysis	55
3.6. Results	56
3.6.1. Erythrocyte membrane fatty acid analysis	56
3.6.2. HDFM analysis	58
3.7. Conclusions.....	65
3.8. References.....	66
Chapter 4: Alzheimer’s Disease.....	71
4.1. Introduction.....	71
4.2. Alzheimer’s disease (AD).....	72
4.3. ApoE4 in the pathogenesis of AD.....	73
4.4. Experimental part	75

4.4.1. In vitro studies	75
4.4.2. Membrane fatty acid analysis	76
4.4.3. Statistical analysis	76
4.5. Results	76
4.6. Conclusions.....	84
4.7. References.....	85
Chapter 5: <i>Trans</i> liposomes	91
5.1. Introduction.....	91
5.2. Liposome properties	92
5.3. Liposome preparation.....	94
5.3.1. Sonication.....	96
5.3.2. Extrusion.....	96
5.4. Liposome characterization.....	97
5.4.1. Dynamic Light Scattering (DLS).....	98
5.4.2. Atomic Force Microscopy (AFM)	99
5.5. Liposome applications.....	100
5.6. Experimental part.....	102
5.6.1. Synthesis and purification of PEPC	103
5.6.2. Liposome preparation.....	103
5.6.3. Dye encapsulation.....	104
5.6.4. Encapsulation Efficiency (EE%)	104
5.6.5. In vitro release study	105
5.6.6. Lipid extraction and GC analysis.....	105
5.6.7. Dynamic Light Scattering (DLS).....	106
5.6.8. Atomic Force Microscopy (AFM).....	106
5.6.9. Statistical analysis	106
5.7. Results	107
5.7.1. Effect of TFAs on size and ζ -potential.....	107
5.7.2. Effect of TFAs on stability	110
5.7.3. Effect of TFAs on morphology and rigidity	111
5.7.4. Effect of TFAs on encapsulation	113
5.7.5. Effect of TFAs on release.....	116
5.8. Conclusions.....	117
5.9. References.....	118
Chapter 6: DHA	122
6.1. Introduction.....	122
6.2. Importance of DHA.....	124
6.3. Experimental part.....	128
6.3.1. Synthesis of mono- <i>trans</i> DHA-Me isomers	130
6.3.1.1. Synthesis by Photolysis	130
6.3.1.2. Synthesis by Epoxidation – Elimination	131
6.3.2. Isomerization of fish oil by Photolysis.....	132
6.3.3. Nutraceutical analysis	132
6.4. Results	132
6.4.1. Synthesis by Photolysis	132
6.4.2. Synthesis by Epoxidation – Elimination	134
6.4.3. NMR Analysis	139
6.4.4. Isomerization of fish oil	141
6.4.5. Nutraceutical analysis	143
6.5. Conclusions.....	149
6.6. References.....	150

Chapter 7: Conclusions..... 155
Appendices 158

List of Abbreviations

Aβ	β -Amiloide
AD	Alzheimer's disease
Ag-TLC	Silver-ion thin layer chromatography
AgNO₃	Silver nitrate
ALA	α -linolenic acid
ANOVA	Analysis of variance
ApoE	Apolipoprotein E
APP	Amyloid precursor protein
ARA	Arachidonic acid
ASD	Autism spectrum disorder
CAM	Cerium ammonium molybdate
C₆D₆	Deuterated benzene
CARS	Childhood Autism Rating Scale
CDCl₃	Deuterated chloroform
CHOL	Cholesterol
CNS	Central nervous system
COX	Cyclooxygenase
DGLA	Dihomo- γ -linolenic Acid
DHA	Docosahexaenoic acid
DHA-Me	Docosahexaenoic acid methyl ester
D/L	Dye-to-lipid ratio
DLS	Dynamic light scattering
DPPC	1,2-dipalmitoyl, phosphatidylcholine
EDTA	Ethylenediamine tetraacetic acid
EDP	Epoxy-docosapentaenoic acid
EE%	Encapsulation efficiency (%)
EFA	Essential fatty acid
EPA	Eicosapentaenoic acid
FA	Fatty acid
FAME	Fatty acid methyl ester
FBS	Fetal bovine serum
FDA	Food and Drug Administration
FFA	Free fatty acid
FID	Flame ionization detector

GC	Gas chromatography
GC-MS	Gas chromatography-mass spectrometry
GUV	Giant unilamellar vesicle
HDL	High density lipoprotein
HDMF	Hyperspectral dark-field microscopy
HMBC	Heteronuclear multiple bond correlation
HSQC	Heteronuclear single-quantum coherence
KOH	Potassium hydroxide
LA	Linoleic acid
LC-PUFA	Long chain polyunsaturated fatty acid
LDL	Low density lipoprotein
LOX	Lipoxygenase
LPL	Lysophospholipid
LT	Leukotriene
LUV	Large unilamellar vesicle
LUVET	Large unilamellar vesicle by extrusion technique
LX	Lipoxin
MAR	Maresine
MLV	Multilamellar vesicle
MTMAB	Myristyl trimethyl ammonium bromide
MUFA	Monounsaturated fatty acid
MVV	Multivesicular vesicle
m/z	Mass-to-charge ratio
Na₂SO₄	Sodium sulphate
NaHCO₃	Sodium bicarbonate
NFT	Neurofibrillary tangle
NH₄OH	Ammonium hydroxide
NMR	Nuclear magnetic resonance
NP	Neuroprotectin
OLV	Oligo lamellar vesicle
OR	Odds ratio
PBS	Phosphate buffered saline
<i>P</i>	Packing parameter
PC	Phosphatidylcholine
PCA	Principal components analysis

PDI	Polydispersity index
PEPC	1-palmitoyl, 2-elaidoyl, phosphatidylcholine
PG	Prostaglandin
PGI2	Prostacyclin
PI	Peroxidation index
PL	Phospholipid
PLA	Phospholipase
POPC	1-palmitoyl, 2-oleoyl, phosphatidylcholine
POPE	1-palmitoyl, 2-oleoyl, phosphatidylethanolamine
ROC	Receiver operating characteristic
ROI	Region of interest
RV	Resolvin
SAM	Spectral angle mapper
SD	Standard deviation
SEM	Scanning electron microscopy
SFA	Saturated fatty acid
SFM	Scanning force microscopy
SUV	Small unilamellar vesicle
PUFA	Polyunsaturated fatty acid
RBC	Red blood cell
R_f	Retention factor
ROS	Reactive oxygen species
RSS	Reactive sulfur species
TEM	Transmission electron microscopy
TFA	<i>Trans</i> fatty acid
TLC	Thin layer chromatography
TX	Thromboxane
UFA	Unsaturated fatty acid
UI	Unsaturation index
VLDL	Very low-density lipoprotein
WHO	World Health Organization

Abstract

Cell membrane plays a crucial role in several biological processes, such as the regulation of molecule and ion exchange, protein functioning and lipid signalling. Inappropriate lifestyles or stress situations can enhance the production of free radicals that, in their turn, are able to trigger chain reactions leading to the damage of the main cell constituents. Normally, the cell possesses physiological mechanisms to counteract the increase of radical stress, but when it is no longer able to do so, deterioration of biomolecules can occur, from which inflammation may start and be perpetuated, thus leading to pathological conditions.

Changes in the lipid compositions at the membrane level can be monitored by fatty acid-based lipidomics, which represents a powerful diagnostic tool for the detection of membrane impairments and their association with different physiological and pathological conditions. It is known that, under radical stress, polyunsaturated fatty acids (PUFA) moieties are the most susceptible to oxidative damages, and lipid peroxidation can be monitored by the loss of PUFAs from membranes. Membrane peroxidation can compete with a reaction induced by sulfur-centered radicals, that is called *cis-trans* isomerization, in which the conversion of the *cis* double bonds of the unsaturated fatty acids to the unnatural *trans* geometry occurs. *Trans* fatty acids (TFAs) can affect the membrane functionality by reducing the membrane permeability and fluidity, however more information is needed to evaluate the extent at which such unnatural molecules affect health. TFAs can also be generated by chemical and physical processes, used also in food industry, such as partial hydrogenation and deodorization. As matter of facts, radical chemistry and nutritional research both evidenced the formation of TFAs. In particular, studies about deodorized fish oils used for nutraceutical supplementation, regarded the ω -3 mono-*trans* PUFA isomers. The impact of fatty acids on health is nowadays well understood, especially as for the inadequate intake of PUFAs is concerned, which is known to strongly affect the pathophysiology of neurological pathologies, such as Autism, and neurodegenerative diseases, such

as Alzheimer. Therefore, the molecular profiles obtained from lipidomic studies can contribute to the development of a multidisciplinary approach for the diagnosis of these diseases.

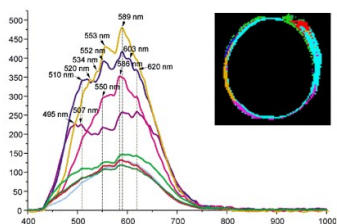
The experimental work described in this thesis started with our focusing on the lipidomic profile of children affected by Autism Spectrum Disorder (ASD), a group of neurodevelopmental disorders characterized by social and behaviour impairments. A dual approach centered on the erythrocyte membranes was for the first time applied to a group of healthy and ASD children. It consisted of the erythrocyte membrane fatty acid analysis combined with the detection of spectral properties related to the membrane organization by using an innovative biophotonic methodology called hyperspectral enhanced dark field microscopy (HDFM). The multidisciplinary collaboration with a medical unit for the clinical evaluation and biophysic researchers brought to an important result of membrane-based diagnostics with high predictive value for ASD, published in *Scientific Reports* in August 2017.

The PhD thesis was also carried out within the frame of a Marie Curie network called ClickGene, which was focused on studying possible membrane cooperative aspects to be used for innovative oxidative damage-based antitumoral strategies. As an Early Stage Researcher of this network, I had the chance to take part in the “Free Radicals in Bio- and Nano-Technology” Group, at the National Institute of Scientific Research “Demokritos” in Athens, where I had the opportunity to deepen three subjects related to cell membranes:

- 1) the membrane involvement in several physiological and pathological processes, using in vitro experiments on a neuroblastoma cell line. In particular, the membrane remodeling induced by two different isoforms of apolipoproteins, ApoE4 and ApoE3, was examined, being apolipoproteins involved in the cholesterol and lipid transport in the brain and the $\epsilon 4$ allele, that codifies for ApoE4, the major genetic risk factor for Alzheimer’s disease. The results, that were published in *BBA Biomembranes* in July 2017, showed consistent differences in the membrane fatty acid profiles in the presence of both isoforms, opening a debate about the role of nutritional and metabolic adaptations as epigenetic determinants over the genetic predisposition;
- 2) the biophysical and biotechnological meaning of *trans* fatty acids in cell membranes using liposome formulations, as models of cell membrane or as nanocarriers for the delivery of substances. Depending on whether liposomes contained natural *cis* or unnatural *trans* fatty acid residues, consistent differences in the lipid bilayer properties (rigidity, diameter, ζ -potential) and in their encapsulation/release abilities were established. These results, published in the journal *Molecules* in November 2017, foresee the insertion of toxic *trans* fatty acids in tumor cell membranes, which would lead to a synergic antitumoral approach;

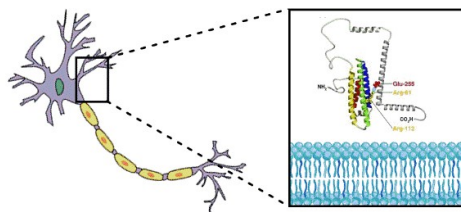
3) the chemical and analytical characteristics of the mono-*trans* isomers of DHA as the first unnatural isomers produced by the application of chemical and physical reagents to the natural *cis* DHA. For the first time the complete characterization using a dual synthetic approach, that allowed the identification of the six DHA mono-*trans* isomers by gas chromatography and nuclear magnetic resonance, has been performed. This characterization has been useful for analyses of nutraceutical formulations available in the market, and identification of *trans* isomer contaminants, harmful for the health. The work was published in *Chemical Research in Toxicology* in February 2018.

Taken together, these results could better clarify the role of fatty acids in the composition of cellular membranes, which is affected by environmental, nutritional and metabolic conditions, providing also a palette of methodologies for the examination of membrane behaviors, impairments and changes linked with the fatty acid geometry and types. The contribution of this PhD thesis will be multidisciplinary in the fields of free radicals in medicine, membrane behavior in different culture conditions, biotechnology of liposomes and lipid analysis of nutraceuticals.



Biophysics/Diagnostics

Membrane impairments in Autism Spectrum Disorder: HDFM and lipidomics for membrane-based diagnostics

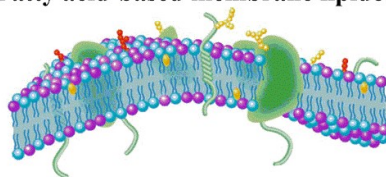


Bioscience/Cellular Biology

Neuroblastoma cell models for Alzheimer's Disease: Membrane fatty acid remodeling induced by ApoE4

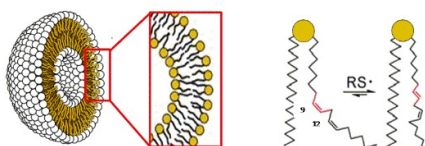
Multi-disciplinary approach

Fatty acid-based membrane lipidomics



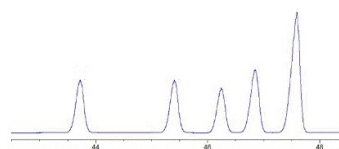
Biomimetics/Biotechnology

Lipid geometry effects on membrane properties: Liposome models containing *trans*-phospholipids



Nutraceuticals/Analytics

Characterization of mono-*trans* DHA isomers: Protocols for the quality control of ω -3 supplements



Chapter 1

Introduction

1.1. Cell membrane

Cell membrane is a mixture of fluid state lipids, in which proteins and other molecules are embedded. It intervenes in many cellular processes [1].

Its role is to delimit the cell externally, defining a physical barrier that separates the intracellular cytoplasmic components from the extracellular environment, thus allowing nutritional exchange and communication with the surrounding environment, essential to ensure the cellular life. Indeed, the cell membrane can be freely crossed by small liposoluble molecules, but it is almost impenetrable by the water-soluble ones.

Several transport mechanisms (either passive or active) allow it to selectively regulate what enters and exits the cell. Cell membrane also takes part in signal transduction, being a source of lipid mediators, which can be mobilized in response to specific stimuli [2].

The most abundant lipid components of the cell membrane are the phospholipids (**Figure 1.1**), consisting of a L-glycerol molecule in which the hydroxyl groups in positions 1 and 2 are esterified with two fatty acids and the hydroxyl group in position 3 is esterified with a phosphate group, which in turn is bound to small polar molecules such as choline, serine, ethanamine or inositol.

The presence of two hydrophobic hydrocarbon chains and a polar head confers amphipathic characteristics to these molecules, but also a cylindrical shape, that prevents them from forming spherical micelles.

Due to their nature, in fact, phospholipids spontaneously aggregate to bury their hydrophobic tails in the membrane inner layer and expose their hydrophilic heads to water, thus forming a continuous bilayer, where the hydrophobic tails are sandwiched between the hydrophilic head groups [3].

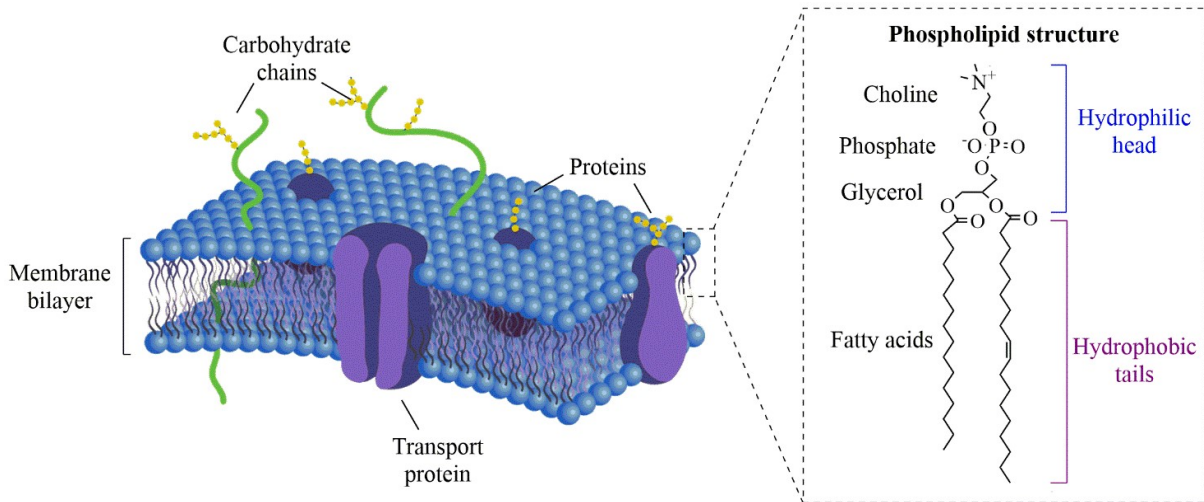


Figure 1.1. Structure of a membrane phospholipid bilayer. The enlargement shows the molecular structure of a representative phospholipid (1-palmitoyl, 2-oleoyl phosphatidylcholine).

The tails are made of fatty acids, that may differ for the length of the carboxylic chain (normally between 14 and 24 carbon atoms) or for the presence (or absence) - and number - of double bonds.

Using the classification based on the structure of the hydrocarbon chain (**Figure 1.2**), fatty acids can be distinguished in:

- Saturated fatty acids (SFAs), which do not contain double bonds within the acyl chain;
- Unsaturated fatty acids (UFAs), which are the ones that possess at least one double bond.

They can be distinguished in:

- Monounsaturated fatty acids (MUFAs), which present a single double bond in their structure;
- Polyunsaturated fatty acids (PUFAs), which are characterized by the presence of two or more double bonds along the acyl chain. Depending on the position of the double bonds, PUFAs can be further distinguished between ω -3 and ω -6 PUFAs.

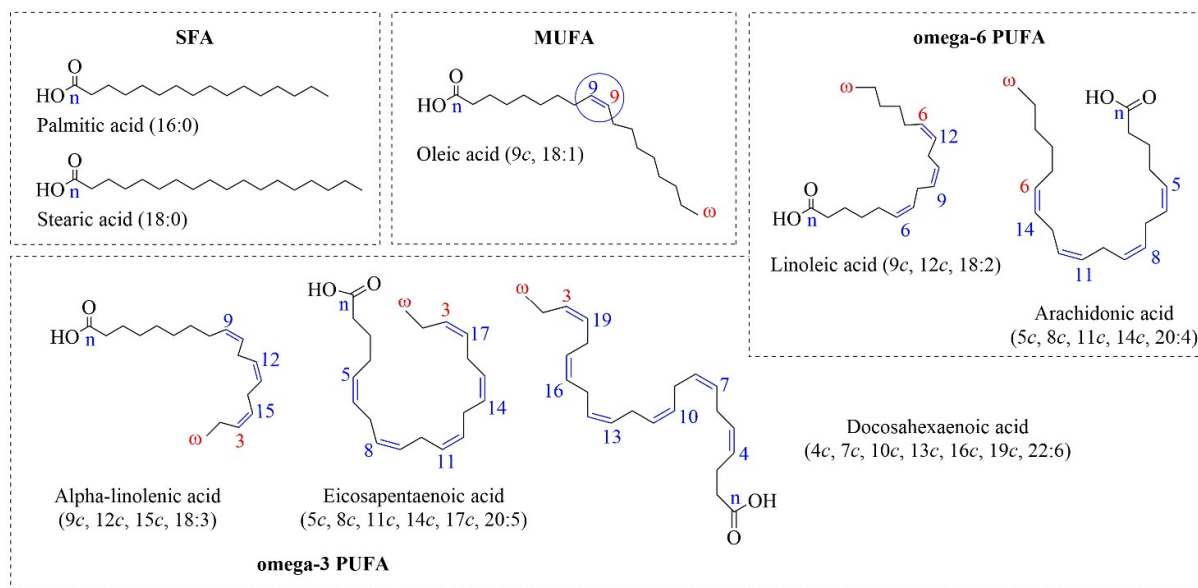


Figure 1.2. Molecular structures of representative components of the main fatty acid families. The spatial hindrance varies according to the number and the configuration of the double bonds in the acyl chain.

In literature, fatty acids are usually reported (**Table 1.1**) with their non-systematic historical common names, which are concise and generally univocal.

However, the most technically clear and descriptive nomenclature is the one based on the IUPAC directives, which has been established in 1979 to give uniformity and avoid ambiguities. Counting begins from the carboxylic acid end and double bond geometry, when necessary, is indicated with *Z*- or *E*-, whether the substituents are on the same side (*Z*, from German *zusammen* = together) or on opposite sides (*E*, from German *entgegen* = opposite) of the double bond [4].

Some abbreviated descriptions, which usually indicate the number of carbons constituting the acyl chain, and the number of double bonds if present, are also in use. These are usually reported as C:D, where C represents the number of carbon atoms in the fatty acid chain and D is the number of double bonds. For example, a fatty acid that consists of 18 carbon atoms and has no double bonds is indicated as 18:0, whereas 18:1 describes an 18-carbon chain with one double bond in it. This notation can be ambiguous because different fatty acids can have the same length and the same numbers of double bonds, but each double bond can be either in a *cis*- or in a *trans*- configuration and take a specific position, therefore, not all the 18:1 fatty acids (for example) are identical. Consequently, the C:D notation is usually paired with other abbreviations that take into account the position of the double bonds along the acyl chain.

The double bond location is usually numbered starting from the carboxylic group, in which case the notation is Δ -n, where n represents the number of carbons that separate the double bond from the carboxylic group. There is a second notation in use, called ω -n, in which the numbering of carbon atoms starts from the terminal methyl group (CH₃) rather than from the carboxyl group and n indicates the number of methyl groups that outdistance the unsaturation from the end of the acyl chain.

Based on this last classification, PUFAs can be further classified in two families, omega-3 (ω -3 or n-3) and omega-6 (ω -6 or n-6), according to the location of the last double bond relative to the terminal methyl end of the molecule. Such classification also reflects the fact that ω -6 and ω -3 fatty acids belong to different families, as they are synthesized starting from two different precursors that cannot be produced through physiological enzymatic pathways and need to be taken up with diet. These two fatty acid precursors are linoleic acid (LA, 9*c*,12*c*, 18:2), the precursor of the ω -6 series, and α -linolenic acid (ALA, 9*c*,12*c*,15*c*, 18:3), the precursor for the ω -3 series; both linoleic and α -linolenic acids are considered essential fatty acids (EFAs).

Table 1.1. Examples of the different nomenclatures of some common fatty acids.

Common name	IUPAC name	C:D	Δ -n	ω -n
Palmitic acid	Hexadecanoic acid	16:0	/	/
Stearic acid	Octadecanoic acid	18:0	/	/
Oleic acid	9Z-Octadecenoic acid	18:1	<i>cis</i> - Δ 9	ω -9
Elaidic acid	9E-Octadecenoic acid	18:1	<i>trans</i> - Δ 9	ω -9
Linoleic acid	9Z,12Z-Octadecadienoic acid	18:2	All- <i>cis</i> - Δ 9, Δ 12	ω -6
α -Linolenic acid	9Z,12Z,15Z-Octadecatrienoic acid	18:3	All- <i>cis</i> - Δ 9, Δ 12, Δ 15	ω -3
Dihomo- γ -linolenic acid	8Z,11Z,14Z-Eicosatrienoic acid	20:3	All- <i>cis</i> - Δ 8, Δ 11, Δ 14	ω -6
Arachidonic acid	5Z,8Z,11Z,14Z-Eicosatetraenoic acid	20:4	All- <i>cis</i> - Δ 5, Δ 8, Δ 11, Δ 14	ω -6

1.2. Lipid geometry

Double bonds in unsaturated fatty acids may have either the *cis* or the *trans* configuration, *cis* meaning that the two alkyl groups, R₁ and R₂, are on the same side of the C=C (**Figure 1.3 A**), *trans* meaning that the two alkyl groups are on opposite sides of the C=C (**Figure 1.3 B**). In eukaryotes, naturally occurring double bonds are in the *cis* configuration. This specific geometry induces a chain kink of 30°, responsible for the characteristic angled structure that distinguishes unsaturated from saturated fatty acids. This kink has important effects on membrane organization. Indeed, saturated fatty acids are characterized by a linear shape that makes saturated acyl chains to form an ordered and tightly packed state in the phospholipid bilayer. On the other hand, unsaturated fatty acids, having *cis*-double bonds that produce the characteristic kinks in the phospholipid acyl chains, can disrupt the regularly packed assembly of saturated phospholipids, creating free spaces within the membrane bilayer. This disordered arrangement increases membrane permeability and fluidity, which in turn affect molecular exchanges within the membrane.

Double bonds with *cis* geometry are generated during the biosynthesis of MUFAs and PUFAs by the regioselective and stereospecific activity of desaturase enzymes, which act only in specific positions of the carboxy chain and always mediate the formation of *cis* bonds [5].

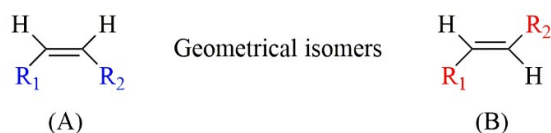


Figure 1.3. *Cis* (A) and *trans* (B) configurations of double bonds.

The *trans* geometric arrangement is not naturally present in mammalian cells because eukaryotic enzymes, at variance with prokaryotic ones, do not have the ability to form *trans* double bonds or to carry out a *trans* isomerization.

On the other hand, bacteria, such as *Pseudomonas aeruginosa*, *Vibrio cholera* and others, are endowed with an enzyme called isomerase, which, under environmental stress conditions, can convert the double bonds of the membrane phospholipids from the *cis* to the *trans* configuration. This is considered a short-term reversible defense mechanism, where the *cis* restitution passage is 500 times slower than the *cis* to *trans* isomerization. In fact, the *trans* configuration, by reducing the permeability and increasing the rigidity of the membrane, allows bacteria to survive to temperature increases or in the presence of disinfectants [6,7].

Since phospholipids are the main components of the membrane, their structure regulates the supramolecular organization and the properties of the double layer. If one considers only the degree of unsaturation, a general rule on lipid assembly is that the lowest the number of double bonds, the higher the packing order of lipids. Thus, lipids are assembled with increasing rigidity according to this order: saturated > *trans*-unsaturated > *cis*-unsaturated acyl chain. The linear configuration of *trans* fatty acids (TFAs) generates strong intermolecular chain–chain interactions, resulting in a higher gel-liquid phase transition temperature (T_m) for TFA chain melting. T_m is the temperature required to induce a change in lipid physical state, from the ordered gel phase, where the lipid chains are stretched, to the liquid crystalline phase, where the lipid chains are randomly oriented. For example, in the case of phosphatidylcholines (PCs) (**Figure 1.4**), keeping fixed the fatty acid in position 1 as palmitic acid (16:0), the variation from stearic (18:0) to elaidic (9*t*, 18:1) and oleic (9*c*, 18:1) acids in position 2, produces changes in the T_m value from 41.5, to 35 and -3 °C, respectively [8,9].

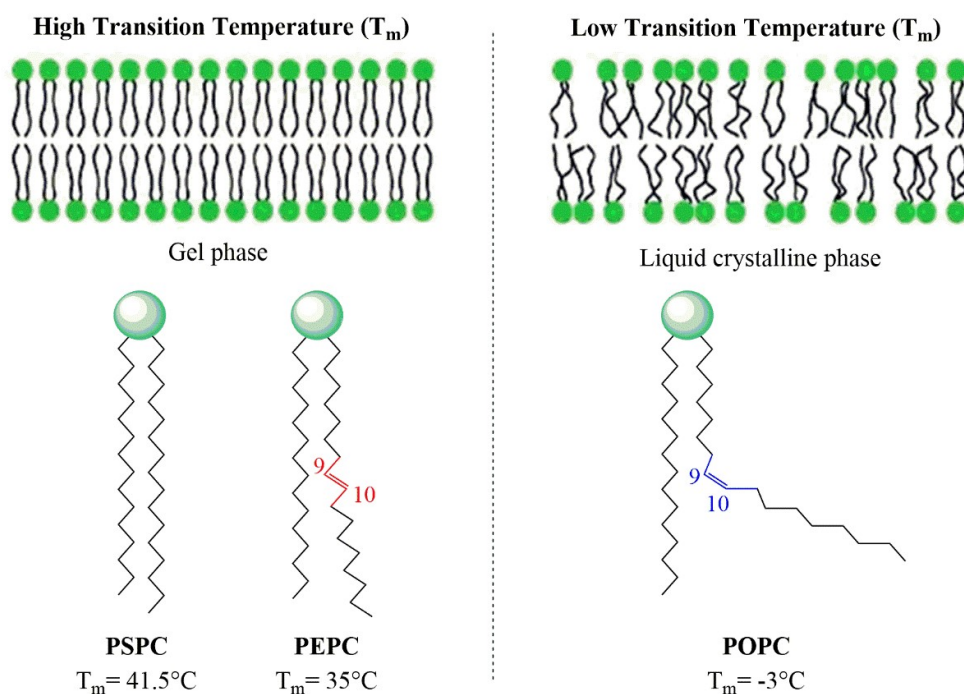


Figure 1.4. Effects of lipid composition on membrane fluidity. 1-palmitoyl, 2-stearoyl, phosphatidylcholine (PSPC), 1-palmitoyl, 2-elaidoyl, phosphatidylcholine (PEPC) and 1-palmitoyl, 2-oleoyl, phosphatidylcholine (POPC) differ for fatty acids in position R_2 : stearic (18:0), elaidic (9*t*, 18:1) and oleic (9*c*, 18:1) acids, respectively.

The presence of TFAs has been reported for the first time in nutrition-related researches. TFAs can be found in foods that underwent industrial procedures such as partial hydrogenation and deodorization but also in dairy and meat products due to the microbial biohydrogenation process that

takes place in ruminants. It is now known that *trans* lipids can also derive from endogenous processes such as radical reactions involving sulfur-reactive species, which catalyze in vivo the *cis-trans* isomerization of double bonds. Here nutrition science meets free radical science, since both deal with understanding the role of the lipid geometry in membrane functionality, as well as in metabolic and signalling processes involving fatty acids. Indeed, since physiological mechanisms and membrane equilibria are based on the natural *cis* geometry of membrane fatty acids, the presence of the *trans* configuration in biological structures, either induced by radical stress or due to industrial manipulation, can lead to significant metabolic and pathological consequences.

1.3. Effect of radical stress on lipids

Cell membrane functionality is guaranteed by the correct quantitative balance among the fatty acid families mentioned above. Imbalances in favor of one family can lead to physio-pathological problems. It has been reported that excessive radical stress induced by free radical molecules can alter the lipid composition of cell membrane and compromise its functionality. Free radicals are highly unstable and reactive molecules, characterized by the presence of an unpaired electron in their outer orbital. The peculiar electronic distribution makes free radicals very unstable and prone to reach a more stable state by interacting with other radicals or by subtracting hydrogen atoms from other molecules.

Reactive Oxygen Species (ROS) and other reactive radical species are endogenously produced by the cells during normal physiological processes. Indeed, free radicals can derive from enzymatic processes like electron transport in the respiratory chain, phagocytosis, peroxysomal activity and detoxification mechanisms involving cytochrome P450. For example, the superoxide radical $O_2^{\bullet(-)}$ can be formed by interaction of molecular oxygen with electrons that occasionally escape the respiratory chain, especially in the oxo-reductive passage between coenzyme Q and cytochromes at the level of NADH-ubichinone reductase and ubichinone-cytochrome C reductase enzymes [10].



Another well-known biological mechanism is the Fenton reaction, which involves metal ions (such as Fe^{2+} and Cu^{2+}) and gives rise to the hydroxyl radical ($\bullet OH$) [11].



During inflammatory processes, cyclooxygenase (COX) and lipoxygenase (LOX) enzymes convert fatty acids into prostaglandins and thromboxanes through a specific free radical-catalyzed mechanism [12,13].

However, radical species can also have exogenous origins. Ionizing radiations (e.g. radioactive sources such as ^{60}Co) or light (e.g. UV radiation) can induce omolytic processes with enough energy to omolytically break a covalent bond and produce free radical species [14].

In physiological conditions, living systems possess endogenous antioxidant defense mechanisms that counterbalance the effects of oxidants and protect structural and functional biomolecules from free radical attack. Superoxide dismutase, catalase, and glutathione peroxidase are the primary enzymes involved in direct elimination of ROS, whereas glutathione reductase and glucose-6-phosphate dehydrogenase intervene later to maintain a steady concentration of glutathione and NADPH, necessary for optimal functioning of the primary antioxidant enzymes [15-18].

In these processes, micronutrients such as selenium, iron, copper, zinc, and manganese are required as cofactors for optimal catalytic activity and effective antioxidative defense. [19]. Additionally, glutathione, iron-binding transferrin, copper-binding ceruloplasmin, α -tocopherol (Vitamin E), carotenoids, and ascorbic acid (Vitamin C) are also involved in the anti-ROS defense system [20-22].

The production of radical substances may increase in some physiological conditions and in many pathological processes, such as inflammation, infections, cancerogenesis and aging. On the other hand, the endogenous production of antioxidant molecules and enzymes may be deficient for genetic, environmental or age-related reasons. Stressful lifestyle and bad habits, like excessive ozone exposure, cigarette smoking or unhealthy diet, can further compromise the equilibrium between the production and the elimination of radical species by antioxidant defenders.

When the ROS levels exceed the antioxidant capacity of the cell, a condition known as oxidative stress, free radicals can quickly react with biological macromolecules, such as DNA, lipids and proteins, and lead to cell death via apoptosis or necrosis [23]. For this reason, oxidative stress is associated with numerous chronic conditions such as cardiovascular disorders (i.e. atherosclerosis, ischemia, stroke), diabetes, cancer, neurodegenerative diseases (i.e. Parkinson's and Alzheimer's diseases) and developmental disorders such as autism [24-29].

1.3.1. Lipid peroxidation

At a membrane level, ROS can attack lipid chains of fatty acids (FAs) and start a process known as lipid peroxidation [30]. The main targets of this reaction are PUFAs, which are present in high concentrations in the cellular membrane phospholipids.

Lipid peroxidation (**Figure 1.5**) proceeds through three sequential phases:

- Initiation
- Propagation
- Termination

The initiation of lipid peroxidation in membranes results from free radical attack that abstracts a hydrogen from a bisallyl methylene group of PUFA by an oxygen radical, generally the hydroxyl radical $\bullet\text{OH}$, generating a carbon-centered lipid radical ($\text{L}\bullet$).

In the propagation phase, $\text{L}\bullet$ rearranges to produce a conjugated diene, which then readily reacts with molecular oxygen to yield a lipid hydroperoxyl radical ($\text{LOO}\bullet$).

$\text{LOO}\bullet$ can propagate the oxidizing chain reaction by abstracting electrons from other susceptible PUFAs, forming another carbon-centered radical and a lipid hydroperoxide (LOOH).

The reaction is interrupted when two radical species combine in various ways to give non-radical products or by termination in the presence of a hydrogen or an electron donor.

At the cell membrane level, peroxidated or degraded lipids are removed by phospholipase (PLA) action and this results in loss of PUFAs and increased permeability of the membrane to substances such as calcium ions.

In this way, lipid peroxidation can seriously alter the membrane functionality and integrity, since it can lead to loss of enzyme and receptor activity and can have deleterious effects on secretory functions [31].

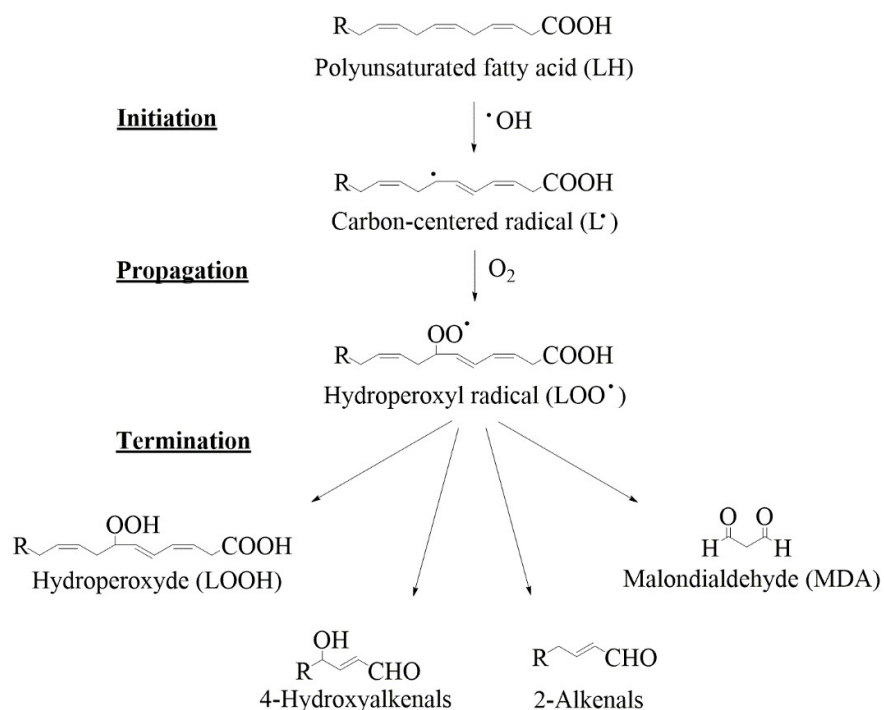


Figure 1.5. Reaction mechanism of lipid peroxidation induced by reactive oxygen species.

Depending on the membrane fatty acid composition, the membrane vulnerability to peroxidation can substantially differ, with PUFAs being generally the most vulnerable. Therefore, membrane susceptibility to peroxidation can be expressed by the peroxidation index (PI), which considers the relative percentages and susceptibility to peroxidation damage of the different fatty acids (**Figure 1.6**).

High values of PI correlate with high percentages of PUFAs in the membrane and reflects high susceptibility to peroxidation. On the other hand, low PI values are correlated with a reduced content of PUFAs in favour of SFAs and MUFAs, and for this reason to a high resistance to ROS attack [32-34].

$$\text{PI} = \left[\begin{array}{l}
 (\% \text{ monoenoic FA} \times 0.025) + \\
 (\% \text{ dienoic FA} \times 1) + \\
 (\% \text{ trienoic FA} \times 2) + \\
 (\% \text{ tetraenoic FA} \times 4) + \\
 (\% \text{ pentaenoic FA} \times 6) + \\
 (\% \text{ hexaenoic FA} \times 8)
 \end{array} \right]$$

Figure 1.6. Peroxidation index equation.

1.3.2. *Cis-trans* isomerization

It is well documented that sulfur-centered radicals can compete with ROS to give lipid damage [35]. Sulfur-centered radicals can attack MUFAs and PUFAs and catalyze the conversion from *cis* to *trans* geometry of lipid double bonds, in a reaction known as *cis-trans* isomerization.

Several radicals (e.g. $\text{RS}\cdot$, $\text{RSe}\cdot$, $\text{RSO}_2\cdot$, $\text{NO}_2\cdot$) and atoms (such as $\text{Br}\cdot$ or $\text{I}\cdot$) can induce the *cis-trans* isomerization reaction but among them the most relevant from a biological point of view are the thiyl radicals ($\text{RS}\cdot$) [36].

$\text{RS}\cdot$ can be formed from sulfur-containing molecules such as free molecules (e.g. H_2S and CH_3SH), amino acids (e.g. cysteine and methionine), peptides or proteins (e.g. glutathione, Met-enkephalin, albumin, β -amyloid and metallothionein) [37-39].

The reaction mechanism consists of an addition-elimination reaction (**Figure 1.7**). Initially, the $\text{RS}\cdot$ sulfur radical attacks the double bond, forming a radical intermediate that evolves into a very rapid monomolecular process with fragmentation of the radical species and restoration of the double bond. However, when the double bond is restored, it has a different geometry, the *trans* one, that is thermodynamically and kinetically more stable than the *cis* configuration. In this process only geometric *trans* isomers can be obtained because there is no possibility of double bond rearrangement that would lead to positional isomers.

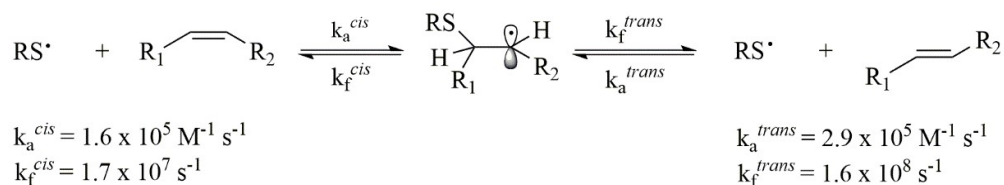


Figure 1.7. Mechanism of *cis-trans* isomerization catalyzed by thiyl radicals ($\text{RS}\cdot$). The rate constants obtained at 22°C are reported.

In the *cis-trans* isomerization reaction, the radical acts as a catalyst as it is regenerated at each isomerization step. It can carry out a catalytic cycle that reaches the value of about 300 molecules per cycle, depending on the conditions and molecules involved.

Various methods for reproducing the endogenous *cis-trans* isomerization reaction in the laboratory are provided in the literature. They involve the use of various thiol compounds, which differ not only for the molecular structure but also for their partition coefficient. Among the various compounds tested, the one that has proved to be the most widely applicable for the study of this reaction is 2-

mercaptoethanol (HOCH₂CH₂SH). Indeed, having amphiphilic properties, 2-mercaptoethanol makes it possible to study the *cis-trans* isomerization reaction in both organic and aqueous solvents, with no restrictions related to the distribution coefficient.

For the generation of sulfur-centered radical species, various techniques can be employed. Among them, photolysis, that requires a UV lamp (254 nm) with low pressure mercury vapor (5.5 W), can be used to induce the homolytic breakdown of a thiol S-H bond (RSH) and generate a thiyl radical (RS•) (**Figure 1.8**).



Figure 1.8. Mechanism of formation of thiyl radicals (RS•) induced by photolysis.

Another technique that can be used to form thiyl radicals is gamma (γ)-radiolysis, which causes the radiolysis of water (**Figure 1.9**) to give rise to a hydroxyl radical (•OH) and a hydrogen atom (H•). The generated radicals are in their turn able to extract a hydrogen atom from a thiol, thus producing a thiyl radical (RS•).

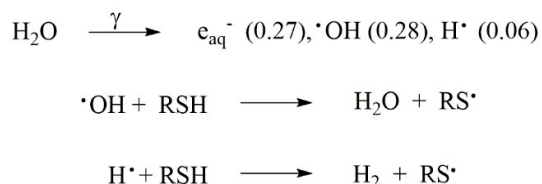


Figure 1.9. Radiolysis of water induced by γ-radiolysis and formation of thiyl radicals (RS•).
In brackets the values representing the radiation yields (G) expressed in μmol J⁻¹.

The isomerization reaction is a step-by-step reaction (**Figure 1.10**). This means that if the reaction occurs in the presence of PUFAs, the double bonds are isomerized one by one, so that the first product consists of mono-*trans* isomers, from which di-*trans*, tri-*trans* and so on, can also be formed.

When the *cis-trans* isomerization reaction takes place in a homogeneous solution, every *cis* double bond is isomerized with the same efficacy independently from the position of the double bond along the chain. Therefore, mono-*trans* isomers, as well as being the first products to be formed, are also obtained in the same amounts for all the double bonds involved.

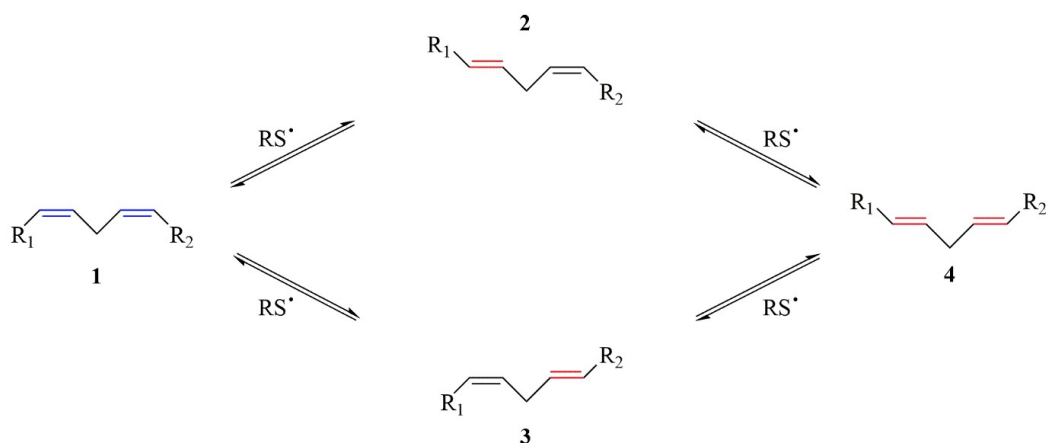


Figure 1.10. Step-by-step mechanism of *cis-trans* isomerization in PUFAs. The reaction of the thiyl radical (RS^\bullet) with the all-*cis* isomer (**1**) leads to the formation of two mono-*trans* isomers (**2** and **3**), that are precursors of the di-*trans* isomer (**4**).

However, in the biological environment, fatty acids (FAs) are constituents of the cell membrane and for this reason the *cis-trans* isomerization is influenced by the supramolecular organization of the phospholipids. Indeed, thiyl radicals must penetrate in the depth of the cellular membrane prior to give rise to the isomerization reaction. This means that the double bonds are not as equivalently reactive as they were in solution because the double bonds that are close to the polar head are more exposed and easily attacked by free radicals than the ones hidden in the hydrophobic bilayer depth.

1.4. Exogenous sources of *trans* fatty acids

In addition to *cis-trans* isomerization catalyzed by sulfur-centered radicals, *trans* fatty acids (TFAs) can be formed during specific industrial processes and enter the biological structures and metabolism after ingestion of *trans* containing foods.

1.4.1. Partial Hydrogenation

Hydrogenation [40] is a chemical process that leads to saturation (or partial saturation) of PUFAs present in vegetable oils by addition of hydrogen atoms to the double bonds (**Figure 1.11**).

A big limitation for companies on the use of PUFA-rich oils is that PUFA double bonds are highly unstable and susceptible to oxidation, causing fat rancidity and flavor alterations of foods. Hydrogenated fats find large application in the industrial preparation of baked goods and in the composition of margarines because, having a reduced number of unsaturated bonds, they display

higher chemical stability to oxidation compared to unsaturated lipids. For this reason, hydrogenated fats have replaced unsaturated oils in the preparation of biscuits, snacks, ice creams and junk food, since they represent the cheaper alternative to other saturated animal derivatives, like butter and lard, and they increase the durability, consistency and palatability of commercial products [41].

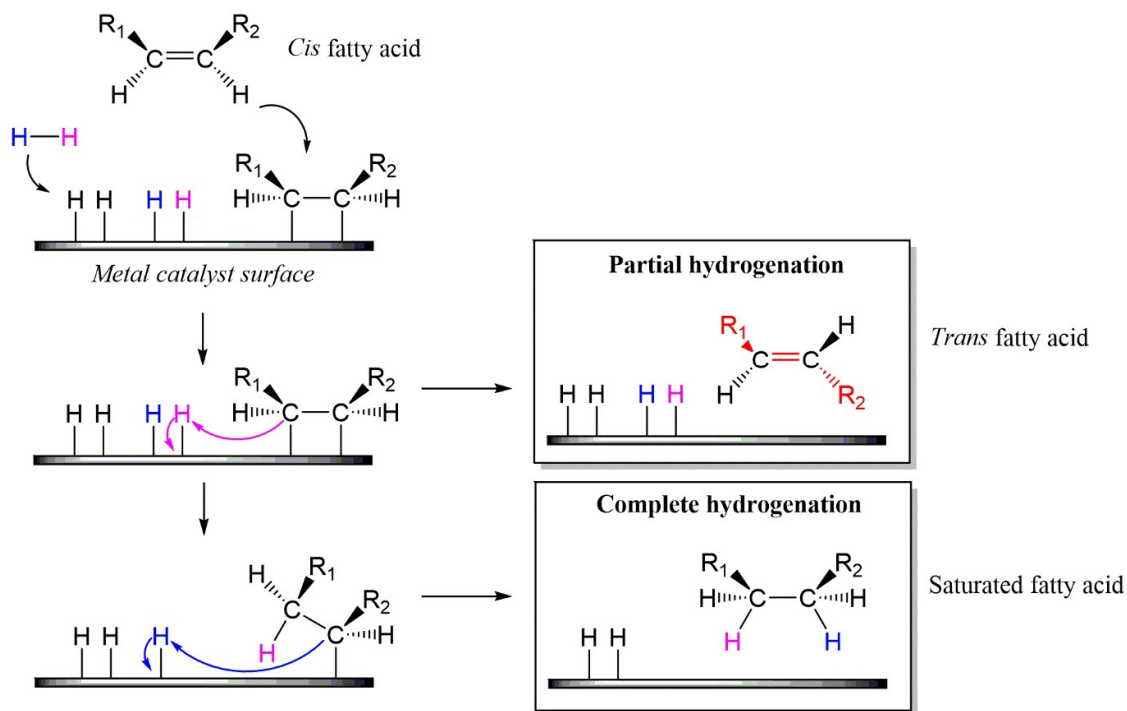


Figure 1.11. Mechanism of formation of *trans* fatty acids (TFAs) during the hydrogenation process.

Often, during the hydrogenation process, saturation fails leading to significant alterations in the structure of FAs, that is the conversion from *cis* to *trans* double bond geometry and the formation of TFAs [42].

TFA levels depend on several parameters, such as the initial lipid composition, the type of catalyst employed and other hydrogenation conditions such as temperature, pressure and stirring conditions. For example, low hydrogen pressure, moderate stirring speed and high temperatures lead to scarcity of hydrogen on the catalyst surface, which in turn favors the formation of TFAs [43].

TFAs produced during these processes can be either in the form of geometric isomers, when the *trans* double bond remains in the same position, and positional isomers, when the *trans* double bond migrates sideways in either direction along the acyl chain. (**Figure 1.12**).

oil to food occurs. Among the several physical and chemical modifications like oxidation, pyrolysis, polymerization, hydrolysis that occur, *cis-trans* isomerization reaction also takes place [49].

The formation of TFAs during food frying is closely related to the temperature reached and to the times oil is used [50]. When partially hydrogenated fats are used, the final concentration of TFAs is even higher, due to the high initial content of these fatty acids in the starting materials [51].

1.4.4. Microbial biohydrogenation

Some foods naturally contain TFAs, such as, for example, meat, milk and other dairy products from ruminants, such as cattle, sheeps and goats [52]. This phenomenon is related to the gastrointestinal physiology of ruminants which undergo bacterial fermentation of the digestive content. During the digestive process, the microorganism activity results in the conversion of *cis* fatty acids into TFAs, that can be absorbed into the intestine and consequently secreted in milk and/or accumulated in the meat. *Trans*-vaccenic acid (11*t*, 18:1), whose metabolism and functions have been widely studied, is a typical *trans* isomer derived from bacterial fermentation [53].

Microbial hydrogenation can also lead to the formation of conjugated linoleic acids (CLAs), a group of positional and geometric isomers of linoleic acid (LA, 9*c*, 12*c*, 18:2) which are characterized by the presence of two conjugated double bonds, i.e. bonds that are not separated, as in LA, by methylene groups (-CH₂-). Despite the presence of *trans* unsaturations, CLAs are reported to have antiinflammatory, anticarcinogenic, antiadipogenic, antidiabetic and antihypertensive effects in animal models [54-58].

1.5. Effects of *trans* fatty acids

TFAs have been reported to induce several adverse effects in humans [59]. Among them, TFAs have been associated with higher levels of systemic inflammation markers, in particular tumor necrosis factor- α , interleukin-6 and C-reactive protein, thus suggesting a possible pro-inflammatory activity of TFAs. High intake of TFAs has been related with high levels of intercellular and vascular cell adhesion molecules (sICAM-1 and sVCAM-1), which are circulating markers of endothelial dysfunction.

TFA consumption has been positively correlated with plasma E-selectin concentrations, another endothelial marker, reinforcing the idea that TFAs may compromise endothelial integrity. Although

the action mechanism is not clear, hypotheses about the incorporation of TFAs into cell membrane phospholipids and the alteration of specific membrane receptors have been formulated. Activation of inflammatory responses and endothelial dysfunction may show a connection between TFA consumption and risk of coronary heart disease and diabetes. In animal studies, TFA intake alters adipocyte gene expression of peroxisome proliferator-activated receptor, resistin, and lipoprotein lipase [60]. TFAs also influence adipocyte fatty acid metabolism in humans [61].

TFAs have been implicated in the incidence of obesity and many adverse effects of TFAs have been related to cardiovascular and coronary complications [40,62]. TFAs, similarly to SFAs, tend to increase total cholesterolemia and low-density lipoproteins (LDLs), whose accumulation within the vascular walls can result in the formation of atherosclerotic plaques with increased risk of mortality. Lipid profile changes are aggravated by the fact that TFAs reduce the plasma levels of the high-density lipoproteins (HDLs), which represent the antiatherogenic fraction [63].

A study demonstrated that elaidic acid (*9t*,18:1) increases plasma cholesteryl ester transfer protein activity in comparison with oleic acid (*9c*, 18:1), resulting in increased transfer of TFA-enriched cholesteryl esters from HDL to LDL [64,65]. Higher plasmatic levels of *trans*-18:2 and lower levels of *trans*-18:1 fatty acids have been associated with fatal ischemic heart disease and sudden cardiac death have been reported. This association might also be due to proarrhythmic effects of *trans*-18:2 [66]. A high consumption of TFAs during pregnancy has been reported to affect intrauterine development [67].

Additionally, studies on the incorporation and metabolism of *cis*- and *trans*-MUFAs in developing and mature brain, have shown that elaidic acid can be incorporated into phospholipids in similar rates as the *cis* isomer but is preferentially esterified to the 1-position of phosphoglycerides, probably due to its similarity with stearic acid, the corresponding SFA. This suggests that the brain does not ensure metabolic exclusion of these potentially deleterious components from the brain membrane lipids, although there may be a mechanism for a more rapid removal of TFAs [68].

TFA analysis has gained more importance since the establishment of maximum TFA daily intake to 1% of total ingested calories by the World Health Organization (WHO), which corresponds to no more than 2-2.5 grams per day of TFAs. In order to comply with such restrictions, the Food and Drug Administration (FDA) has required to list the TFA content among the nutritional values on product labels [69].

1.6. Lipid signalling

Lipids have long since been recognized as crucial bioactive molecules involved in several physiological responses to regulate metabolic homeostasis, signal transduction and molecular recognition pathways. Indeed, lipids can respond to physiological, pathological and environmental variations through the dynamic remodeling of membrane lipids, which consist in the redistribution of FAs in membrane phospholipids. The FA remodeling usually involves two enzymes, phospholipase A₁ (PLA₁) and phospholipase A₂ (PLA₂), which hydrolyze the acyl bond in positions 1 and 2, respectively, to release a free FA (FFA) and a lysophospholipid (LPL).

This mechanism is important not only for the physiological lipid turnover but also for the host defence, since it removes damaged phospholipids and initiates signalling pathways. Indeed, PUFAs, that usually occupy position 2 of membrane phospholipids, can be easily peroxidated by ROS, resulting in a structural and functional alteration of the membrane.

PLA₂ can remove these fatty acids at the level of the double lipid layer, replacing them with fatty acids present in the cytoplasmic pool. The bioactive lipids generated from LPLs include lysophosphatidylcholine, platelet activating factor, lysophosphatidic acid, sphingosine-1-phosphate and endocannabinoids.

Depending on the nature of phospholipids involved, over two dozens of bioactive lipid mediators can be formed from FFAs, some of which have pro-inflammatory effects, while others have anti-inflammatory and pro-resolution properties. For example, ARA, an ω -6 fatty acid, can give rise to eicosanoid metabolites. They consist of prostaglandins (PGs) and thromboxanes (TXs) generated via the action of cyclooxygenases 1 and 2 (COX-1 and COX-2), or leukotrienes (LTs), generated via the action of 5-lipoxygenase (5-LOX). All these mediators are involved in the inflammatory cascade. However, recent studies indicate that, as inflammation proceeds, neutrophils within confined exudates, influenced by cells and substrates in the local environment, can change their phenotype and start converting ARA into lipoxins (LXs), that intervene to actively terminate inflammation and promote resolution [70-72]. Inflammation resolution consists in the reduction or removal of leukocytes and debris from inflamed sites, thus enabling the return to homeostasis.

Literature reports three other new families of bioactive mediators, named (neuro)protectins (NPs), resolvins (RVs) and maresins (MARs) which have anti-inflammatory and pro-resolution properties. These mediators are biosynthesized from essential FA precursors of the ω -3 series, EPA and DHA (**Figure 1.13**) [73,74].

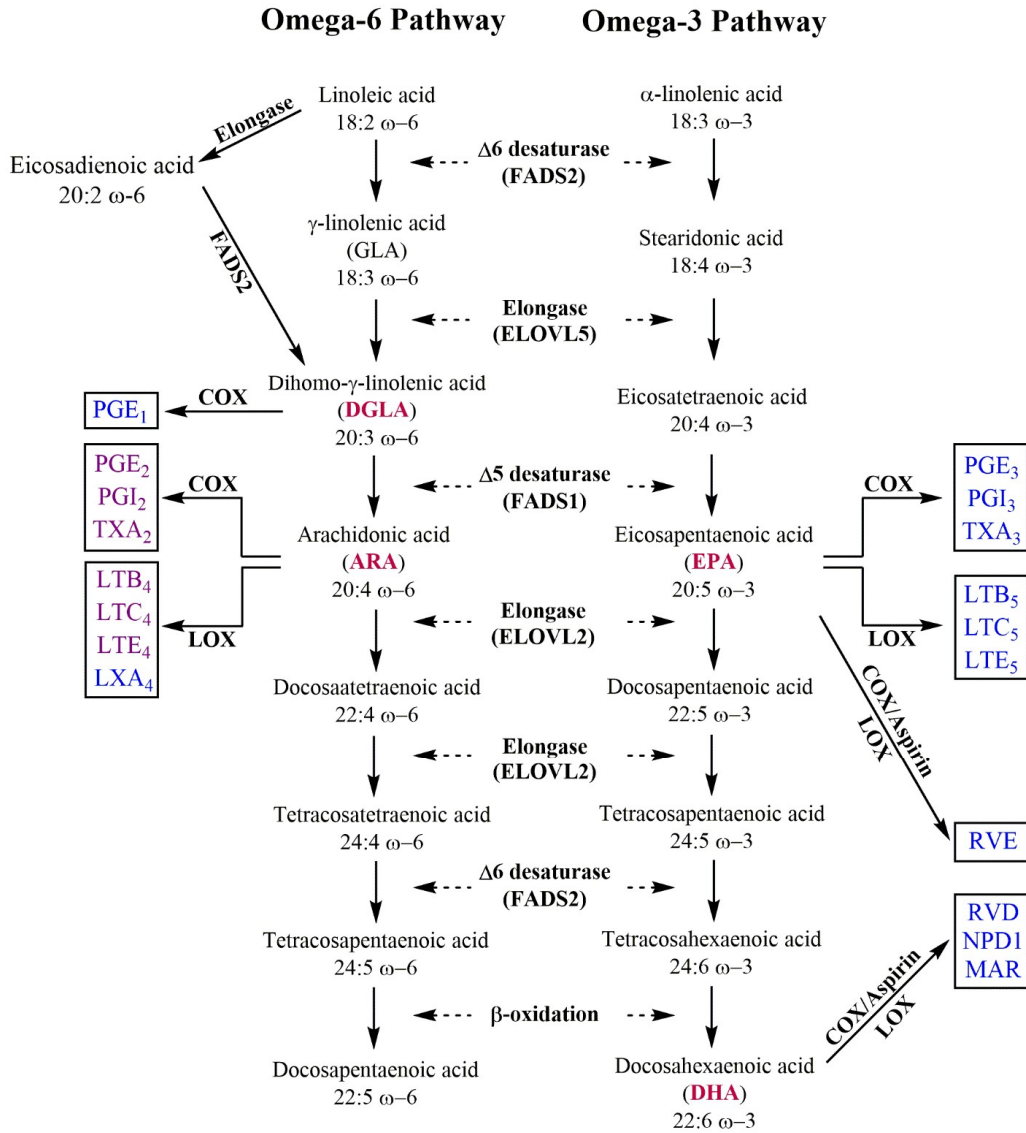


Figure 1.13. Omega-3 and omega-6 fatty acid metabolic pathways with main eicosanoid derivatives of DGLA, ARA, EPA and DHA. PGE: prostaglandin E, PGI: prostacyclin, TXA: thromboxane A, LTB: leukotriene B, LTC: leukotriene C, LTE: leukotriene E, LXA: lipoxin A, RVE: resolvin E, RVD: resolvin D, NPD: neuroprotection D, MAR: maresines. Adapted from [77,78].

Uncontrolled inflammation has been associated with many diseases that had not previously been considered to be classic inflammatory diseases, including atherosclerosis, cancer, asthma and several neurological disorders, such as Alzheimer's disease and Parkinson's disease. In this view, a close connection between nutrition, dietary supplementation and biosynthesis of lipid mediators, must be considered.

As previously mentioned (**Chapter 1, Paragraph 1.1**), the precursors of the ω-6 and ω-3 series, that are linoleic acid (LA, 18:2 ω-6) and α-linolenic acid (ALA, 18:3 ω-3), respectively, are both essential fatty acids (EFAs) that have to be introduced through the diet because the human body cannot

synthesize them due to the lack of specific desaturase enzymes. Often, dietary assumption of these precursors is not sufficient to supply the correct amount of their important long chain derivatives. Indeed, ARA can be synthesized from LA by alternative chain desaturation and elongation steps. However, conversion of ALA to DHA is limited, resulting in lower blood levels of DHA than those obtained through direct uptake.

Western diets over the last decades tends to be largely unbalanced towards the ω -6 fatty acids, showing deficiencies of ω -3 fatty acids and consequently increasing the ω -6 to ω -3 ratio (ω -6/ ω -3) [75]. Because of lifestyle, nutrition, metabolism and stress, imbalances in lipid signalling pathways can contribute to disease progression in chronic inflammation, autoimmunity, allergy, cancer, atherosclerosis, hypertension, heart hypertrophy, metabolic and degenerative diseases [76].

1.7. Lipidomics for lipid biomarker discovery

Variations in the composition of human body lipids can be monitored through lipidomics, which represents a powerful diagnostic tool to assess the quantity and quality of FA constituents and to monitor the remodeling of membrane FA composition associated with various physiological and pathological conditions [79].

Lipidomics aims at understanding membrane lipid role in the functioning and regulation of cellular behaviour. Indeed, it is possible to detect lipid variations occurring in health and disease situations, in order to gain knowledge on their connections with complex mechanisms of cellular homeostasis and signalling. The "dynamic" perspective offered by lipidomics allows the possibility of deepening the knowledge about the individual heritage and lipid transformation and of relating lipid type and quantity with health conditions. It is now possible to identify, for each tissue, the normality ranges for membrane FA composition in standard health conditions.

To date, lipidomic analytical strategies are applied to a wide variety of biological samples, such as blood, plasma, serum, cerebrospinal fluid, urine and biological tissue derived from animal models or clinical patients. In particular, red blood cells (RBCs) can be ideal reporters for evaluating individual values and possible deviations connected with intrinsic or extrinsic metabolic reasons (e.g. inflammation, stress and dysfunctional diet). Indeed, unlike traditional analyses, which are carried out on plasma and give information about FA dietary intakes of a few weeks before withdrawal, RBC lipidomic analyses account for more stable information obtained from metabolic transformations together with stabilized dietary contributions.

In this view, the lipidomics approach could contribute to underline alterations in the lipid metabolism or in both physiological and pathological conditions, information that can be used as guidance for personalized medicine, dietary intervention, as well as in biomarker discovery. Indeed, lipidomics has been successfully applied to discover biomarkers for a variety of diseases, such as metabolic and cardiovascular disease.

Moreover, lipidomics can play a key role in mechanistic studies, risk prediction, and therapeutic monitoring for such pathologies in which aberrant lipid metabolism occur, such as diabetes and obesity. Since lipids play important roles in cell growth and metabolism, which are essential for rapidly proliferating cancer cells, lipidomics has been used to report changes in lipid metabolism and homeostasis undergone by cancer cells.

Lipidomic analysis also clarified the role of some lipid-derived bioactive molecules that are involved in ophthalmological processes related with eye disease [80].

Lipidomics has been used as well to understand diet-induced changes in the structure, composition, and function of cellular lipids. Additionally, lipidomics might be useful for evaluating chronic effects associated with the dietary intake of specific components and for providing nutritional advice and lifestyle corrections.

The ultimate goal is to integrate the lipidomic knowledge with therapeutical, nutritional and nutraceutical aspects, and include lipids as important elements for prevention strategies and integrated medicine.

1.8. Thesis Goals and Objectives

In view of the above-mentioned importance of cell membrane lipid composition in health and disease, during my PhD I focused my interest on four different topics.

The first task has been the study of the cell membrane involvement in Autism Spectrum Disorder (ASD), a heterogeneous group of neurodevelopmental disorders caused by a combination of complex genetic traits and environmental factors. We designed an innovative diagnostic approach focused on the erythrocyte membranes, which included the lipidomic analysis of mature erythrocytes and their hyperspectral characterization by means of hyperspectral enhanced dark field microscopy (HDFM), with the aim of detecting differences between ASD and healthy subjects in the membrane fatty acid composition and in the scattering spectra and of finding correlations with clinical features of ASD.

Within the “ClickGene” Marie Curie network, having as objective the study of membrane cooperative effects for innovative antitumoral strategies based on oxidative damages, I carried out some experiments at the National Center of Scientific Research “Demokritos”, in Athens, focused on three different aspects, the first being a study related to the major neurodegenerative and disabling disorder in the elders, Alzheimer’s disease (AD), that has long been correlated with enhanced oxidative stress and altered lipid metabolism. The study was aimed at investigating whether expressing the $\epsilon 4$ allele of the apoE gene (considered to be predisponent to the disease) or the $\epsilon 3$ allele (considered to be protective) induced changes in the membrane lipidomics.

Another study carried out at the Demokritos Center concerned the biophysical and biotechnological implications of the presence of *trans* fatty acids in cell membranes, where the development of specific liposomal formulations was used to study whether different concentrations of *trans* fatty acid-containing phospholipid affected liposome diameter, fluidity and permeability.

Finally, the chemical and analytical characterization of the six mono-*trans* isomers of DHA, an essential ω -3 fatty acid, was performed using two different synthetic approaches combined with gas chromatography and nuclear magnetic resonance. Such characterization was finalized to the building of a molecular reference library to be used for the identification of DHA *trans* isomers in nutraceutical formulations.

1.9. References

1. Dowhan, W.; Bogdanov, M.; Mileykovskaya, E. Functional roles of lipids in membranes. In *Biochemistry of lipids, lipoproteins and membranes*, 6th ed.; Vance, J.E., Vance, D., Eds.; Elsevier Science, Amsterdam, Netherlands, **2002**, pp- 1-40
2. Yeagle, P.L. Lipid regulation of cell membrane structure and function. *The FASEB journal* **1989**, 3(7), 1833-1842
3. Cullis, P.T. ; De Kruijff, B. Lipid polymorphism and the functional roles of lipids in biological membranes. *Biochim. Biophys. Acta (BBA)-Reviews on Biomembranes* **1979**, 559(4), 399-420
4. Firestone, D.A.; Horwitz, W.I. IUPAC gas chromatographic method for determination of fatty acid composition: collaborative study. *J. Assoc. Off. Anal. Chem.* **1979**, 62(4), 709-721
5. Cook, H.W.; McMaster, C.R. Fatty acid desaturation and chain elongation in eukaryotes. *New comprehensive biochemistry* **2002**, 36, 181-204.
6. Heipieper, H.J.; Meinhard, F.; Segura, A. The cis-trans isomerase of unsaturated fatty acids in *Pseudomonas* and *Vibrio*: biochemistry, molecular biology and physiological function of a unique stress adaptive mechanism. *FEMS Microbiol. Lett.* **2003**, 229, 1-7
7. Diefenbach, R.; Heipieper, H.J.; Keweloh, H. The conversion of cis into trans unsaturated fatty acids in *Pseudomonas putida* P8: evidence for a role in the regulation of membrane fluidity. *Applied Microbiology and Biotechnology* **1992**, 38(3), 382-387
8. Ferreri, C.; Pierotti, S.; Barbieri, A.; Zambonin, L.; Landi, L.; Rasi, S.; Luisi, P.L.; Barigelletti, F.; Chatgililoglu, C. Comparison of phosphatidylcholine vesicle properties related to geometrical isomerism. *Photochem. Photobiol.* **2006**, 82(1), 274-280
9. Cevc, G. (Ed.). *Phospholipids handbook*. CRC Press, Marcel Dekker Inc., New York, USA, **1993**
10. Cadenas, E.; Boveris, A.; Ragan, C.I.; Stoppani, A.O. Production of superoxide radicals and hydrogen peroxide by NADH-ubiquinone reductase and ubiquinol-cytochrome c reductase from beef-heart mitochondria. *Arch. Biochem. Biophys.* **1977**, 180(2), 248-257
11. Babbs, C.F. Free radicals and the etiology of colon cancer. *Free Radic. Biol. Med.* **1990**, 8(2), 191-200.
12. Yamamoto, S. "Enzymatic" lipid peroxidation: Reactions of mammalian lipoxygenases. *Free Radic. Biol. Med.* **1991**, 10(2), 149-159
13. Halliwell, B. Free radicals, reactive oxygen species and human disease: a critical evaluation with special reference to atherosclerosis. *Br. J. Exp. Pathol.* **1989**, 70(6), 737-757
14. Lunec, J. Free radicals: their involvement in disease processes. *Ann. Clin. Biochem.* **1990**, 27(3), 173-182
15. Gutteridge, J.M.C. The protective action of superoxide dismutase on metal-ion catalysed peroxidation of phospholipids. *Biochem. Biophys. Res. Commun.* **1977**, 77(1), 379-386

16. Maehly, A.; Chance, B. The assay of catalases and peroxidases, In *Methods of Biochemical Analysis*, Glick, D. Ed., Interscience Publishers, New York, **1954**, Volume 1, pp. 357-424
17. Maddipati, K.R.; Marnett, L.J. Characterization of the major hydroperoxide-reducing activity of human plasma. Purification and properties of a selenium-dependent glutathione peroxidase. *J. Biol. Chem.* **1987**, *262*(36), 17398–17403
18. Vendemiale, G.; Grattagliano, I.; Altomare, E. An update on the role of free radicals and antioxidant defense in human disease. *Int. J. Clin. Lab. Res.* **1999**, *29*(2), 49-55
19. Halliwell, B.; Gutteridge, J.M.C. Role of free radicals and catalytic metal ions in human disease: an overview. *Methods Enzymol.* **1990**, *186*, 1-85
20. Erden-Inal, M.; Sunal, E.; Kanbak, G. Age-related changes in the glutathione redox system. *Cell. Biochem. Funct.* **2002**, *20*(1), 61–66
21. Gutteridge, J.M.C.; Richmond, R.; Halliwell, B. Oxygen free-radicals and lipid peroxidation: inhibition by the protein caeruloplasmin. *FEBS Lett.* **1980**, *112*(2), 269–272
22. Loeffler, D.A.; Connor, J.R.; Juneau, P.L.; Snyder, B.O.S.; Kanaley, L.; DeMaggio, A.J.; Nguyen, H.; Brickman, C.M.; LeWitt, P.A. Transferrin and iron in normal, Alzheimer's disease, and Parkinson's disease brain regions. *J. Neurochem.* **1995**, *65*(2), 710–724
23. Birben, E.; Sahiner, U.M., Sackesen, C.; Erzurum, S.; Kalayci, O. Oxidative stress and antioxidant defense. *World Allergy Organ. J.* **2012**, *5*(1), 9-19
24. Dhalla, N.S.; Temsah, R.M.; Netticadan, T. Role of oxidative stress in cardiovascular diseases. *J. Hypertens.* **2000**, *18*(6), 655-673
25. Baynes, J.W. Role of oxidative stress in development of complications in diabetes. *Diabetes* **1991**, *40*(4), 405-412
26. Valko, M.; Rhodes, C.; Moncol, J.; Izakovic, M.M.; Mazur, M. Free radicals, metals and antioxidants in oxidative stress-induced cancer. *Chem. Biol. Interact.* **2006**, *160*(1), 1-40
27. Barnham, K.J.; Masters, C.L.; Bush, A.I. Neurodegenerative diseases and oxidative stress. *Nat. Rev. Drug Discov.* **2004**, *3*(3), 205-214
28. Jenner, P. Oxidative stress in Parkinson's disease. *Ann. Neurol.* **2003**, *53*(S3), S26-36
29. Chauhan, A.; Chauhan, V. Oxidative stress in autism. *Pathophysiology*, **2006**, *13*(3), 171-181
30. Halliwell, B.; Chirico, S. Lipid peroxidation: its mechanism, measurement, and significance. *Am. J. Clin. Nutr.* **1993**, *57*(5S), S715-724
31. Shils, M.E.; Shike, M. (Eds.). *Modern nutrition in health and disease*. 10th ed.; Lippincott Williams & Wilkins, Philadelphia, USA, **2006**
32. Hulbert, A.J. Explaining longevity of different animals: is membrane fatty acid composition the missing link?. *Age(Dordr)* **2008**, *30*(2-3), 89-97
33. Naudí, A.; Jové, M.; Ayala, V.; Portero-Otín, M.; Barja, G.; Pamplona, R. Membrane lipid unsaturation as physiological adaptation to animal longevity. *Front. Physiol.* **2013**, *4*, 372

34. Yun, J.M.; Surh, J. Fatty acid composition as a predictor for the oxidation stability of Korean vegetable oils with or without induced oxidative stress. *Prev. Nutr. Food Sci.* **2012**, *17*(2), 158-165
35. Mihaljevic, B.; Tartaro, I.; Ferreri, C.; Chatgililoglu, C. Linoleic acid peroxidation vs. isomerization: a biomimetic model of free radical reactivity in the presence of thiols. *Org. Biomol. Chem.*, **2011**, *9*, 3541-3548
36. Ferreri, C.; Chatgililoglu, C. Geometrical trans lipid isomers: a new target for lipidomics. *ChemBioChem.* **2005**, *6*(10), 1722-1734
37. Chatgililoglu, C.; Ferreri, C.; Lykakis, I.N.; Wardman, P. *trans*-Fatty acids and radical stress: What are the real culprits?. *Bioorg. Med. Chem.* **2006**, *14*(18), 6144-6148
38. Chatgililoglu, C.; Ferreri, C.; Melchiorre, M.; Sansone, A.; Torreggiani, A. Lipid geometrical isomerism: from chemistry to biology and diagnostics. *Chem. Rev.* **2014**, *114*(1), 255-284
39. Ferreri, C.; Manco, I.; Faraone-Mennella, M.R.; Torreggiani, A.; Tamba, M.; Chatgililoglu, C. A biomimetic model of tandem radical damage involving sulfur-containing proteins and unsaturated lipids. *ChemBioChem*, **2004**, *5*(12), 1710-1712
40. Willett, W.C.; Stampfer, M.J.; Manson, J.E.; Colditz, G.A.; Speizer, F.E.; Rosner, B.A.; Sampson, L.A.; Hennekens, C.H. Intake of trans fatty acids and risk of coronary heart disease among women. *Lancet* **1993**, *341*(8845), 581-585.
41. Ascherio, A.; Willett, W.C. Health effects of trans fatty acids. *Am. J. Clin. Nutr.* **1997**, *66*(4S), 1006S-1010S
42. Hill, E.G.; Johnson, S.B.; Lawson, L.D.; Mahfouz, M.M.; Holman, R.T. Perturbation of the metabolism of essential fatty acids by dietary partially hydrogenated vegetable oil. *Proc. Natl. Acad. Sci. U.S.A.* **1982**, *79*, 953-957
43. Ackman, R.G.; Mag, T.K. Trans fatty acids and the potential for less in technical products. In *Trans Fatty Acids in Human Nutrition*, Christie, W.W.; Sebedio, J.L. Eds.; The Oily Press, Dundee, UK, **1998**, pp. 35-58
44. Fournier, V.; Destailats, F.; Hug, B.; Golay, P. A.; Joffre, F.; Juaneda, P.; Semon, E.; Dionisi, F.; Lambelet, P.; Sebedio, J.L.; Berdeaux, O. Quantification of eicosapentaenoic and docosahexaenoic acid geometrical isomers formed during fish oil deodorization by gas-liquid chromatography. *J. Chromatogr. A* **2007**, *1154*(1-2), 353-359
45. Ferreri, C.; Grabovskiy, S.A.; Aoun, M.; Melchiorre, M.; Kabal'nova, N.; Feillet-Coudray, C.; Fouret, G.; Courdray, C.; Chatgililoglu, C. Trans fatty acids: chemical synthesis of eicosapentaenoic acid isomers and detection in rats fed a deodorized fish oil diet. *Chem. Res. Toxicol.* **2012**, *25*(3), 687-694
46. Smith, L.M., Clifford, A.J., Creveling, R.K., & Hamblin, C.L. Lipid content and fatty acid profiles of various deep-fat fried foods. *J. Am. Oil Chem. Soc.* **1985**, *62*(6), 996-999
47. Tsuzuki, W.; Matsuoka, A.; Ushida, K. Formation of trans fatty acids in edible oils during the frying and heating process. *Food Chem.* **2010**, *123*(4), 976-982

48. Mjøs, S.A.; Solvang, M. Geometrical isomerisation of eicosapentaenoic and docosahexaenoic acid at high temperatures. *Eur. J. Lipid Sci. Technol.* **2006**, 108(7), 589-597
49. Moreno, M.; Olivares, D.M.; Lopez, F.J.A.; Adelantado, J.V.G.; Reig, F.B. Determination of unsaturation grade and trans isomers generated during thermal oxidation of edible oils and fats by FTIR. *J. Mol. Struct.* **1999**, 482-483, 551-556
50. Sanibal, E.A.A.; Mancini-Filho, J. Frying oil and fat quality measured by chemical, physical, and test kit analyses. *J. Am. Oil Chem. Soc.* **2004**, 81(9), 847-852
51. Romero, A.; Cuesta, C.; Sánchez-Muniz, F.J. Trans fatty acid production in deep fat frying of frozen foods with different oils and frying modalities. *Nutr. Res.* **2000**, 20(4), 599-608.
52. Parodi, P.W. Distribution of isomeric octadecenoic fatty acids in milk fat. *J. Dairy Sci.* **1976**, 59(11) 1870-1873
53. Santora, J.E.; Palmquist, D.L.; Roehrig, K.L. Trans-vaccenic acid is desaturated to conjugated linoleic acid in mice. *J. Nutr.* **2000**, 130(2), 208-215
54. Viladomiu, M.; Hontecillas, R.; Bassaganya-Riera, J. Modulation of inflammation and immunity by dietary conjugated linoleic acid. *Eur. J. Pharmacol.* **2016**, 785, 87-95
55. Corl, B.A.; Barbano, D.M.; Bauman, D.E. cis-9, trans-11 CLA derived endogenously from trans-11 18:1 reduces cancer risk in rats. *J. Nutr.* **2003**, 133(9), 2893-2900
56. Sisk, M.B.; Hausman, D.B.; Martin, R.J.; Azain, M.J. Dietary conjugated linoleic acid reduces adiposity in lean but not obese Zucker rats. *J. Nutr.* **2001**, 131(6), 1668-1674
57. Moloney, F.; Toomey, S.; Noone, E.; Nugent, A.; Allan, B.; Loscher, C.E.; Roche, H.M. Antidiabetic effects of cis-9, trans-11-conjugated linoleic acid may be mediated via anti-inflammatory effects in white adipose tissue. *Diabetes* **2007**, 56(3), 574-582
58. Inoue, N.; Nagao, K.; Hirata, J.; Wang, Y.M., Yanagita, T. Conjugated linoleic acid prevents the development of essential hypertension in spontaneously hypertensive rats. *Biochem. Biophys. Res. Commun.* **2004**, 323(2), 679-684
59. Mozaffarian, D. Trans fatty acids—Effects on systemic inflammation and endothelial function. *Atheroscler. Suppl.* **2006**, 7(2), 29-32
60. Saravanan, N.; Haseeb, A.; Ehtesham, N.Z.; Ghafoorunissa. Differential effects of dietary saturated and trans-fatty acids on expression of genes associated with insulin sensitivity in rat adipose tissue. *Eur. J. Endocrinol.* **2005**, 153(1), 159-165
61. Micha, R.; Mozaffarian, D. Trans fatty acids: effects on metabolic syndrome, heart disease and diabetes. *Nat. Rev. Endocrinol.* **2009**, 5(6), 335-344
62. Dorfman, S.E.; Laurent, D.; Gounarides, J.S.; Li, X.; Mullarkey, T.L.; Rocheford, E.C.; Sari-Sarraf, F.; Hirsch, E.A.; Hughes, T.E.; Commerford, S.R. Metabolic implications of dietary trans-fatty acids. *Obesity (Silver Spring)* **2009**, 17(6), 1200-1207
63. Mensink, R.P.; Katan, M.B. Effect of dietary trans fatty acids on high-density and low-density lipoprotein cholesterol levels in healthy subjects. *N. Engl. J. Med.* **1990**, 323(7), 439-445

64. Lagrost, L.; Barter, P.J. Effects of various nonesterified fatty acids on the transfer of cholesteryl esters from HDL to LDL induced by the cholesteryl ester transfer protein. *Biochim. Biophys. Acta* **1991**, *1085*(2), 209-216
65. Abbey, M.; Nestel, P.J. Plasma cholesteryl ester transfer protein activity is increased when trans-elaidic acid is substituted for cis-oleic acid in the diet. *Atherosclerosis* **1994**, *106*(1), 99-107
66. Lemaitre, R.N.; King, I.B.; Mozaffarian, D.; Sotoodehnia, N.; Rea, T.D.; Kuller, L.H.; Tracy, R.P.; Siscovick, D.S. Plasma phospholipid trans fatty acids, fatal ischemic heart disease, and sudden cardiac death in older adults. *Circulation* **2006**, *114*(3), 209-215
67. Decsi, T.; Koletzko, B. Do trans fatty acids impair linoleic acid metabolism in children?. *Ann. Nutr. Metab.* **1995**, *39*(1), 36-41
68. Cook, H.W. Incorporation, metabolism and positional distribution of trans-unsaturated fatty acids in developing and mature brain. Comparison of elaidate and oleate administered intracerebrally. *Biochim. Biophys. Acta, Lipids Lipid Metab.* **1978**, *531*(3), 245-256
69. Moss, J. Labeling of trans fatty acid content in food, regulations and limits-the FDA view. *Atheroscler. Suppl.* **2006**, *7*(2), 57-59
70. Serhan, C.N. A search for endogenous mechanisms of anti-inflammation uncovers novel chemical mediators: missing links to resolution. *Histochem. Cell. Biol.* **2004**, *122*(4), 305-321
71. Levy, B.D.; Clish, C.B.; Schmidt, B.; Gronert, K.; Serhan, C.N. Lipid mediator class switching during acute inflammation: signals in resolution. *Nature Immunol.* **2001**, *2*(7), 612-619
72. Serhan, C.N.; Clish, C.B.; Brannon, J.; Colgan, S.P.; Chiang, N.; Gronert, K. Novel functional sets of lipid-derived mediators with antiinflammatory actions generated from omega-3 fatty acids via cyclooxygenase 2-nonsteroidal antiinflammatory drugs and transcellular processing. *J. Exp. Med.* **2000**, *192*(8), 1197-1204
73. Serhan, C.N.; Chiang, N.; Van Dyke, T.E. Resolving inflammation: dual anti-inflammatory and pro-resolution lipid mediators. *Nat. Rev. Immunol.* **2008**, *8*(5), 349-361
74. Serhan, C.N.; Yang, R.; Martinod, K.; Kasuga, K.; Pillai, P.S.; Porter, T.F.; Oh, S.F.; Spite, M. Maresins: novel macrophage mediators with potent antiinflammatory and proresolving actions. *J. Exp. Med.* **2009**, *206*(1), 15-23
75. Patterson, E.; Wall, R.; Fitzgerald, G.F.; Ross, R.P., Stanton, C. Health implications of high dietary omega-6 polyunsaturated fatty acids. *J. Nutr. Metab.* **2012**, 539426
76. Wymann, M.P.; Schneider, R. Lipid signalling in disease. *Nat. Rev. Mol. Cell. Biol.* **2008**, *9*(2), 162-176
77. Schmitz, G.; Ecker, J. The opposing effects of n-3 and n-6 fatty acids, *Prog. Lipid Res.* **2008**, *47*(2), 147-155

78. Hidaka, B.H.; Li, S.; Harvey, K.E.; Carlson, S.E.; Sullivan, D.K.; Kimler, B.F.; Zalles, C.M.; Fabian, C. J. Omega-3 and omega-6 Fatty acids in blood and breast tissue of high-risk women and association with atypical cytomorphology. *Cancer Prev. Res. (Phila)* **2015**, *8*(5), 359-364
79. Yang, K.; Han, X. Lipidomics: techniques, applications, and outcomes related to biomedical sciences. *Trends Biochem. Sci.* **2016**, *41*(11), 954-969
80. Gordon, W.C.; Bazan, N.G. Mediator lipidomics in ophthalmology: targets for modulation in inflammation, neuroprotection and nerve regeneration. *Curr. Eye Res.* **2013**, *38*(10), 995-1005

Chapter 2

Analytical Methodologies

2.1. Lipid analyses

Lipidomic approach is used to study complex mixtures containing different lipid classes. The analytical techniques for the detection and quantification of lipids are characterized by high selectivity, that is the ability to determine the analyte in the presence of interferents in the matrix.

The lipid analysis of a sample usually involves some common key steps [1]:

- extraction of the lipid fraction from the starting matrix;
- isolation of the lipid fractions of interest;
- derivatization of the lipid components;
- identification and quantification of FAs.

The accuracy of the analysis is influenced by the effectiveness of each single step. For this reason, the analytical method of extraction should be developed taking into account the following requirements:

- ability to inhibit the action of enzymes such as lipases and phospholipases, in order to avoid lipid degradation during the analysis;
- ability to limit oxidative and isomerization phenomena of the double bonds during extraction (generally induced by high temperatures and unsuitable solvents);
- ability to extract all the constituents of the lipid fraction;

- ability to separate lipids from other low polarity components (apolar interferents) that could compromise the quality of the analysis.

2.2. Lipid extraction

Lipid extraction permits to isolate lipids from biological matrices and remove any sources of interference, such as proteins and sugars. Lipids are usually characterized by hydrophobic properties that make them immiscible with water and soluble in non polar (organic) solvents. However, due to the broad variety of lipids, some classes of lipids, such as phospholipids, have amphiphilic properties, that confer them greater polarity.

For this reason, the most efficient lipid extraction method is the liquid-liquid extraction proposed by Folch in 1957, which suggested the use of a chloroform/methanol mixture (2:1 v/v) for quantitative lipid isolation. [2]. Even if other effective mixtures were identified, aimed at reducing the solvent toxicity and increasing selectivity, Folch method remains the most commonly used procedure for the extraction of lipids from biological matrices.

2.3. Thin Layer Chromatography (TLC)

After the extraction step, thin layer chromatography (TLC) can be used to verify in a fast and relatively unexpensive way the efficiency of the extraction method [3]. Usually, it is particularly suitable for carrying out qualitative or semi-quantitative evaluations as well as to follow the progress of a chemical reaction.

Like all chromatographic techniques, TLC is based on the different distribution of similar substances between a stationary phase and a mobile phase, depending on the affinity of each substance with the substrates. Molecules with high affinity for the mobile phase will migrate faster along the plate, while molecules with high affinity for the stationary phase will stuck close to the baseline, without significantly migrating. The TLC plate is usually coated with a suitable adsorbing material, such as silice gel or alumina, that constitutes the stationary phase. The mobile phase is a solvent (or a mixture of solvents) that is characterized by a low affinity with the stationary phase and a good ability to separate the components of interest. Depending on the polarity of the lipid families present in the sample, different mobile phases can be employed.

The procedure consists on the deposition of a small amount of the lipid sample on the TLC plate, that is then immersed in a chamber saturated with the appropriate mobile phase. Over time, the solvent moves up the TLC plate due to capillary forces and separates different lipid fractions based on their affinity for the absorbing material. Standard reference substances are usually spotted beside the lipid mixture to allow recognition and assignment of the lipid components.

Since most lipids are colorless and TLC spots cannot be seen, stains can be applied at the end of the separation by spraying - or by dipping the plate into - a staining solution, to form colored compounds that can be identified by direct observation or UV analysis.

For these set of experiment, cerium ammonium molybdate (CAM) was chosen as staining technique, due to its sensitivity and wide applicability. CAM can be prepared by dissolving 1.5 g of phosphomolybdic acid and 1.0 g of cerium (IV) sulfate in a mixture of 6 ml of sulfuric acid (H₂SO₄) and 94 ml of distilled water. After exposure to heating conditions, Mo⁵⁺ and Mo⁴⁺ compounds are formed and green to blue colored spots on a yellow background appear on the plate.

Each substance has a specific retention factor (R_f), corresponding to the distance of the spot from the origin compared with the distance covered by the solvent (solvent front). By comparing the distance reached by the experimental spots with that of standards of known composition, it is possible to identify the lipids present in the original mixture (**Figure 2.1**).

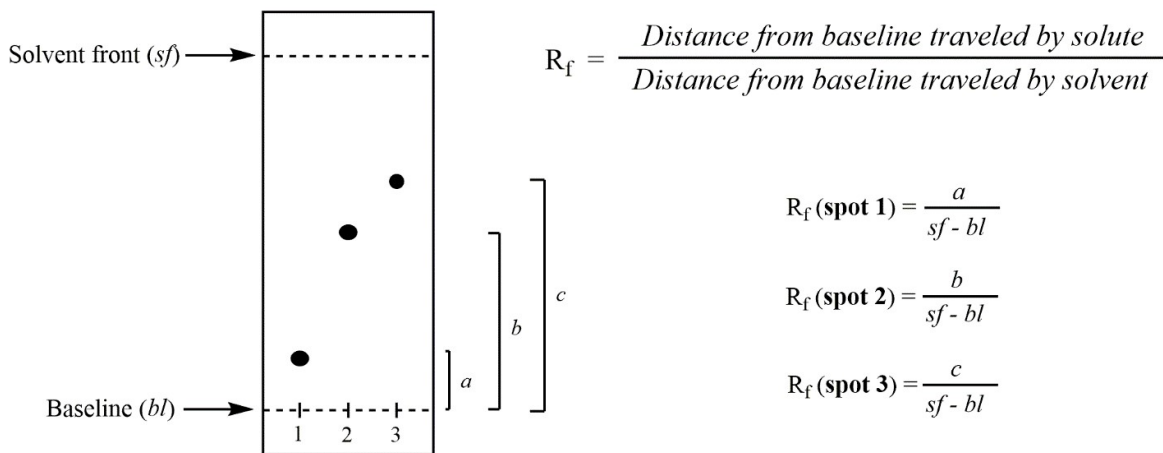


Figure 2.1. Schematic representation of a TLC plate and R_f definition.

2.3.1. Silver-ion thin layer chromatography (Ag-TLC)

Silver-ion thin layer chromatography (Ag-TLC) is a well-known analytical method for monitoring the isomerization reaction since it allows the separation of *cis* and *trans* lipid isomers [4].

The separation by Ag-TLC is based on the ability of unsaturated organic compounds to form complexes with transition metals, specifically with silver ion Ag (I). Indeed, the pi electrons of double bonds in the lipid fatty acyl residues reversibly react with silver ions to form polar complexes; the greater the number of double bonds, the stronger the complexation effect.

The formation of the lipid-Ag⁺ complex involves a charge transfer, in which the unsaturated compound acts as an electron donor and the Ag⁺ ion acts as an electron-acceptor (**Figure 2.2**).

On this regard, the current model assumes the formation of a sigma-type bond between the occupied 2p orbitals of an olefinic double bond and the free 5s and 5p orbitals of the transition metal ion, and a (probably weaker) pi acceptor backbond between the occupied 4d orbitals of the metal ion and the free antibonding 2p pi* orbitals of the olefinic bond [5,6].

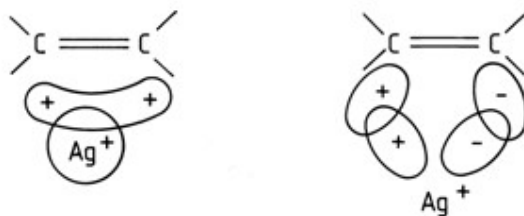


Figure 2.2. Interaction between Ag⁺ and an olefinic double bond. Image from <http://lipidlibrary.aocs.org>.

The complex formation efficiency is influenced by the ease with which the overlapping of the orbitals can occur, which is determined by steric factors. Generally, fully saturated lipids do not form complexes and migrate to the top of the plate, while those containing one or more unsaturated bonds come next. This technique is exploited for the separation of geometrical isomers, since the isomers in the *cis* configuration form a more stable complex with the stationary phase and are retained more compared to their *trans* analogues. By optimizing the mobile phase to yield the suitable separation, *trans*-isomers have higher R_f, while *cis*-isomers run slower on the Ag-TLC plate.

A 5% w/v silver nitrate solution (AgNO₃) in acetonitrile was prepared dissolving 2.5 g of AgNO₃ in 50 mL of acetonitrile. The silica-based plates with glass support were immersed for 15 minutes in this solution of 5% AgNO₃ in acetonitrile protected from light, and subsequently dried in an oven for one hour. The surface-functionalized TLC plates can be stored in a dry and dark place for a maximum of one week. The spots can be detected by spraying with CAM stain and by heating until blue brown

spots on a yellow background could be observed. When employed for preparative use, Ag-TLC plates are treated with CAM only on a small portion, to allow the recovery of the unaltered compounds from the remaining portion.

2.4. Gas Chromatography (GC)

The step that follows lipid extraction is the fatty acid derivatization to more volatile compounds, using the transesterification reaction that leads to fatty acid methyl ester (FAME) derivatives.

FAMEs can be analyzed by gas chromatography (GC), that is the election technique for lipid separation and quantification. The derivatization step is necessary since most lipids have low volatility and some tendency to degrade at high temperatures.

The transesterification procedure to FAMEs can take place with both acidic or basic reagents as catalysts. The most efficient derivatization method to obtain FAMEs is the transesterification reaction carried out in a basic environment [7]. The conditions usually require anhydrous methanol (CH₃OH) in the presence of a basic catalyst, usually potassium hydroxide (KOH), which facilitates the exchange between methanol and glycerol of the O-acyl lipids, such as triglycerides and phospholipids (**Figure 2.3**).

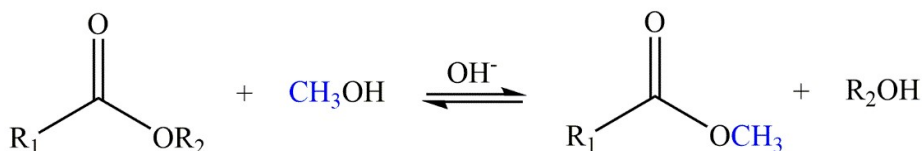


Figure 2.3. Base-catalysed transesterification mechanism of an acyl chain to its methyl ester derivative.

In this step, not only the base but also the molarity and type of solvent used become determinative for the quantitative success of the reaction. In basic conditions, the reaction takes place in a very short time without inducing isomerization and migration phenomena, processes that easily take place in acidic environment. Attention must be paid to exclude the presence of water in the reaction environment and to prevent the occurrence of hydrolysis and FFA formation. Water is used to quench the reaction, since it neutralizes the anions present, and FAMEs can be extracted with hexane and, once anhydriified, can be injected in the GC.

GC equipment (**Figure 2.4**) consists of a sample injection system, connected to a capillary column that is flushed with the carrier gas in a thermostated chamber (oven). The column leads to a detector that is connected to an external unit equipped with software for data processing. In gas

chromatography, the mobile phase is a carrier gas, usually an inert gas such as helium or an unreactive gas such as nitrogen. The sample is heated in the injection chamber to volatilize the FAMES and then carried into the separating column by a heated carrier gas.

To inject a liquid phase sample into a capillary column, spit or splitless modes can be used. In the split mode, 1 μL of the sample is introduced into the injector, but only a small percentage of steam generated within the liner enters in the column, while the remaining part is removed through the operation of a valve. This mode guarantees high resolution separations thanks to the high flow rate at the split point. In the case of trace compound analyses, however, the splitless mode is more indicated, which involves the processing of the full injected sample in the column.

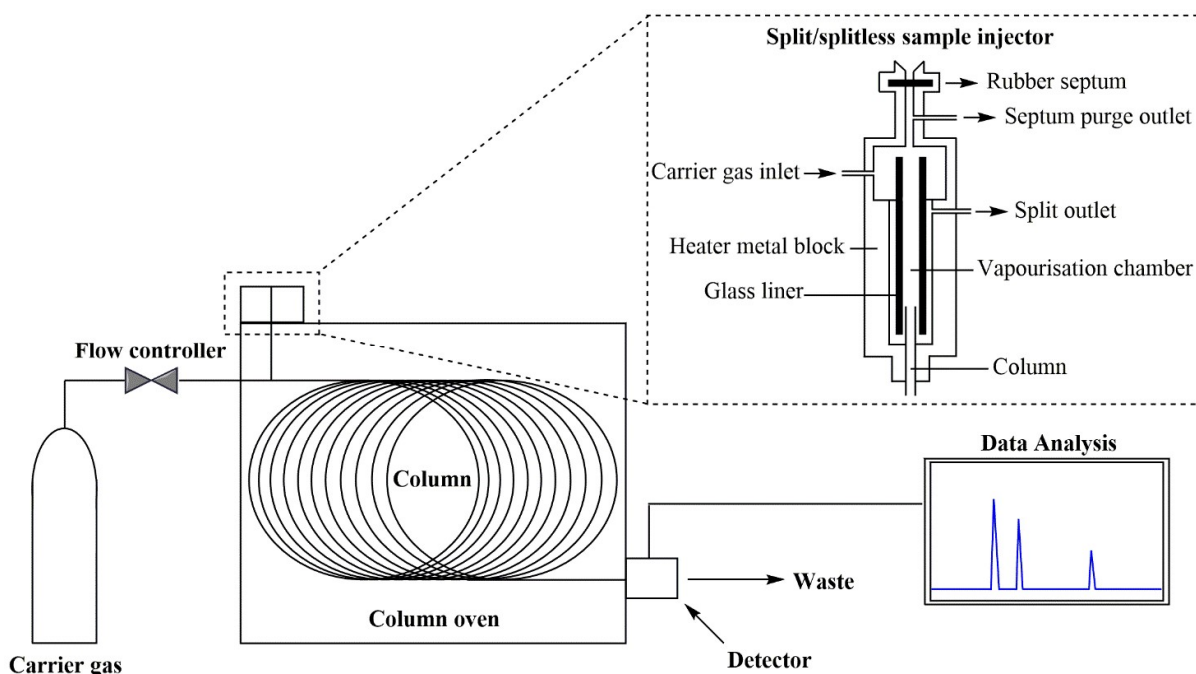


Figure 2.4. Schematic representation of a gas chromatogram equipped with a spit/splitless sample injector.

FAMES in the mixture can be separated because of their differing affinities for the matrix in the column. The stronger the affinity between a specific molecule and the matrix the slower it passes through the column. After being separated by the column, each molecule passes by a suitable detector that allows its quantification.

For the GC analyses reported in this thesis, a gas chromatograph (GC) equipped with a 60 meters capillary column in fused silica having a stationary phase consisting of (50%-cyanopropyl)-methylpolysiloxane (DB-23, Agilent, USA), was used. The GC is connected to a flame ionization

detector (FID). The operating mechanism of FID provides the detection of ions formed by organic compound combustion on a hydrogen flame, that is proportional to the concentration of organic species in the sample gas stream. The molar response of hydrocarbons is usually equal to the number of carbon atoms in their molecule, while oxygenated lipids and other species that contain heteroatoms tend to have a lower response factor.

For more details regarding gas carrier, volume of injection, oven temperature program and operating pressures, please refer to the experimental sections of each chapter.

The specificities of DB-23 column, including the length and the medium polarity of the stationary phase, combined with the oven temperature set up, guarantee the selectivity and efficiency required for the resolution of complex FAME mixture and achieve the separation of a high number of geometrical isomers.

With the conditions set up in our laboratory, elution order depends on the number of carbon atoms and the number of double bonds in the acyl chain. For example, the retention time of FAMES increases as the number of carbons increases, being short chain fatty acids the first ones to elute and long chain fatty acids the last ones ($14:0 < 16:0 < 18:0 < 20:0 < 22:0$). When chains differ in the number or in the position of unsaturated bonds rather than in the chain length, SFAs are usually the first ones to elute, while MUFAs and PUFAs strongly interact with the stationary phase and are retained with increasing strength inside the column ($18:0 < 18:1 < 18:2 < 18:3$).

Considering the position of the double bonds, usually FAMES with the unsaturation closer to the carboxylic group are eluted first ($9c,18:1 < 11c,18:1$), and the same happens when the double bond has *trans* geometry ($9t,18:1 < 11t,18:1$). In analogy with saturated FAMES, when the only difference is the configuration of the double bond, *trans* isomers are less retained compared to the *cis* analogues ($9t,18:1 < 9c,18:1$).

However, these should only be considered general indications, because for FAMES with more than 18 carbon atoms, the separation of *trans* isomers does not comply with these elution criteria. The unpredictable elution of PUFA methyl esters with more than 18 carbons reinforces the need of molecular reference libraries of standards for the precise interpretation of GC chromatograms. The most common FAMES with the *cis* geometry are commercially available. However, for the mono-*trans* isomers of our interest, such as ARA [8] and EPA [9], it was necessary to build up synthetic methods for the full characterization and the correct allocation of the peaks.

GC presents many advantages, since it requires small samples (typically 1-2 μL) and is characterized by high resolution and high sensitivity for effect of the capillary columns. Depending on the length of the column and the set up of the oven ramp, the analyses can require longer analysis times.

2.5. References

1. Christie, W.W.; Han, X. Isolation, Separation, Identification and Lipidomic Analysis. In *Lipid analysis*, 4th ed.; The Oily Press, Bridgwater, U.K., **2010**
2. Folch, J.; Lees, M.; Sloane Stanley, G.H. A simple method for the isolation and purification of total lipids from animal tissues, *J. Biol. Chem.* **1957**, *226*(1), 497-509
3. Fuchs, B.; Süß, R.; Teuber, K.; Eibisch, M.; Schiller, J. Lipid analysis by thin-layer chromatography- a review of the current state. *J. Chromatogr. A* **2011**, *1218*(19), 2754-2774
4. Kiran, C.R.; Reshma, M.V.; Sundaresan, A. Separation of cis/trans fatty acid isomers on gas chromatography compared to the Ag-TLC method. *Grasas y aceites* **2013**, *64*(1), 95-102.
5. Morris, L.J. Separations of lipids by silver ion chromatography, *J. Lipid Res.*, **1966**, *7*(6), 717-732
6. Momchilova, S.M.; Nikolova-Damyanova, B.M. Advances in Silver Ion Chromatography for the analysis of fatty acids and triacylglycerols - 2001 to 2011, *Anal. Sci.* **2012**, *28*(9), 837-844
7. Christie, W.W. Preparation of ester derivatives of fatty acids for chromatographic analysis. In *Advances in Lipid Methodology*, The Oily Press, Bridgwater, U.K., **1993**, Volume 2, pp- 69-111
8. Ferreri, C.; Faraone Mennella, M.R.; Formisano, C.; Landi, L.; Chatgililoglu, C. Arachidonate geometrical isomers generated by thiyl radicals: the relationship with trans lipids detected in biological samples, *Free Rad. Bio & Med.* **2002**, *33*(11), 1516-1526
9. Ferreri, C.; Grabovskiy, S.A.; Aoun, M.; Melchiorre, M.; Kabal'nova, N.; Feillet-Coudray, C.; Fouret, G.; Courdray, C.; Chatgililoglu, C. Trans fatty acids: chemical synthesis of eicosapentaenoic acid isomers and detection in rats fed a deodorized fish oil diet. *Chem. Res. Toxicol.* **2012**, *25*(3), 687-694

Chapter 3

Autism Spectrum Disorder

3.1. Introduction

Autism Spectrum Disorder (ASD) is a major neurodevelopmental disorder, which affects the ability of interaction and social communication, induces repetitive behaviors and drastically limits the interest for external events. Currently, ASD is an incurable condition whose causes are both genetic and environmental.

Increasing evidences support the involvement of altered FA metabolic pathways in the nervous system malfunctioning and their contribution to autism spectrum disorder.

Compared with other organs, the brain presents a high intrinsic concentration of polyunsaturated lipids, which increase its vulnerability to ROS damage, as further induced by high metabolism and high levels of iron compared to relatively low levels of enzymes encharged of free fradical depletion.

Since the diagnosis is actually based only on clinical symptoms, the development of comprehensive diagnostic tools will be useful, in order to help the pediatrician to make as early a diagnosis as possible; it is hoped that an early intervention, comprehensive of nutritional advice, may be useful for a milder prognosis.

In this thesis we show preliminary data of an integrated approach based on biophotonics, lipidomics and clinical evaluation as powerful strategy for an early ASD diagnosis. Specifically, we focused on RBCs of autistic children, mapping the cell surface by hyperspectral dark-field microscopy (HDFM) and in parallel monitoring membrane phospholipid FA composition by lipidomic analysis.

These results foresee the use of biophotonic methodologies combined with other clinical evaluations to better define an ASD diagnostic panel and design a personalized and targeted plan of intervention.

3.2. Autism Spectrum Disorder (ASD)

ASD is a neurodevelopmental disorder characterized by impairment of social interaction and deficiencies of verbal and nonverbal communication, which causes interest deficits and repetitive behaviors [1].

This condition is characterized by behavioural alterations that can be classified in three main areas and be employed as diagnostic parameters [2,3]:

- **Social Impairment:** it refers to the inability of establishing social and/or emotional relationships with other people. Usually ASD children show little interest in other children or adults, do not react when called by name and become aggressive in noisy and unusual environments.
- **Communication:** it refers to the inability of expressing ideas and feelings. Usually, delay or total lack of language are seen. If language is present, it is often abnormal and consisting of repeated sounds or single words which cannot be organized in sentences. They also display problems in understanding conversations and concepts.
- **Rigidity and perseveration:** it refers to a constant dedication to one or more types of interest with exaggerated reactions to specific topics or events (i.e. ability to memorize with no efforts name lists, historical events, sportive charts or to solve mathematic problems). The activities of children affected by ASD are usually characterized by repetitive and stereotyped behaviors. They repeatedly perform purposeless motor movements and they show persistent attachment to objects or toys that reflects anxiety and resistance to changes.

Finally, other typical autistic behaviors are abrupt mood swings, hyperactivity or apathy, self-aggressive behaviors such as hand biting or hair grabbing, phobias, sleep disturbances and eating disorders.

Since the variety of symptoms makes it difficult to provide a consistent clinical description, within the ASD definition are included several pathologies or syndromes characterized by the same behaviors, although at different degrees of intensity. The severity of the pathological disorder and the appearance of the symptoms are very variable, and this fact makes autism diagnosis and personalized interventions very difficult.

The incidence of the disorder in 2007 was reported to be of 6.6 cases per thousand children [4], but the US Centers for Disease Control and Prevention have recently reported the prevalence of ASD in 14.7 per thousand of 8-years-old children. This suggests that the incidence of ASD has dramatically increased. There is a marked difference in prevalence among males and females: for every ASD female with autism there are three to four males with the same disorder [5].

Parents usually notice the first signs within the baby's first two years of life and reliable diagnosis can often be made within the thirty months of life. For the diagnosis the Childhood Autism Rating Scale (CARS), a widely recognized investigation tool for ASD, can be employed [6].

CARS consists on the evaluation of children referring to a list of 15 items related to the main behavioral areas. For each point, a seven-degree scale can be used to indicate how much the subject behavior deviates from the norm relating to his age, assessing 1 as the normal behavior and 7 as the most abnormal one. The final CARS score allows to distinguish mild to medium ASD from the more severe cases.

3.3. Lipidomics for ASD biomarkers

ASD is a multifactorial disorder [7,8] which is thought to have correlations with genetic, epigenetic, environmental and immunological factors, with oxidative stress as linking mechanism [9-13].

The brain is highly vulnerable to oxidative stress; the reason can be found in the limited antioxidant ability of this organ and in its high requirement of energy, especially in the form of lipids and iron. Therefore, neuron functionality is the first one to be compromised in the presence of ROS and shortage of antioxidant.

Children have a natural deficit in detoxification capacity and associated lower levels of glutathione compared to adults [14]. Additionally, environmental factors that induce oxidative stress were found to accumulate in the placenta and to be found in higher concentration in infants [15].

Taken together, these studies suggest that children are highly vulnerable to oxidative stress and that certain conditions could compromise normal neurodevelopment and increase the risk of neurodevelopmental disorders such as autism.

Plasmatic levels of lipid peroxidation indicators were found to be increased in ASD children compared to developmentally normal, aged-matched children [16]. Several studies have suggested alterations in the antioxidant enzymes. Children with ASD showed reduced activity of glutathione peroxidase in plasma and erythrocytes, lower levels of total glutathione, and decreased catalase and

SOD activity in erythrocytes [17,18]. Additionally, other antioxidant proteins, transferrin and ceruloplasmin, were found to be reduced in autistic children. Being transferrin an iron-binding protein and ceruloplasmin a copper-binding protein, abnormalities in the iron and copper metabolism have been suggested to have, together with oxidative stress, a pathological role in autism [19,20].

In a recent study from our group, we described erythrocyte membrane alterations in autistic children. In particular, an increase in MUFAs, a decrease EPA and DHA, and a consequently increased ω -6/ ω -3 ratio that was associated with a reduction of the erythrocyte membrane fluidity, were observed. Increased levels of thiobarbituric acid reactive substances, urinary isoprostane, and hexanoyl-lysine, together with a significant reduction of Na^+/K^+ -ATPase activity were also reported [16].

There are increasing evidences of abnormalities in membrane lipid metabolism and in immune and inflammatory responses in autism [21,22]. Other studies focused on the role of fatty acid deficiencies or imbalances in the appearance of neurodevelopmental disorders such as attention-deficit/hyperactivity disorder, dyslexia, dyspraxia, and autistic spectrum disorders [23,24]. Scientific evidences have been collected on the deficiency of EFAs, possibly correlated with overactive/over-expressed PLA₂ enzymes [25,26].

Plasma methionine and S-adenosylmethionine to S-adenosylhomocysteine ratio, an indicator of methylation capacity, were significantly decreased in ASD. In addition, plasma levels of cysteine, glutathione, and the ratio of reduced to oxidized glutathione, an indication of antioxidant capacity and redox homeostasis, were significantly decreased, suggesting that impairment in the methylation ability might occur in autism [27].

In addition to high levels of oxidative stress, a state of neuroinflammation with activation of the microglia and high levels of proinflammatory cytokines have been found to play a key role in the development of histopathological alterations [28]. Recently, the possible role of *trans* lipids in this disease has been discussed [29].

The efficacy of ω -3 fatty acid supplementation to children with autism has been investigated in a number of studies [30]. ω -3 supplements were found to reduce hyperactivity and stereotypies in children with ADS after six-week treatment [31]; caregivers reported improvements in cognitive and motor skills, concentration, sleep quality and sociability as well as reductions in irritability, hyperactivity and aggression in children supplemented with ω -3-rich oils [25].

Taken together, these evidences support the idea of lipid membrane homeostasis as a therapeutic target in ASD. We focused on RBC membranes, since erythrocytes are a sort of observational window to understand the health conditions of the whole organism [32]. We combined the lipidomic analysis

of RBCs from ASD patients and matched control subjects with the hyperspectral characterization and cell surface mapping of RBCs, using hyperspectral dark-field microscopy.

3.4. Hyperspectral dark-field microscopy (HDFM)

Given the importance of RBCs to monitor the health status of patients and the ease of obtaining blood samples, a large number of blood-based analytical techniques have been developed for many pathologies. Microscopic examination of blood samples is generally used to detect defects in the morphology of blood cells or the presence of bacteria and parasites. While bacterial and eukaryotic parasites can be studied by optical microscopy, albeit with limits in resolution capacity, electron microscopy, requiring more complex preparation techniques, can be used for virus identification.

Hyperspectral dark-field microscopy (HDFM) is an emerging biophotonic imaging methodology, patented by CytoViva, Inc., that finds many applications in life and material sciences [33-35]. Indeed, HDFM technique is a highly versatile method that provides simultaneous spatial and spectroscopic characterization of nonfluorescent samples in a single measurement and does not require contact between the object and the sensor.

In typical dark-field microscopy, the sample is illuminated by indirect light to enhance the image contrast of unstained samples. To do so, a disk is placed underneath the condenser lens so that only the light that is scattered from the analyzed objects can be collected to produce an image. The CytoViva technology (**Figure 3.1**) provides numerous advantages compared to traditional dark field microscopes. The main difference between an optical image and a hyperspectral image, although apparently similar, is that the latter provides, for each pixel, the complete reflectance spectral response of that pixel's spatial area within the visible and near-infrared spectral range (VNIR 400 nm–1000 nm). This enables nondestructive spectral measurements at a nanoscale level in the full spatial context of the sample image. More specifically, CytoViva's patented enhanced dark-field illumination system, unlike standard microscope condensers, works by coupling the source illumination directly to the condenser optics and creates a very narrow illumination angle that can be precisely focused into the sample but bypasses the objective. The result is a very intense scatter from nanoscale samples against a very dark background. Additionally, non-fluorescent live cells and pathogens can be easily observed with such precision that cannot be reached with traditional optical imaging techniques. Finally, signal-to-noise ratio in CytoViva's enhanced darkfield microscope optics is ten times higher than that obtained in standard darkfield optics, enabling particles down to 10-20 nm size to be properly imaged.

CytoViva's technology simultaneously captures the optical spectrum of each point in the image by combining motion of the microscope stage with digital imaging spectroscopy. In this way, samples can be imaged by acquiring hundreds of contiguous wavelengths or bands, which associate scattering spectral information to every pixel [36].

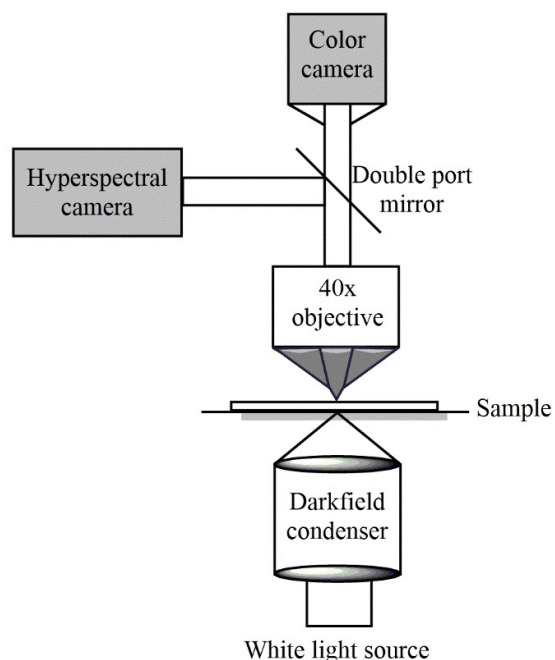


Figure 3.1. Diagram of the CytoViva microscope used for dark-field enhanced hyperspectral image acquisition.

Abundant literature is available on surface mapping and material identification; in the biological field, HDFM was applied in the field of drug delivery using metallic nanoparticles; at present, it shows potentials for spectral characterization of bacteria and pathogens in the blood [37,38], in the cytological diagnosis of cancerous tissues [39,40], as well as in the spectral characterization of gold nanoparticle distribution and pathogens in the blood [37,41]. An initial approach to HDFM analysis of blood cells evidenced the possibility to detect light scattering changes of blood cells induced by morphological alterations [42].

There is growing interest for studies aimed at clarifying morphological characteristics that can be obtained from the scattering spectrum of blood cells. In fact, alterations in the erythrocyte shape could reflect chemical variances or physical abnormalities of RBC membrane itself or of its content [43]. The shape is critical for RBC functioning, and emerging evidence indicates oxidative stress as a key factor for erythrocyte shape alteration [44-46]. Additionally, a high percentage of altered RBC shapes, predominantly elliptocytes, combined with erythrocyte membrane oxidative damage, and β -actin

alterations was observed in ASD patients [47]. Scattering spectra obtained by HDFM analyses depend on the thickness, shape, refractive index, anisotropy and geometry of the membrane compartment and, at molecular level, are affected by the structures and properties of the light-intercepting components.

A study from our group demonstrated that it is possible to correlate the presence of bands in the RBC spectral library with information about phospholipids, hemoglobin, spectrin, cholesterol and protoporphyrin moieties [48].

Since alterations in lipid composition, possibly important in regulating membrane fluidity, have been reported in ASD, we investigated whether RBCs from patients and age-matched controls could be distinguished by HDFM analysis. The combination of HDFM and lipidomic analyses could represent an innovative and promising diagnostic tool for ASD pathology, potentially helpful for early diagnosis and design of specific nutritional interventions and supplementations.

3.5. Experimental part

Chloroform, methanol and *n*-hexane (HPLC grade) were purchased from Merck (Darmstadt, Germany). Sodium sulphate anhydrous (Na₂SO₄) was purchased from Carlo Erba (Milan, Italy). Potassium hydroxide (KOH) and protoporphyrin IX were purchased from Sigma Aldrich (St. Louis, MO, USA). Phospholipid egg lecithin was available from Avanti Polar Lipids (Alabaster, AL, USA). All FAMES used as standard references for GC analysis were purchased from Sigma Aldrich or Fluka (Switzerland) and used without further purification.

3.5.1. Erythrocyte membrane fatty acid analysis

Blood samples were provided by the Child Neuropsychiatric Unit of the Bellaria Hospital (IRCCS, Bologna) which took care of recruitment, clinical diagnostic assessment and comprehensive neurological work up of the patients. A total of 41 children, 21 with ASD (15 Males and 6 Females, mean age 7.2 ± 0.8 years) and 20 with a typical development (13 Males and 7 Females, mean age 9.0 ± 0.9 years), were recruited.

The present study was carried out according to the guidelines laid down in the Declaration of Helsinki and the Ethical Committee of Bologna Health Authority approved all procedures involving human

patients (authorization n. 13062). Blood testing and clinical data collection were authorized by children parents, which gave written informed consent.

Autism diagnosis was made according to the currently accepted clinical evaluation panels, however this was not a topic of the present PhD Thesis; for more information please refer to [49].

In all 21 patients any medical, genetic and neurological comorbidity was excluded. Control group children were healthy typically developing children, recruited in the local community, with no sign of cognitive, learning and psychiatric involvement, as clinically and anamnestically determined by experienced clinicians. All control group children were attending mainstream school and had not been subjected to stressful events. Dietary habits were assessed by a food questionnaire. All patients and controls were on a typical Mediterranean diet. Both ASD and control groups were drug and supplementation free.

An aliquote (250 μ L) of blood sample was processed for lipidomic analysis. The erythrocyte membrane pellet for fatty acid membrane profile analysis was obtained as described in literature [50]. For this study, a specific erythrocyte fraction corresponding to the aged erythrocytes (RBC age > 3 months) was selected due to their higher density and smaller diameter compared to the average erythrocyte population [51-53]. Whole blood was firstly centrifuged at 2000 g \times 5 minutes to remove plasma, and subsequently centrifuged at 4000g \times 4 $^{\circ}$ C \times 5 minutes to yield a stratification by cell density. The phospholipid fraction was extracted using the well known Folch Method (**Chapter 2, Paragraph 2.2**). Briefly, the mature RBC pellet was treated with chloroform/methanol (2:1 v/v) and washed with brine to remove proteins and other water-soluble substances. Organic extracts were dried with anhydrous Na₂SO₄. A TLC using *n*-hexane/ethyl ether/acetic acid (7:3:0.1 v/v) as mobile phase [54] was performed to ascertain the presence of phospholipids and cholesterol, the main lipid membrane constituents. The residue was subjected to transesterification reaction using 0.5 M KOH/methanol solution and kept under stirring for 10 minutes at 22 $^{\circ}$ C and then quenched with brine solution [55]. This procedure led to the formation of FAME derivatives of membrane phospholipids, that were extracted using *n*-hexane. The hexane phase was collected and dried with anhydrous Na₂SO₄. After filtration, the solvent was eliminated by evaporation using a rotary evaporator, and the thin white film corresponding to FAMEs dissolved in a small volume of *n*-hexane. Approximately 1 μ L of this solution was injected into the GC.

An Agilent 6850 gas chromatograph, equipped with a (50%-cyanopropyl)-methylpolysiloxane (DB-23, Agilent, USA) capillary column (60 m \times 0.25 mm i.d. \times 0.25 μ m film thickness) was used for the analysis. The instrument had a flame ionization detector (FID) that required air (450 mL/min) and hydrogen (40 mL/min) and was kept at 250 $^{\circ}$ C. The method used for the analysis started from an

initial temperature of 165 °C held for 3 min, followed by an increase of 1 °C/min up to 195 °C, held for 40 minutes. A final ramp, with a temperature increase of 10 °C/min up to a maximum temperature of 240 °C, was maintained for 10 minutes for column purge.

After the acquisition of the chromatograms, FAMES were identified by comparison with the retention times of commercially available standards or *trans* fatty acid references, synthesized by known protocols described elsewhere [56].

3.5.2. HDFM analysis

Dark-field images were recorded using an enhanced dark-field illumination system (CytoViva, Auburn, AL) attached to an Olympus microscope (EDFM). The system consisted of a CytoViva 150 dark field condenser in place of the microscope original condenser attached via a fiber optic light guide to a 150 W quartz halogen light source (Dolan Jenner DC-950, Massachusetts, USA), which covers the full spectrum from 400 nm to 2500 nm. A 100x oil immersion colour corrected objective with numerical aperture of 1.35–0.55 (Olympus UPlanAPO fluorite) was integral to the system. The optical images consisted of 700.000 pixels with 2 nm resolution.

3.5.2.1. HDFM analysis of RBCs

5 µl of whole blood (EDTA-treated) obtained from control and ASD children, were loaded in the centre of a glass slide and sandwiched with coverslip; samples were left 120 minutes to stabilize prior to proceed with optical acquisition to avoid image blurring. For reproducibility, the protocol required to include approximately thirty regularly shaped RBCs and no other blood cells. Two acquisitions were carried out for each sample.

The optical images obtained from control samples, after background subtraction, were used to create a spectral library. Pixel regions with similar features were identified and selected as region of interest (ROI). Spectra were then characterized for number of peaks, maximum wavelengths and overall spectral shape. Setting the maximum angle on single value and keeping it at 0.1 radian with the spectral angle mapper (SAM) function, eight spectra were individuated which satisfied the requirements of optimal coverage of the optical image. Results are reported as relative spectral distribution \pm SD.

3.5.2.2. HDFM analysis of phospholipids

4.8 mM egg lecithin phospholipid suspension was prepared in tri-distilled water according to known procedures [57]. Liposome vesicles were formed, and the average vesicle diameter size of 200 nm was detected by dynamic light scattering (DLS) measurements (Zetasizer Nano Z, Malvern Instruments). From an optical image made of 700.000 pixels, after background subtraction, the ROI was selected and the hyperspectral image of the sample was acquired. The obtained spectrum is shown in **Figure 3.6**. Bands at 525, 563, 595, 620 nm are observed [48].

3.5.2.3. HDFM analysis of Protoporphyrin IX

6.5 mM protoporphyrin IX was dissolved in tri-distilled water and vortexed at 300 rpm for 1 hour at 37 °C, as previously described [48], to respect the biological concentration [58]. The same procedure described above for the selection of ROI was followed. The resulting spectrum is shown in **Figure 3.6**. Typical bands at 505, 555, 564, 605, 618 nm were observed.

3.5.3. Statistical analysis

Statistical analyses were carried out by a group of expert statisticians, which considered the heterogeneity of the groups and the confounding factors. Statistical analysis was performed using SAS v. 9.2 and STATA 12. To compare groups, normality tests to determine whether data sets followed a Gaussian distribution were applied to all numeric variables. Appropriate parametric tests (ANOVA, Student's t test for independent data) or the nonparametric equivalent (Wilcoxon-Mann-Whitney) were used. In detail, analysis of variance (ANOVA) was used to compare the difference between the internal variability of two or more groups and the variability between the groups. Student's t test for independent data was used to establish if there was a statistically significant difference between the means in two unrelated groups. Wilcoxon-Mann-Whitney test was applied when it was necessary to compare the means of two groups of independent samples, in which a Gaussian distribution could not be assumed. Non-parametric correlation (Spearman's rho), a measure of the linear relationship between two variables, was used to correlate clinical features and biochemical data in the ASD group (non-parametric ANOVA for cognitive/developmental level). Differences were considered significant at p value < 0.05 . Spectrum 4 and DHA value were found to differ in a statistically significant way by ANOVA test with p values of 0.0021 and 0.0344, respectively. Receiver operating characteristic (ROC) curves were also used to estimate the

performance of a given parameter as a binary classifier, i.e. the ability of a test to assign a specific subject to either one of two groups - in this case healthy controls (negative group) or ASD patients (positive group). Plotting the true positive rate, or sensitivity, against the false positive rate, or specificity, at various threshold settings, creates the curve. The sensitivity is the ability to correctly classify positive cases (patients), whereas the specificity is the ability to correctly classify negative cases (controls). The ROC curves were used in conjunction with the Youden Index (J), as a way of summarizing the performance of the diagnostic test. Its value ranges from 0 to 1, a value of 1 indicating the absence of false positives or false negatives. ROC curve analyses were based on non-parametric methods. The confidence intervals of ROC curves were set at 95%.

$$J = \text{sensitivity} + \text{specificity} - 1$$

When two parameters were combined, such as in the case of HDFM data and DHA values, a mathematical treatment to eliminate the measurement unit has been applied. Principal components analysis (PCA) is a statistical method that uses an orthogonal transformation to sort out affinities among different variables; the higher the value of “factorial weights”, the higher the affinity of a variable to that specific factor. It was carried out for the different variables reported in this study finding four factors that gather > 90% of the variability of the data. Factor 2 contains DHA values and Spectrum 4 together with “cc”, which is the variable that discriminates cases and controls, and the CARS total score. Therefore, PCA indicates that these four parameters belong to the same factor, putting clinical, biophotonic and molecular data together with the variable that discriminates cases and controls.

3.6. Results

3.6.1. Erythrocyte membrane fatty acid analysis

A sample of fresh whole blood treated with ethylenediaminetetraacetic acid (EDTA) as anticoagulant, was collected from all subjects and used for membrane lipidome analysis and HDFM measurements. An aliquot of blood sample (250 μ L) from healthy and ASD children was processed for FA analysis of membrane phospholipids. The corpusculated portion of blood, consisting of RBCs, was treated with a robotic protocol performed at Lipinutragen srl. This procedure allowed the isolation of membrane phospholipids of mature RBCs, as they are effective reporters for metabolism and nutritional conditions, reflecting the balance established between fatty acids that come from biosynthesis or diet. A cluster of 12 FAs (10 *cis* and 2 *trans*) was chosen since it represents more

than the 98% of the total peaks in the GC chromatogram (**Figure 3.2**). The RBC membrane FAs of healthy and ASD subjects are reported in **Table 3.1**.

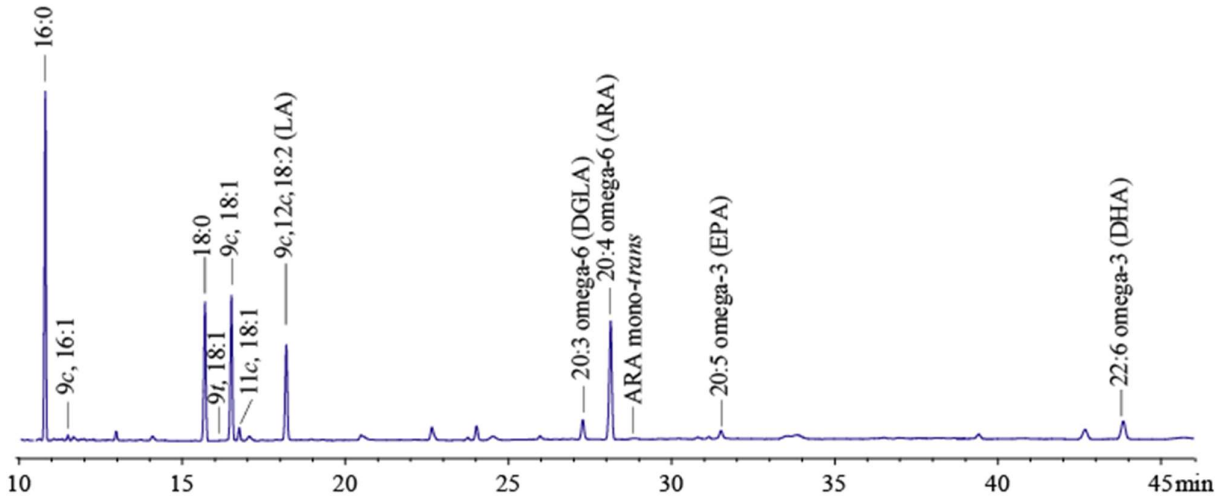


Figure 3.2. Representative GC chromatogram obtained from the analysis of erythrocytes.

Table 3.1. Fatty acid obtained from RBC cell membrane phospholipid analysis of healthy (CTR) and ASD children.

FAME	CTR children (n=20)	ASD children (n=21)	p values
16:0	24.8 ± 1.32	25.23 ± 0.86	0.7557
9c, 16:1	0.31 ± 0.04	0.29 ± 0.04	0.3549
18:0	18.20 ± 0.57	18.17 ± 0.69	0.8711
9t, 18:1	0.12 ± 0.03	0.12 ± 0.04	0.9443
9c, 18:1	16.42 ± 0.33	17.07 ± 0.84	0.0960
11c, 18:1	1.24 ± 0.11	1.22 ± 0.08	0.9350
LA	12.82 ± 0.50	12.40 ± 0.60	0.2851
DGLA	2.05 ± 0.20	2.14 ± 0.19	0.2973
ARA	18.56 ± 1.29	18.60 ± 0.86	0.7660
∑ARA mt	0.09 ± 0.03	0.07 ± 0.03	0.5415
EPA	0.55 ± 0.09	0.51 ± 0.07	0.4066
DHA	4.81 ± 0.56	4.14 ± 0.41	0.0424*

The values obtained from GC analysis of FAMES are reported as relative percentage (%rel) of the total fatty acid peak areas detected in the GC chromatograms, corresponding to >98% of the total peaks. Results are expressed as mean ± SD. mt= mono-trans

The interest in RBC membrane fatty acid composition derives from the fact that mature RBCs have a stable and representative composition that reflects the general state of the organism, connected to an *in vivo* exchange with tissues and lipoproteins that occurs during normal cellular metabolism.

Erythrocytes have a cell turnover of about 120 days: we decided to extract and to analyze the fraction corresponding to mature erythrocytes, because they are considered efficient reporters of the general metabolic and nutritional status, which reflects the balance established between FAs coming from the biosynthesis and FAs taken from the diet [59].

GC analysis showed that the most abundant SFA is palmitic acid (16:0), followed by stearic acid (18:0). Among the MUFAs, the most abundant fatty acid is oleic acid (9*c*, 18:1) while the most abundant PUFAs correspond to linoleic (LA, 9*c*,12*c*, 18:2) and arachidonic (ARA, 20:4 ω -6) acids. The analytical conditions employed and the sensitivity of the instrument allowed to identify the presence of mono-*trans* derivatives of oleic acid, LA and ARA, but no significant differences were found between the two groups.

Lipidomic analyses evidenced a significant DHA decrease in ASD subjects (p value = 0.0424), as already reported for a previously studied cohort [16,60]. Using ANOVA test to compare the two groups, the DHA decrease in ASD was found to be significant (p value = 0.0344). This decrease was not attributable to dietary differences between the two groups, since food questionnaire reported fish consumption for both groups (data not shown).

3.6.2. HDFM analysis

For HDFM analyses, 5 μ l of whole blood (EDTA-treated) from healthy and ASD children were loaded in the centre of glass slide and sandwiched with coverslip and left 120 minutes to stabilize prior to proceed with optical acquisitions. For reproducibility reasons, we established that each optical image of RBCs acquired by HDFM technology should be characterized by the presence of approximately thirty RBCs of round shape. Therefore, erythrocytes with altered morphology, such as echinocytes and stomatocytes, were not included in the optical field, in order to avoid an increase in the intrinsic variability of the procedure, notwithstanding the fact that RBCs with irregular shape are increased in subjects with ASD [60, 47]. Indeed, RBC shape deformation can also depend from pH and other blood parameters [61].

Accurate collection of the spectral reflectance from RBCs gave rise to eight spectra in the 430–800 nm wavelength region (**Figure 3.3**), that using a small spectral angle (0.1 in radians) gave a

fingerprint of the region of interest (ROI), with optimal coverage of the optical image (>98%) as shown in **Figure 3.4**.

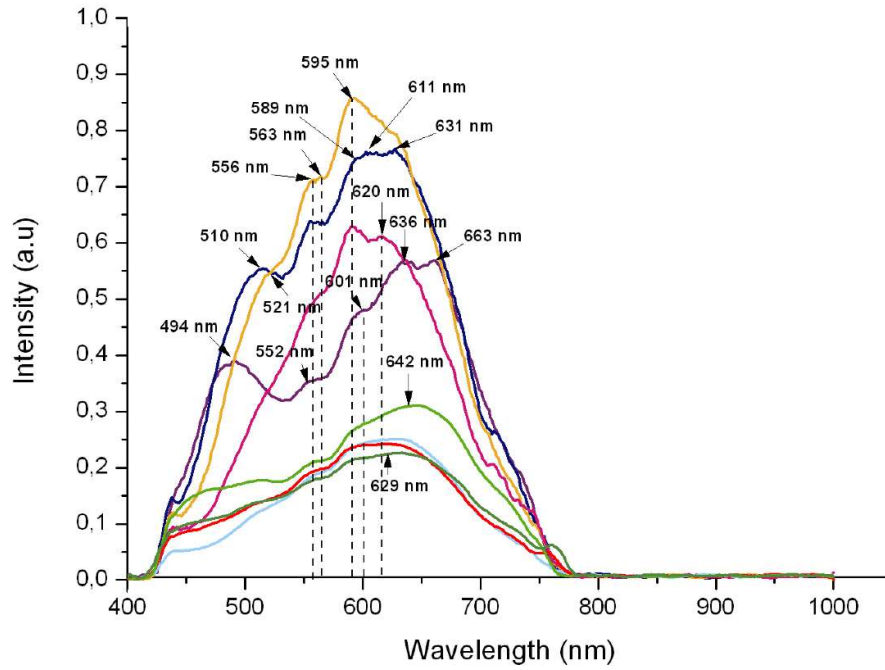


Figure 3.3. The HDFM spectral library identified for RBC imaging.

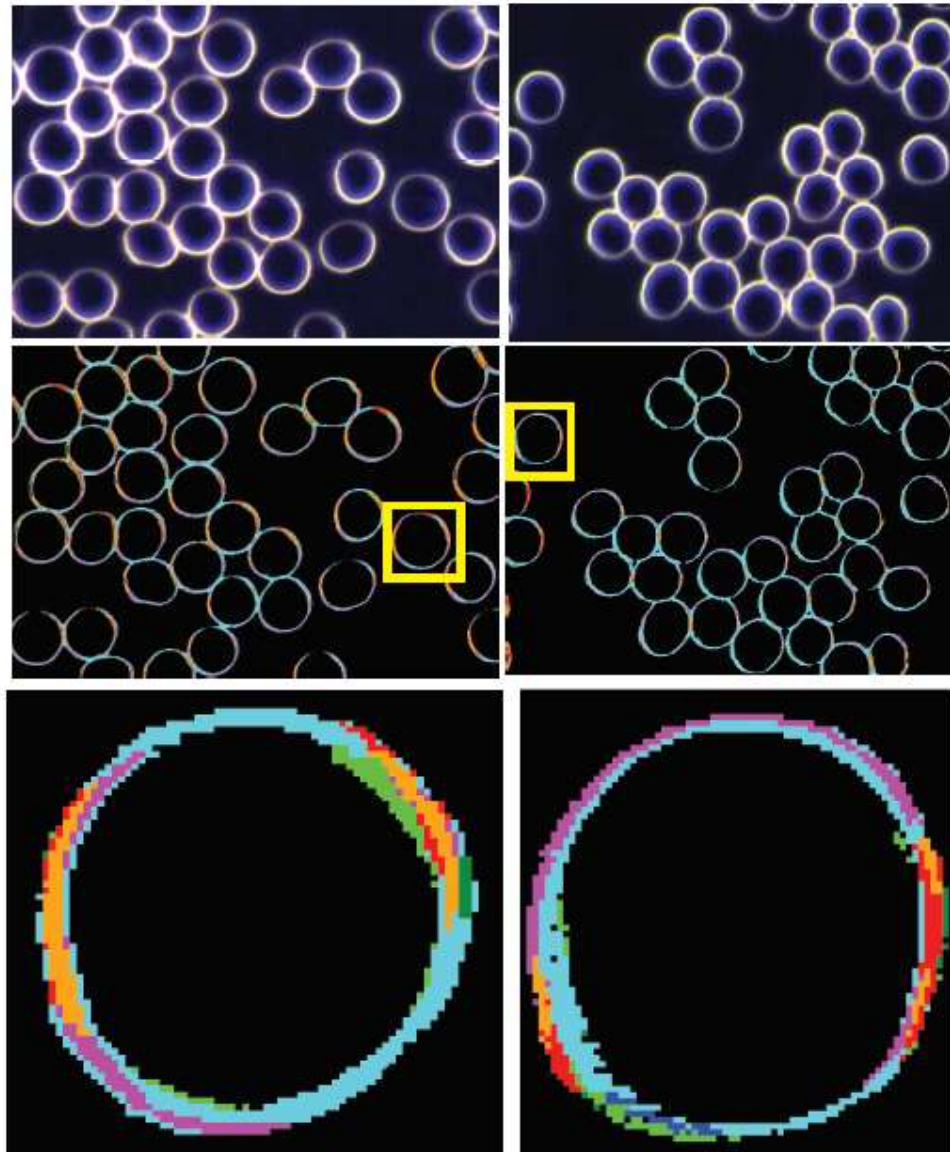


Figure 3.4. RBC optical images and the corresponding hyperspectral image for healthy (left panels) and ASD (right panels) children. In yellow box a selected RBC for which an enlarged view is given below, where it is clearly seen the satisfactory matching of the optical and hyperspectral images. Coloured areas indicate regions whose reflectance spectra match with the spectral end-members of the library.

It is known that the cell membrane curvature is determined by the orientation of the blood cells relative to the propagation vector of the illuminating electro-magnetic field. When a biconcave-shaped RBC interacts with a linearly polarised light beam, it tends to orient its long axis in the direction of the electric field of the incident beam, due to RBC's intrinsic birefringence. In our conditions, the light source was an unpolarized halogen light source, thus no “forced” orientation of the cells was observed. The lamp normalization routine was used in order to eliminate the background light, improving method robustness compared to previously published data [42].

Under these careful set-up conditions, we constantly obtained a good match by mapping of the eight end-members spectral library with the small spectral angle onto images taken from different blood samples. Therefore, we could conclude that the identified spectral signatures are not sensitively affected by the cell orientation, but probably result from a curvature of the membrane surface connected to the morphological status. Indeed, the cell orientation dependency could be observed when differently shaped RBCs are examined, such as stacked RBCs forming rouleaux and echinocytes, giving rise to different spectral end-members [42], that are currently under investigation for the biological importance of these changes.

After the library was created to give the optimal surface match, the relative spectral distribution of the eight endmembers could be obtained using Spectral Angle Mapper (SAM) software. The mean distribution values with standard errors for the two children cohorts are reported in **Table 3.2**.

Table 3.2. Relative distribution of the HDFM spectral patterns of the RBC samples of healthy and ASD children.

Spectrum	Control children (n=20)	ASD children (n=21)	p values
1	0.46 ± 0.25	0.67 ± 0.67	0.5030
2	2.15 ± 1.17	1.72 ± 1.043	0.5375
3	7.42 ± 2.89	6.75 ± 1.71	0.6520
4	13.10 ± 2.39	19.66 ± 3.80	0.0021**
5	53.43 ± 9.02	53.53 ± 5.75	0.9835
6	10.71 ± 3.00	7.91 ± 2.05	0.0883
7	7.53 ± 4.01	6.24 ± 3.34	0.5775
8	5.20 ± 3.00	3.53 ± 1.30	0.2494

By analysis of variance (ANOVA) the spectrum 4 distribution resulted significantly different between healthy and ASD children (p value = 0.0021).

Statistical analysis for the diagnostic performance of spectrum 4 distribution values was carried out using the receiver operating characteristic (ROC) curve analysis [62].

ROC curve analysis is a statistical method that is becoming more and more widely applied in the biomedical field since it permits to evaluate the accuracy of a diagnostic procedure [63].

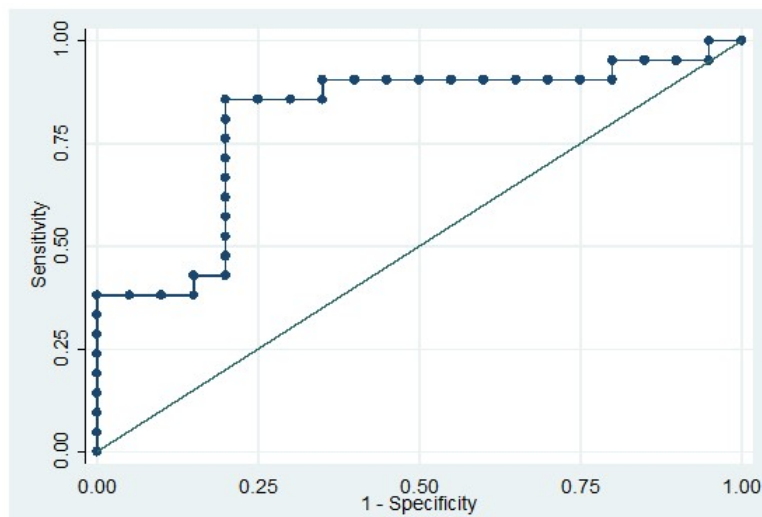
The ROC graph plots on the y-axis sensitivity, that is the ability of a test to correctly identify patients with the disease, and on the x-axis (1-specificity), where specificity represents the ability of the test to correctly identify those without the disease.

The parameter of interest is represented by the area under the curve.

The diagonal line from the bottom left to the top right corners, represents points where sensitivity = 1-specificity, meaning there is the same chance to have a negative result in the presence of the disease (false negative) and a positive one in case of no disease (false positive). The test in this case is unreliable, since positive or negative results cannot be related to the true disease status.

The top left corner of the ROC box is the point where sensitivity = 100% (no false negatives) and (1-specificity) = 0%, or better specificity = 100% (no false positives): this point represents the ideal test. The closer the ROC curve get to the top left corner, the better the test is overall. 100% sensitivity) and 100% specificity).

When we performed the ROC analysis for spectrum 4 (**Figure 3.5**), very high statistical significance (p value = 0.0008) and a cut-off value at 16.225 were determined.



AUC	Cut off	Sensitivity	Specificity	J
0.8071	16.225	85.71%	80.00%	0.6571

Figure 3.5. ROC curves and J values for HDFM spectrum 4.

Additionally, the odds ratio (OR), that expresses the level of association between two factors, was calculated. In the case of spectrum 4 and ASD pathology, OR was found to be significant and corresponding to 24 (p value < 0.0001; IC 95%: [4.6488–123.9035]),

Therefore, statistic analyses evidenced that individuals with distribution values of spectrum 4 higher than 16.225 (cut-off value) have a probability of being autistic 24 times higher than those having values of spectrum 4 lower than 16.225.

Looking closely at spectrum 4, and comparing its spectral profile with the spectra obtained from the analysis of membrane components [48], similarities were found with the maximum HDFM peaks (564, 587, 595, 620 nm) of phospholipid and protoporphyrin IX, which are important component of the RBC membranes (**Figure 3.6**).

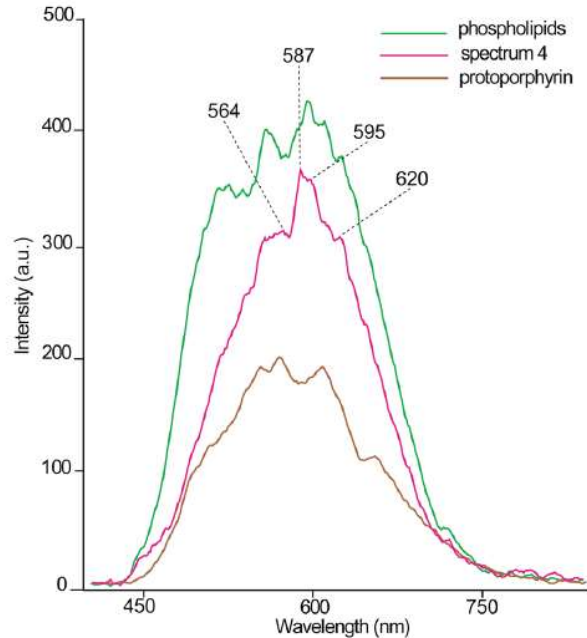


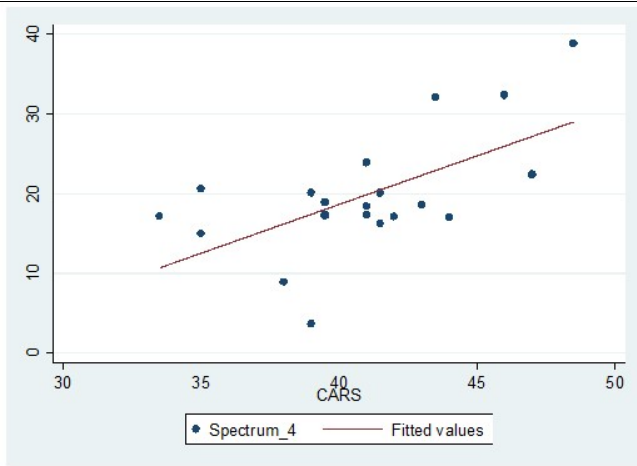
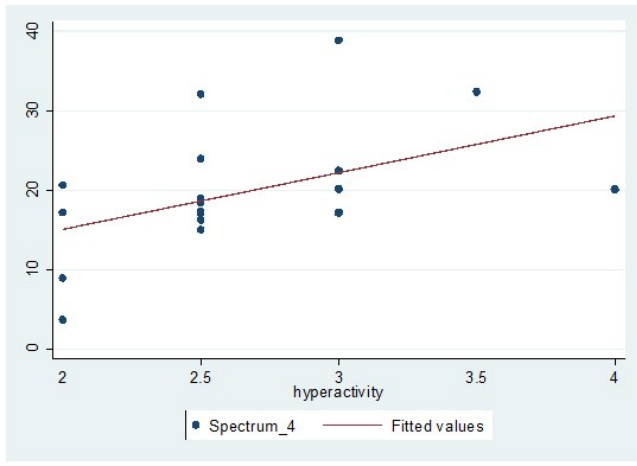
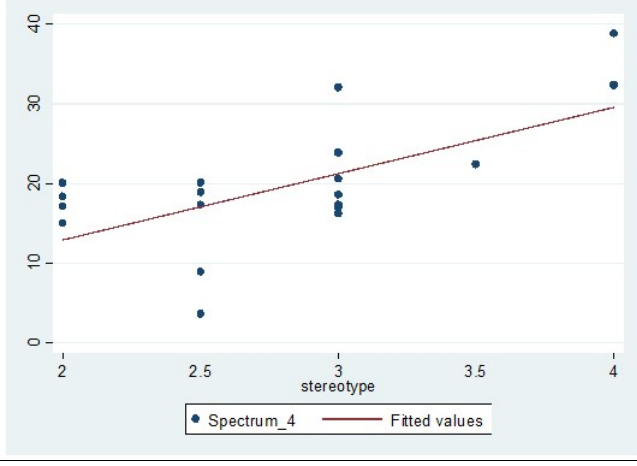
Figure 3.6. Superimposition of spectrum 4 with two reference compounds, phospholipids as liposome suspension (green) and protoporphyrin IX (brown). Principal bands of spectrum 4 are indicated.

It is worth underlining that the phospholipid sample was prepared as aqueous liposome suspension¹⁸, an aggregation that mimics the membrane lipid organization. Some of the spectral bands in common between spectrum 4 and the two membrane components can be seen. However, further work is needed to make an unequivocal assignment of the spectral bands in RBCs.

Spearman's non-parametric correlations were calculated for spectrum 4 vs. a number of subject's demographic and clinical features. The correlations found to be statistically significant are shown in **Table 3.3**.

Again, the spectrum 4 was found to be positively and significantly correlated with CARS total scores ($P = 0.0248$), hyperactivity ($P = 0.0279$), stereotypies ($P = 0.0225$).

Table 3.3. Statistically significant Spearman's non parametric correlations calculated for spectrum 4.

Correlation of HDFM spectrum 4 and CARS	
	<p>Variable: CARS</p> <p>Spearman's rho: 0.4881</p> <p>P value: 0.0248</p>
Correlation of HDFM spectrum 4 and hyperactivity	
	<p>Variable: CARS</p> <p>Spearman's rho: 0.4794</p> <p>P value: 0.0279</p>
Correlation of HDFM spectrum 4 and stereotypes	
	<p>Variable: Stereotypes</p> <p>Spearman's rho: 0.4950</p> <p>P value: 0.0225</p>

3.7. Conclusions

The lipidomic analysis of 41 children, 21 with ASD and 20 with typical development was performed. This study showed that the erythrocyte membranes of autistic children presented significantly reduced levels of DHA.

Additionally, the characterization of human RBCs using hyperspectral optical imaging was provided. In particular, a reference spectral library made of 8 scattering spectra was built up from which it was possible to derive the relative spectral distribution for all samples.

With this study we demonstrated that HDFM spectra can comprehensively describe the contribution of erythrocyte components with their organization and packing at the level of membrane and sub-membrane regions. Indeed, some of the bands of the HDFM spectra matched the bands obtained by typical RBC molecular components, such as phospholipids and protoporphyrin IX, demonstrating the possibility of mapping single molecules (e.g. proteins) as well as obtaining information on the membrane phospholipid assembly.

By setting up this innovative approach, the potentiality and effectiveness of hyperspectral imaging of RBC and its components for clinical applications can be envisaged.

HDFM results, obtained through this fast, easy and reproducible protocol, can encourage further studies extended to larger cohorts, to explore the potentiality of RBC mapping in the presence different health conditions. This technique can be integrated with other diagnostic and intervention tools, such as personalized lipidomic profiles, to design personalized membrane-targeted therapies.

To summarize, this study represents the proof of concept that hyperspectral imaging, being a fast and non-expensive screening methodology, can be used to gather comprehensive information on the erythrocyte cell membrane components and their organization, that are the premise of using HDFM methodology for clinical targets. This also opens the field to integrated approaches for the determination of cell impairment due to unbalances of its molecular components, such as those targeted to cell membranes using lipidomics.

3.8. References

1. American Psychiatric Association. *Diagnostic and Statistical Manual of Mental Disorders*, 4th ed. Text Revision (DSM-IV-TR). Washington, DC: American Psychiatric Association, **2000**
2. Rapin, I.; Tuchman, R.F. Autism: definition, neurobiology, screening, diagnosis. *Pediatr. Clin. North Am.* **2008**, *55*(5), 1129-1146
3. Baird, G.; Cass, H.; Slonims, V. Diagnosis of autism. *BMJ* **2003**, *327*(7413), 488-493
4. Johnson, C.P.; Myers, S.M. Identification and evaluation of children with autism spectrum disorders. *Pediatrics*, **2007**, *120*(5), 1183-1215
5. Loomes, R.; Hull, L.; Mandy, W.P.L. What Is the Male-to-Female Ratio in Autism Spectrum Disorder? A Systematic Review and Meta-Analysis. *J. Am. Acad. Child Adolesc. Psychiatry*, **2017**, *56*(6), 466-474
6. Schopler, E.; Reichler, R.J.; DeVellis, R.F.; Daly, K. Toward objective classification of childhood autism: Childhood Autism Rating Scale (CARS). *J. Autism Dev. Disord.* **1980**, *10*(1), 91-103
7. Bourgeron T. The genetics and neurobiology of ESSENCE: The third Birgit Olsson lecture. *Nord J Psychiatry* **2016**, *70*(1), 1-9
8. Robinson, E.B.; St Pourcain, B.; Anttila, V.; Kosmicki, J.A.; Bulik-Sullivan, B.; Grove, J.; Maller, J.; Samocha, K.E.; Sanders, S.J.; Ripke, S.; Martin, J.; Hollegaard, M.V.; Werge, T.; Hougaard, D.M.; iPSYCH-SSI-Broad Autism Group., Neale B.M.; Evans, D.M.; Skuse, D.; Mortensen, P.B.; Børglum, A.D.; Ronald, A.; Smith, G.D.; Daly, M.J. Genetic risk for autism spectrum disorders and neuropsychiatric variation in the general population. *Nat. Genet.* **2016** *48*(5), 552-555
9. Keller, F.; Persico, A.M. The neurobiological context of autism. *Mol. Neurobiol.* **2003**, *28*(1), 122
10. Beaudet, A.L. Is medical genetics neglecting epigenetics? *Genet. Med.* **2002**, *4*(5), 399-402
11. London, E.A. The environment as an etiologic factor in autism: a new direction for research. *Environ. Health Perspect* **2000**, *108*(suppl 3), 401-404
12. Szachta, P.; Skonieczna-Żydecka, K.; Adler, G.; Karakua-Juchnowicz, H.; Madlani, H.; Ignyś, I. Immune related factors in pathogenesis of autism spectrum disorders. *Eur. Rev. Med. Pharmacol. Sci.* **2016**, *20*(14), 3060-3072
13. Chauhan, A.; Chauhan, V. Oxidative stress in autism. *Pathophysiology* **2006**, *13*(3), 171-181
14. Ono, H.; Sakamoto, A.; Sakura, N. Plasma total glutathione concentrations in healthy pediatric and adult subjects. *Clin. Chim. Acta* **2001**, *312*(1-2), 227-229

15. Walker, C.K.; Krakowiak, P.; Baker, A.; Hansen, R.L.; Ozonoff, S.; Hertz-Picciotto, I. Preeclampsia, placental insufficiency, and autism spectrum disorder or developmental delay. *JAMA Pediatr.* **2015**, *169*(2), 154-162
16. Ghezzi, A.; Visconti, P.; Abruzzo, P.M.; Bolotta, A.; Ferreri, C.; Gobbi, G.; Malisardi, G.; Manfredini, S.; Marini, M.; Nanetti, L.; Pipitone, E.; Raffaelli, F.; Resca, F.; Vignini, A.; Mazzanti, L. Oxidative Stress and Erythrocyte Membrane Alterations in Children with Autism: Correlation with Clinical Features. *PLoS One* **2013**, *8*(6), e66418
17. Yorbik, O.; Sayal, A.; Akay, C.; Akbiyik, D.I.; Sohmen, T. Investigation of antioxidant enzymes in children with autistic disorder, *Prostaglandins Leukot. Essent. Fatty Acids* **2002**, *67*(5), 341–343
18. James, S.J.; Cutler, P.; Melnyk, S.; Jernigan, S.; Janak, L.; Gaylor, D.W.; Neubrandner, J.A. Metabolic biomarkers of increased oxidative stress and impaired methylation capacity in children with autism, *Am. J. Clin. Nutr.* **2004**, *80*(6), 1611-1617
19. Chauhan, A.; Chauhan, V.; Brown, W.T.; Cohen, I. Oxidative stress in autism: Increased lipid peroxidation and reduced serum levels of ceruloplasmin and transferrin - the antioxidant proteins. *Life Sci.* **2004**, *75*(21), 2539–2549
20. Zoroglu, S.S.; Armutcu, F.; Ozen, S.; Gurel, A.; Sivasli, E.; Yetkin, O.; Meram, I. Increased oxidative stress and altered activities of erythrocyte free radical scavenging enzymes in autism, *Eur. Arch. Psychiatry Clin. Neurosci.* **2004**, *254*(3), 143-147
21. Rose, S.; Melnyk, S.; Pavliv, O.; Bai, S.; Nick, T.G.; Frye, R.E.; James, S.J. Evidence of oxidative damage and inflammation associated with low glutathione redox status in the autism brain. *Transl. Psychiatry*, **2012**, *2*, e134
22. Tamiji, J.; Crawford, D.A. The neurobiology of lipid metabolism in autism spectrum disorders. *Neurosignals* **2010**, *18*(2), 98-112
23. Richardson, A.J. Clinical trials of fatty acid treatment in ADHD, dyslexia, dyspraxia and the autistic spectrum. *Prostaglandins Leukot. Essent. Fatty Acids* **2004**, *70*(4), 383-390
24. Vancassel, S.; Durand, G.; Barthelemy, C.; Lejeune, B.; Martineau, J.; Guilloteau, D.; Andres, C.; Chalon, S. Plasma fatty acid levels in autistic children. *Prostaglandins Leukot. Essent. Fatty Acids* **2001**, *65*(1), 1-7
25. Bell, J.G.; MacKinlay, E.E.; Dick, J.R.; MacDonald, D.J.; Boyle, R.M.; Glen, A.C.A. Essential fatty acids and phospholipase A2 in autistic spectrum disorders. *Prostaglandins Leukot. Essent. Fatty Acids* **2004**, *71*(4), 201-204
26. Yao, J.K. Abnormalities of fatty acid metabolism in red cells platelets and brain in schizophrenia, in *Phospholipid Spectrum Disorders in Psychiatry and Neurology*, Peet, M.; Glen, A.I.M.; Horrobin, D.F. (Eds.), Marius Press, Carnforth, UK, **2003**, pp. 193–212
27. James, S.J.; Cutler, P.; Melnyk, S.; Jernigan, S.; Janak, L.; Gaylor, D.W.; Neubrandner, J.A. Metabolic biomarkers of increased oxidative stress and impaired methylation capacity in children with autism. *Am. J. Clin. Nutr.* **2004**, *80*(6), 1611-1617

28. Vargas, D.L.; Nascimbene, C.; Krishnan, C.; Zimmerman, A.W.; Pardo, C.A. Neuroglial activation and neuroinflammation in the brain of patients with autism. *Ann. Neurol.* **2005**, *57*(1), 67-81
29. Bu, B.; Ashwood, P.; Harvey, D.; King, I.B.; Van de Water, J.; Jin, L.W. Fatty acid compositions of red blood cell phospholipids in children with autism. *Prostaglandins Leukot. Essent. Fatty Acids* **2006**, *74*(4), 215-221
30. Bent, S.; Bertoglio, K.; Hendren, R.L. Omega-3 fatty acids for autistic spectrum disorder: a systematic review. *J. Autism Dev. Disord.* **2009**, *39*(8), 1145-1154
31. Amminger, G.P.; Berger G.E.; Schäfer M.R.; Klier C.; Friedrich M.H.; Feucht, M. Omega-3 fatty acids supplementation in children with autism: a double-blind randomized, placebo-controlled pilot study. *Biol. Psychiatry* **2007**, *61*(4), 551-553
32. Ferreri, C.; Masi, A.; Sansone, A.; Giacometti, G.; Larocca, A. V.; Menounou, G.; Scanferlato, R.; Tortorella, S.; Rota, D.; Conti, M.; Deplano, S.; Louka, M.; Maranini, A.R.; Salati, A.; Sunda, V.; Chatgililoglu, C. Fatty Acids in Membranes as Homeostatic, Metabolic and Nutritional Biomarkers: Recent Advancements in Analytics and Diagnostics. *Diagnostics (Basel)* **2017**, *7*(1), 1
33. Sorg, B.S.; Moeller, B.J.; Donovan, O.; Cao, Y.; Dewhirst, M.W. Hyperspectral imaging of hemoglobin saturation in tumor microvasculature and tumor hypoxia development. *J. Biomed. Opt.* **2005**, *10*(44004), 1083-3668
34. Martin, M.E.; Wabuyele, M.B.; Chen, K.; Kasili, P.; Panjehpour, M.; Phan, M.; Overholt, B.; Cunningham, G.; Wilson, D.; Denovo, R.C.; Vo-Dinh, T. Development of an advanced hyperspectral imaging (HSI) system with applications for cancer detection. *Ann. Biomed. Eng.* **2006**, *34*(6), 1061-1068
35. Leavesley, S.J.; Annamdevula, N.; Boni, J.; Stocker, S.; Grant, K.; Troyanovsky, B.; Rich, T.C.; Alvarez, D. F. Hyperspectral imaging microscopy for identification and quantitative analysis of fluorescently-labeled cells in highly autofluorescent tissue. *J. Biophotonics* **2012**, *5*(1), 67-84
36. Grahn, H.; Geladi, P. (Eds.). *Techniques and applications of hyperspectral image analysis*. John Wiley & Sons, Chichester, **2007**
37. Schultz, R.A.; Nielsen, T.; Zavaleta, J.R.; Ruch, R.; Wyatt, R.; Garner, H.R. Hyperspectral imaging: a novel approach for microscopic analysis. *Cytometry Part A* **2001**, *43*(4), 239-247
38. Park, B.; Seo, Y.; Yoon, S.C.; Hinton Jr, A.; Windham, W.R.; Lawrence, K.C. Hyperspectral microscope imaging methods to classify gram-positive and gram-negative foodborne pathogenic bacteria. *Transactions of the ASABE* **2015**, *58*(1), 5-16
39. Darwiche, K.; Zarogoulidis, P.; Krauss, L.; Oezkan, F.; Walter, R.F.; Werner, R.; Theegarten, D.; Sakkas, L.; Sakkas, A.; Hohenforst-Schmidt, W.; Zarogoulidis, K.; Freitag, L. "One-stop shop" spectral imaging for rapid on-site diagnosis of lung cancer: A future concept in nanomedicine. *Int. J. Nanomedicine* **2013**, *8*, 4533-4542
40. Martin, M.E.; Wabuyele, M.B.; Chen, K.; Kasili, P.; Panjehpour, M.; Phan, M.; Overholt, B.; Cunningham, G.; Wilson, D.; Denovo, R.C.; Vo-Dinh, T. Development of an advanced

hyperspectral imaging (HSI) system with applications for cancer detection, *Ann. Biomed. Eng.* **2006**, *34*, 1061-1068

41. Rocha, A.; Zhou, Y.; Kundu, S.; Gonzalez, J.M.; BradleighVinson, S.; Liang, H. In vivo observation of gold nanoparticles in the central nervous system of *Blaberus discoidalis*, *J. Nanobiotechnology* **2011**, *9*, 5
42. Verebes, G.S.; Melchiorre, M.; Garcia-Leis, A.; Ferreri, C.; Marzetti, C.; Torreggiani, A. Hyperspectral enhanced dark field microscopy for imaging blood cells. *J. Biophotonics* **2013**, *6*(11), 960-967
43. Sheetz, M.P.; Singer, S.J. On the mechanism of ATP-induced shape changes in human erythrocyte membranes. I. The role of the spectrin complex. *J. Cell. Biol.* **1977**, *73*(3), 638-646
44. Ciccoli, L.; Signorini, C.; Alessandrini, C.; Ferrali, M.; Comporti, M. Iron release, lipid peroxidation, and morphological alterations of erythrocytes exposed to acrolein and phenylhydrazine. *Exp. Mol. Pathol.* **1994**, *60*(2), 108-118
45. Srour, M.A.; Bilot, Y.Y.; Juma, M.; Irhimeh, M.R. Exposure of human erythrocytes to oxygen radicals causes loss of deformability, increased osmotic fragility, lipid peroxidation and protein degradation. *Clin. Hemorheol. Microcirc.* **2000**, *23*(1), 13-21
46. Lucantoni, G.; Pietraforte, D.; Matarrese, P.; Gambardella, L.; Metere, A.; Paone, G.; Bianchi, E.L.; Straface, E. The red blood cell as a biosensor for monitoring oxidative imbalance in chronic obstructive pulmonary disease: an ex vivo and in vitro study. *Antioxid. Redox Signal.* **2006**, *8*(7-8), 1171-1182
47. Ciccoli, L.; De Felice, C.; Paccagnini, E.; Leoncini, S.; Pecorelli, A.; Signorini, C.; Belmonte, G.; Guerranti, R.; Cortelazzo, A.; Gentile, M.; Zollo, G.; Durand, T.; Valacchi, G.; Rossi, M.; Hayek, J. Erythrocyte shape abnormalities, membrane oxidative damage, and β -actin alterations: an unrecognized triad in classical autism. *Mediators Inflamm.* **2013**, 432616
48. Conti, M.; Scanferlato, R.; Louka, M.; Sansone, A.; Marzetti, C.; Ferreri, C. Building up spectral libraries for mapping erythrocytes by hyperspectral dark field microscopy. *Biomed. Spectrosc. Imaging* **2016**, *5*(2), 175-184
49. Giacometti, G.; Ferreri, C.; Sansone, A.; Chatgialloglu, C.; Marzetti, C.; Spyratou, E.; Georgakilas, A.G.; Marini, M.; Abruzzo, P.M.; Bolotta, A.; Ghezzi, A.; Minguzzi, R.; Posar, A.; Visconti, P. High predictive values of RBC membrane-based diagnostics by biophotonics in an integrated approach for Autism Spectrum Disorders. *Sci. Rep.* **2017**, *7*(1), 9854
50. Viviani Anselmi, C.; Ferreri, C.; Novelli, V.; Roncarati, R.; Bronzini, R.; Marchese, G.; Somalvico, F.; Condorelli, G.; Montenero, A.S.; Puca, A.A. Fatty acid percentage in erythrocyte membranes of atrial flutter/fibrillation patients and controls. *J. Interv. Card. Electrophysiol.* **2010**, *27*(2), 95-99
51. van der Vegt, S.G.; Ruben, A.M.; Werre, J.M.; Palsma, D.M.; Verhoef, C.W.; de Gier, J.; Staal, G.E. Counterflow centrifugation of red cell populations: a cell age related separation technique. *Br. J. Hematol.* **1985**, *61*(3), 393-403

52. Rennie, C.M.; Thompson, S.; Parker, A.C.; Maddy, A. Human erythrocyte fractionation in "Percoll" density gradients. *Clin. Chim. Acta* **1979**, *98*(1-2), 119-125
53. Corash, L.M.; Piomelli, S.; Chen, C.; Seaman, C.; Gross, E. Separation of erythrocytes according to age on a simplified density. gradient. *J. Lab. Clin. Med.* **1974**, *84*,147-151
54. Fukunaga, N; Wada, M; Honjo, M; Setaishi, Y; Hayashinaka, N; Takada, Y; Nishikawa, J. Effects of temperature and salt on lipid and fatty acid compositions of a bacterium isolated from the bottom layer of Lake Vanda, Antarctica. *Gen. Appl. Microbiol.* **1995**, *41*(3), 191-205
55. Kramer, J.K.G.; Fellner, V.; Dugan, M.E.; Sauer, F.D.; Mossoba, M.M.; Yurawecz, M.P. Evaluating acid and base catalysts in the methylation of milk and rumen fatty acids with special emphasis on conjugated dienes and total trans fatty acids. *Lipids*, **1997**, *32*(11), 1219-1228
56. Ferreri, C.; Kratzsch, S.; Brede, O.; Marciniak, B.; Chatgililoglu, C. Trans lipid formation induced by thiols in human monocytic leukemia cells. *Free Rad. Biol. Med.* **2005**, *38*(9), 1180-1187
57. Ferreri, C.; Sassatelli, F.; Samadi, A.; Landi, L.; Chatgililoglu, C. Regioselective cis-trans isomerization of arachidonic double bonds by thiyl radicals: the influence of phospholipid supramolecular organization. *J. Am. Chem. Soc.* **2004**, *126*, 1063-1072
58. Froom, P.; Kristal-Boneh, E.; Benbassat, J.; Ashkanazi, R.; Ribak, J. Predictive value of determinations of zinc protoporphyrin for increased blood lead concentrations, *Clin. Chem.* **1998**, *44*(6 Pt 1), 1283-1288
59. Sun, Q.; Ma, J.; Campos, H.; Hankinson, S.E.; Hu, F.B. Comparison between plasma and erythrocyte fatty acid content as biomarker of fatty acid intake in US women, *Am. J. Clin. Nutr.*, **2007**, *86*(1), 74-81
60. Cortelazzo, A.; De Felice, C.; Pecorelli, A.; Belmonte, G.; Signorini, C.; Leoncini, S.; Zollo, G.; Capone, A.; Giovampaola, C.D.; Sticozzi, C.; Valacchi, G.; Ciccoli, L.; Guerranti, R.; Hayek, J. Beta-Actin deficiency with oxidative posttranslational modifications in Rett syndrome erythrocytes: insights into an altered cytoskeletal organization. *PLoS One* **2014**, *9*(3), e93181
61. Gedde, M.M.; Davis, D.K.; Huestis, W.H. Cytoplasmic pH and human erythrocyte shape. *Biophys. J.* **1997**, *72*(3), 1234-1246
62. Abruzzo, M.A.; Ghezzi, A.; Bolotta, A.; Ferreri, C.; Minguzzi, R.; Vignini, A.; Visconti, P.; Marini, M. Perspective biological markers for autism spectrum disorders: advantages of the use of receiver operating characteristic curves in evaluating marker sensitivity and specificity. *Dis. Markers* **2015**, Article ID 329607
63. Hajian-Tilaki, K. Receiver operating characteristic (ROC) curve analysis for medical diagnostic test evaluation. *Caspian J. Intern. Med.* **2013**, *4*(2), 627-635

Chapter 4

Alzheimer's Disease

4.1. Introduction

Lipidomics is considered very important to investigate lipid signalling, metabolism, trafficking, and homeostasis that are associated with neurological disorders. The neuronal system is the second organ for concentration in lipids, exceeded only by adipose tissue.

Disorders in the lipid metabolism in the central nervous system (CNS) have been associated with neurodegenerative diseases, such as Alzheimer's Disease (AD). Indeed, it has already been mentioned that lipids are a large group of molecules which can act as cell membrane structure components, signalling molecules for normal cellular functions and energy storage. At a CNS level, changes in brain lipid balance due to impaired synthesis or metabolism may result in homeostatic dysregulation and ultimately in neurodegeneration [1].

In AD, a neurodegenerative, progressive and irreversible disease that affects the brain, 'lipidic granules' in glial cells, suggesting aberrant lipid metabolism, have been reported [2]. Alterations in brain cholesterol metabolism were also observed in the cerebrospinal fluid and plasma of AD patients. In addition, the hypothesis of peroxisomal dysfunctions and/or of abnormal desaturase and elongase activities linked with some fatty acid alteration was formulated [3].

However, a connection between AD and aberrant lipid metabolism was seriously considered only when the $\epsilon 4$ allele variant of the apolipoprotein E (APOE) gene was identified as the strongest genetic risk factor for late-onset AD.

In the current state of knowledge, the mechanism of action of apoE4 has not been clarified yet. Since many studies support a possible link between lipid metabolism disorders and the pathogenesis of AD,

there has been a stronger focus on lipidomic studies to identify lipid biomarkers of AD. Taking into account the diagnostic significance of fatty acid-based membrane lipidomics for human health [4,5], we have planned a preliminary study to investigate whether fatty acid remodeling of cell membranes occurs in the presence of apoE proteins, since little is known about the effects of apoE on membrane fatty acid profile. In particular, the fatty acid remodeling of human neuroblastoma cell line (SK-N-SH) exposed to apoE3 and apoE4 isoforms is reported.

Results showed that the treatment with either apoE3 or apoE4 isoforms induced significantly different changes in the organization of the membrane fatty acids, which predominantly influence membrane properties and peroxidation susceptibility.

This study was realized in collaboration with the group of Dr. Chroni, in Athens, which synthesized and purified ApoE isoforms and set up the biological assays.

4.2. Alzheimer's disease (AD)

Alzheimer's disease (AD) is a chronic multifactorial neurodegenerative disease [6] that is considered the most common cause of age-related dementia. The clinical symptoms involve progressive decline in memory, starting with short-term memory loss, problems with language, mood swings, disorientation and loss of independence [7].

AD is characterized by the accumulation of abnormally folded amyloid β peptide ($A\beta$) in plaques and neurofibrillary tangles (NFTs), containing hyperphosphorylated tau protein, which can induce loss of neurons and synapses in the cerebral cortex and some subcortical regions, brain atrophy and inflammation [8].

$A\beta$ peptide is generated by fragmentation induced by γ - and β -secretases of amyloid precursor protein (APP), a transmembrane protein that is critical for neuron growth, survival, and post-injury repair. This fragment gives rise to fibrils of amyloid β that form clumps, which can deposit outside neurons in dense formations known as senile plaques.

$A\beta$ can alterate the signalling pathways involved in the phosphorylation of the microtubule-associated protein tau, blocking its function of stabilizing the cytoskeleton and expelling potentially toxic proteins. Moreover, $A\beta$ can inhibit the functionality of proteasome that is responsible for hyperphosphorylated tau degradation. Therefore, these two proteins and their associated signalling pathways represent important therapeutic targets for AD.

Although these have long been considered as the most important factors in the onset of AD, the first observations of patients with dementia also reported the presence of 'adipose inclusions' or 'lipoidic granules' in glial cells, suggesting aberrant lipid metabolism.

Strong evidences now suggest the altered expression of the isoform APOE- ϵ 4 in the apolipoprotein E (ApoE) gene being the most firmly established genetic risk factor in AD.

4.3. ApoE4 in the pathogenesis of AD

ApoE is the predominant apolipoprotein in the brain and is crucial for cholesterol transport with a role in neuroplasticity-related phenomena, since it intervenes in lipid changes and cholesterol dependent function [9]. ApoE can regulate triglyceride metabolism throughout the body by enhancing triglyceride-rich lipoprotein particle uptake, triglyceride utilization and cholesteryl ester hydrolysis in macrophages [10]. In the peripheral nervous system, apoE influences neuronal growth and differentiation. ApoE is of critical importance for membrane repair and remodeling since it participates in the lipid removal from degenerated neurons, and for this reason its expression can be induced in response to stress or injury [11].

At a gene level, several single-nucleotide polymorphisms lead to three common isoforms of ApoE, that differ only for two aminoacids: apoE2 (cys112, cys158), apoE3 (cys112, arg158), and apoE4 (arg112, arg158) [12]. These proteins are coded by three different alleles, among which ϵ 4 allele is considered the major risk factor for AD, while ϵ 2 allele (the least common) and ϵ 3 allele (the most frequently encountered worldwide) have protective properties [13-16].

However, the mechanisms that elucidate the association of ApoE4 with AD have not been clarified yet. It has been proposed that apoE can bind A β and induce changes in A β conformation. In addition, apoE can modulate A β accumulation and deposition in the brain in an isoform- and lipidation status-dependent manner [17-19].

Several model studies pointed out the importance of the lipidation status of apoE since it can influence the protein conformation [20], the interaction of apoE with lipid transporters that are involved in the cellular lipid homeostasis [21] and the affinity of apoE for A β peptides [22]. The apoE lipidation status can also alter its ability to promote the degradation and clearance of A β from brain [23].

It is known that ApoE can exert protective effects against free radicals but that the response is isoform dependent, with ApoE4 being the less efficient free radical scavenger and the more sensitive to free radical attack [24,25]. Other studies have associated the differential effects of apoE isoforms on AD

pathogenesis with differences in their ability to affect neuronal repair and brain lipid transport or metabolism.

In addition, massive disruption of the total membrane lipid bilayers caused by A β 1–40 was reported in the presence of apoE4 but not of apoE3, individuating apoE4 as promotive element for A β fibrillation and membrane oxidative damage [26].

It has been demonstrated that apoE4 is much more susceptible to proteolysis than apoE3 and apoE2 and carboxyl-terminal truncated forms of apoE4 have been found in brains of AD patients and apoE4 transgenic mice [27-29]. Specific apoE4 fragments have been linked with early events in the pathogenesis of AD including neuroinflammation, tau pathology, and accumulation of A β 42 in neurons accompanied with the induction of oxidative stress [30,31].

In the current state of knowledge, a few data are available on the molecular effects of apoE regarding lipid remodeling using in vitro experiments. Apolipoprotein E isoforms were found to enhance triglyceride-rich lipoprotein particle uptake, triglyceride utilization and cholesteryl ester hydrolysis in macrophages [32].

ApoE4-165 fragment was found to strongly reduce sphingomyelin levels in SKN-SH cells, thus inducing changes in the micro-fluidity [33]. Incorporation of sphingomyelin rather than phosphatidylcholines in lipid emulsion models of lipoproteins reduced the binding of apoE to the emulsions and the apoE-mediated uptake of the emulsions by human hepatoma HepG2 cells [34]. Very recently, the importance of cholesterol and phospholipid levels for the protein functioning in neuronal cells and their involvement in neurological diseases was assessed [35,36].

Thus, we hypothesized there could be a lipid coordination effect driven by the structure related to the unique properties of ApoE4, that might clarify the molecular bases of AD.

Thanks to the recent and successful developments in revealing membrane unbalance and identifying specific biomarkers of pathological conditions, lipidomic analysis could be the means of achieving this aim. Cell membrane can be used as a mirror to identify specific fatty acid impairments induced by radical and oxidative processes, since it is the result of biophysical, biochemical and dietary processes. This work could provide molecular-level information of ApoE-membrane interactions and of its isoform-specific affinity, offering hints about the pathology of AD.

To better understand the mechanism of interaction of ApoE4 with membrane lipids, we decided to study the possible effects of ApoE3 and ApoE4 isoforms on the membrane lipid remodelling. For these in vitro experiments SK-N-SH neuroblasma cell line was used since it exhibits a neuronal

phenotype with a variety of neurochemical markers that make it an ideal target to study neurodegenerative diseases like AD [37-38].

4.4. Experimental part

Human neuroblastoma SK-N-SH cells were purchased from American Type Culture Collection – ATCC (Manassas, VA, USA). Fetal bovine serum (FBS) was purchased from Biosera (France). Minimum Essential Medium (Eagle), L-glutamine, nonessential amino acids, sodium pyruvate and sodium bicarbonate were from Biochrom AG (Berlin, Germany). Antibiotics (penicillin and streptomycin) and Phosphate-buffered saline (PBS) were purchased by Sigma Aldrich (St. Louis, MO, USA); 0.05% trypsin solution and potassium hydroxide were purchased by Merck Millipore (Bedford, MA, USA). Chloroform, methanol and *n*-hexane (HPLC grade), were purchased by Merck (Darmstadt, Germany) and used without further purification.

Silica gel thin-layer chromatography was performed on Merck silica gel 60 plates (0.25 mm thickness) and the spots were detected by spraying the plate with cerium ammonium sulfate reagent. Standard FAME references were commercially available from Supelco (USA) and all compounds were used without further purification.

4.4.1. *In vitro* studies

Human neuroblastoma SK-N-SH cells were cultured in Minimum Essential Medium Eagle medium supplemented with 2 mM L-glutamine, 0.1 mM nonessential amino acids, 1 mM sodium pyruvate, 1.5 g/l sodium bicarbonate, 10% (v/v) FBS and antibiotics. Care was taken to use the same FBS batch in all experiments. Cells were plated on 100-mm Petri dishes at a density of 10^6 cells/dish and cultured for 24 h at 37 °C in the presence of 5% CO₂. The cells were then washed and incubated with fresh serum-free medium in the presence or absence of 1 μM of lipid-free apoE3 or apoE4 for 24 h. The expression and purification of apoE4 and apoE3 was carried out according to protocols already described before [39,40]. At the end of the treatment, cells were thoroughly washed using PBS and pelleted by centrifugation at 2500 rpm × 10 min × 4 °C using a Heraeus, Labofuge 400R table centrifuge (Thermo Scientific, Rockford, IL, USA).

4.4.2. Membrane fatty acid analysis

Cell membrane PL were isolated using the well-established Folch method (**Chapter 2, Paragraph 2.2**). Briefly, the pellet was re-suspended in pure water and lipids were extracted with chloroform/methanol (2:1 v/v). Thin layer chromatography using chloroform/methanol/water (65:25:4 v/v) was performed to determine the purity of the PL fraction [41]. The PL residue was transesterified with a 0.5 M KOH/methanol solution for 10 minutes at 22 °C.

The corresponding fatty acid methyl esters (FAMES) were extracted with *n*-hexane and analyzed by Agilent 7890B GC system equipped with a flame ionization detector and a (50%-cyanopropyl)-methylpolysiloxane (DB-23, Agilent, USA) capillary column (60 m, 0.25 mm i.d., 0.25 µm film thickness). The initial temperature was 165 °C, held for 3 minutes, followed by an increase of 1 °C/min up to 195 °C, held for 40 minutes, followed by a second increase of 10 °C/min up to 240 °C, held for 10 minutes. The carrier gas was hydrogen, held at a constant pressure of 16.482 psi. All the FAMES were identified by comparison with the retention times of standard references either commercially available or obtained by synthesis, as already described elsewhere [42].

4.4.3. Statistical analysis

Results are given as means ± SD. Six samples were included in each group. Statistical significance (p values) of the results was calculated by unpaired two-tailed Student's t-test using GraphPad Prism™ software version 6.01 for Windows (GraphPad Software Inc., La Jolla, CA, USA). The threshold for significance was set up at 0.05.

4.5. Results

SK-N-SH cells were incubated in the presence or in the absence of lipid-free full-length apoE3 or apoE4 for 24 hours. Care has been taken in using FBS from the same batch to avoid external influence of lipid supply. The choice to use lipid free apoE was based on the knowledge that apoE secreted by brain cells (astrocytes, microglia, neurons) can scavenge lipids from cells and be lipidated in situ [43,44]. Therefore, the exogenously added apoE isoforms were expected to behave similarly to apoE secreted from brain cells.

After cell treatment, membrane fatty acid composition was determined using known methodologies for membrane pellet formation, phospholipid isolation and transesterification to FAME derivatives, that were analyzed by GC.

Six samples for each group were analyzed. Controls were cells incubated in the same conditions but in the absence of apoE proteins. Fatty acid quantities are reported as percentages of the main peak areas obtained from GC analyses, calibrated and recognized with appropriate references, as already described [42,45].

The GC chromatograms obtained had very similar profiles (**Figure 4.1**). A cluster of twelve fatty acids (FAs) was chosen since it was representative of the total fatty acid contribution in SK-N-SH cell membranes. The most abundant FAs was the MUFA oleic acid (9*c*, 18:1), followed by two SFAs, palmitic (16:0) and stearic (18:0) acids. Among the MUFAs, palmitoleic (9*c*, 16:1) and vaccenic (11*c*, 18:1) acids were found in similar percentages. Another significant contribution in the membrane fatty acid composition was given by the ω -6 PUFAs ARA (20:4 ω -6), that was found in concentrations comparable to DHA (22:6 ω -3), the main ω -3 PUFA. The analytical conditions and the sensitivity of the instrument allowed to detect the presence of mono-*trans* derivatives of oleic acid and ARA.

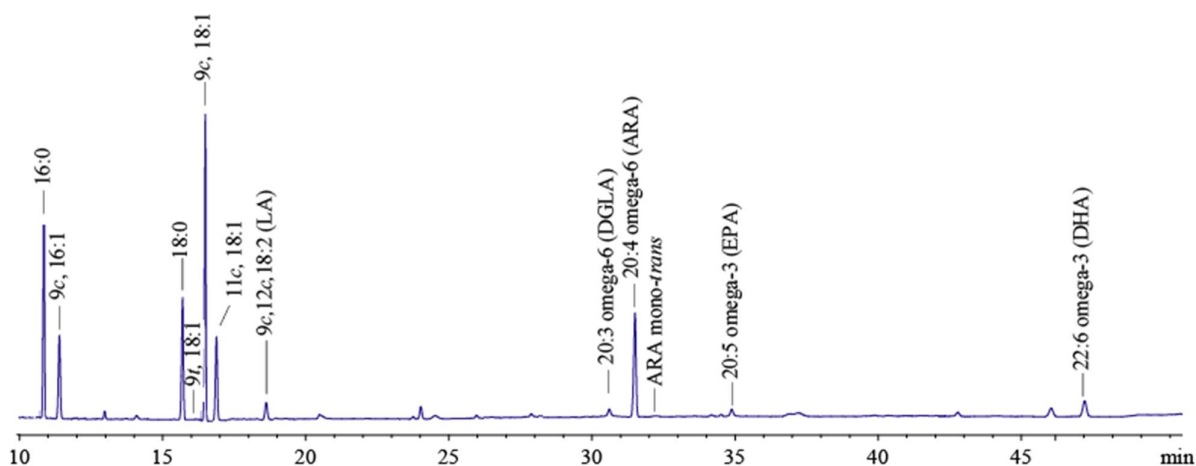


Figure 4.1. Representative GC chromatogram showing the FAME peaks of SK-N-SH cells.

Tables 4.1 and **4.2** show the membrane fatty acid composition, the main membrane fatty acid families and the index of the SK-N-SH cells after 24 h incubation in the presence or absence of apoE3 or apoE4.

Table 4.1. Fatty acids obtained from SK-N-SH cell membrane phospholipids after incubation with 1 μ M of apoE3 or apoE4 for 24 h. Controls are cells cultured for 24 h in the absence of these proteins.

FAME	Control	apoE3	apoE4	apoE3 vs. apoE4
	n=6	n=6 (p value) ^a	n=6 (p value) ^b	(p value) ^c
16:0	25.70 \pm 0.45	26.60 \pm 0.82 (0.0396)	26.91 \pm 0.18 (0.0001)	0.4020
9c, 16:1	6.55 \pm 0.72	6.91 \pm 0.69 (0.4014)	8.20 \pm 0.38 (0.0006)	0.0025
18:0	9.72 \pm 0.33	10.70 \pm 0.58 (0.0049)	9.22 \pm 0.14 (0.0043)	0.0002
9t, 18:1	0.03 \pm 0.01	0.04 \pm 0.04 (0.4072)	0.06 \pm 0.04 (0.1065)	0.5435
9c, 18:1	36.76 \pm 0.71	36.54 \pm 0.59 (0.5668)	35.40 \pm 0.36 (0.0018)	0.0024
11c, 18:1	7.03 \pm 0.20	7.47 \pm 0.14 (0.0014)	7.23 \pm 0.04 (0.0432)	0.0023
LA	1.51 \pm 0.04	1.47 \pm 0.03 (0.0653)	1.53 \pm 0.04 (0.4581)	0.0134
DGLA	0.42 \pm 0.00	0.47 \pm 0.02 (<0.0001)	0.39 \pm 0.02 (0.0200)	<0.0001
ARA	5.59 \pm 0.12	4.95 \pm 0.04 (<0.0001)	5.63 \pm 0.12 (0.5377)	<0.0001
Σ ARA mt	0.16 \pm 0.06	0.12 \pm 0.01 (0.1819)	0.14 \pm 0.02 (0.5071)	0.0420
EPA	0.87 \pm 0.06	0.69 \pm 0.04 (0.0001)	0.83 \pm 0.04 (0.1741)	<0.0001
DHA	5.66 \pm 0.26	4.05 \pm 0.13 (<0.0001)	4.46 \pm 0.14 (<0.0001)	0.0004

The values obtained from GC analysis of FAMES are reported as relative percentage (%rel) of the total fatty acid peak areas detected in the GC chromatograms, corresponding to >98% of the total peaks. mt= mono-*trans*

^a Significance between control and ApoE3.

^b Significance between control and ApoE4.

^c Significance between ApoE3 and ApoE4.

Table 4.2. Main FAME families and membrane homeostasis indexes obtained from the data of **Table 4.1**.

FAME	Control	apoE3	apoE4	apoE3 vs. apoE4
	n = 6	n = 6 (p value) ^a	n = 6 (p value) ^b	p value ^c
Total SFA ^d	35.42 ± 0.36	37.30 ± 0.75 (0.0003)	36.12 ± 0.21 (0.0022)	0.0043
Total MUFA ^e	50.34 ± 0.16	50.92 ± 0.59 (0.0449)	50.83 ± 0.08 (<0.0001)	0.7254
ω-3 PUFA ^f	6.53 ± 0.24	4.73 ± 0.16 (<0.0001)	5.29 ± 0.17 (<0.0001)	0.0002
ω-6 PUFA ^g	7.51 ± 0.14	6.89 ± 0.06 (<0.0001)	7.55 ± 0.15 (0.6701)	<0.0001
Total PUFA	14.05 ± 0.24	11.62 ± 0.21 (<0.0001)	12.84 ± 0.31 (<0.0001)	<0.0001
Total TFA ^h	0.19 ± 0.08	0.17 ± 0.04 (0.5007)	0.20 ± 0.04 (0.7824)	0.1631
SFA/MUFA ratio	0.70 ± 0.01	0.73 ± 0.02 (0.0379)	0.71 ± 0.00 (0.2959)	0.0652
SFA/PUFA ratio	2.52 ± 0.07	3.21 ± 0.12 (<0.0001)	2.81 ± 0.08 (<0.0001)	<0.0001
EPA/ARA ratio	0.16 ± 0.01	0.14 ± 0.01 (0.0191)	0.15 ± 0.00 (0.1284)	0.0478
ω-6/ω-3 ratio	1.15 ± 0.05	1.46 ± 0.04 (<0.0001)	1.43 ± 0.03 (<0.0001)	0.1736
PUFA Balance ⁱ	46.51 ± 1.10	40.72 ± 0.65 (<0.0001)	41.19 ± 0.43 (<0.0001)	0.1718
Unsaturation Index (UI) ^j	115.29 ± 1.52	102.76 ± 1.66 (<0.0001)	108.50 ± 1.41 (<0.0001)	<0.0001
Peroxidation Index (PI) ^k	76.49 ± 1.93	59.95 ± 1.38 (<0.0001)	66.77 ± 1.75 (<0.0001)	<0.0001

The values are given as mean ± SD.

^a Significance between control and ApoE3.

^b Significance between control and ApoE4.

^c Significance between ApoE3 and ApoE4.

^d SFA = %16:0 + %18:0.

^e MUFA = %9c-16:1 + %9c-18:1 + %11c-18:1.

^f PUFA ω-3= %EPA + %DHA.

^g PUFA ω-6= %LA + %DGLA + %ARA.

^h TFA= %9t-18:1 + %∑mono-trans ARA.

ⁱ PUFA balance = [(%EPA + %DHA) / total PUFA] × 100.

^j UI= (%MUFA × 1) + (%LA × 2) + (%DGLA × 3) + (%ARA × 4) + (%EPA × 5) + (%DHA × 6).

^k PI = (%MUFA × 0.025) + (%LA × 1) + (%DGLA × 2) + (%ARA × 4) + (%EPA × 6) + (%DHA × 8).

In **Figures 4.2** and **4.3** the main fatty acid and family values are graphically represented as relative percentage differences from controls, together with their statistical significance against controls and between the two apoE isoforms.

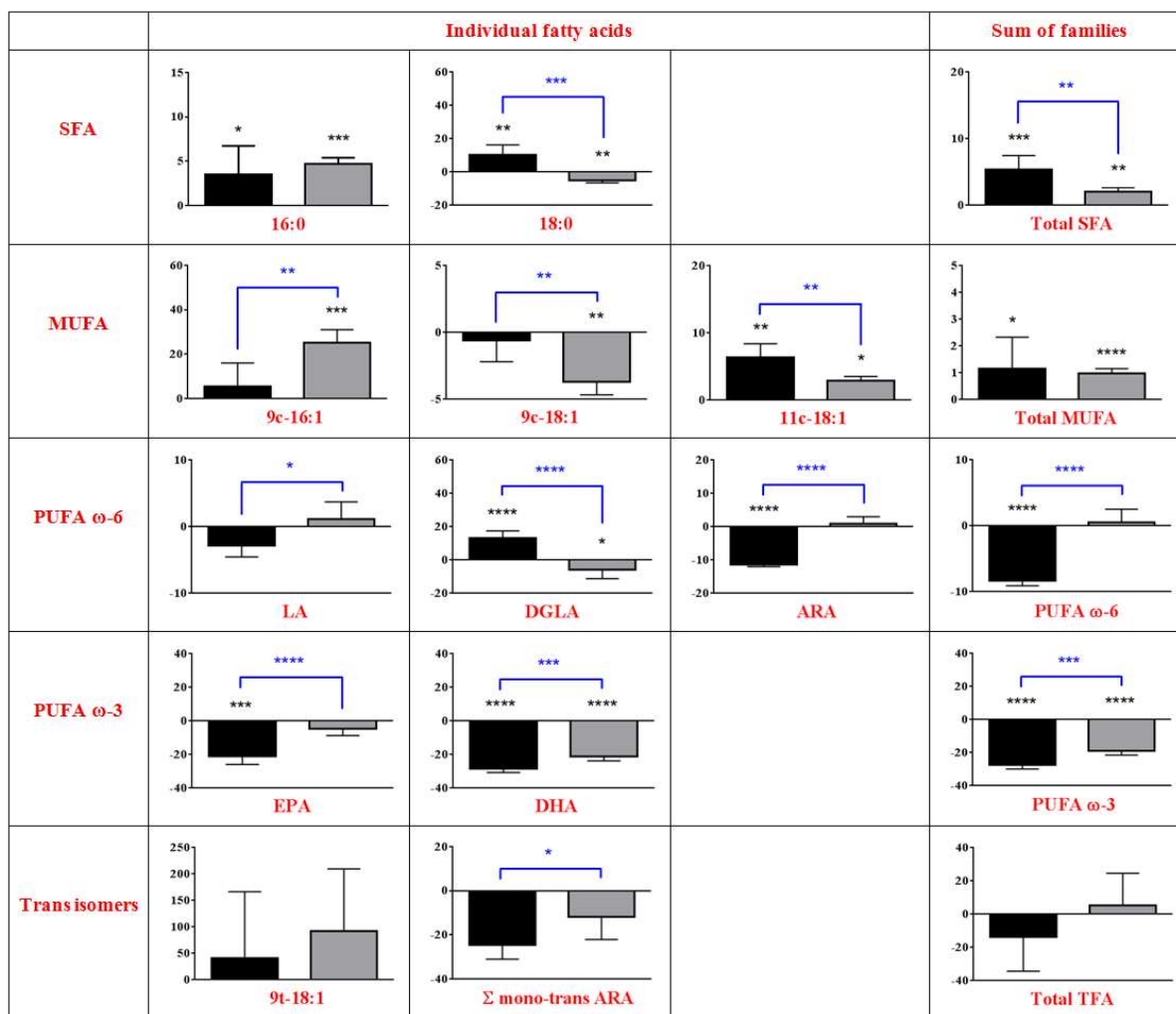


Figure 4.2. Percentage differences compared to controls for each type of fatty acid in the SK-N-SH cell membranes following incubation with 1 μ M apoE3 (black) or apoE4 (grey) after 24 h. The values are given as mean \pm SD (n=6). Each member of the fatty acid family is given in a row, the last column being the sum of the corresponding fatty acid family. Values significantly different from the control: (*) $p < 0.05$, (**) $p < 0.01$, (***) $p < 0.001$, (****) $p < 0.0001$. Black asterisks indicate the significance between control and apoE isoforms, blue asterisks indicate the significance between the two apoE isoforms.

A more specific evaluation of single fatty acids present in the membrane phospholipids yielded interesting differences between the two treatments with different apoE isoforms. The SFA stearic acid (18:0) and the ω -6 DGLA (20:3 ω -6) were both decreased after incubation of cells with apoE4 ($p < 0.01$ and $p < 0.05$, respectively) and increased after incubation with apoE3 ($p < 0.01$ and $p < 0.0001$, respectively). The ω -6 ARA (20:4 ω -6) was significantly diminished after incubation of cells with the apoE3 isoform ($p < 0.0001$) and negligibly increased after incubation with apoE4. These fatty acids were the only ones found with opposite trends for the two protein isoforms. Concerning the ω -3 fatty acids, EPA (20:5 ω -3) and DHA (22:6 ω -3) levels were found to be lower after incubation of the cells with either of the two apoE isoforms, as compared to untreated cells, but the decrease was

of a greater extent after incubation with the apoE3 isoform as compared to apoE4 ($p < 0.0001$ and $p < 0.001$, respectively).

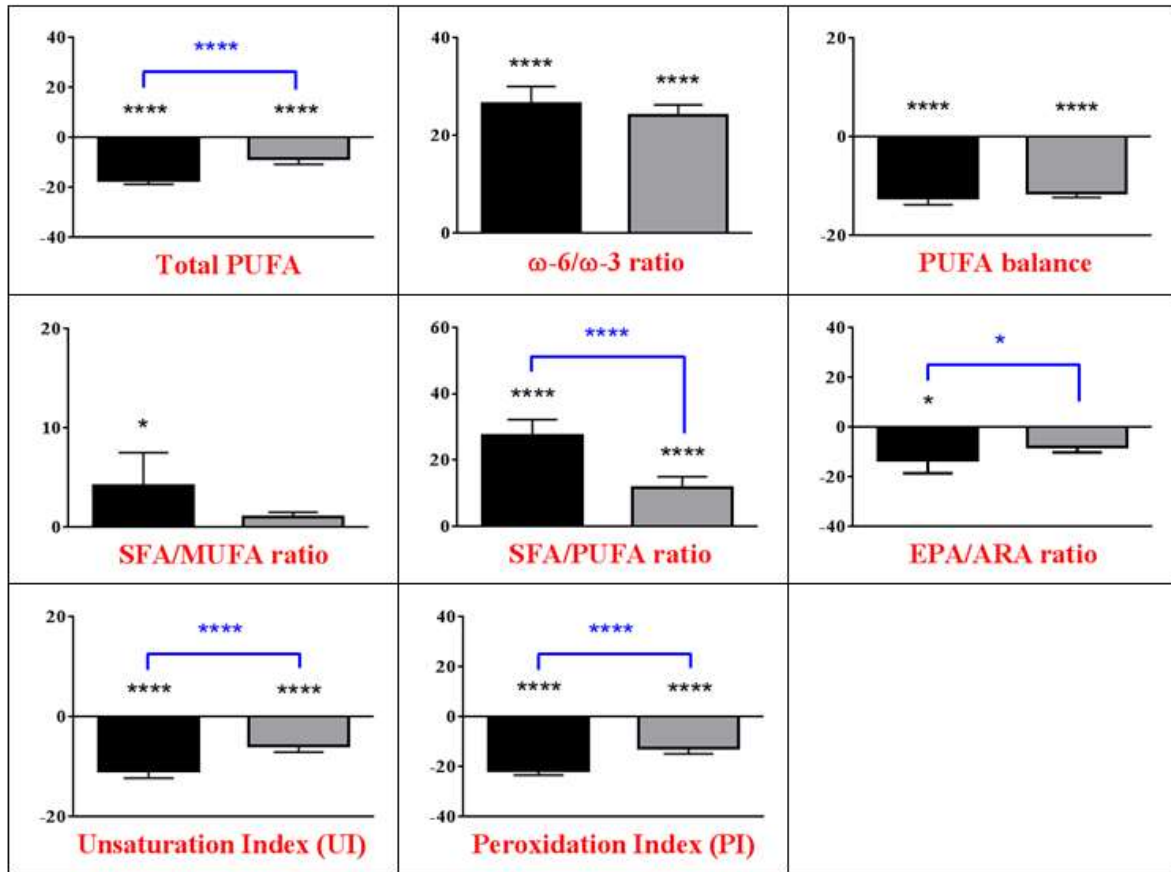


Figure 4.3. Membrane homeostasis indexes in the SK-N-SH cells recorded after 24 h treatment with 1 μ M apoE3 (black) or apoE4 (grey). Upper row: total PUFA, ω -6/ ω -3 ratio and PUFA balance; Middle row: SFA/MUFA, SFA/PUFA and EPA/ARA ratios; Lower row: unsaturation and peroxidation indexes. The values are given as mean \pm SD ($n = 6$). Values significantly different from the control: (*) $p < 0.05$, (**) $p < 0.01$, (***) $p < 0.001$, (****) $p < 0.0001$. Black asterisks indicate the significance between control and apoE isoforms, blue asterisks indicate the significance between the two apoE isoforms.

Expanding the vision to the whole membrane, these single fatty acid variations affect the corresponding indicators of the membrane status (**Table 4.2 and Figure 4.3**). Among them, the SFA/PUFA ratio in membranes was significantly increased after incubation with both isoforms ($p < 0.0001$), with apoE3 resulting in a higher increase compared to apoE4 ($p < 0.0001$). Also the ω -6/ ω -3 ratio (Fig. 2) was increased after incubation of cells with either apoE isoforms ($p < 0.0001$), whereas both peroxidation and unsaturation index (PI and UI) were lower than controls ($p < 0.0001$), with apoE3 inducing a greater decrease than apoE4 ($p < 0.0001$). The decrease of ω -3 affected also the PUFA balance indicator [46] with respect to control ($p < 0.0001$). In general, the effects of the addition of the apoE isoforms resulted in decreasing membrane fluidity, due to SFA increase and

PUFA loss. Other indicators of this significant decreasing trend, expressed as peroxidation index (PI) and unsaturation index (UI) [47] are shown in **Table 4.2**; for both indices, the difference from controls was higher with apoE3 than with apoE4 ($p < 0.0001$).

Changes in the fatty acid composition of membrane phospholipids due to the addition in the medium of apolipoproteins is a novel finding, and may be valuable for the understanding of the membrane properties and of the cell predisposition to metabolic responses originated from membrane constituents.

The effects of different fatty acids on the biophysical properties of cell membranes have been discussed by many Authors [48,49]. The increase in SFAs and the decrease in PUFAs, observed in the presence of both apoE isoforms, can influence membrane fluidity and permeability as measured by the PI and UI indexes, consequently bringing to a more rigid packing of the bilayer. It is interesting to note that apoE3 resulted in a more consistent reduction of the PI and UI indexes, thus suggesting a different influence of the two apoE isoforms on the properties of plasma membrane microenvironment. Indeed, biophysical and biological modifications induced by individual fatty acids deserve more attention in the apolipoprotein studies, as suggested by former observations on the palmitic acid-induced increase of de novo synthesis of ceramide in astroglia, known for being involved in A β production and in tau-protein hyperphosphorylation [50]. Notably, in the early stages of AD, sphingolipid balance is shifted towards ceramide accumulation and ceramide levels have been found to be increased in the brain, the CSF and the plasma of AD patients, as compared to the age matched neurologically normal control subjects [51-53]. Moreover, the observed changes can have important consequences on the cellular signalling. In fact, change in the membrane phospholipid fatty acids following apoE supplementation have direct connections with the signalling cascades mediated by eicosanoids, since ω -6 and ω -3 fatty acids are the precursor of signalling lipids after they are detached from membranes by the action of PLA₂ [54]. ω -6 fatty acids are precursors of different molecules with respect to ω -3 fatty acids; in fact, the former regulate cell functions with inflammatory, atherogenic and prothrombotic signals, whereas the latter directly inhibit the pro-inflammatory NF- κ B activity, by binding peroxisome proliferator activated receptors and thus controlling several genes involved in lipid metabolism and cytokine production (**Chapter 1, Paragraph 1.6**). More specifically, the ω -6 DGLA is a precursor of series-1 prostaglandins and other oxidation metabolites with anti-inflammatory and anti-proliferative effects [55]. DGLA is the metabolic precursor of ARA and is converted to ARA by the activity of Δ 5 desaturase. Therefore, its biological roles are determined by the partition into these two different pathways that must be evaluated in each specific condition. In this study, incubation of SK-NSH cells with apoE3 increased

the levels of DGLA and decreased the levels of ARA as compared to control cells. In contrast, incubation of cells with apoE4 had moderated diminution effect on DGLA levels and no significant effect on ARA levels.

The effect of apoE3, but not of apoE4, on ARA could be attributed either to: i) a metabolic negative influence on DGLA transformation (desaturase and elongase enzymes), which correspondently increases in the glycerophospholipids of SK-N-SH cells, or ii) a different affinity of the two apoE isoforms for the two ω -6 containing lipids, influencing their distribution to cells and availability for membrane phospholipid biosynthesis.

On the other hand, multiple mechanisms can be synergically operative. It was described that apoE4, but not apoE3, triggers a significant elevation of cytokines (IL6 and IL8, both implicated in AD) in SHSY5Y human neuroblastoma cells [56], through its connection with the formation of apoERelA transcriptional complex (RelA: v-rel avian reticuloendotheliosis viral oncogene homolog A/nuclear factor NF-kB p65 subunit – subunit of the NF-kB complex). As matter of facts, in our cell model apoE3 facilitates the increase of DGLA content in membrane phospholipids thus increasing the probability for protective molecular pathways. The role of DGLA and its transformations in AD have not been considered so far, and our results suggest a more comprehensive understanding of neurological functions including an evaluation of the balance among membrane fatty acid content and production of lipid mediators in neuronal cells [57]. ω -6 fatty acid involvement in AD is already well documented. Altered neuroinflammatory markers and upregulation of the ARA cascades have already been widely described, supporting the association of ARA metabolism and cytokine production with neuronal damage in AD brains [58].

Moreover, the low ability of apoE4 to act as a radical scavenger is supported by our results, showing differences in the amount of *trans* ARA isomers in neuronal membranes (see **Table 4.1**). Indeed, *trans* fatty acids are generated endogenously, resulting from the radical stress of sulfur-centered radicals that convert the *cis* double bonds of fatty acids (**Chapter 1, Paragraph 1.3.2**). It appears that the apoE3 isoform is able to maintain a lower amount of *trans*-ARA in cell membranes than the apoE4 isoform. Excess of *trans*-ARA could affect membrane integrity and contribute to alter lipid organization and cell responses. Moreover, the addition of the apoE3 isoform caused a higher reduction in the PI than apoE4, imparting to the cells greater stability against lipid oxidation. In a previous study, we found that an apoE4 fragment, the apoE4-165, promotes amyloid peptide β 42 (A β 42) accumulation in SK-N-SH cells and increases intracellular reactive oxygen species formation [33]. ApoE4 fragments are produced at the onset of AD and co-exist with the full-length protein in the brain during the progression of the disease. The limited capacity of apoE4 to decrease the PI may

facilitate the formation of apoE4 fragments, which are related to oxidative damage in neurons. In fact, increased lipid peroxidation was found in post-mortem brains expressing the apoE4 isoform [59,60].

While the functions of lipoproteins in the brain and the recruitment of lipids by the ApoE isoforms have been thoroughly investigated [61], our work expands the scenario to the observation of the membrane lipid composition, which is certainly influenced by the different availability of fatty acids. The results provided by these in vitro experiments are the first to connect molecular observations on membrane lipids to the systemic effects observed in the brain cells and tissues and to the clinical findings. Further targeted studies can be thus envisaged on the effects of supplementation with ω -3 or other lipids, also in consideration of the fact that a higher-than-normal ω -6/ ω -3 ratio has been described in cell membranes of people carrying the apoE4 isoform [6].

Thus, membrane lipidomics may help to reach a better understanding of the observed differences between apoE3 and apoE4 allele carriers and of the nexus between apoE isoforms and AD onset.

4.6. Conclusions

This work is a preliminary in vitro study aimed at investigating the membrane fatty acid remodeling in the presence of either apoE3 or apoE4. For this model, SK-N-SH neuroblastoma cell line was used.

Although it is established that carrying the lipid binding proteins apoE3 or apoE4 is associated with opposite effects as for AD onset, with apoE4 being the major risk factor for AD, the effect of these protein isoforms on brain cells membrane fatty acid composition was largely unexplored. We found that cell incubation in the presence of either apoE3 or apoE4 induced fatty acid remodeling.

The main results can be summarized as follows:

- SFAs were significantly increased after incubation of cells with apoE3 or apoE4 ($p < 0.001$, $p < 0.01$, respectively), but the increase was higher in the presence of apoE3 than apoE4 ($p < 0.01$);
- MUFAs were significantly increased after incubation with both apoE3 and apoE4 ($p < 0.05$, $p < 0.0001$, respectively), with apoE4 mainly increasing palmitoleic acid concentration ($p < 0.001$).
- ω -6 PUFAs were significantly diminished in the cell membranes after incubation with apoE3 ($p < 0.0001$) but their concentration was unchanged after incubation with apoE4.
- ω -3 PUFAs were significantly diminished in the membrane of cells treated with both apoE forms if compared with untreated samples ($p < 0.0001$), but the decrease was of greater

magnitude in the presence of apoE3 ($p < 0.001$). The decrease of ω -3 affected also the PUFA balance indicator with respect to control ($p < 0.0001$).

- TFAs tended to decrease after incubation of the cells with apoE3. On the contrary, the TFA content in cell membranes appeared to increase in the presence of apoE4.

More specifically, ApoE3 increased the membrane level of stearic acid and of DGLA, whereas apoE4 had opposite effects. The addition of both apoE3 and apoE4 increased membrane SFAs and MUFAs, ω -6/ ω -3 ratio and decreased total PUFAs, but with various intensities. Moreover, both apoE isoforms decreased membrane homeostasis indexes such as PUFA balance, UI and PI.

The present results highlight membrane property changes connected to the apoE isoforms, suggesting that membrane lipidomics could be inserted in future model studies of apolipoproteins in health and disease. The membrane remodeling induced by the addition of apolipoproteins encourages further in vitro studies to better understand synergies between fatty acid-based membrane lipidomics and apolipoprotein lipid distribution, including the effects of different dietary conditions and lipid supplementation.

4.7. References

1. Mielke, M.M.; Lyketsos, C.G. Lipids and the pathogenesis of Alzheimer's disease: is there a link? *Int. Rev. Psychiatry* **2006**, *18*(2), 173-186
2. Di Paolo, G.; Kim, T.W. Linking lipids to Alzheimer's disease: cholesterol and beyond. *Nat. Rev. Neurosci.* **2011**, *12*(5), 284-296
3. Zarrouk, A.; Debbabi, M.; Bezine, M.; Karym, E.M.; Badreddine, A.; Rouaud, O.; Moreau, T.; Cherkaoui-Malki, M.; El Ayeb, M.; Nasser, B.; Hammami, M.; Lizard, G. Lipid Biomarkers in Alzheimer's Disease. *Curr. Alzheimer Res.* **2017**, *14*(9)
4. Ferreri, C.; Chatgialiloglu, C.; *Membrane Lipidomics for Personalized Health*, John Wiley and Sons, New York, **2015**
5. Ferreri, C.; Chatgialiloglu, C. Role of fatty acid-based functional lipidomics in the development of molecular diagnostic tools. *Expert Rev. Mol. Diagn.* **2012**, *12*(7), 767-780
6. Ballard, C.; Gauthier, S.; Corbett, A.; Brayne, C.; Aarsland, D.; Jones, E. Alzheimer's disease. *Lancet* **2011**, *377*(9770), 1019-1031
7. McKhann, G.; Drachman, D.; Folstein, M.; Katzman, R.; Price, D.; Stadlan, E.M. Clinical diagnosis of Alzheimer's disease Report of the NINCDS-ADRDA Work Group* under the auspices of Department of Health and Human Services Task Force on Alzheimer's Disease. *Neurology* **1984**, *34*(7), 939

8. Kim, J.; Basak, J.M.; Holtzman, D.M. The role of apolipoprotein E in Alzheimer's disease. *Neuron* **2009**, *63*(3), 287–303
9. Hirsch-Reinshagen, V.; Zhou, S.; Burgess, B.L.; Bernier, L.; McIsaac, S.A.; Chan, J.Y.; Tansley, G.H.; Cohn, J.S.; Hayden, M.R.; Wellington, C.L. Deficiency of ABCA1 impairs apolipoprotein E metabolism in brain. *J. Biol. Chem.* **2004**, *279*(39), 41197-41207
10. Schwiegelshohn, B.; Presley, J.F.; Gorecki, M.; Vogel, T.; Carpentier, Y.A.; Maxfield, F.R.; Deckelbaum, R.J. Effects of apoprotein E on intracellular metabolism of model triglyceride-rich particles are distinct from effects on cell particle uptake. *J. Biol.Chem.*, **1995**, *270*(4), 1761-1769
11. Xu, Q.; Bernardo, A.; Walker, D.; Kanegawa, T.; Mahley, R.W.; Huang, Y. Profile and regulation of apolipoprotein E (apoE) expression in the CNS in mice with targeting of green fluorescent protein gene to the ApoE locus. *J. Neurosci.* **2006**, *26*(19), 4985-4994
12. Lehtimäki, T.; Pirttilä, T.; Mehta, P.D.; Wisniewski, H.M.; Frey, H.; Nikkari, T. Apolipoprotein E (apoE) polymorphism and its influence on ApoE concentrations in the cerebrospinal fluid in Finnish patients with Alzheimer's disease. *Hum. Genet.* **1995**, *95*(1), 39-42
13. Corder, E.H.; Saunders, A.M.; Strittmatter, W.J.; Schmechel, D.E.; Gaskell, P.C.; Small, G.W.; Roses, A.D.; Haines, J.L.; Pericak-Vance, M.A. Gene dose of apolipoprotein E type 4 allele and the risk of Alzheimer's disease in late onset families. *Science* **1993**, *261*(5123), 921-923
14. Strittmatter, W.J.; Saunders, A.M.; Schmechel, D.; Pericak-Vance, M.; Enghild, J.; Salvesen, G.S.; Roses, A.D. Apolipoprotein E: high-avidity binding to beta-amyloid and increased frequency of type 4 allele in late-onset familial Alzheimer disease. *Proc. Natl. Acad. Sci. U.S.A.* **1993**, *90*(5), 1977-1981
15. Chartier-Harlin, M.C.; Parfitt, M.; Legrain, S.; Pérez-Tur, J.; Brousseau, T.; Evans, A.; Berr, C.; Vidal, O; Roques, P.; Gourlet, V.; Fruchart, J.C. Apolipoprotein E, epsilon 4 allele as a major risk factor for sporadic early and late-onset forms of Alzheimer's disease: analysis of the 19q13. 2 chromosomal region. *Hum. Mol. Genet.* **1994**, *3*(4), 569-574
16. Mayeux, R.; Ottman, R.; Maestre, G.; Ngai, C.; Tang, M.X.; Ginsberg, H.; Chun, M.; Tycko B.; Shelanski, M. Synergistic effects of traumatic head injury and apolipoprotein-epsilon4 in patients with Alzheimer's disease. *Neurology* **1995**, *45*(3), 555-557
17. Deane, R.; Sagare, A.; Hamm, K.; Parisi, M.; Lane, S.; Finn, M.B.; Holtzman, D.M.; Zlokovic, B.V. ApoE isoform-specific disruption of amyloid β peptide clearance from mouse brain. *J. Clin. Invest.* **2008**, *118*(12), 4002-4013
18. Bu, G. Apolipoprotein E and its receptors in Alzheimer's disease: pathways, pathogenesis and therapy. *Nat. Rev. Neurosci.* **2009**, *10*(5), 333-344
19. Tai, L.M.; Mehra, S.; Shete, V.; Estus, S.; Rebeck, G.W.; Bu, G.; LaDu, M.J. Soluble apoE/A β complex: mechanism and therapeutic target for APOE4-induced AD risk. *Mol. Neurodegener.* **2014**, *9*(1), 2

20. Fisher, C.A.; Ryan, R.O. Lipid binding-induced conformational changes in the N-terminal domain of human apolipoprotein E. *J. Lipid Res.* **1999**, *40*(1), 93-99
21. Krimbou, L.; Denis, M.; Haidar, B.; Carrier, M.; Marcil, M.; Genest, J. Molecular interactions between apoE and ABCA1 impact on apoE lipidation. *J. Lipid Res.* **2004**, *45*(5), 839-848
22. Tokuda, T.; Calero, M.; Matsubara, E.; Vidal, R.; Kumar, A.; Permanne, B.; Zlokovic, B.; Smith, J.D.; Ladu, M.J.; Rostagno, A.; Frangione, B.; Ghiso, J. Lipidation of apolipoprotein E influences its isoform-specific interaction with Alzheimer's amyloid β peptides. *Biochem. J.* **2000**, *348*(Pt 2), 359-365
23. Jiang, QLee, C.D.; Mandrekar, S.; Wilkinson, B.; Cramer, P.; Zelcer, N.; Mann, K.; Lamb, B.; Willson, T.M.; Collins, J.L.; Richardson, J.C.; Smith, J.D.; Comery, T.A.; Riddell, D.; Holtzman, D.M.; Tontonoz, P.; Landreth, G.E. ApoE promotes the proteolytic degradation of A β . *Neuron* **2008**, *58*(5) 681-693
24. Christen, Y. Oxidative stress and Alzheimer disease. *Am. J. Clin. Nutr.* **2000**, *71*(2), 621s-629s
25. Miyata, M.; Smith, J.D. Apolipoprotein E allele-specific antioxidant activity and effects on cytotoxicity by oxidative insults and beta-amyloid peptides. *Nat. Genet.* **1996**, *14*(1), 55-61
26. Legleiter, J.; Fryer, J.D.; Holtzman, D.M.; Kowalewski, T. The modulating effect of mechanical changes in lipid bilayers caused by apoE-containing lipoproteins on A β induced membrane disruption. *ACS Chem. Neurosci.* **2011**, *2*(10), 588-599
27. Huang, Y.; Liu, X.Q.; Wyss-Coray, T.; Brecht, W.J.; Sanan, D.A.; Mahley, R.W. Apolipoprotein E fragments present in Alzheimer's disease brains induce neurofibrillary tanglelike intracellular inclusions in neurons. *Proc. Natl. Acad. Sci. U.S.A.* **2001**, *98*(15), 8838-8843
28. Harris, F.M.; Brecht, W.J.; Xu, Q.; Tesseur, I.; Kekoni, L.; Wyss-Coray, T.; Dee Fish, J.; Masliah, E.; Hopkins, P.C.; Searce-Levie, K.; Weisgraber, K.H.; Mucke, L.; Mahley, R.W.; Huang, Y. Carboxyl-terminal-truncated apolipoprotein E4 causes Alzheimer's disease-like neurodegeneration and behavioral deficits in transgenic mice. *Proc. Natl. Acad. Sci. U.S.A.* **2003**, *100*(19), 10966-10971
29. Brecht, W.J.; Harris, F.M.; Chang, S.; Tesseur, I.; Yu, G.Q.; Xu, Q.; Dee Fish, J.; Wyss-Coray, T.; Buttini, M.; Mucke, L.; Mahley, R.W.; Huang, Y. Neuron-specific apolipoprotein e4 proteolysis is associated with increased tau phosphorylation in brains of transgenic mice. *J. Neurosci.* **2004**, *24*(10), 2527-2534
30. Dafnis, I.; Argyri, L.; Sagnou, M.; Tzinia, A.; Tsilibary, E.C.; Stratikos, E.; Chroni, A. The ability of apolipoprotein E fragments to promote intraneuronal accumulation of amyloid beta peptide 42 is both isoform and size-specific. *Sci. Rep.* **2016**, *6*, 30654
31. Dafnis, I.; Tzinia, A.; Tsilibary, E.C.; Zannis, V.I.; Chroni, A. An apolipoprotein E4 fragment affects MMP9, TIMP1 and cytokine levels in brain cell lines. *Neuroscience* **2012**, *210*, 21-32
32. Schwiegelshohn, B.; Presley, J.F.; Gorecki, M.; Vogel, T.; Carpentier, Y.A.; Maxfield, F.R.; Deckelbaum, R.J. Effects of apoprotein E on intracellular metabolism of model triglyceride-

- rich particles are distinct from effects on cell particle uptake. *J. Biol. Chem.* **1995**, *270*, 1761-1769
33. Dafnis, I.; Stratikos, E.; Tzinia, A.; Tsilibary, E.C.; Zannis, V.I.; Chroni, A. An apolipoprotein E4 fragment can promote intracellular accumulation of amyloid peptide beta 42. *J. Neurochem.* **2010**, *115*(4), 873-884
 34. Morita, S.; Okuhira, K.; Tsuchimoto, N.; Vertut-Doi, A.; Saito, H.; Nakano, M.; Handa, T. Effects of sphingomyelin on apolipoprotein E-and lipoprotein lipase-mediated cell uptake of lipid particles. *Biochim. Biophys. Acta* **2003**, *1631*(2), 169-176
 35. Mahley, R.H. Central nervous system lipoproteins: ApoE and regulation of cholesterol metabolism. *Arterioscler. Thromb. Vasc. Biol.* **2016**, *36*(7), 1305-1315
 36. Gao, X.; Campbell IV, W.A.; Chaibva, M.; Jain, P.; Leslie, A.E.; Frey, S.L.; Legleiter, J. Cholesterol modifies Huntingtin binding to, disruption of, and aggregation on lipid membranes. *Biochemistry* **2016**, *55*(1), 92-102
 37. Thanh Nam, D.; Arseneault, M.; Zarkovic, N.; Waeg, G.; Ramassamy, C. Molecular regulations induced by acrolein in neuroblastoma SK-N-SH cells: relevance to Alzheimer's disease. *J. Alzheimers Dis.* **2010**, *21*(4), 1197-1216
 38. Peng, Y.; Lee, D.Y.W.; Jiang, L.; Ma, Z.; Schachter, S.C.; Lemere, C.A. Huperzine A regulates amyloid precursor protein processing via protein kinase C and mitogen-activated protein kinase pathways in neuroblastoma SK-N-SH cells over-expressing wild type human amyloid precursor protein 695. *Neuroscience* **2007**, *150*(2), 386-39
 39. Argyri, L.; Skamnaki, V.; Stratikos, E.; Chroni, A. A simple approach for human recombinant apolipoprotein E4 expression and purification. *Protein Expr. Purif.* **2011**, *79*(2), 251-257
 40. Georgiadou, D.; Stamatakis, K.; Efthimiadou, E.K.; Kordas, G.; Gantz, D.; Chroni, A.; Stratikos, E. Thermodynamic and structural destabilization of apoE3 by hereditary mutations associated with the development of lipoprotein glomerulopathy. *J. Lipid Res.* **2013**, *54*(1), 164-176
 41. Fuchs, B.; Süß, R.; Teuber, K.; Eibisch, M.; Schiller, J. Lipid analysis by thin-layer chromatography- a review of the current state. *J. Chromatogr. A* **2011**, *1218*(19), 2754-2774
 42. Cohen, G.; Shamni, O.; Avrahami, Y.; Cohen, O.; Broner, E.C.; Filippov-Levy, N.; Chatgililoglu, C.; Ferreri, C.; Kaiser, N.; Sasson, S.; Beta cell response to nutrient overload involves phospholipid remodelling and lipid peroxidation. *Diabetologia* **2015**, *58*(6), 1333-1343
 43. Holtzman, D.M.; Bales, K.R.; Wu, S.; Bhat, P.; Parsadanian, M.; Fagan, A.M.; Chang, L.K.; Sun, Y.; Paul, S.M. Expression of human apolipoprotein E reduces amyloid- β deposition in a mouse model of Alzheimer's disease. *J. Clin. Invest.* **1999**, *103*(6), R15-R21
 44. Getz, G.S.; Reardon, C.A. Apoprotein E as a lipid transport and signaling protein in the blood, liver and artery wall. *J. Lipid Res.* **2009**, *50*, S156-S161

45. Bolognesi, A.; Chatgililoglu, A.; Polito, L.; Ferreri, C. Membrane lipidome reorganization correlates with the fate of neuroblastoma cells supplemented with fatty acids. *PLoS One* **2013**, *8*(2), e55537
46. Abbott, S.K.; Else, P.A.; Atkins, T.A.; Hulbert, A.J. Fatty acid composition of membrane bilayers: importance of diet polyunsaturated fat balance, *Biochim. Biophys. Acta* **2012**, *1818*(5), 1309-1317
47. Puca, A.A.; Novelli, V.; Viviani, C.; Andrew, P.; Somalvico, F.; Cirillo, N.A.; Chatgililoglu, C.; Ferreri, C. Lipid profile of erythrocyte membranes as possible biomarker of longevity. *Rejuvenation Res.* **2008**, *11*(1), 63-72
48. Maulucci, G.; Cohen, O.; Daniel, B.; Sansone, A.; Petropoulou, P.I.; Filou, S.; Spyridonis, A.; Pani, G.; De Spirito, M.; Chatgililoglu, C.; Ferreri, C.; Kypreos, K.E.; Sasson, S. Fatty acid related modulations of membrane fluidity in cells: detection and implications. *Free Radic. Res.* **2016**, *50*(sup1), S40-S50
49. Holthuis, C.M.J.; Menon, A.K. Lipid landscapes and pipelines in membrane homeostasis, *Nature* **2014**, *510*(7503), 48-57
50. Patil, S.; Melrose, J.; Chan, C. Involvement of astroglial ceramide in palmitic acid-induced Alzheimer-like changes in primary neurons. *Eur. J. Neurosci.* **2007**, *26*(8), 2131-2141
51. Han, X.; Holtzman, M.D.; McKeel, D.W. Jr.; Kelley, J.; Morris J.C. Substantial sulfatide deficiency and ceramide elevation in very early Alzheimer's disease: potential role in disease pathogenesis. *J. Neurochem.* **2002**, *82*(4), 809-818
52. Cutler, R.G.; Kelly, J.; Storie, K.; Pedersen, W.A.; Tammara, A.; Hatanpaa, K.; Troncoso, J.C.; Mattson, M.P. Involvement of oxidative stress-induced abnormalities in ceramide and cholesterol metabolism in brain aging and Alzheimer's disease. *Proc. Natl. Acad. Sci. U.S.A.* **2004**, *101*(7), 2070-2075
53. He, X.; Huang, Y.; Li, B.; Gong, C.X.; Schuchman, E.H. Deregulation of sphingolipid metabolism in Alzheimer's disease. *Neurobiol. Aging* **2010**, *31*(3), 398-408
54. Schmitz, G.; Ecker, J. The opposing effects of n-3 and n-6 fatty acids. *Progr. Lipid Res.* **2008**, *47*(2), 147-155
55. Wang, X.; Lin, H.; Gu, Y. Multiple roles of dihomo-gamma-linolenic acid against proliferation diseases. *Lipids Health Dis.* **2012**, *11*, 25
56. Theendakara, V.; Peters-Libe, C.A.; Spilman, P.; Poksay, K.S.; Bredesen, D.E.; Rao, R.V. Direct transcriptional effects of apolipoprotein E. *J. Neurosci.* **2016**, *36*(3), 685-700
57. Bazinet, R.P.; Layé, S. Polyunsaturated fatty acids and their metabolites in brain function and disease. *Nat. Rev. Neurosci.* **2014**, *15*(12), 771-785
58. Rao, S.; Rapoport, S.I.; Kim, H.W. Altered neuroinflammatory, arachidonic acid cascade and synaptic markers in postmortem Alzheimer's disease brain, *Transl. Psychiatry* **2011**, *1*(8), e31
59. Ramassamy, C.; Averill, D.; Beffert, U.; Bastianetto, S.; Theroux, L.; Lussier-Cacan, S.; Cohn, J.S.; Christen, Y.; Davignon, J.; Quirion, R.; Poirier, J. Oxidative damage and

protection by antioxidants in the frontal cortex of Alzheimer's disease is related to the apolipoprotein E genotype, *Free Radic. Biol. Med.* **1999**, 27(5-8), 544-553

60. Ramassamy, C.; Averill, D.; Beffert, U.; Theroux, L.; Lussier-Cacan, S.; Cohn, J.S.; Christen, Y.; Schoofs, A.; Davignon, J.; Poirier, J. Oxidative insults are associated with apolipoprotein E genotype in Alzheimer's disease brain, *Neurobiol. Dis.* **2000**, 7(1), 23-37
61. Wang, H.; Heckel, R.H. What are lipoproteins doing in the brain? *Trends Endocrinol. Metab.* **2014**, 25(1), 8-14
62. Chouinard-Watkins, R.; Plourde, M. Fatty acid metabolism in carriers of apolipoprotein E epsilon 4 allele: is it contributing to higher risk of cognitive decline and coronary heart disease? *Nutrients* **2014**, 6(10), 4452-4471

Chapter 5

Trans liposomes

5.1. Introduction

Liposomes, which are constituted by phospholipids, served as membrane models in the field of biomimetic chemical biology; at the same time, they have been extensively studied in medicinal chemistry for their potential in drug delivery.

The biophysical characteristics of liposomes strongly depend on the fatty acid moieties. The influence of lipid double bond configuration has not been considered so far when evaluating the competence of liposomes in drug delivery; however, one should remember that natural unsaturated lipids are always in the *cis* configuration.

The study we carried out focused on possible changes in the molecular properties of liposomes induced by the conversion of the double bonds from *cis* to *trans* geometry. In particular, we report on the effects of the addition of *trans*-phospholipids to other lipid constituents on size, ζ -potential and stability of liposomal formulations and on liposome ability to encapsulate two dyes, rhodamine B and fluorescein.

From a biotechnological point of view, *trans*-containing liposomes proved to have different characteristics from those containing the *cis* analogues, and to influence the incorporation and release of the dyes. These results open new perspectives in the use of the unnatural lipid geometry, with the purpose of changing liposome behavior and/or of obtaining molecular interferences, also in view of synergic effects on cell toxicity, especially in antitumoral strategies.

5.2. Liposome properties

Liposomes are small artificial vesicular structures characterized by the presence of one or more phospholipid bilayers, that delimit a hydrophilic core.

As previously mentioned for cell membrane (**Chapter 1, Paragraph 1.1**), phospholipids are amphiphilic molecules that expose their polar heads towards the surrounding aqueous environment or towards the internal aqueous cavity, while the apolar tails (the hydrophobic portion of the molecules) are buried in the inner core, where they interact each with the other; the lipidic bilayers surround an internal aqueous cavity. Therefore, liposomes can remain immersed in an aqueous environment while simultaneously hosting an aqueous content in which active principles or other water-soluble molecules are dispersed. The release of polar molecules located in the inner aqueous volume is generally prevented, effectively isolating the liposome content.

Liposomes can be classified according to different criteria, such as size, structure and preparation method. Depending on the structure and the number of double phospholipid layers, it is possible to distinguish liposomes as:

- Unilamellar liposomes, that consist of a single phospholipid bilayer that encloses a hydrophilic core. Depending on their size, unilamellar liposomes can be further classified into:
 - Small unilamellar vesicles (SUVs) whose diameter may vary from 20 nm to 100 nm;
 - Large unilamellar vesicles (LUVs) whose diameter may vary from 100 nm to 1 μm ;
 - Giant unilamellar vesicles (GUVs) whose diameter is greater than 1 μm .
- Multilamellar vesicles (MLVs), that are characterized by the presence of concentric lipid layers (usually more than five), separated by aqueous phases (onion organization). Multilamellar liposomes can reach diameters between 500 and 10.000 nm. Oligolamellar vesicles (OLVs), consisting of few concentric phospholipid bilayers (less than five), are also included in this group.
- Multivesicular vesicles (MVs), that are characterized by the presence of a double phospholipid layer enclosing other not concentric liposomes (**Figure 5.1**).

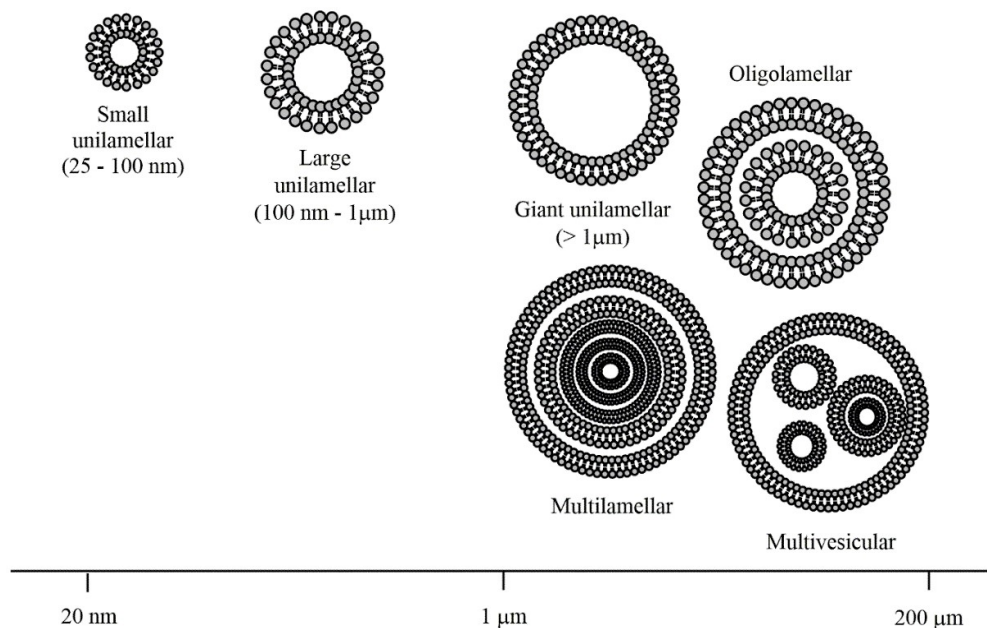


Figure 5.1. Liposome classification based on size and structural characteristics.

Not all phospholipids have the propensity to form liposomes. The aggregation structure is influenced by the phospholipid shape, which depends on the relative dimensions of their polar and apolar tails. The molecular self-assembly structure can be predicted by a factor known as packing parameter, P . This parameter, is defined as the ratio between the effective hydrophobic chain volume (V), and the product of the effective headgroup area (A_0) by the alkyl chain length, (l_c) (**Figure 5.2**).

P parameter underlines the importance of the area ratio occupied by the cross section of the hydrophobic portion with respect to the hydrophilic portion [1].

When the head group and the lipid scaffold have similar cross section areas ($P > 1/2$), the molecules have a cylindrical shape and form spherical vesicles, that are thermodynamically favoured over planar bilayers. This is the case of phosphatidylcholine and phosphatidylserine, the most abundant phospholipids found in cell membranes.

Lipids with a head occupying a relatively large surface area when compared with the cross-sectional area occupied by the hydrophobic chains ($P < 1/2$), as for example in the case of lysophospholipids, usually prefer micellar (non-inverted) structures.

In contrast, lipids with a relatively small polar head and acyl chains occupying an extended area ($P > 1$), such as phosphatidylethanolamine, tend to adopt an inverse hexagonal phase H_{II} .

This lipid polymorphism has been considered of crucial importance in physiological processes such as the generation of curvatures that occurs in the formation of lipid vesicles or during membrane fusion.

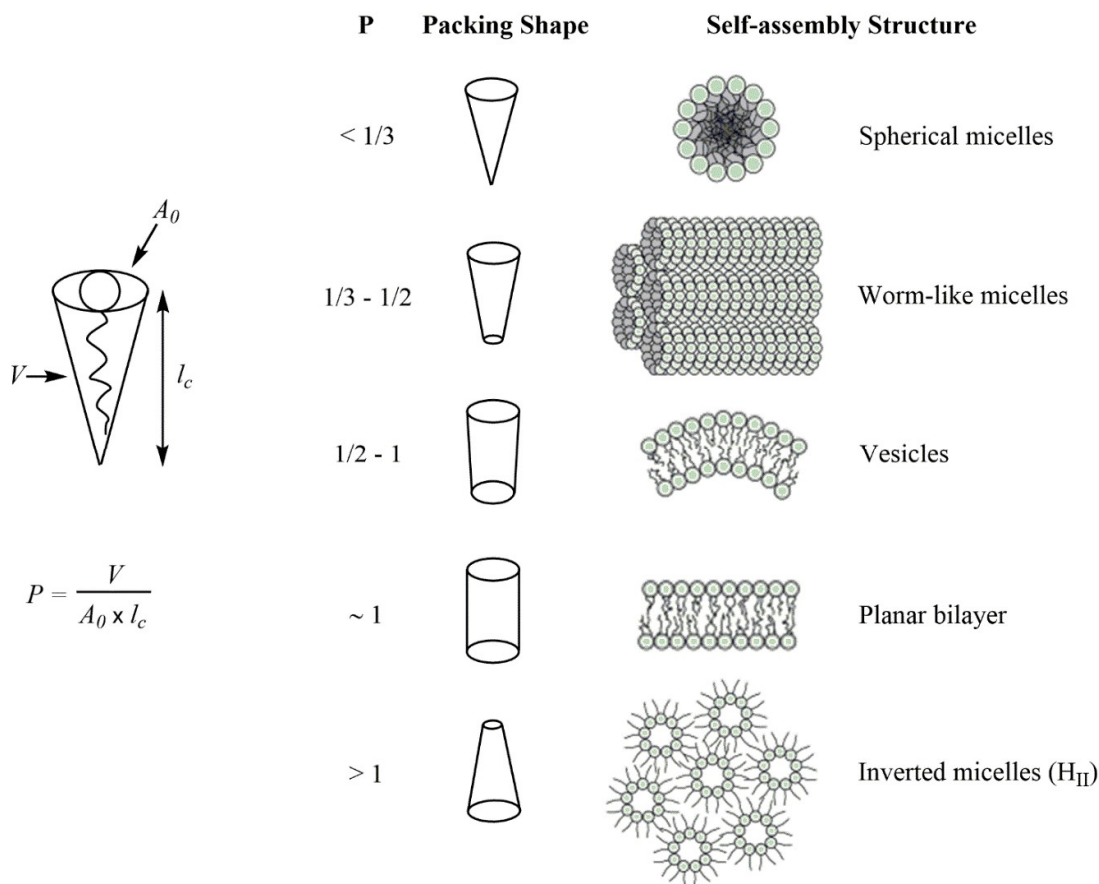


Figure 5.2. Schematic representation of the liposome structure as a function of the lipid packing parameter (P).

5.3. Liposome preparation

Liposomes can be prepared at a lab-scale level using reproducible and robust protocols that can be modified to suit specific needs [2,3].

The choice of the proper liposome preparation method depends on the physico-chemical characteristics of the material to be entrapped and consequently of the medium in which they are dispersed. Additionally, it is important to consider the effective concentration of the entrapped substance, its potential toxicity but also the size distribution and the shelf-life of the vesicles for the intended applications [4,5].

The first step of liposome preparation consists in dissolving the phospholipids (or a mixture of lipid components) in an organic solvent, such as chloroform or chloroform/methanol mixtures, to assure the formation of a homogeneous mixture of lipids.

Lipid solutions are usually prepared at a 10-20 mg lipid/mL concentration, however higher concentrations may be used, based on the lipid solubility and mixing capacity. Once the lipids are

thoroughly mixed in the organic solvent, the solvent is removed to yield a homogeneously distributed lipid film. Depending on the solvent volume, inert gas stream (i.g. nitrogen or argon) or rotary evaporation can be used to evaporate the solvent. The residual traces of organic solvent can be removed by placing the vial or bottom round flask on a vacuum pump at least one hour prior to proceed with the rehydration step.

Hydration of the dry lipid film can be achieved by adding an aqueous medium, followed by agitation. Attention should be paid to the temperature of use, which should be above the gel-to-liquid crystal transition temperature (T_m) of the lipid with the highest T_m , and should be maintained constant until the end of the process. In the presence of a phospholipid mixture, the temperature to be used should be considered with caution since high temperatures can facilitate oxidative processes or induce lipid degradation. Hydration time may differ depending on the lipid species and structures, however hydrating and vigorous shaking usually lead to high homogeneity of the suspension and reduction in size of the vesicles.

The hydration mediums are usually water or buffers, depending on the applications, to respect physiological pH and osmolarity, the desired surface charge for the electrostatic interactions with the encapsulated molecules, but also the preparation method. For example, if the liposome procedure requires lyophilization, a cryoprotectant in the hydration medium is required.

The product of hydration is a stable suspension composed by MLVs, analogous in structure to an onion, which can be downsized by a variety of techniques, including sonication or extrusion (**Figure 5.3**).

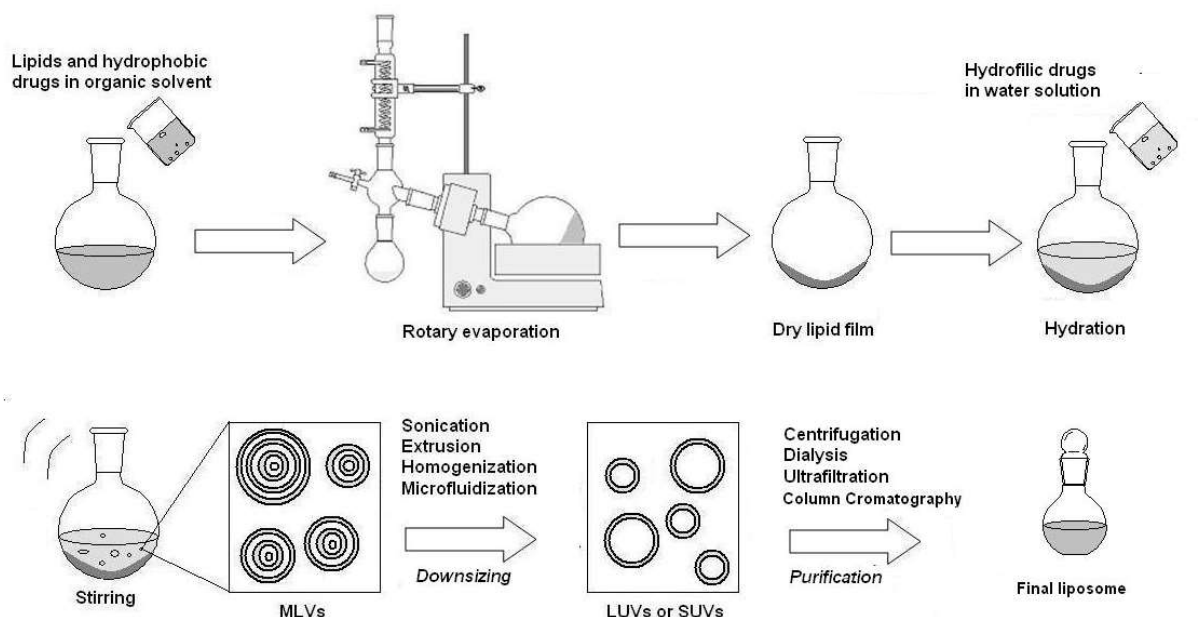


Figure 5.3. Liposome preparation (image from <http://www.intechopen.com/source/html/44386/media/image7.png>).

5.3.1. Sonication

Sonication method is usually accomplished by placing a vial containing the MLV suspension to be downsized in a bath sonicator and sonicating for 5-10 minutes above the T_m of the lipid mixture. Sonication of MLVs typically produces SUVs with diameters in the range of 15-50 nm. Approaching homogeneity and nanometric sizes, the suspension becomes transparent, however different factors, such as concentration, temperature, sonication time and power, can influence the nanoparticle size distribution. Despite being a quick and inexpensive technique, sonication hardly gives reproducible results and chances of scale-up.

5.3.2. Extrusion

An alternative to sonication is represented by the extrusion technique [6].

Extrusion consists in the forced passage of a MLV suspension through small, regular pores of a resistant membrane by applying an external pressure. The passage through the pores destroys the large aggregates and produces liposomes similar in size to the membrane pore diameter. For this purpose, the extrusion apparatus is composed of two syringes that should fit tight into a central support containing the membranes with suitable pore diameters (**Figure 5.4**). Membrane supports and o-rings are also included in the system to guarantee the hermetic sealing of the downsizing chamber and to

avoid suspension leakage. The temperature can be controlled by placing the extruder heating block on a hot plate. After equilibrating the temperature and pre-wetting of the instrument with clean buffer, the suspension can be inserted in one of the two syringes and gently pushed from the plunger to the second syringe and again back to the original syringe. This step can be repeated several times since the more passages through the membrane are accomplished, the more homogenous the suspension becomes. The final extrusion should fill the alternate syringe, in order to reduce contamination from larger particles or undesired material (i.g. dust) that did not pass through the membrane.

The method is simple and reproducible, but it is usually time-wasting and difficult to scale-up because it is limited to processing small volumes.

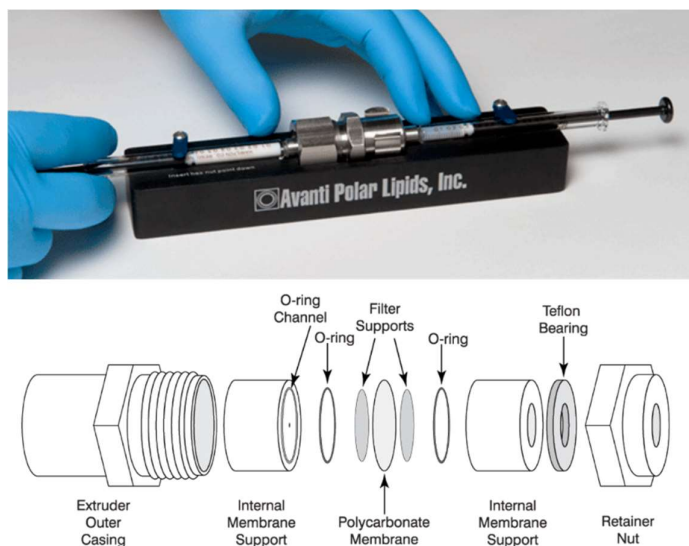


Figure 5.4. Extruder system (image from www.avantilipids.com).

5.4. Liposome characterization

The quality of the liposomes obtained by the methods previously described can be assessed by monitoring various parameters. From the analytical point of view, the most important features include the average mean diameter, the polydispersity and the morphology. Other commonly monitored parameters for the therapeutic use of liposomes are the encapsulation efficiency and the surface charge.

5.4.1. Dynamic Light Scattering (DLS)

Dynamic light scattering (DLS) is the most commonly used technique for liposome size and surface charge measurements [7].

The sample is illuminated by a laser beam, and the variations in light intensity diffused by the sample are measured as a function of time. The intensity variations measured by the detector are generated by the Brownian movement of the particles at the origin of the scattering.

The phenomenon at the basis of DLS is that, in the same conditions of temperature and viscosity, 'small' particles move quickly, creating rapid variations in the scattering intensity. On the contrary, 'big' particles move more slowly, creating slow intensity variations.

Thanks to an auto correlator, the speed of the intensity variations can be measured, and the particle diffusion coefficient calculated by the correlation function. Stokes–Einstein equation (**Figure 5.5**), where D is the diffusion constant, k_B is Boltzmann's constant, T is the absolute temperature, η is the dynamic viscosity and r is the radius of the spherical particle, allows then to convert the diffusion coefficient into the hydrodynamic diameter.

$$D = \frac{K_B \times T}{6\pi \eta r}$$

Figure 5.5. Stokes-Einstein equation.

Additionally, through this technique it is possible to obtain information regarding the surface charge of the nanoparticles, also known as zeta (ζ -) potential. ζ -potential is useful to predict the stability of the dispersions or the electrostatic interactions. Most of the nanoparticles dispersed in water have a surface charge, induced by ionization or absorption of charged species. The charged particles in solution are surrounded by different ionic layers, whose composition is different from that of the bulk. When moving in solution, the particles move together with a double ionic layer.

The ζ -potential appears to be the main force of interactions between the particles, and for this reason allows to predict the stability of a suspension. In fact, a high ζ -potential value (i.e. $<-30\text{mV}$ and $>+30\text{mV}$) indicate particles that reject each other keeping the formulation stable. On the other hands, ζ -potential values close to neutrality are associated with the high tendency of particles to interact, thus giving rise to aggregation and flocculation phenomena.

5.4.2. Atomic Force Microscopy (AFM)

Atomic force microscopy (AFM), also known as scanning force microscopy (SFM), is one of the most common techniques for morphological characterization of liposomes [8,9]. AFM is largely exploited in the field of nanoparticles since it provides high nanoscale spatial resolution combined with minimal sample preparation that preserves unaltered the sample characteristics. Indeed, compared to scanning electron microscopy (SEM) and transmission electron microscopy (TEM), which require complex sample preparation such as chemical fixing or metal coating, AFM leaves unaltered the surface to be scanned [10,11].

In AFM technique (**Figure 5.6**), the sample is mounted on a stage and a sharp tip, which is fixed to a cantilever, is placed in proximity to the sample surface. Weak interaction forces between the tip and the sample are established and transduced into changes of the cantilever motion. Several different aspects of the cantilever motion can be used to quantify the interaction between the tip and sample, most commonly the value of the deflection, the amplitude of an imposed oscillation of the cantilever, or the shift in resonance frequency of the cantilever. The deflection and motion of the cantilever are recorded by a detector.

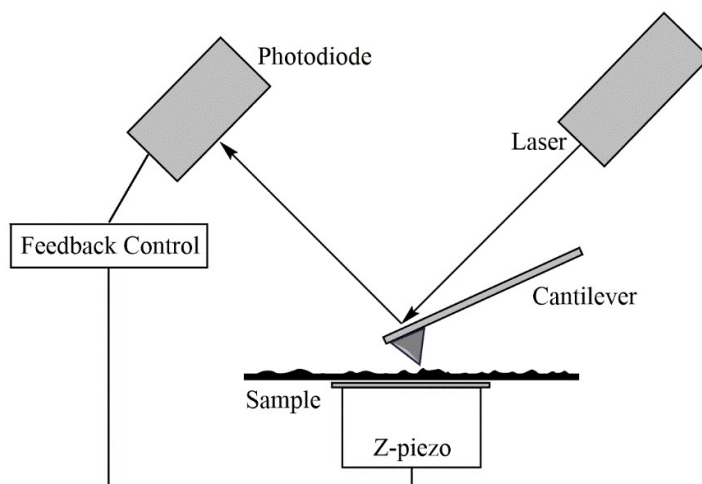


Figure 5.6. Schematic representation of the operation of the AFM technique.

There are several ways to scan the sample surface, depending on the application and the nature of the tip motion. Imaging modes can be in general be classified as static, also called contact, or dynamic, or tapping, modes [12].

In contact mode, the tip is gently dragged over the sample surface and the details of the surface can be measured either by directly measuring the deflection of the cantilever or by using the feedback

signal required to keep the cantilever at a constant position. In the contact mode, the forces involved are mainly repulsive. The main drawback in contact mode is that side forces could possibly distort the image and capillary forces due to a fluid layer can cause significant hindrance to the probe-sample interaction.

In tapping mode, the cantilever is driven by a small piezo element to vibrate or oscillate up and down near its resonance frequency. The frequency and amplitude of the driving signal are kept constant to have a constant amplitude of the cantilever oscillation in the absence of drift or interaction with the surface. The interaction of forces acting on the cantilever when the tip and the surface enter in contact, such as Van der Waals, dipole-dipole or electrostatic interactions, cause the amplitude of the cantilever's oscillation to change (usually decrease) as the tip gets closer to the sample. This amplitude is monitored by an electronic servo that adjusts the height of the cantilever to maintain constant the oscillation amplitude along the sample scanning. By imaging the force of the intermittent contacts of the tip with the sample surface, a tapping AFM image is produced. Tapping mode imaging is usually favourable for the visualization of lipid vesicles, since it is gentler than contact mode and does not modify the sample characteristics, thus is suitable for elastic materials. Additional information can be collected observing the height of the sample. As a result, the height/diameter ratio can be calculated [13].

5.5. Liposome applications

Thanks to their characteristics, liposomes can find multifold applications, from the medical to the pharmaceutical and to the cosmetic field, due to their high affinity with the epidermal stratum corneum. Regarding the medical and pharmaceutical applications, however, liposomes can be employed both for therapeutic and diagnostic purposes. The ability of liposomes to isolate their contents from the outer environment is particularly useful in the delivery of perishable substances (such as, for example, proteins and nucleic acids). At the same time, liposomes can be exploited to reduce the toxicity of certain drugs. This is the case, for example, of doxorubicin - an anticancer drug largely used for ovarian and prostate cancer - that, if encapsulated in long-range liposomes, shows altered pharmacokinetics, as well as reduced toxicity and improved effectiveness.

Liposomes were initially proposed as simplified models of cell membranes since they faithfully reproduce the arrangement of phospholipids in membrane bilayers [14].

Over the years, liposomes have gained attention for their ability of carrying therapeutics, thanks to their high versatility combined with their high biological compatibility. Indeed, due to their

amphiphilic properties, drugs with different partition coefficients can be incorporated into liposomes allowing control of the degradation rate and the harmful side effects. Moreover, the similarity of liposomes to biological membranes makes them non-immunogenic, physiologically inert and highly tolerated by the organism [15].

Liposome surface and composition can be finely modulated to achieve the desired distribution and pharmacokinetics, promoting controlled and sustained drug release together with drug accumulation in the targeted site of action [16,17].

To face the complexity and multifactoriality of many disease states and healing processes, several strategies can be combined in the so-called stimuli responsive liposomes, going from internal (biologically occurring) stimuli such as pH, temperature, redox microenvironment, to external stimuli, such as magnetic field, ultrasound, light and heat.

As far as the fatty acid residues of the membrane phospholipids are concerned, changes of the unsaturation index and of the double bond geometry of natural fatty acids affect physical properties of the membrane bilayer, such as fluidity and permeability, with consequences on the surface interactions, protein functioning and lipid signalling.

In particular, we were interested in the geometry of the double bonds, given the evidence that in bacteria the conversion from *cis* to *trans* geometry is enzymatically induced to create a membrane barrier, as a protective mechanism against high temperatures or high toxic substance concentrations of the surrounding environment (**Chapter 1, Paragraph 1.2**). In humans, such enzymatic transformation does not occur.

In the last two decades the occurrence of *trans* lipids has been reported in foods that have undergone industrial procedures such as partial hydrogenation and deodorization (**Chapter 1, Paragraph 1.4**) but also as the results of endogenous reactions induced by sulfur centered radicals, that cause the *cis-trans* double bond isomerization of biological lipids (**Chapter 1, Paragraph 1.3.2**).

The idea that TFA incorporation in the fluid mosaic of cell membranes affects their assembly properties and in vivo functions is sustained by the effect of high dietary consumption of these unnatural lipids. In fact, cell membrane incorporation of TFAs is associated with the rise in several endothelial dysfunction markers - including ICAM-1 intercellular cell adhesion molecules, VCAM-1 vascular cell adhesion molecules and E-selectin - and with the loss of vasodilatory endothelium-mediated response (**Chapter 1, Paragraph 1.5**).

So far, the *trans* geometry of the cell membrane fatty acid pool has been poorly addressed. Some preliminary differences between *cis*- and *trans*-containing monounsaturated liposomes, regarding

diameter and fluidity properties, were found, which could be related to the molecular shapes [18,19]. Whether such variations induced by *trans*-phospholipids might be used for imparting differences in drug encapsulation efficiency or release profile, influencing liposome stability and drug leakage, it is not known so far.

In this study we report the effects induced by the presence of *trans*-phospholipids on size, ζ - potential and stability of liposomal formulations. In liposome formulations containing known components (such as cholesterol, neutral phospholipids and cationic surfactants) and differing for their *cis*- or *trans*-phospholipid geometry, the encapsulation efficiency and the in vitro release of two different dyes, rhodamine B and fluorescein (commonly used to study the properties of different nanocarriers [20,21], were compared. In perspective, the results suggest that *trans*-phospholipids may be interesting players in antitumoral formulations, because of their ability to influence the liposome behavior; the synergy of the drug effect with the *trans* geometry of phospholipids can be envisioned as an innovative antitumoral strategy. It is worth mentioning that the formation of *cis* double bonds (stearic to oleic acid transformation) is a crucial enzymatic pathway involved in tumorigenesis [22,23].

5.6. Experimental part

1,2-dipalmitoyl, phosphatidylcholine (DPPC), 1-palmitoyl,2-oleoyl, phosphatidylcholine (POPC), and 1-palmitoyl,2-oleoyl, phosphatidylethanolamine (POPE) were purchased from NOF American Corporation (Irvine, CA, USA). Sodium sulfate anhydrous, phosphate-buffered saline (PBS) tablets, cholesterol and myristoyl trimethylammonium bromide (MTMAB) were purchased from Sigma Aldrich (St. Louis, MO, USA). Rhodamine B was purchased from Janssen Chimica (Beerse, Belgium) and fluorescein was purchased from Merck (Darmstadt, Germany). 2-mercaptoethanol (98% purity) was purchased by Alfa Aesar (Karlsruhe, Germany). 30% ammonium hydroxide (NH₄OH) aqueous solution was purchased from Panreac Quimica SA (Barcelona, Spain). Potassium hydroxide (KOH) was purchased from Riedel De Haen AG (Seelze, Hannover, Germany). isopropanol (Analytical grade) and chloroform (HPLC grade) were purchased from Fisher Scientific (Atlanta, GA, USA). Methanol and *n*-hexane, were purchased from Macron Fine Chemicals (Center Valley, PA, USA). Silica gel thin-layer chromatography was performed on Merck silica gel 60 plates (0.25 mm thickness) and the spots were detected by spraying the plate with cerium ammonium sulphate reagent. Standard methyl ester references (FAME mix C14-C22 and 37 component FAME mix) were commercially available from Supelco (Bellefonte, PA, USA) and were used without further

purification. *Trans* FAME references were synthesized according to previously reported protocols [18, 24].

5.6.1. Synthesis and purification of PEPC

A solution of 1-palmitoyl,2-oleoyl, phosphatidylcholine, POPC (60 mg, ca. 0.079 mmol) in isopropanol (4 mL) was placed in a vial and degassed with argon for 20 minutes. Then, 2-mercaptoethanol (2.73 mg; 0.035 mmol) was added, and the solution was irradiated for 1h (dose rate = 2.84 Gy/min). The crude reaction product was purified to pure phospholipids (59 mg; 0.077 mmol; 98% yield) using the chromatographic procedure described in literature [18]. Briefly, the solvent was evaporated and the crude reaction product was dissolved in chloroform and charged on a silica column conditioned with chloroform/methanol (8:2 v/v). The sample was collected in one fraction procedure using chloroform/methanol/water/30% NH₄OH aq (20:10:0.4:0.2 v/v) mixture as mobile phase. The purity of phosphatidylcholine was verified by TLC using the above specified eluent (R_f = 0.5). A small aliquot underwent GC analysis to determine the *trans* isomer content. In the product, 60% of oleic acid was converted in the corresponding *trans* isomer, elaidic acid. To this phosphatidylcholine mixture was given the name of 60-PEPC.

5.6.2. Liposome preparation

LUVETs were prepared using the hydration-extrusion technique. Briefly, POPC (76 mg; 0.1 mmol) or a mixture of phospholipids with the same molarity were dissolved in chloroform/methanol (2:1 v/v) until a clear lipid solution was obtained. The organic solvent was removed using a rotary evaporator to yield a homogeneous lipid film on the sides of a round bottom flask. The lipid film was thoroughly dried to remove residual organic solvent by placing the vial or flask on a vacuum pump for 1 h. The dried lipid film was left to hydrate for 30 minutes in PBS and then vortexed for 10 minutes until a milky mono-phasic solution containing MLVs was obtained. For high transition lipids, PBS 1X was warmed up above the phase transition temperature (T_m) of the lipid with the highest T_m before adding to the dry lipid, and all the steps that follow were done under the same conditions. Once a stable suspension was formed, MLVs were downsized to LUVETs using a LiposoFast hand extrusion device (Avestin Inc., Ottawa, ON, Canada) equipped with 100 nm pore size polycarbonate filters through which the lipid suspension was passed 19 times, controlling the temperature with a heat block when required. The resulting suspension was used in the encapsulation and release experiments with the same molarity (i.e., 10 mM).

5.6.3. Dye encapsulation

Rhodamine B (MW 479.02 g/mol) and fluorescein (MW 332.31 g/mol), were chosen as inexpensive and common luminophore drug models.

Starting from a 5 mM total lipid concentration, 1:1, 1:10, 1:50 and 1:100 dye/lipid ratio were tested in order to determine the optimal encapsulation conditions. Lipids were first dissolved in chloroform then dried to form a thin lipid film using the rotary evaporator and left under vacuum for 30 minutes. 10 mM stock solutions of rhodamine B (in PBS) and fluorescein (in methanol) were used to prepare the dye-containing diluted solutions used to rehydrate the thin lipid film. In the case of rhodamine B, the diluted solution could be immediately used to rehydrate the lipid film, while fluorescein solution in methanol was added to the lipid film prior to the vacuum step in order to remove any trace of organic solvent. The lipid suspension was left 30 minutes to hydrate and then vortexed for 10 minutes. When freeze-annealing-thaw cycles were required, the samples were frozen at -196 °C using liquid nitrogen (3 minutes), left to anneal at 0 °C in an ice bath (30 minutes) and then thawed at 40 °C in a liquid bath (30 minutes). Four different procedures were tested. *Method A*: samples underwent 10 minutes vortexing performed at 22 °C; *Method B*: the vortexing step of 10 minutes duration was carried out at 40 °C, followed by two sonication cycles, each one of 5 minutes; *Method C*: after 10 minutes vortexing at 22 °C, samples underwent two freeze-annealing-thaw cycles; *Method D*: samples were vortexed for 10 minutes at 22 °C and then subjected to five freeze-annealing-thaw cycles. The non-encapsulated dye was removed by sequential centrifugations (18000 g × 4 °C × 30 min) and washed with fresh PBS until a transparent supernatant was obtained. Rhodamine B concentration was determined by measuring its absorbance at 553 nm using a V-560 Jasco UV/Vis Spectrophotometer. The dose-response curve was linear ($r= 0.999$) in the concentration range of 0.1-10 µM. Fluorescein concentration was determined by measuring its absorbance at 491 nm and its fluorescence at 512 nm, using a Fluorostar OPTIMA Spectrophotometer. The dose-response curve was linear in the concentration range of 0.5-100 µM in absorbance ($r= 0.9994$) and 0.01-5 µM in fluorescence ($r= 1$). The measurements were recorded both in PBS 1X and in 30% ethanol.

5.6.4. Encapsulation Efficiency (EE%)

After removal of the non-encapsulated dye, the pellet of dye-containing liposomes was dissolved in 30% ethanolic aqueous solution and thoroughly sonicated in order to fully disrupt the liposome pellet and release the encapsulated dye (Direct method). This method was preferred over the commonly used detergent treatment with 10% Triton X-100 because this latter one induced a significant

quenching in the fluorescence. The encapsulated amount of dyes was confirmed by measuring the not encapsulated dye (Indirect method) using the following equation:

$$\text{Encapsulation Efficiency (EE\%)} = \frac{(\text{Initial}_{\text{Dye}}) - (\text{Free}_{\text{Dye}})}{\text{Initial}_{\text{Dye}}} \times 100$$

5.6.5. *In vitro* release study

Cellulose dialysis membranes with a MWCO of 12-14000 Daltons and 28.6 mm diameter (Visking Medicell International, London, UK) were hydrated using PBS 1X. 0.5 mL of the dye-loaded liposome suspension (10 mM lipids, pH 7.4) was placed into the dialysis bag, which was then transferred into a becker containing 10 mL of PBS 1X. The becker was put on a magnetic stirrer and kept continuously under stirring. The dye release was monitored at 22 and 37 °C to simulate storage and physiological conditions, respectively. For comparison, a solution of free dye dissolved in PBS was analysed under the same conditions. Samples of 1 mL volume were withdrawn at fixed time intervals (30 minutes, 1, 2, 4, 8 and 24 hours) and analyzed by UV/Vis or fluorescence spectroscopy.

5.6.6. Lipid extraction and GC analysis

Liposome phospholipids were isolated using the well-established Folch Method (**Chapter 2, Paragraph 2.2**). Briefly, the liposomal suspension in PBS 1x was treated with 2:1 chloroform/methanol (2:1 v/v) mixture. The organic phase was collected and dried using anhydrous sodium sulphate, evaporated and left under vacuum for 30 minutes. A small fraction was analyzed by thin layer chromatography using chloroform/methanol/water (65:25:4 v/v) as eluent to check the purity of the phospholipid fraction, according to published procedures [25]. The residue was treated with a 0.5 M KOH/methanol solution and left under stirring for 10 minutes at 22 °C to convert the fatty acid residues of the phospholipids into their corresponding fatty acid methyl esters (FAMES). The reaction was quenched with water and FAMES were extracted using *n*-hexane (3 x 2 mL); the organic phase was collected and dried with anhydrous sodium sulphate. The solvent was eliminated by evaporation using a rotary evaporator, and the thin white film of the FAME was subsequently dissolved in a small volume of *n*-hexane and injected into the GC.

An Agilent 7890B gas chromatograph, with a flame ionization detector and a (50%-cyanopropyl)-methylpolysiloxane (DB-23, Agilent, USA) capillary column (60 m, 0.25 mm i.d., 0.25 µm film thickness) was used for the analysis. The initial temperature was 165°C, held for 3 minutes, followed

by an increase of 1 °C/min up to 195 °C, held for 40 minutes, followed by a second increase of 10 °C/min up to 240 °C, held for 10 minutes. The carrier gas was hydrogen, held at a constant pressure of 16.482 psi. All the methyl esters were identified by comparison with the retention times of standard references either commercially available or obtained by synthesis, as described elsewhere [18,24].

5.6.7. Dynamic Light Scattering (DLS)

Hydrodynamic diameter and ζ -potential of LUVETs were measured using DLS technique (Malvern Instruments Series, NanoZS) with a detection angle of 173°. The optimal concentration for size distribution was 1 mM, while 0.1 mM concentration was used to measure ζ -potential. All measurements were recorded at 25 °C. In the present study, the data reported are the mean values obtained from 3 measurements, each one including 10 runs of 10 seconds. The polydispersity of the sample, a reverse parameter to describe the homogeneity of the system, is reported as polydispersity index (PDI).

5.6.8. Atomic Force Microscopy (AFM)

Morphological characteristics were monitored using AFM. Tapping mode was chosen for recording image parameters. The probes used were Bruker RTESPA-300 model, unmounted Si (n-type doped Sb) with nominal constant 40-80 N/m and resonance 300-400 kHz. 20 μ L of a 10 mM liposome solution were deposited on a mica support. After 2 minutes of incubation at 22 °C, the excess of liquid was removed from a corner using a kimtech tissue. Samples were analyzed in triplicates. Results are expressed as mean \pm SD.

5.6.9. Statistical analysis

All data reported are presented as mean or percentage \pm SD (n=3). Statistical significance (p values) of the results was calculated by unpaired two-tailed Student's t-test using GraphPad Prism version 6.01 for Windows. Differences were considered statistically significant when $p < 0.05$.

5.7. Results

Trans-phospholipids were prepared by a synthetic procedure using γ -radiation (Cobalt-60 source) on the natural 1-palmitoyl,2-oleoyl, phosphatidylcholine (POPC), having the natural oleic acid (9*c*, 18:1) as monounsaturated chain, in the presence of 2-mercaptoethanol [24,26]. Thiyl radical, generated from thiol, catalyzed the conversion of oleic moiety to the corresponding geometrical isomer (9*t*, 18:1). More specifically, the product of the reaction was a *trans* fatty acid-containing phosphatidylcholine mixture, composed by 60% by 1-palmitoyl,2-elaidoyl, phosphatidylcholine (PEPC) and 40% POPC. The *trans* content was established after purification and conversion of a small sample fraction to the corresponding FAMES followed by GC analysis. This phospholipid mixture was named 60-PEPC. Another phospholipid mixture containing an intermediate percentage of elaidic acid, i.e., consisting of 30% PEPC and 70% POPC, was prepared and named 30-PEPC. Multilamellar vesicles (MLVs) were obtained from a 0.01M phosphate buffered saline (PBS) suspension of 5 mM *cis* and *trans*-containing phospholipids. The MLV suspensions were then downsized by extrusion technique using 100 nm polycarbonate membrane filters to form large unilamellar vesicles (LUVETs), which are more suitable for drug delivery purposes. Liposomes were analyzed by DLS, that gives information about the size distribution, the homogeneity and the surface charge of the liposomal suspensions, as well as on aggregation or disruptive phenomena.

5.7.1. Effect of TFAs on size and ζ -potential

The results of the particle sizing and ζ -potential measurements of the various liposomal formulations are summarized in **Table 5.1** and **Figure 5.7**.

The simplest formulation to investigate the differences due to the percentages of *cis* and *trans* bonds consisted of the natural POPC in comparison with formulations having 30-PEPC and 60-PEPC. A decrease in size was observed as the *trans* phospholipid percentage increased (**Table 5.1** - Formulation A0, A30, A60). A significant drop in size, from 149.1 ± 0.18 nm to 117.4 ± 0.55 nm ($p \leq 0.0001$), was observed by replacing POPC with 60-PEPC. As for the Polydispersity Index (PDI), that provides information about the size distribution of the suspensions, and for the average surface charge of the particles, indicated as ζ -potential, no large differences were noticed among the three formulations.

The inclusion of cholesterol in the formulation, used in a phospholipid/cholesterol molar ratio of 70:30 [27], induced an increase in size compared to natural phosphatidylcholine liposomes (**Table 5.1** - Formulations B0, B30, B60). This is one of the expected changes due to the cholesterol

interactions within the lipid bilayer, which are known to influence lipid order, bilayer width and properties, such as permeability and fluidity [28-30]. The presence of 60-PEPC (B60), but not 30-PEPC (B30), led to a decrease in size and PDI and an increase in ζ -potential compared to POPC (B0). The decrease caused by the *trans* geometry to the size and PDI in the presence of cholesterol is worth of note, since at the 60% PEPC concentration in the bilayer the cholesterol effect seems to be annihilated. This aspect could suggest an interesting connection with the role of cholesterol in the *cis-trans* isomerization process in bacteria, as protection against environmental changes (Chapter 1, Paragraph 1.2). In all cases the presence of cholesterol decreased the ζ -potential value that is a known effect such as in case of Na⁺ ion binding with the lipid head group [31], although in the presence of 60-PEPC the decrease is much less.

Due to the expanding field of gene therapy, that requires positively charged liposomes to carry negatively charged oligonucleotides, a cationic formulation containing the cationic surfactant, myristoyl trimethyl ammonium bromide (MTMAB), was also tested. In particular, formulations containing a mixture of POPC/DPPC/CHOL/POPE/MTMAB 25:25:20:15:15 or the analogous 30-PEPC or 60-PEPC in replacement of POPC, were prepared (**Table 5.1** - Formulations C0, C30, C60). Components able to synergize in the enhancement of the membrane stability were chosen in such formulations. In fact, a) 1,2-dipalmitoyl, phosphatidylcholine (DPPC) is important to preserve the thermostability of liposomes in physiological conditions, due to its high transition temperature [32,33]; b) 1-palmitoyl,2-oleoyl, phosphatidylethanolamine (POPE) is a phosphatidylethanolamine (PE) that can form stable bilayers at physiological pH when intercalated with other amphiphilic molecules, although protonation of its carboxylic group in an acidic environment causes the shift to the inverted hexagonal phase that destabilizes the liposome structure. For this reason, PE is widely used in cancer gene therapy since it can lead to lysosome destabilization and selective drug release in the acidic extracellular tumour environment [34,35]; c) MTMAB is a quaternary surfactant able to enhance the cellular internalization and the DNA transfection in gene therapy [36,37]. Indeed, cationic liposomes appear to be the safest and cheapest alternative to viral vectors for protecting DNA from enzymatic degradation and efficiently delivering high molecular weight molecules without provoking dangerous immunological responses [38-40]. The diameter range of the three cationic formulations was smaller compared to the above-mentioned ones and their ζ -potentials were close to +20 mV. The presence of surface positive charges, as observed in this case, induces electrostatic repulsions that prevent formation of aggregates or flocculation of liposomes. Moreover, positive net charges could promote the interaction of liposomes with cells, due to the asymmetric membrane lipid distribution of phosphatidylserine that confers a negative charge to cell membranes [41]. Very small

values of PDI (< 0.15) were recorded for POPC and 60-PEPC formulations, which indicates narrow monodisperse systems.

Table 5.1. Average size diameter, polydispersity index and ζ -potential of various liposomal formulations. The values are given as mean \pm SD. Each experiment was performed in triplicate ($n=3$).

Formulation	Composition	Size (nm)	PDI	ζ -potential (mV)
A0	POPC	149.1 \pm 0.18	0.18 \pm 0.01	-6.03 \pm 1.05
A30	30-PEPC	144.45 \pm 0.78	0.11 \pm 0.06	-4.35 \pm 0.95
A60	60-PEPC	117.40 \pm 0.55	0.16 \pm 0.01	-2.98 \pm 0.86
B0	POPC/CHOL 7:3	170.70 \pm 2.19	0.31 \pm 0.01	-7.52 \pm 1.23
B30	30-PEPC/CHOL 7:3	167.80 \pm 2.51	0.32 \pm 0.01	-7.22 \pm 0.56
B60	60-PEPC/CHOL 7:3	156.60 \pm 1.03	0.17 \pm 0.01	-3.45 \pm 0.97
C0	POPC/DPPC/CHOL/POPE/MTMAB 25:25:20:15:15	138.2 \pm 0.95	0.09 \pm 0.03	+20.5 \pm 1.45
C30	30-PEPC/DPPC/CHOL/POPE/MTMAB 25:25:20:15:15	134.7 \pm 1.85	0.31 \pm 0.12	+20.9 \pm 0.98
C60	60-PEPC/DPPC/CHOL/POPE/MTMAB 25:25:20:15:15	134.5 \pm 0.28	0.13 \pm 0.19	+19.2 \pm 1.11

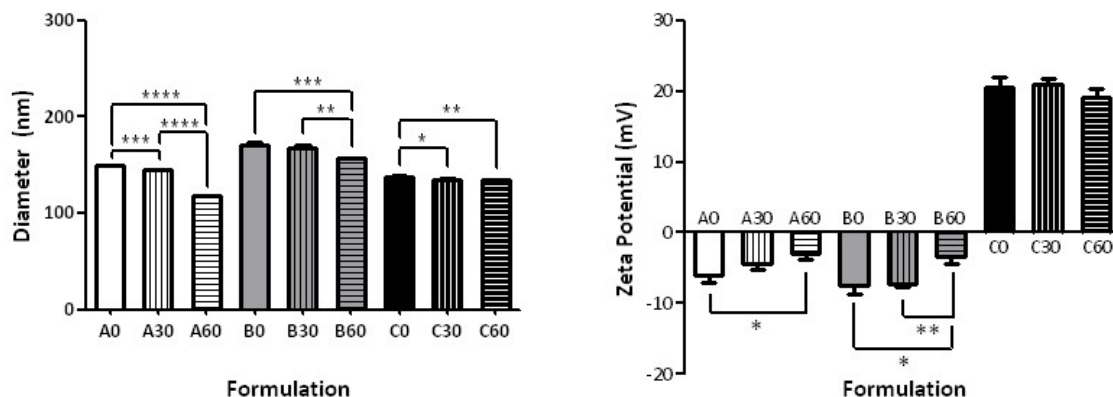


Figure 5.7. Size distribution and ζ -potential of various liposomal formulations (taken from **Table 5.1**). Significant differences (p value) are reported as follow: (*) $p \leq 0.05$, (**) $p \leq 0.01$, (***) $p \leq 0.001$, (****) $p \leq 0.0001$.

In general, it was observed that, as the *trans* content in the membrane increases, the mean particle size decreased. Only small differences with the *cis* formulations were observed when 30-PEPC is used. Particle diameters greater than 100 nm, the size of the filter pores, can be explained by the interaction of the phospholipid heads with buffer ions in the surrounding environment; on the other hand, the fact that the liposome size is still <200 nm is important for the escape from complement

recognition and uptake by the mononuclear phagocytic system [42]. Smaller sizes are desired to exploit the passive targeting due to the so-called enhanced permeability and retention effect (EPR) where extravasation of liposomes into solid tumours is essential [43]. The accumulation of liposomes in tumours is size-dependent, as tumour capillaries have larger pores (100 to 700 nm in diameter) than normal blood vessels (typically <50 nm). Thus liposomes between 90 and 200 nm in diameter are able to selectively penetrate tumour capillaries [44,45].

5.7.2. Effect of TFAs on stability

Since formulations with 60-PEPC gave better results in terms of size and PDI compared to the 30-PEPC formulations, further studies were performed to understand the effect of *trans*-inclusion in liposomal membrane in comparison with *cis*-analogues. Stability studies were conducted by storing the formulations at the temperatures 22, 37 and 45 °C for 72 hours and by analyzing them by DLS, GC and TLC.

Figure 5.8 shows the DLS results for the formulations A0, B0 and C0 using commercially available POPC (left side) and for the analogous formulations using 60-PEPC (right side). The formulation A0 showed aggregation phenomena when stored at 37 and 45 °C. The formulation A60 reduced this tendency but the aggregation, driven by the neutral charge of the phospholipid employed for this preparation, could not be avoided [46].

Addition of cholesterol improved the stability of the formulations at all the temperatures, both in the presence of POPC (B0) and 60-PEPC (B60).

Good stability was also observed when the cationic formulation was tested, regardless of the inclusion of *trans* lipids (C0 and C60). Reasonably, the presence of surface charges reduced the tendency of liposomes to flocculate and form bigger particle aggregates.

TLC and GC analyses, useful to detect formation of by-products or oxidative consumption of unsaturated lipids, did not evidence any alteration in lipid composition (data not shown).

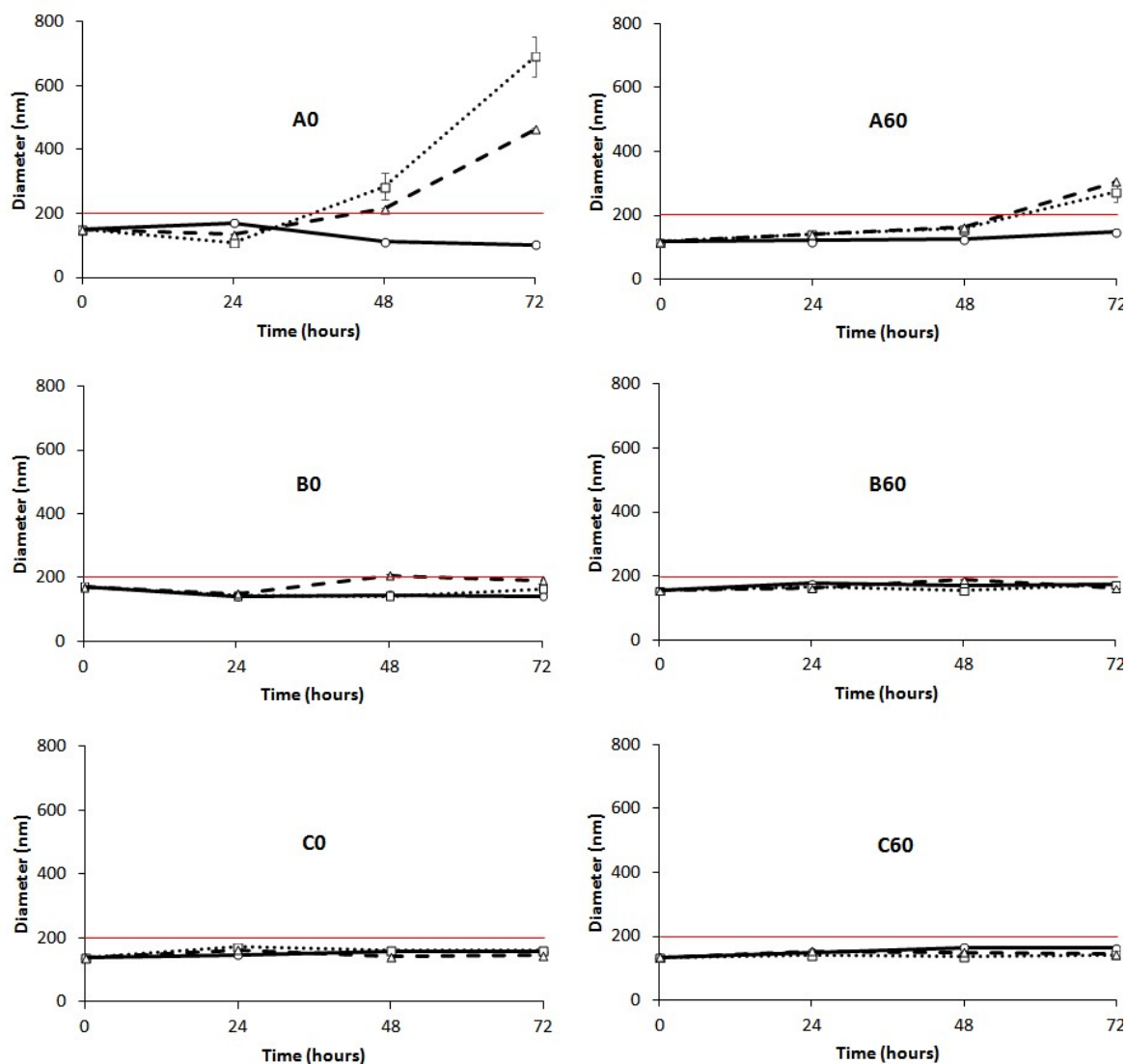


Figure 5.8. DLS measurements of liposomes at 22 °C (solid line), 37 °C (spotted line) and 45 °C (dashed line) versus time. Left side: POPC formulation A0, B0 and C0; Right side: 60-PEPC formulation A60, B60 and C60. The red line shows the size threshold of 200 nm.

5.7.3. Effect of TFAs on morphology and rigidity

POPC and 60-PEPC liposomes were analyzed by AFM, which is one of the most common techniques for liposome description. AFM provides high nanoscale spatial resolution combined with minimal sample preparation that preserves unaltered the sample characteristics. Indeed, compared to other scanning techniques, such as SEM and TEM, which require complex sample preparation such as chemical fixing or metal coating, AFM leaves unaltered the surface to be scanned. High sensitivity is reached using the tapping mode that, through small oscillations of the cantilever, permits to collect information about nanocarrier morphology and thickness. As a result, differences in rigidity can be

observed and numerically expressed by the height/diameter ratio. Measurements of approximately 10 liposome diameters were performed for each sample. The results are provided (as mean of triplicate measurements) in the **Table 5.2** and in the **Figure 5.9** a representative AFM image is shown for POPC and 60-PEPC liposomes.

Table 5.2. AFM analysis of POPC and 60-PEPC.

	POPC	60-PEPC
Diameter (nm)	145.00 ± 37.98	122.78 ± 13.15
Height (nm)	6.04 ± 1.22	9.28 ± 1.80
Height/diameter ratio	0.04	0.08

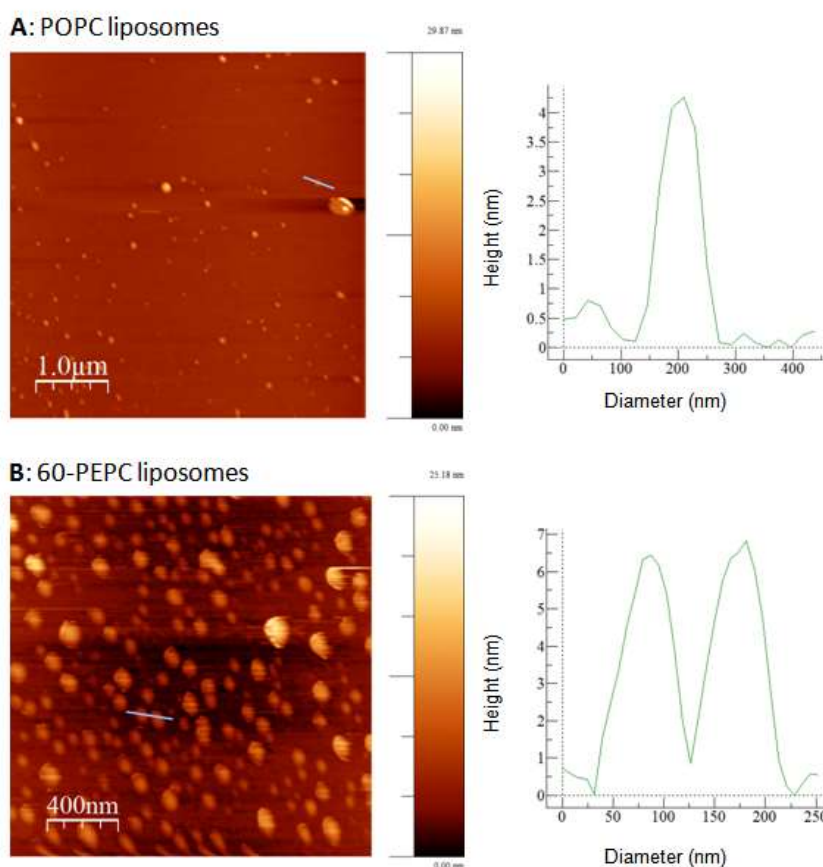


Figure 5.9. Representative AFM images (on the left) and cross-section profiles (on the right) of POPC (A) and 60-PEPC (B) liposome acquired with tapping mode.

Both formulations showed spherical shape with homogeneous distribution. POPC liposomes resulted to be larger if compared with 60-PEPC. Considering the liposome height, POPC liposomes resulted to be collapsed on the support. This property can be expressed by the height/diameter ratio that gives

general information about the liposome rigidity. Indeed, the higher the height/diameter ratio, the more rigid the system is.

These scanning probe microscopy measurements confirm the different properties of *trans*-containing liposomes compared to *cis*-containing ones, as previously shown by other techniques, detailing the features of dimensions and rigidity.

5.7.4. Effect of TFAs on encapsulation

Four different conditions were tested to ensure the maximal drug encapsulation yield, as summarized in **Table 5.3**. The conditions were optimized on the POPC formulations (A0, A30, and A60) using rhodamine B as drug model. Since rhodamine B is an aminoxanthene with amphiphilic characteristics, it was dissolved in the aqueous solution and used to rehydrate the phospholipid film. Briefly, the effect of vortexing at 22 °C and 40 °C, followed by sonication or freeze-annealing-thaw cycles was studied. The molar ratio between the dye and the lipids (D/L) played a crucial role in the successful encapsulation of the fluorescent molecule. Four different D/L of 1:1, 1:10, 1:50, and 1:100 were tested.

Table 5.3. Methods used to optimize the liposomal encapsulation of rhodamine B.

Method	Procedure
A	Vortexing (10 minutes, 22 °C)
B	Vortexing (10 minutes, 40 °C) + 2 sonication cycles (5 minutes each)
C	Vortexing (10 minutes, 22 °C) + 2 freeze-annealing-thaw cycles
D	Vortexing (10 minutes, 22 °C) + 5 freeze-annealing-thaw cycles

Results are reported in **Figure 5.10**. With the lowest D/L ratio, when the suspensions were vortexed at 22 °C for 10 minutes at maximum speed (*Method A*), only 20 to 40% of dye encapsulation efficiency (EE) was observed.

Warming up of the buffer to 40 °C prior to the hydration step, followed by two brief sonication cycles of 5 minutes (*Method B*), resulted in a significant improvement of rhodamine B loading in the liposomal vesicles. Among the three formulations, POPC liposomes (A0) were the most efficient in including the dye in the inner aqueous volume. Probably, the presence of cholesterol decreased the

encapsulation efficiency of the fluorescent molecule since it induced membrane condensation and directly competes with rhodamine B in the bilayer assembly [47].

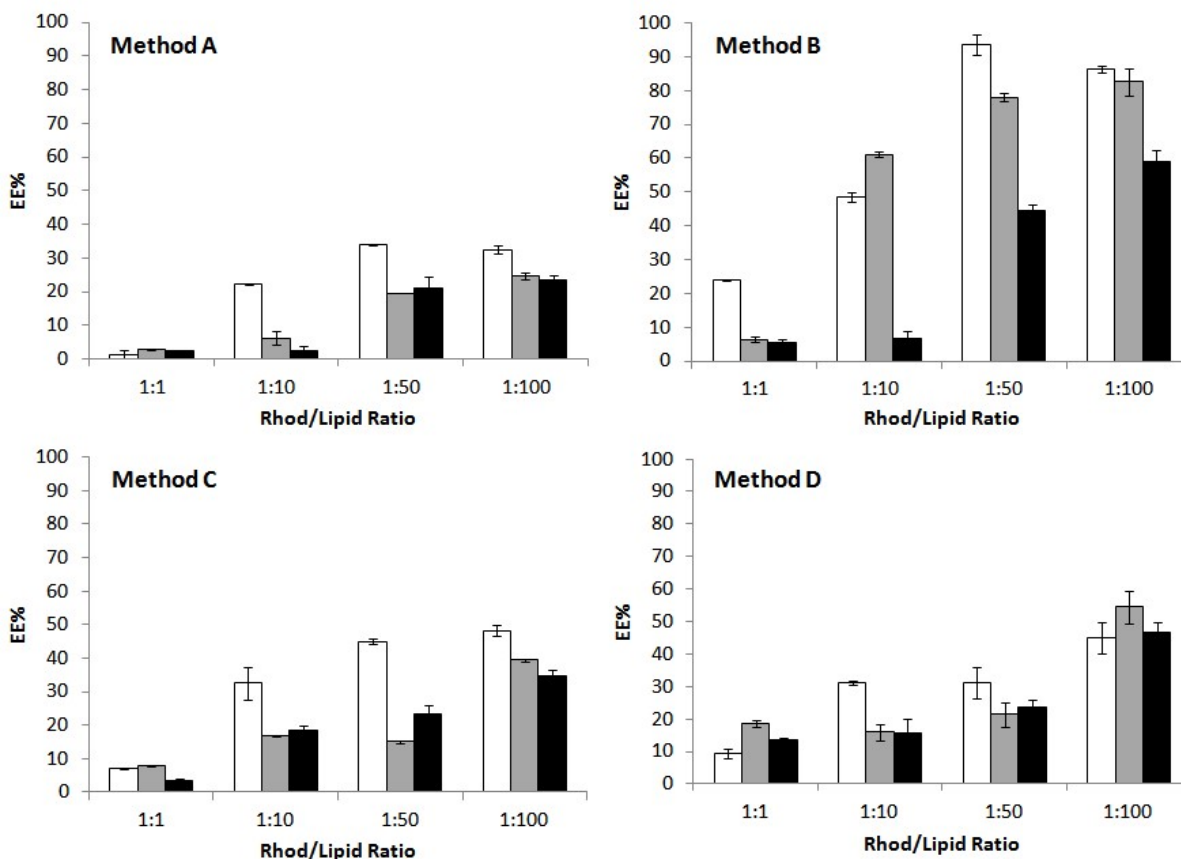


Figure 5.10. Effect of the encapsulation technique on the encapsulation efficiency (EE%) of rhodamine B in liposomes formulations A0 (white), B0 (grey) and C0 (black). The procedures are described in **Table 5.3**.

Another important technique often used to enhance drug encapsulation into nanocontainers is the freeze-thaw procedure [48,49], but high variability in the number of cycles has been reported in literature [50,51].

In this work, the sample underwent two (*Method C*) or five (*Method D*) freeze-anneal-thaw cycles (freezing to $-196\text{ }^{\circ}\text{C}$ with liquid nitrogen, annealing at $0\text{ }^{\circ}\text{C}$ for 30 minutes in ice bath, thawing at $40\text{ }^{\circ}\text{C}$ in a water bath), since drug diffusion occurring in the frozen state and fusion/destabilization of liposomes led to higher EE compared to the traditional method [52].

Apparently, an increase in the number of freeze-anneal-thaw cycles gave higher percentages of encapsulated dye but not as much as sonication. Probably, the steric hindrance of the molecule to be encapsulated does not favour its entrapment and interaction with the lipid fraction.

It is worth to underline that the molar ratio between dye and lipid was very important, since by varying the D/L it is possible to optimize the drug loading and release from liposomal formulation [53]. In this set of experiments, 1/100 was chosen as the best D/L not only because it allowed to reach 60 to 90% of EE using *Method B*, but also because using higher D/L ratio could induce drug precipitation and membrane bilayer destabilization [54]. In these formulations the total lipid concentration was 10 mM.

In the light of these results, *Method B*, that combines temperature and sonication effects, and a 1:100 dye/lipid ratio, for the best encapsulation efficiency, was chosen as the most favorable encapsulation conditions to be applied with the 60-PEPC containing formulations, i.e., A60, B60 and C60 (**Figure 5.11**).

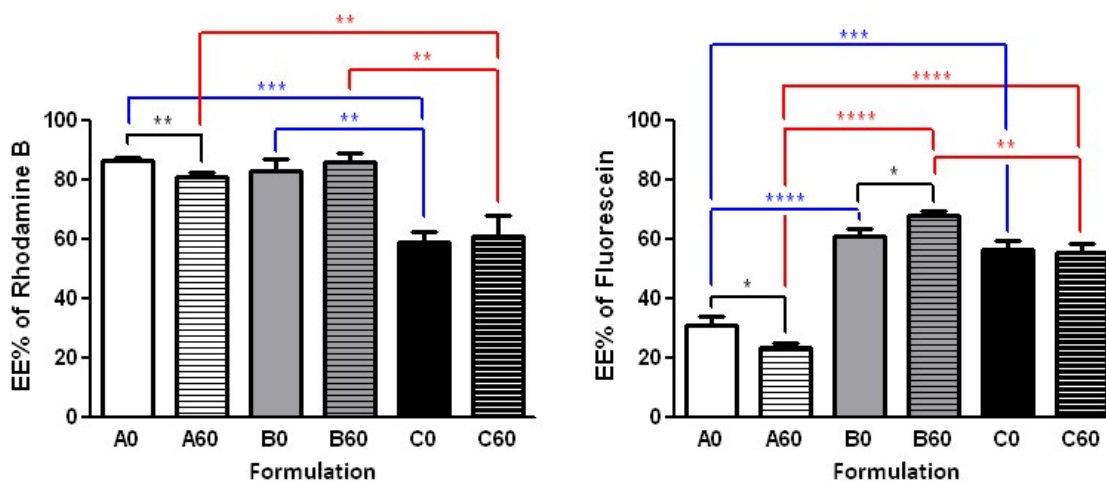


Figure 5.11. Encapsulation efficiency (EE) of rhodamine B (left side) and fluorescein (right side): in liposomes formulations A0, B0 and C0, and the corresponding formulations containing 60-PEPC (A60, B60 and C60 respectively). The encapsulation procedure was carried out at 40 °C using two sonication cycles of 5 minutes each (*Method B*) and 1:100 dye/lipid ratio. Experiments were run in triplicate. Results are shown as mean EE% \pm SD. Significant differences (p value) are reported as follow: (*) $p \leq 0.05$, (**) $p \leq 0.01$, (***) $p \leq 0.001$, (****) $p \leq 0.0001$. Differences between *cis* and *trans* containing liposomes having the same formulation (black), but also between *cis* containing formulations (blue) and *trans* containing formulations (red), are reported.

Comparing the effects of the three different formulations in the EE of rhodamine B, only the charged liposomes were less prone to incorporate the dye (**Figure 5.11**, left side). Comparing the effects of the *trans* geometry of the phospholipid (60-PEPC), the reduction of the EE was significant in case of the simplest formulation (cf., A0 vs. C0, A60 and B60 vs. C60), indicating the direct effect of the packing of these liposomes compared to simple phospholipids and cholesterol assemblies.

The same procedure was used to encapsulate a different dye, fluorescein (**Figure 5.11**, right side), an oxyxanthene insoluble in water. Here, the effect due to the hydrophobic nature of this dye is clear, leading in all formulations to a diminished incorporation compared to rhodamine B. However, both

the addition of cholesterol and of the charged lipids significantly increased EE (cf., A0 vs. B0 and C0). The effects of the *trans* geometry (60-PEPC) on these liposomes is again evident in the simplest composition (A0 vs. A60), whereas cholesterol brought a significant increase of EE for the *trans* lipid, confirming the spacing effect created by the sterol presence in the bilayer (B0 vs. B60). The charged surface of liposomes in the case of C0 and C60 resulted into an intermediate effect on EE. The presence of cationic lipids in the “C” formulation can also have a stabilizing effect on the incorporation of fluorescein, which is negatively charged at pH 7.4 ($pK_{a1} = 4.45$; $pK_{a2} = 6.8$).

5.7.5. Effect of TFAs on release

The *in vitro* release of rhodamine from the liposomal formulations at 22 °C and 37 °C was tested. Dialysis bags containing 0.5 mL of dye-containing liposomes were dialyzed against 10 mL of PBS 1 X under continuous stirring. A solution of pure rhodamine B dissolved in PBS, was used as a control to show the ability of liposome to give a controlled and sustained release over time.

In all cases the dialysis of the free dye is evidently different from the encapsulated dye formulations. They reach the same dye release in the end of the process, and no differences are seen at 22 °C (data not shown). Instead, at 37 °C the B formulation gave the best effect of retardation when 60-PEPC is present (**Figure 5.12**). In the formulations A and B, the release detected at the first hours are always reduced in the 60-PEPC liposomes, whereas in cationic liposomes these effects are lost. This could be due to the different partition coefficient of the dyes used for the experiments. It is possible that fluorescein, having hydrophobic characteristics, is localized in the proximity or in the depth of the double lipid layer and this causes it to be less retained by the liposomal structure. On the contrary, rhodamine B, which has amphiphilic characteristics, can be localized both in the internal cavity created by the liposomal bilayer and in the depth of the liposome membrane itself and for this reason it is released slower than fluorescein.

The data presented here using dyes can be extrapolated to drug encapsulation and release behaviors, highlighting the role of *trans*-containing liposomes as potential carriers with additional properties compared to the known phospholipid formulations. Resistance and release experiments, either using human plasma and cell cultures, will be required and our results suggest the utility of further work where advantages of the liposomal lipid diversity could be explored, also considering the double bond geometrical features.

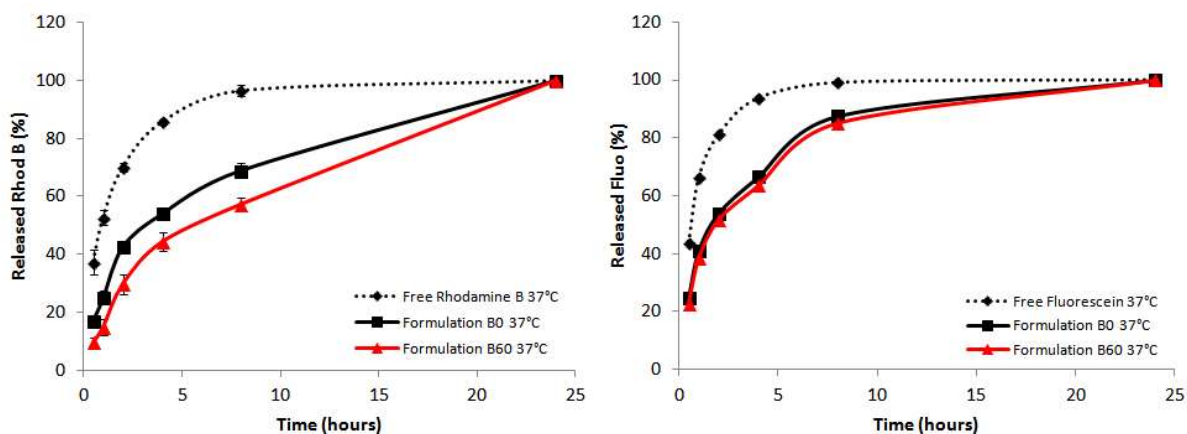


Figure 5.12. *In vitro* release of rhodamine B (left side) and fluorescein performed at 37 °C (right side). The POPC containing formulations (in black) were compared with the corresponding 60-PEPC containing ones (in red). The release profiles of free rhodamine B and free fluorescein (dashed lines) are also reported.

5.8. Conclusions

In this study, the effects of TFAs on the membrane properties of liposomal models have been investigated. In particular, different formulations containing increasing percentages of *trans*-phospholipids have been characterized in their size, surface charge (ζ -potential) and morphology. Additionally, the stability in size over time at different temperature has been monitored. Finally, since *trans* lipids are known to induce changes in the membrane permeability, the efficiency of encapsulation of two different fluorescent compounds, rhodamine B and fluorescein, and their release profiles have been described.

It emerged that *trans*-phospholipids included in membrane composition are able to affect the bilayer properties. *Trans*-containing liposomes showed reduced diameter compared to their *cis*-analogues. Moreover, AFM analyses showed that *trans*-phospholipids enhanced the rigidity of the nanoparticles, as expressed by the height/diameter ratio.

Concerning the encapsulation efficiency of the two dyes, the main differences were due to the encapsulation procedure, to the lipid formulation of liposomes and to the dye characteristics, and not to the double bond geometry.

Finally, a slightly slower release profile of rhodamine B encapsulated into *trans*-containing liposomes compared to their *cis*-analogues was observed, thus encouraging further experiments about the use of *trans*-phospholipids in drug delivery applications for the optimization of pharmacokinetics and pharmacodynamics.

The results suggest further experiments where such effects would be explored in biological membranes, where *trans* lipids can be formed by endogenous or exogenous sources. Because of the distinct features imparted to the membrane by the presence of *trans* lipids, the use of TFA-containing liposomes could be exploited for synergic effects in antitumoral strategies.

5.9. References

1. Israelachvili, J.N.; Marcelja, S.; Horn, R.G. Physical principles of membrane organization. *Q. Rev. Biophys.* **1980**, *13*(2), 121-200
2. Dua, J.S.; Rana, A.C.; Bhandari, A.K. Liposome: methods of preparation and applications. *Int. J. Pharm. Stud. Res.* **2012**, *3*(2), 14-20
3. Woodle, M.C.; Papahadjopoulos, D. Liposome preparation and size characterization. *Methods Enzymol.* 1989, *171*, 193-217
4. Gomez-Hens, A.; Fernandez-Romero, J.M. Analytical methods for the control of liposomal delivery systems, *Trends Anal. Chem.* **2006**, *25*(2), 167-178
5. Mozafari, M.R.; Johnson, C.; Hatziantoniou, S.; Demetzos, C. Nanoliposomes and their applications in food nanotechnology, *J. Liposome Res.* **2008**, *18*(4), 309-327
6. Olson, F.; Hunt, C.A.; Szoka, F.C.; Vail, W.J.; Papahadjopoulos, D. Preparation of liposomes of defined size distribution by extrusion through polycarbonate membranes. *Biochim. Biophys. Acta- Biomembranes* **1979**, *557*(1), 9-23
7. Egelhaaf, S.U.; Wehrli, E.; Müller, M.; Adrian, M.; Schurtenberger, P. Determination of the size distribution of lecithin liposomes: a comparative study using freeze fracture, cryoelectron microscopy and dynamic light scattering. *J. Microsc.* **1996**, *184*(3), 214-228
8. Ruozi, B.; Belletti, D.; Tombesi, A.; Tosi, G.; Bondioli, L.; Forni, F.; Vandelli, M.A. AFM, ESEM, TEM, and CLSM in liposomal characterization: A comparative study. *Int. J. Nanomed.* **2011**, *6*, 557-563
9. Ruozi, B.; Tosi, G.; Forni, F.; Fresta, M.; Vandelli, M.A. Atomic force microscopy and photon correlation spectroscopy: Two techniques for rapid characterization of liposomes. *Eur. J. Pharm. Sci.* **2005**, *25*(1), 81-89
10. Spyratou, E.; Mourelatou, E.A.; Makropoulou, M.; Demetzos, C. Atomic force microscopy: A tool to study the structure, dynamics and stability of liposomal drug delivery systems. *Expert Opin. Drug Deliv.* **2009**, *6*(3), 305-317
11. Spyratou, E.; Mourelatou, E.A.; Demetzos, C.; Makropoulou, M.; Serafetinides, A.A. Characterization of new drug delivery nanosystems using atomic force microscopy. In Proceedings of the SPIE 9447, 18th International School on Quantum Electronics: Laser Physics and Applications, Sozopol, Bulgaria, 8 January 2015

12. Binnig, G.; Quate, C.F.; Gerber, Ch. Atomic Force Microscope. *Phys. Rev. Lett.* **1986**, *56*(9), 930-933
13. Teschke, O.; De Souza, E.F. Liposome structure imaging by atomic force microscopy: Verification of improved liposome stability during adsorption of multiple aggregated vesicles. *Langmuir* **2002**, *18*(17), 6513-6520
14. Bangham, A.D.; Hill, M.W.; Miller, N.G.A. Preparation and use of liposomes as models of biological membranes. In *Methods in membrane biology*, Plenum Press, **1974**, pp. 1-68
15. Pattni, B.S.; Chupin, V.V.; Torchilin, V.P. New developments in liposomal drug delivery. *Chem. Rev.* **2015**, *115*(19), 10938-10966
16. Ganta, S.; Devalapally, H.; Shahiwala, A.; Amiji, M. A review of stimuli-responsive nanocarriers for drug and gene delivery. *J. Control. Release* **2008**, *126*(3), 187-204
17. Sercombe, L.; Veerati, T.; Moheimani, F.; Wu, S.Y.; Sood, A.K.; Hua, S. Advances and challenges of liposome assisted drug delivery. *Front. Pharmacol.* **2015**, *6*, 286
18. Ferreri, C.; Pierotti, S.; Barbieri, A.; Zambonin, L.; Landi, L.; Rasi, S.; Luisi, P.L.; Barigelletti, F.; Chatgililoglu, C. Comparison of phosphatidylcholine vesicle properties related to geometrical isomerism. *Photochem. Photobiol.* **2006**, *82*(1), 274-280
19. Ferreri, C.; Pierotti, S.; Chatgililoglu, C.; Barbieri, A.; Barigelletti, F. Probing the influence of cis-trans isomers on model lipid membrane fluidity using cis-parinaric acid and a stop-flow technique. *Chem. Commun.* **2006**, *5*, 529-531
20. Berkland, C.; Kipper, M.J.; Narasimhan, B.; Kim, K.K.; Pack, D.W. Microsphere size, precipitation kinetics and drug distribution control drug release from biodegradable polyanhydride microspheres. *J. Control. Release* **2004**, *94*(1), 129-141
21. Ge, J.; Neofytou, E.; Cahill, T.J.; Beygui, R.E.; Zare, R.N. Drug Release from Electric-Field-Responsive Nanoparticles. *ACS Nano* **2012**, *6*(1), 227-233
22. Igal, A.R. Roles of stearylCoA desaturase-1 in the regulation of cancer cell growth, survival and tumorigenesis. *Cancers (Basel)* **2011**, *3*(2), 2462-2477
23. Kamphorst, J.J.; Cross, J.R.; Fan, J.; de Stanchina, E.; Mathew, R.; White, E.P.; Thompson, C.B.; Rabinowitz, J.D. Hypoxic and Ras-transformed cells support growth by scavenging unsaturated fatty acids from lysophospholipids. *Proc. Natl. Acad. Sci. U.S.A.* **2013**, *110*(22), 8882-8887
24. Chatgililoglu, C.; Ferreri, C.; Ballestri, M.; Mulazzani, Q.G.; Landi, L. Cis-trans isomerization of monounsaturated fatty acid residues in phospholipids by thiyl radicals. *J. Am. Chem. Soc.* **2000**, *122*(19), 4593-4601
25. Fuchs, B.; Süß, R.; Teuber, K.; Eibisch, M.; Schiller, J. Lipid analysis by thin-layer chromatography- a review of the current state. *J. Chromatogr. A* **2011**, *1218*(19), 2754-2774
26. Ferreri, C.; Costantino, C.; Chatgililoglu, C.; Landi, L.; Mulazzani, Q.G. The thiyl radical-mediated isomerization of cis-monounsaturated fatty acid residues in phospholipids: A novel path of membrane damage? *Chem. Commun.* **1999**, *5*, 407-408

27. Briuglia, M.L.; Rotella, C.; McFarlane, A.; Lamprou, D.A. Influence of cholesterol on liposome stability and on in vitro drug release. *Drug Deliv. Transl. Res.* **2015**, *5*(3), 231-242
28. Bhattacharya, S.; Haldar, S. Interactions between cholesterol and lipids in bilayer membranes. Role of lipid headgroup and hydrocarbon chain-backbone linkage. *Biochim. Biophys. Acta Biomembr.* **2000**, *1467*(1), 39-53
29. Lee, S.C.; Lee, K.E.; Kim, J.J.; Lim, S.H. The effect of cholesterol in the liposome bilayer on the stabilization of incorporated retinol. *J. Liposome Res.* **2005**, *15*(3-4), 157-166
30. van Meer, G.; Voelker, D.R.; Feigenson, G.W. Membrane lipids: Where they are and how they behave. *Nat. Rev. Mol. Cell Biol.* **2008**, *9*(2), 112-124
31. Magarkar, A.; Dhawan, V.; Kallinteri, P.; Viitala, T.; Elmowafy, M.; Róg, T.; Bunker, A. Cholesterol level affects surface charge of lipid membranes in saline solution. *Sci. Rep.* **2014**, *4*, 5005
32. Kneidl, B.; Peller, M.; Winter, G.; Lindner, L.H.; Hossann, M. Thermosensitive liposomal drug delivery systems: State of the art review. *Int. J. Nanomed.* **2014**, *9*, 4387-4398
33. Chang, H.I.; Yeh, M.K. Clinical development of liposome-based drugs: Formulation, characterization, and therapeutic efficacy. *Int. J. Nanomed.* **2012**, *7*, 49-60
34. Seddon, J.M.; Cevc, G.; Marsh, D. Calorimetric studies of the gel-fluid (L.beta.-L.alpha.) and lamellar-inverted hexagonal (L.alpha.-HII) phase transitions in dialkyl-and diacyl-phosphatidylethanolamines. *Biochemistry* **1983**, *22*, 1280-1289
35. Lai, M.Z.; Vail, W.J.; Szoka, F.C. Acid-and calcium-induced structural changes in phosphatidylethanolamine membranes stabilized by cholesteryl hemisuccinate. *Biochemistry* **1985**, *24*(7), 1654-1661
36. Pinnaduwege, P.; Schmitt, L.; Huang, L. Use of a quaternary ammonium detergent in liposome mediated DNA transfection of mouse L-cells. *Biochim. Biophys. Acta* **1989**, *985*(1), 33-37
37. Llères, D.; Weibel, J.M.; Heissler, D.; Zuber, G.; Duportail, G.; Mély, Y. Dependence of the cellular internalization and transfection efficiency on the structure and physicochemical properties of cationic detergent/DNA/liposomes. *J. Gene Med.* **2004**, *6*(4), 415-428
38. Obata, Y.; Saito, S.; Takeda, N.; Takeoka, S. Plasmid DNA-encapsulating liposomes: Effect of a spacer between the cationic head group and hydrophobic moieties of the lipids on gene expression efficiency. *Biochim. Biophys. Acta Biomembr.* **2009**, *1788*(5), 1148-1158
39. Thomas, C.E.; Ehrhardt, A.; Kay, M.A. Progress and problems with the use of viral vectors for gene therapy. *Nat. Rev. Genet.* **2003**, *4*(5), 346-358
40. Yin, H.; Kanasty, R.L.; Eltoukhy, A.A.; Vegas, A.J.; Dorkin, J.R.; Anderson, D.G. Non-viral vectors for gene-based therapy. *Nat. Rev. Genet.* **2014**, *15*(8), 541-555
41. Fadeel, B.; Xue, D. The ins and outs of phospholipid asymmetry in the plasma membrane: Roles in health and disease. *Crit. Rev. Biochem. Mol. Biol.* **2009**, *44*(5), 264-277

42. Hupfeld, S.; Holsaeter, A.M.; Skar, M.; Frantzen, C.B.; Brandl, M. Liposome size analysis by dynamic/static light scattering upon size exclusion-/field flow-fractionation. *J. Nanosci. Nanotechnol.* **2006**, *6*(9-19), 3025-3031
43. Yuan, F.; Dellian, M.; Fukumura, D.; Leunig, M.; Berk, D.A.; Torchilin, V.P.; Jain, R.K. Vascular permeability in a human tumor xenograft: Molecular size dependence and cutoff size. *Cancer Res.* **1995**, *55*(17), 3752-3756
44. Zhu, T.F.; Szostak, J.W. Preparation of large monodisperse vesicles. *PLoS One* **2009**, *4*(4), e5009
45. Liu, D.; Mori, A.; Huang, L. Role of liposome size and RES blockade in controlling biodistribution and tumor uptake of GM1-containing liposomes. *Biochim. Biophys. Acta* **1992**, *1104*(1), 95-101
46. Bozzuto, G.; Molinari, A. Liposomes as nanomedical devices. *Int. J. Nanomed.* **2015**, *10*, 975-999
47. de Meyer, F.; Smit, B. Effect of cholesterol on the structure of a phospholipid bilayer. *Proc. Natl. Acad. Sci. U.S.A.* **2009**, *106*(10), 3654-3658
48. Pick, U. Liposomes with a large trapping capacity prepared by freezing and thawing of sonicated phospholipid mixtures. *Arch. Biochem. Biophys.* **1981**, *212*(1), 186-194
49. Aliño, S.F.; García, M.; Lejarreta, M.; Bobadilla, M.; Pérez-Yarza, G.; Unda, F.J. Trapping drug efficiency in liposomes produced by extrusion of freeze-thaw multilamellar vesicles. *Biochem. Soc. Trans.* **1989**, *17*(6), 1000-1001
50. Colletier, J.P.; Chaize, B.; Winterhalter, M.; Fournier, D. Protein encapsulation in liposomes: Efficiency depends on interactions between protein and phospholipid bilayer. *BMC Biotechnol.* **2002**, *2*, 9
51. Gjetting, T.; Andresen, T.L.; Christensen, C.L.; Cramer, F.; Poulsen, T.T.; Poulsen, H.S. A simple protocol for preparation of a liposomal vesicle with encapsulated plasmid DNA that mediate high accumulation and reporter gene activity in tumor tissue. *Results Pharma Sci.* **2011**, *1*(1), 49-56
52. Costa, A.P.; Xu, X.; Burgess, D.J. Freeze-anneal-thaw cycling of unilamellar liposomes: Effect on encapsulation efficiency. *Pharm. Res.* **2014**, *31*(1), 97-103
53. Johnston, M.J.; Semple, S.C.; Klimuk, S.K.; Edwards, K.; Eisenhardt, M.L.; Leng, E.C.; Karlsson, G.; Yanko, D.; Cullis, P.R. Therapeutically optimized rates of drug release can be achieved by varying the drug-to-lipid ratio in liposomal vincristine formulations. *Biochim. Biophys. Acta Biomembr.* **2006**, *1758*(1), 55-64
54. Johnston, M.J.; Edwards, K.; Karlsson, G.; Cullis, P.R. Influence of drug-to-lipid ratio on drug release properties and liposome integrity in liposomal doxorubicin formulations. *J. Liposome Res.* **2008**, *18*(2), 145-157

Chapter 6

DHA

6.1. Introduction

The ω -3 fatty acid DHA belongs to the family of ω -3 PUFAs, essential components of cell membranes, which play many important biological functions. In vivo, DHA is produced through a nine-step biosynthetic pathway, requiring elongation and desaturation reactions, which starts from α -linolenic acid, its essential precursor introduced by the diet.

The efficiency of the biosynthetic pathway has different degrees of efficiency in humans, therefore the semi-essential nature of DHA is emerging. DHA has gained increased interest over the years, as multiple roles in various molecular pathways and signalling networks have been described in the last decades. Noteworthy, all biological activities are dependent on the naturally occurring polyunsaturated *cis* geometry [1].

As a sign of its recognized importance in biological functions, the main international food safety and health agencies established that 100-200 mg are an adequate daily intake from dietary sources, such as algae or fish, especially for children and pregnant women [2]. This led to an increased marketing of DHA-rich formulas, both as functional foods and as nutraceuticals.

In the industrial process, the unpleasant fishy smell of fish oils is eliminated by deodorization, using high temperature and low-pressure procedures, however such conditions have been found to affect the natural *cis* structure of the PUFAs, converting them to the geometrical unnatural *trans* isomers (**Chapter 1, Paragraph 1.4.1**). The dire consequences of *trans* PUFA uptake for health have been discovered two decades ago and nowadays the presence of *trans* fats in foods is banned in the USA and is matter of careful evaluation in Europe [3].

In the frame of our research on free radical modification of biomolecules, we studied TFAs obtained by sulfur-centered radical-induced isomerization process occurring with an addition-elimination mechanism, where no double bond shift was taking place, so that only *trans* geometrical isomers were produced (**Chapter 1, Paragraph 1.3.2**).

The number of geometrical isomers for the unsaturated fatty acids is equal to 2^n , where n is the number of double bonds. In case of PUFAs, the process yields a complex mixture of isomers; by a biomimetic approach, which makes use of unilamellar liposomes as membrane models, we established that the first isomers to be formed by a step-by-step mechanism of the isomerization reaction, at a low radical concentration, are mono-*trans* fatty acids. Indeed, when ARA is exposed to thiyl radicals produced during oxidative metabolism, its mono-*trans* isomers are the most relevant products thus created, which are distinguishable from those TFAs deriving from dietary intake of chemically manipulated foods [4-6].

We undertook such studies in order to support functional investigations on the biological effects of single TFAs. In fact, the literature on the subject is scanty [7-10], owing to the limits of commercially available molecular libraries of TFAs.

Being able to obtain mono-*trans* isomers of PUFAs by synthetic and efficient routes will allow us to build up a *trans* lipid library, aimed at addressing analytical and biological applications.

Studies from our group reported the formation and the analysis of four mono-*trans* isomers of ARA [11] and of five mono-*trans* isomers of EPA [12] using a combination of GC and of carbon-13 nuclear magnetic resonance (^{13}C NMR) for the assignment of each isomer structure. In the case of EPA, the efficiency of a dual synthetic approach to obtain the five mono-*trans* isomers was tested.

The strategy consisted in the comparison of mono-*trans* isomers obtained by free radical-catalysed isomerization with mono-*trans* isomers isolated and characterized as mono-epoxide precursors (**Figure 6.1**). The separation and assignment of the mono-epoxide structures successfully provided the first unambiguous determination of the *trans* alkene position, thus integrating data already present in the literature [13-15].

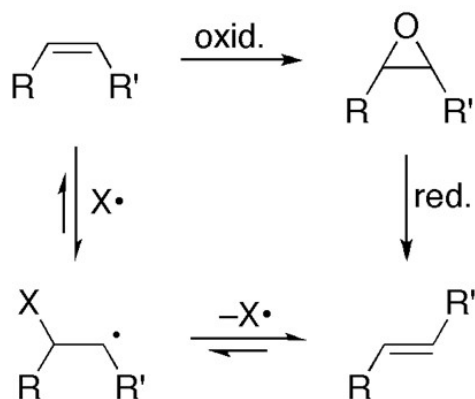


Figure 6.1. Dual synthetic approach from *cis*-alkene to obtain the geometrical *trans* isomer.

We applied the same analytical approach for the synthesis and characterization of the mono-*trans* DHA isomers. For the production of the six mono-epoxides of DHA methyl ester, published methods rely on the classical epoxidation reaction, being the yield for each individual regioisomers higher as the distance between the targeted double bond and the carbomethoxy group increased [16].

Therefore, for the chemically unstable 4,5-epoxy, docosapentaenoic (EDP) derivative, protocols have been developed for the selective synthesis of this mono-epoxide of DHA modifying a previously published three-step procedure [17,18]. In both cases the identification of mono-epoxides is reported by HPLC-MS and GC-MS analyses.

As far as *trans*-DHA isomers are concerned, only the 4-*trans* regioisomer of DHA is commercially available and can be used in GC analysis as reference, whereas all mono-*trans* DHA isomers were described under GC conditions and used to examine the deodorization/isomerization reaction, but the assignment of the *trans*-double bond position was still lacking.

The isomeric mono-*trans* DHA mixture was then characterized by GC analysis and this protocol was useful to follow up the isomerization reaction of a fish oil sample by free radical catalysed process, as well as to analyse commercially available fish oil-containing capsules.

6.2. Importance of DHA

DHA (4*c*,7*c*,10*c*,13*c*,16*c*,19*c*, docosahexaenoic acid) is a long chain polyunsaturated fatty acid (LC-PUFA) belonging to the ω -3 series [19]. Concerning its chemical structure, DHA is a carboxylic acid characterized by 22 carbon atom chain having 6 double bonds in *cis* position (**Figure 6.2**). The last double bond is located three carbons from the methyl end, thus it is a so-called ω -3 fatty acid.

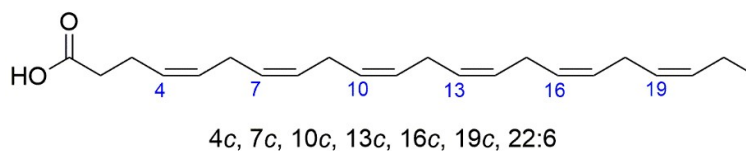


Figure 6.2. Chemical structure of DHA.

Among the PUFAs present in the human body, DHA has the longest acyl chain and the higher number of double bonds. DHA can be endogenously synthesized through enzymatic pathways, or come from dietary exogenous sources.

There are some controversies about the mechanism of DHA biosynthesis in mammals. From a synthetic point of view, DHA can be synthesized de-novo from its precursor, α -linolenic acid, that is an essential fatty acid, through a series of elongation and desaturation steps that alternatively occur in the endoplasmatic reticulum (**Figure 6.3**).

Initially, it was hypothesized that DHA could be directly formed from its immediate precursor 22:5 ω 3 by the action of a Δ 4 desaturase that introduced a double bond in position Δ 4. In lower eukaryotes, like *Thraustochytrium sp.*, the existence of a Δ 4-desaturase has been demonstrated [20], but the presence of this enzyme in mammals has never been ascertained [21].

An alternate route, that involves peroxisomes, known as the “Sprecher pathway”, has been generally accepted [22]. This pathway requires an elongation step to convert 22:5 ω 3 to 24:5 ω 3, followed by a second Δ 6-desaturation step to 24:6 ω 3; the product would finally be β -oxidated in the peroxisome to produce DHA.

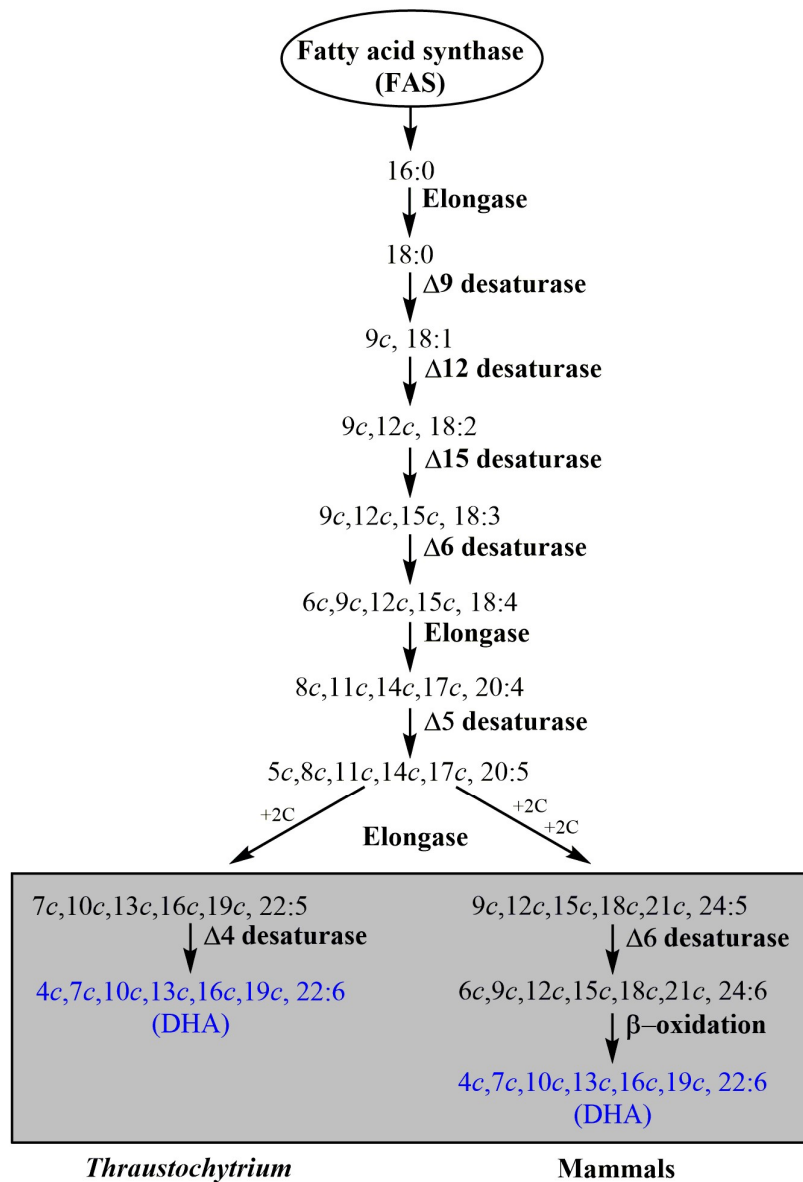


Figure 6.3. Enzymatic pathways for the synthesis of DHA in *Thraustochytrium* and mammals.

De-novo synthesis of DHA is influenced by several factors that modify the catalytic activity of some of the enzymes involved in the process; moreover, some of these enzymes compete for different PUFAs, such as the the ω-6 chain ones.

The desaturation step, carried out by Δ6 desaturase is the first and rate-limiting step of the PUFA synthesis [23,24]. This enzyme, in a similar way as Δ5-desaturase, is inhibited by cholesterol, SFAs and TFAs [Mahfouz 1981]. Additionally, the activity of both desaturases was found to be reduced by alcohol, glucocorticoids, and adrenaline [26] and in hyperlipidemia and hypertension conditions [27].

Finally, competition between α -linolenic acid and 24:5 ω 3 for the enzyme could explain the reduction in DHA levels observed following α -linolenic acid intake beyond certain values [28].

These constraints made it necessary to increase DHA assumption through the diet. In this regard, DHA can be found in discrete quantities in fish, particularly in salmon, mackerel, sardines, herring, tuna and anchovies [29]. Fish meat is enriched with DHA because a preferential fish food is microalgae, such as *Cryptocodinium Cohnii*, *Schizochytrium* and *Ulkenia*, which constitute the main source of DHA in nature [30]. Apart from these foods, DHA's dietary sources are particularly limited. Only small amounts of DHA are found in meat and in eggs, especially if the animal has been fed algae-based fodder [31].

DHA plays a crucial role in the human body. It is found in high levels in the neuronal system and in the retina because it is essential for nervous neurotransmission and visual development [32,33]. For this reason, appropriate amounts of this fatty acid must be introduced during pregnancy and breast feeding to guarantee the proper childhood development. Considerably high levels of DHA are needed in the pregnancy period that immediately precedes birth, that is when cerebral growth occurs and DHA is required for rapidly expanding neuronal cell biosynthesis [34]. Studies report that children which are not breastfed nor supplemented with DHA enriched formulas show mental retardation in comparison with children which received appropriate supplies of DHA. Nutraceutical supplementations in ω -3 fatty acids are a new trend in the prevention approach, to ensure the proper development of brain tissue, visual function and cognitive ability of fetuses and newborns. Moreover, in children affected by attention deficit and hyperactivity disorder, DHA supplementation was reported to reduce aggressivity and improve learning and social relationship ability [35,36].

Although the molecular mechanism is still unknown, DHA is hypothesized to modulate neurotransmission by improving signal transduction processes and ensuring optimum communication between nerve cells: in fact, a study on patients admitted for severe depression and other behavioral disorders (bipolarism and schizophrenia), shows that a balanced ω -3 regime reduces the frequency and intensity of depressive events and stabilized the mood [37].

As mentioned in **Chapter 5**, recent studies from our group on the cellular membrane of autistic children, DHA deficiency was observed and associated with the loss of function of Na^+ / K^+ ATPase of the erythrocyte membrane [38]. Several studies highlighted the possible role of DHA in inhibiting the progressive neurodegeneration, such as Alzheimer's disease, that may occur in the elders [34]. Concerning visual diseases, DHA can prevent senile degeneration of the macula in adults [39].

DHA is also present in considerable quantities in sperm cells, where it participates in the regulation of spermatogenesis and membrane fluidity to guarantee spermatozoa migration from seminiferous tubules to epididymis [40].

Additionally, DHA can be found in the cardiac tissue, where it is considered to reduce triglycerides in the blood. DHA enriched diets were reported to be beneficial for cardiopathic and hypertensive patients, decreasing cardiovascular risk factors, such as atherosclerosis and hypertension that are responsible for heart attacks and stroke [41,42]. Clinical benefits of dietary supplementation with DHA are reported for people suffering from rheumatoid arthritis [43] and ulcerative colitis [44]. Regulation of cell growth by DHA can have a significant impact on the development of certain types of tumors, such as colorectal, prostate and breast cancer [45-47].

Therefore, studies concerning DHA, its chemical transformations and nutraceutical use are of great interest not only for scientific research, but also for industrial and therapeutic applications.

6.3. Experimental part

Chloroform, methanol, *n*-hexane, isopropanol and acetonitrile (HPLC purity) were purchased from Merck, USA. Absolute ethanol was purchased from VWR BDH Prolabo, Poole, UK (Normapur grade) and 2-mercaptoethanol was purchased from Sigma-Aldrich, USA. Silver nitrate (AgNO_3), 30% aq ammonium hydroxide (NH_4OH), sodium bicarbonate (NaHCO_3) and anhydrous sodium sulfate (Na_2SO_4) were purchased from Carlo Erba, Italy. All FAMES used as reference standard for GC analyses were purchased from Sigma Aldrich or Fluka, USA, and used without further purification.

Silica gel thin-layer chromatography (analytical and preparative) was performed on Merck silica gel 60 plates (0.25 and 2 mm thickness, respectively).

Photolysis was carried out in a quartz photochemical reactor (Sigma Aldrich, USA) equipped with a 5.5 W low-pressure mercury lamp. The temperature was maintained at (22 ± 2) °C by means of a thermostat bath.

The gas chromatograph used for the analyses (Agilent 6850, Milan) was equipped with a (50%-cyanopropyl)-methylpolysiloxane (DB-23, Agilent, USA) capillary column (60 m \times 0.25 mm i.d. \times 0.25 μm film thickness). The instrument had a flame ionization detector (FID) that requires air (450 mL/min) and hydrogen (40 mL/min) and was maintained at a temperature of 250 °C.

Two identical equipments were used for the analyses, applying the same injection temperature (230 °C) but different oven conditions and carrier gas.

Method A: the initial temperature was set up at 165 °C and held for 3 minutes, followed by an increase of 1 °C/min up to 195 °C, held for 40 minutes. A final ramp, with a temperature increase of 10 °C/min up to a maximum temperature of 240 °C, was maintained for 10 minutes for column purge. A constant pressure mode (29 psi) was chosen with helium as carrier gas.

Method B: temperature started from 195 °C, held for 26 minutes, followed by an increase of 10 °C/min up to 205 °C, held for 13 minutes, followed by a second increase of 30 °C/min up to 240 °C, held for 10 minutes. A constant pressure mode (29 psi) was chosen with hydrogen as carrier gas.

FAMEs were identified by comparison with the retention times of commercially available standards or *trans* fatty acid references, obtained as described elsewhere [4,12,48,49].

GC/MS spectra were recorded on a Clarus 500 GC apparatus equipped with a Clarus 560S mass spectrometer (GC/MS transfer line temperature 230 °C) and a (50%-cyanopropylphenyl)-dimethylpolysiloxane (DB-225ms, Agilent, USA) column (60 m x 0.25 mm i.d. x 0.25 µm film thickness). Injection temperature was set up at 230 °C, a split ratio of 50:1 was applied and helium as carrier gas was kept at a constant flow of 1.2 mL/min. The oven conditions were the following ones: temperature started from 195 °C, held for 52 minutes, followed by an increase of 3 °C/min up to 205 °C, held for 10 minutes, followed by a second increase of 3 °C/min up to 225 °C, held for 15 minutes and a final increase of 5 °C/min up to 230 °C, held for 10 minutes.

All NMR spectra were collected with a fully automated Agilent NMR system, consisting of a 54-mm bore, 500 MHz (11.7 T) Premium Shielded superconducting magnet, a DD2 Performa IV NMR console and the Agilent OneNMR probe. All samples were dissolved in C₆D₆ and transferred in 3 mm thin wall NMR tubes (Wilmad 335-PP-8). After having calibrated the 90° pulse-width (pw90) for each sample, seven NMR experiments were performed on each sample. 2D spectra were collected with 50% nonuniform sampling (NUS) and F2 spectral width (sw) (¹H): 10 ppm, from -0.5 to 9.5 ppm.

- ¹H NMR spectra: pw 90 was calibrated for each sample, sw: -0.5 to 9.5 ppm
- one gHSQC: F1 sw (¹³C) 135 ppm, from 5.0 to 140 ppm; number of transients (nt) =32; number of increments (ni) =512; resolution (res): 33 Hz (0.26 ppm). F2 sw (¹H): 10 ppm, from -0,5 to 9,5 ppm, NUS: 50%.
- two bsgHSQCAD:
 - *First* F1 sw (¹³C): 60 ppm, from 5.0 to 65 ppm; nt=32; ni=512; res: 15 Hz (0.12 ppm); F2 sw (¹H): 10 ppm, from -0.5 to 9.5 ppm, NUS: 50%.

- Second: F1 sw (^{13}C): 20 ppm, from 120.0 to 140 ppm; nt=32; ni=512; res: 5 Hz (0.04 ppm); F2 sw (^1H): 10 ppm, from -0.5 to 9.5 ppm, NUS: 50%
- one gHMBCAD: F1 sw (^{13}C): 175 ppm, from 5.0 to 180 ppm; nt=64; ni=512; res: 43 Hz (0.34 ppm); F2 sw (^1H): 10 ppm, from -0.5 to 9.5 ppm, NUS: 50%
- two bsgHMBC:
 - First F1 sw (^{13}C): 60 ppm, from 5.0 to 65 ppm; nt=64; ni=512; res: 15 Hz (0.12 ppm); F2 sw (^1H): 10 ppm, from -0.5 to 9.5 ppm, NUS: 50%.
 - Second F1 sw (^{13}C): 60 ppm, from 120.0 to 180 ppm; nt=64; ni=512; res: 15 Hz (0.12 ppm); F2 sw (^1H): 10 ppm, from -0.5 to 9.5 ppm, NUS: 50%

6.3.1. Synthesis of mono-trans DHA-Me isomers

6.3.1.1. Synthesis by Photolysis

A 15 mM solution of all-*cis* DHA methyl ester, (20 mg, 0.058 mmol) in isopropanol (3.87 mL) was transferred into a quartz photochemical reactor (Sigma Aldrich, USA) equipped with a 5.5 W low-pressure mercury lamp. The reaction mixture was degassed with argon for 20 minutes to remove oxygen, then an aliquot of a previously degassed stock solution of 2-mercaptoethanol was added (0.03 mmol) and the UV lamp was turned on for 5 minutes at the temperature of 22 ± 2 °C, kept by means of a thermostat bath. The reaction was monitored by Ag-TLC, spraying the plate with CAM, to evidence the formation of the mono-*trans* fraction and other poly-*trans* products, and stop the reaction when mono-*trans* isomers were prevalently formed, in the presence of remaining *cis*-DHA.

The solvent was removed under vacuum, by addition of chloroform to help the removal of 2-mercaptoethanol. The crude reaction product was subsequently dissolved in 1 mL of *n*-hexane and loaded onto a preparative Ag-TLC plate. A rapid and efficient separation was obtained using diethyl ether/methanol/*n*-hexane/acetic acid (95:10:5:3 v/v) as mobile phase. After elution, the area corresponding to the mono-*trans* isomer fraction ($R_f = 0.58$), detected by spraying a small portion of the plate with CAM, was scraped off.

Silica was washed with chloroform (3 x 5 mL). The solvent was evaporated to give a solid material, which is the Ag-fatty acid complex insoluble in *n*-hexane. This material was dissolved in a 5% aqueous solution of NH_4OH , vigorously stirred (600 rpm) for 10 minutes and extracted with aliquots of *n*-hexane. Finally, the organic phase was dried over Na_2SO_4 , filtered and evaporated. The unreacted all-*cis* DHA-Me was recovered and subjected to a second isomerization cycle. This procedure led to

the collection of a colorless oil that corresponded to the mono-*trans* DHA methyl ester isomer mixture (5.2 mg, 0.0152 mmol, overall yield from two isomerization cycles 26%), that was characterized by GC and NMR analyses.

6.3.1.2. Synthesis by Epoxidation – Elimination

A 5.84 mM solution of *meta*-chloroperoxybenzoic acid in dichloromethane (2.5 mL corresponding to 0.1 eq; 0.0146 mmol; 2.51 mg) was added dropwise to a solution of DHA methyl ester (50 mg; 0.146 mmol) in dichloromethane (2.5 mL). After the addition was completed, the mixture was stirred for 10 minutes at 22 °C under argon atmosphere, following the formation of monoepoxides with traces of di-epoxides by TLC using *n*-hexane/diethyl ether (7:3 v/v) as mobile phase. Work-up was carried out by addition of 5 mL of ice-cold NaHCO₃ (25% w/v) stirred for 2 minutes. Then, the reaction mixture was transferred in a separating funnel, the aqueous layer was discarded and the organic layer was washed two times with NaHCO₃, deionized water and dried over Na₂SO₄.

The crude reaction product was purified with flash chromatography using *n*-hexane/diethyl ether (9:1 v/v) as eluent, to give a first fraction with the pure methyl(*cis*)-4,5-epoxy-all-(*cis*)-7,10,13,16,19-docosapentaenoic acid methyl ester (4,5-EDP-Me) (structure **2** in **Figure 6.8**) colorless oil (5 mg; 0.0134 mmol; 9.2% yield), followed by an inseparable mixture of 16,17-EDP-Me and 13,14-EDP-Me (colorless oil; 8 mg; 0.0223 mmol; 15.3% yield; structures **6** and **5** in **Figure 6.8**, respectively, in a 71:29 ratio, as calculated by the integration of protons of C-22 on ¹H NMR spectrum) with traces of 10,11-EDP-Me (structure **4** in **Figure 6.8**). The structural assignment of each regioisomer in the fractions was performed by dissolving the fractions in C₆D₆ as NMR solvent in which they are stable, and carrying out mono- and bi-dimensional experiments as described in the Method section. EDP-Me regioisomers **5** and **6** were further purified by preparative TLC using toluene/isopropanol (100:0.5 v/v) to give **6** (R_f = 0.5, 3 mg; 0.0084 mmol; 37.5% yield) with only traces of **5** (R_f = 0.4).

A third fraction was then isolated containing an inseparable mixture of 19,20-EDP-Me and 7,8-EDP-Me (colorless oil; 7mg; 0.0195 mmol; 13.4% yield; structures **7** and **3** in **Figure 6.8**, respectively, in a 57:43 ratio, as calculated by the integration of protons of C-22 on ¹H NMR spectrum).

The starting all-*cis* DHA-Me (**1**) was also recovered (30 mg; 0.0877 mmol; 60% yield).

6.3.2. Isomerization of fish oil by Photolysis

A sample of commercially available fish oil, from a company that provides material for ω -3 containing food and nutraceutical preparation, was isomerized following the procedure described for the DHA-Me isomerization by photolysis. The ^1H NMR and ^{13}C NMR spectra of the isomerized oil were recorded. The oil underwent a transesterification reaction as described below for nutraceutical formulas, in order to analyse the *cis* and *trans* fatty acid content by the corresponding fatty acid methyl esters.

6.3.3. Nutraceutical analysis

Nutraceutical products commercially available in Italy and Spain were examined. Lipids were extracted from the products according to the Folck method (**Chapter 2, Paragraph 2.2**). Briefly, approx. 3 mg of each sample were treated with chloroform/methanol (2:1 v/v) and brine; organic phases, containing lipids, were joined and dried over anhydrous Na_2SO_4 . After filtration, the solvent was eliminated using a rotor evaporator and the oily residue was left under vacuum for 10 minutes to remove any possible trace of water. The lipid fraction was controlled by TLC using *n*-hexane/ethyl ether (7:3 v/v) as eluent and then treated with freshly prepared 0.5 M KOH/methanol solution for 30 minutes at 22 °C under stirring. The reaction was quenched using brine and FAMES were extracted using *n*-hexane; the organic phases were collected and dried over anhydrous Na_2SO_4 . After filtration and solvent evaporation, the FAME mixture was dissolved in the appropriate volume of *n*-hexane and analysed by GC.

6.4. Results

6.4.1. Synthesis by Photolysis

According to the scheme represented in **Figure 6.1**, we approached the dual synthetic strategy first by carrying out the direct radical-catalysed isomerization of DHA methyl ester, as previously described by our group for EPA [12], thus obtaining a mixture of the six mono-*trans* DHA isomers. Ag-TLC (Chapter 2.3.1) was used to purify the mono-*trans* DHA isomers from the starting material (**Figure 6.4**).

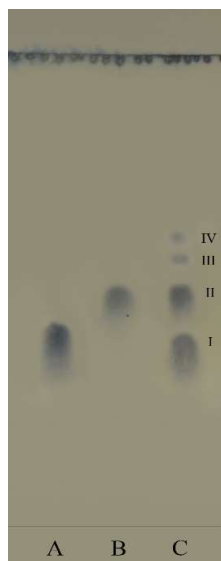


Figure 6.4. Ag-TLC after 5 minutes of isomerization under photolysis in the presence of 2-mercaptoethanol. Commercial standard all-*cis* DHA-Me (A). Mono-*trans* isomers of DHA-Me (B). Reaction mixture (C) containing all-*cis* (I), mono-*trans* (II) and traces of di-*trans* (III) and tri-*trans* (IV) isomers of DHA-Me.

The separation of each mono-*trans* isomer is not realizable at this stage, however satisfactory separation of the isomers could be obtained by gas chromatography, the GC trace showing five out of six separable peaks, meaning that only two isomers are superimposed (**Figure 6.5**). It is also worth noting that one mono-*trans* DHA isomer elutes close to *cis*-DHA.

This separation was previously described under similar conditions [50], but again the assignment of each mono-*trans* isomer was not performed. Only by elution of the commercially available 4-*trans*-DHA-Me, the third eluting peak could be assigned to this isomer.

The mono-*trans* DHA-Me mixture was also analysed by gas chromatography coupled to mass spectrometry (GC/MS). The fragmentation pattern of the mono-*trans* isomers showed the typical mass-to-charge ratios characteristic of ω -3 PUFAs, or rather $m/z=41$, $m/z=55$, $m/z=67$, $m/z=79$, $m/z=91$, $m/z=105$ and $m/z=119$ (**Appendix 1**). No other data worthy of note could be gathered at this point of the study.

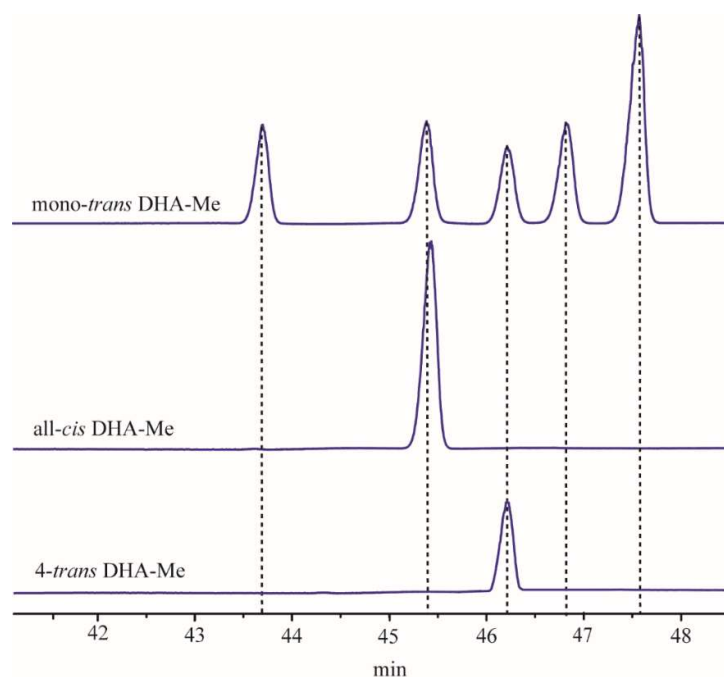


Figure 6.5. GC chromatograms showing the mixture of mono-*trans* DHA methyl ester isomers obtained after free radical isomerization by photolysis, all-*cis* DHA methyl ester and commercially available 4-*trans* DHA methyl ester.

6.4.2. Synthesis by Epoxidation – Elimination

By the second synthetic strategy, DHA-Me was transformed in two-steps to the mono-*trans* alkenes (**Figure 6.1**), via mono-epoxide formation, ring-opening of the epoxide, using the stereoselective formation of the dibromide derivatives followed by elimination reaction, that provides the *trans* geometry of each starting double bond. In this strategy, the key step is the separation and characterization of the mono-epoxide products, to assign the double bond position for the subsequent elimination step. Epoxidation of DHA methyl ester was performed using *meta*-chloroperoxybenzoic acid (*m*-CPBA), followed by purification using flash chromatography with *n*-hexane/diethyl ether (9:1 v/v) as eluent. Preparative TLC using *n*-hexane/diethyl ether (7:3 v/v) provided a separation of three fractions of monoepoxide regioisomers (**Figure 6.6**).

The structures of the six regioisomers expected in the reaction are shown in **Figure 6.7**.

Epoxydocosapentaenoic acids (EDPs) are naturally occurring compounds obtained from DHA by cytochrome P450 enzyme, exhibiting a variety of biological effects in inflammation, pain, angiogenesis and cancer [51]. Actually, cytochrome P450 is able to provide the stereoselective epoxidation of DHA, preferably at the last double bond obtaining 19,20-EDP [52]. However, also

16,17-EDP, 13,14-EDP, 10,11-EDP and 7,8-EDP have been detected and separated by HPLC analysis, whereas 4,5-EDP was reported to be unstable [53,54].

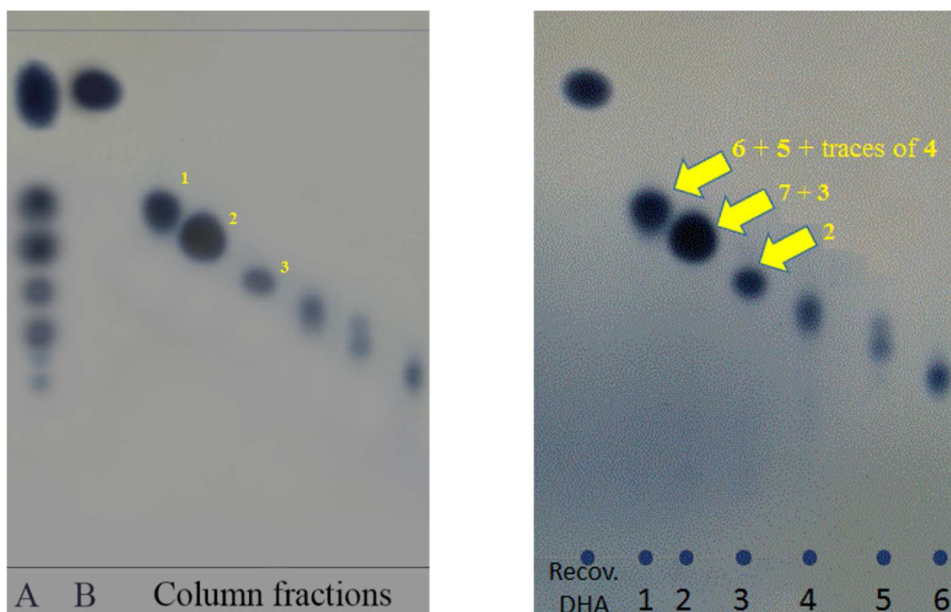


Figure 6.6. TLC after DHA-Me epoxidation and column separation. (A) Reaction mixture, (B) all-*cis* DHA-Me; Epoxide fractions: 1-2-3 mono-epoxide fractions and assignment, (right TLC), separated using *n*-hexane/diethyl ether (7:3 v/v) as mobile phase.

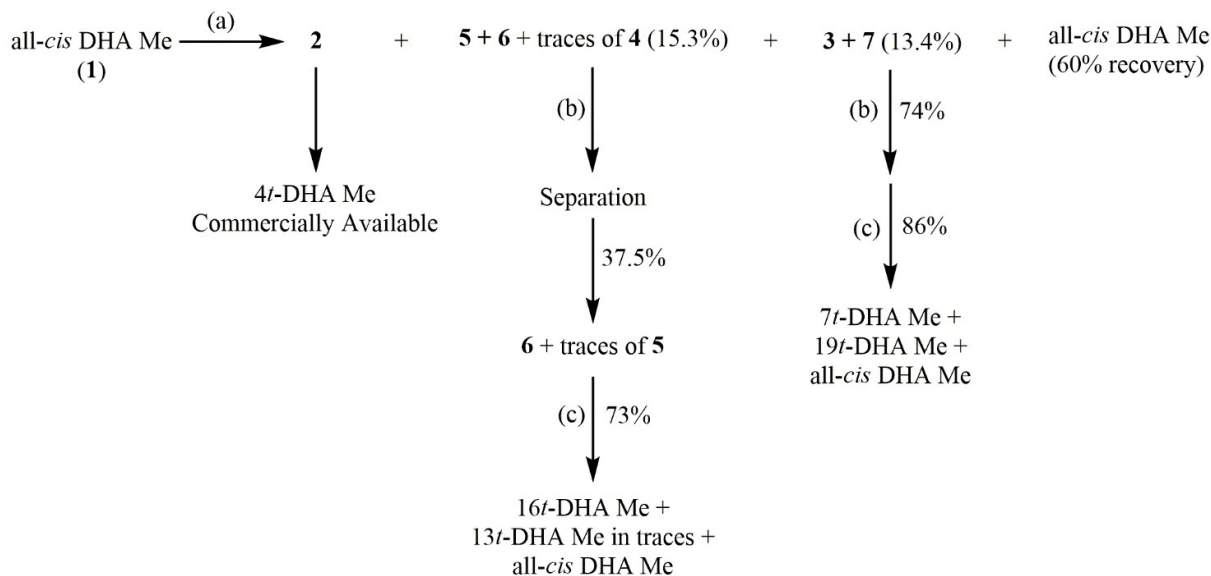


Figure 6.7. (a) *m*-CPBA, DCM, RT, 10 min; quantitative conversion based on the recovery of starting material; (b) dry DCM, pyridine, Ph_3PBr_2 , 5°C, overnight; (c) DMF, activated Zn, AcOH, 0°C, 10 h.

To the best of our knowledge, EDP analysis by NMR spectroscopy has not been reported so far, whereas we were interested to carry out mono- and bi-dimensional NMR experiments in order to

assign the epoxide position in each compounds of the reaction mixture. For stability reasons, NMR measurements were recorded in deuterated benzene (C_6D_6), since deuterated chloroform ($CDCl_3$) creates a slightly acidic environment that induces decomposition of DHA derivatives.

Under our experimental conditions, the 4,5-EDP (product **2** in **Figure 6.8**) was isolated in pure form as first fraction of the chromatography. The fraction was characterized by NMR spectroscopy (^{13}C and 1H) in $CDCl_3$ and in C_6D_6 . The spectral data were identical with those previously reported in $CDCl_3$ [17].

The other regioisomers were obtained in the subsequent two chromatographic fractions, each as mixture of two compounds. In **Table 6.1**, the ^{13}C NMR data of the EDP isomers are collected, showing that the 10,11-EDP regioisomer is present only in traces. The reasons to justify the absence of this stereoisomer were not investigated.

The C resonances were attributed by comparison with the DHA assignment individuating five EDP regioisomers for the resonances for the carbon atoms of the epoxy functionality. The ^{13}C NMR in $CDCl_3$ of two epoxy-isomers, 4,5-EDP and 19,20-EDP, were described in the literature [17,55] and for comparison they were also reported in the table together with the data obtained in this study.

The structures of the five EDP isomers with their proton and carbon atom resonances as assigned in this study are summarized in **Appendix 2**.

The subsequent transformations by ring opening as dibromides and elimination to the corresponding alkenes were performed in one-step for each fraction. The latter reaction sequence was adapted for DHA-Me from a procedure described for arachidonic acid methyl ester [56] and also eicosapentanoic acid methyl ester (EPA) [12].

Table 6.1. ^{13}C NMR Resonances of EDP isomers of DHA-Me.

Literature data (in CDCl_3)		Empirical data (in C_6D_6)						
19,20	4,5	Carbon Atom	DHA-Me	16,17	13,14	19,20	7,8	4,5
173.5	173.33	C1	172.33	172.35	172.35	172.32	172.30	172.35
130.4	132.18	C2	33.65	33.63	33.63	33.64	33.51	30.76
129.3	130.82	C3	22.75	22.75	22.75	22.76	22.83	23.42
128.4	128.74	C4	128.06	128.11	128.11	128.08	130.08	55.32
128.2	128.64	C5	129.08	129.02	129.02	129.06	125.77	56.07
128.2	128.50	C6	25.57	25.57	25.57	25.58	26.23	26.38
128.1	128.09	C7	128.11	127.87	127.87		55.63	124.78
128.1	127.96	C8	128.15	128.32	128.32	128.35 – 127.80	55.65	130.27
127.9	127.85	C9	25.66	25.66	25.78	25.75 – 25.60	26.35	25.86
127.9	127.13	C10	128.15	128.40	130.19		124.78	127.95
124.5	124.33	C11	128.15	127.70	124.76	128.35 – 127.80	130.17	128.42
58.3	56.7	C12	25.56	25.78	26.34	25.75 – 25.60	25.78	25.75
56.5	56.10	C13	128.11	130.19	55.65			128.63/128.38/128.11/128.96
51.6	51.88	C14	128.22	124.76	55.66	128.35 – 127.80	128.35 – 127.80	25.75
34.0	31.14	C15	25.67	26.34	26.35	25.79	25.75 – 25.60	25.75
26.2	26.35	C16	127.91	55.65	124.55	130.03		128.63/128.38/128.11/128.96
25.8	25.96	C17	128.50	55.79	130.53	124.96	128.35 – 127.80	128.11/128.96
25.7	25.77	C18	25.65	26.22	25.68	26.31	25.58	25.66
25.6	25.69	C19	128.11	123.66	126.82	55.75	127.06	127.19
22.8	23.49	C20	131.78	133.81	131.90	57.38	131.82	131.89
21.1	20.70	C21	20.54	20.53	20.53	21.10	20.55	20.66
10.7	14.41	C22	14.08	14.00	14.03	10.45	14.07	14.17
		C1'	50.65	50.65	50.65	50.65	50.66	50.85

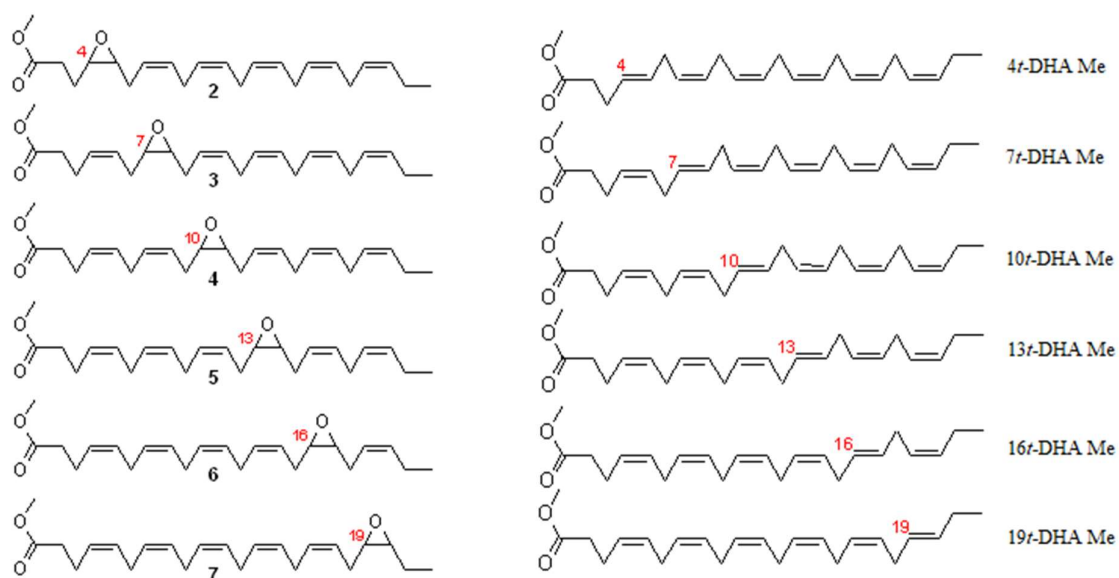


Figure 6.8. Structures of the six EDP regioisomers and the corresponding mono-*trans* DHA methyl ester isomers.

It was observed that, during the *in situ* transformation of epoxides to dibromide derivatives and the subsequent elimination to *trans* alkenes, the concerted elimination is not the only occurring mechanism, indeed *cis*-DHA-Me can be formed. Therefore, after elimination, the resulting mono-*trans* DHA products can be further purified by Ag-TLC using diethyl ether/*n*-hexane/methanol (9:1:0.4 v/v) prior to GC injection, as shown in **Figure 6.9**, in order to have a pure isomeric fraction from the elimination step.

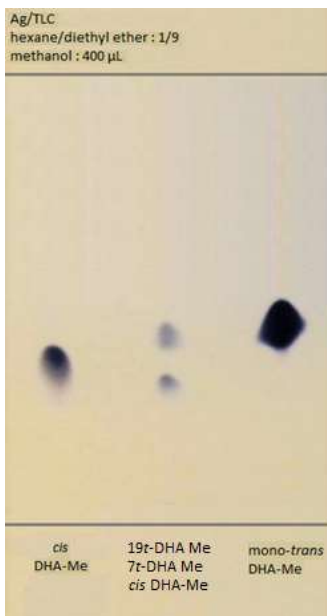


Figure 6.9. Ag-TLC showing all-*cis* DHA-Me (left), 19*trans* and 7*trans* DHA-Me isolated after after bromination and elimination reaction (center) and the mixture of mono-*trans* DHA-Me obtained by photolysis (right).

Using GC analysis after the elimination step of each mono-epoxide fraction, the panel of the mono-*trans* DHA-Me was clarified as shown in **Figure 6.10**. The 16-*trans* isomer was almost overlapping with DHA-Me, and other two mono-*trans* isomers, namely 7-*trans* and 10-*trans*, were superimposed (compare lanes (III) and (IV) corresponding to the transformation of two different mono-epoxide fractions). The 10-*trans* isomer was indeed obtained from the traces of the 9,10-EDP that was found to be the product with the lowest yield among all EDP isomers, as ascertained by the study of the NMR spectra reported in the following section.

Therefore, taking also into account previously reported retention times for some of the mono-*trans* geometrical isomers of DHA-Me, the following GC order of elution could be assigned: 19-*trans* < 16-*trans* = all-*cis* < 4-*trans* < 13-*trans* < 7-*trans* = 10-*trans*.

This is the first time that assignment of mono-*trans* geometrical isomers of the ω-3 fatty acid DHA is made, by a combination of Ag-TLC, NMR spectroscopy, gas chromatography, and this result

completes the overall picture of the non-commercially available *trans* lipid library referred to the most important polyunsaturated fatty acids.

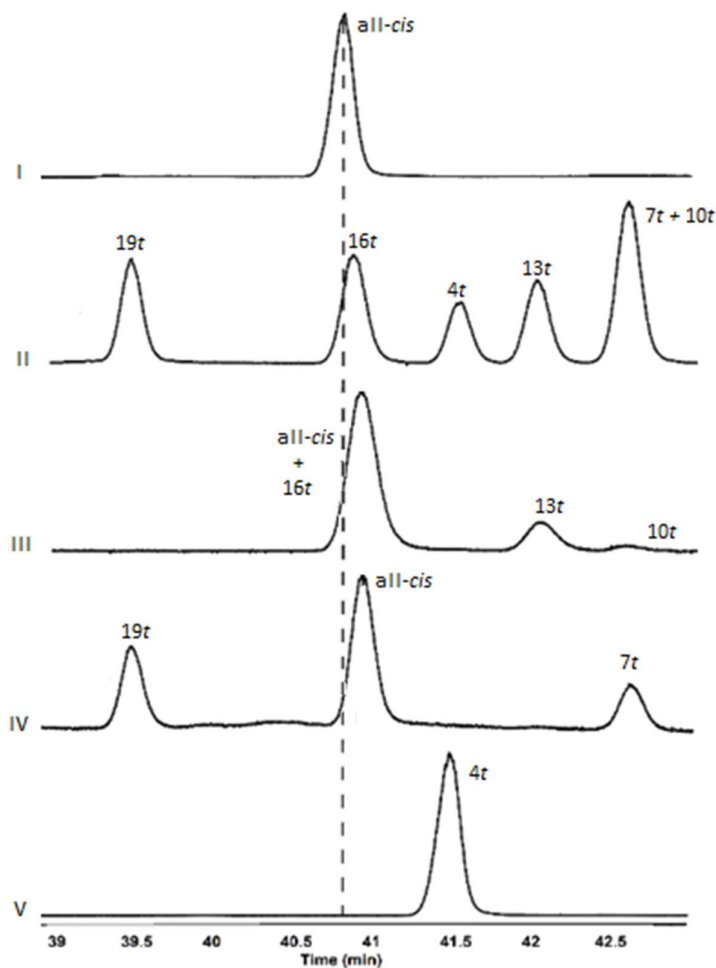


Figure 6.10. GC chromatograms of (I) all *cis*-DHA methyl ester; (II) mixture of mono-*trans* DHA-Me isomers obtained by photolysis; (III) 16-*trans* isomer superimposed with all *cis*-DHA-Me, 13-*trans* and traces of 10-*trans* isomers; (IV) 19-*trans*, all-*cis* and 7-*trans* DHA-Me; and (V) 4-*trans* DHA-Me.

6.4.3. NMR Analysis

As previously mentioned, the examination of the ^1H and ^{13}C NMR resonances were carried out in C_6D_6 to avoid decomposition of these compounds. A careful examination of the spectra obtained from the EDP isomer formed during the epoxidation allowed the structures of these regioisomers to be assigned, using mono- and bi-dimensional experiments.

A first observation came from the ^1H NMR spectra of the EDP regioisomers (see **Appendix 3,4,5**), where the terminal methyl group (C-22) appears as triplet in the 0.80-0.91 ppm region and is

influenced by the relative position of the epoxide functional group. As shown in **Figure 6.11**, in Me-DHA the triplet is centered at 0.885 ppm (trace I), whereas the pure 4,5-EDP isomer shows the triplet centered at 0.888 ppm (trace IV). Two fractions obtained from the EDP separation contained the other four isomers: i) a mixture with the 16,17-EDP isomer with the triplet centered at 0.853 ppm and the 13,14-EDP isomer with the triplet centered at 0.880 ppm, with traces of the 10,11-EDP isomer (trace II); ii) a mixture with the 19,20-EDP isomer with the triplet at 0.838 ppm (major isomer) and the 7,8-EDP isomer with the triplet centered at 0.892 ppm. The assignment of the triplet was made by correlation experiments, crossing the ^1H and ^{13}C resonances of the methyl group and epoxide carbon atoms, respectively.

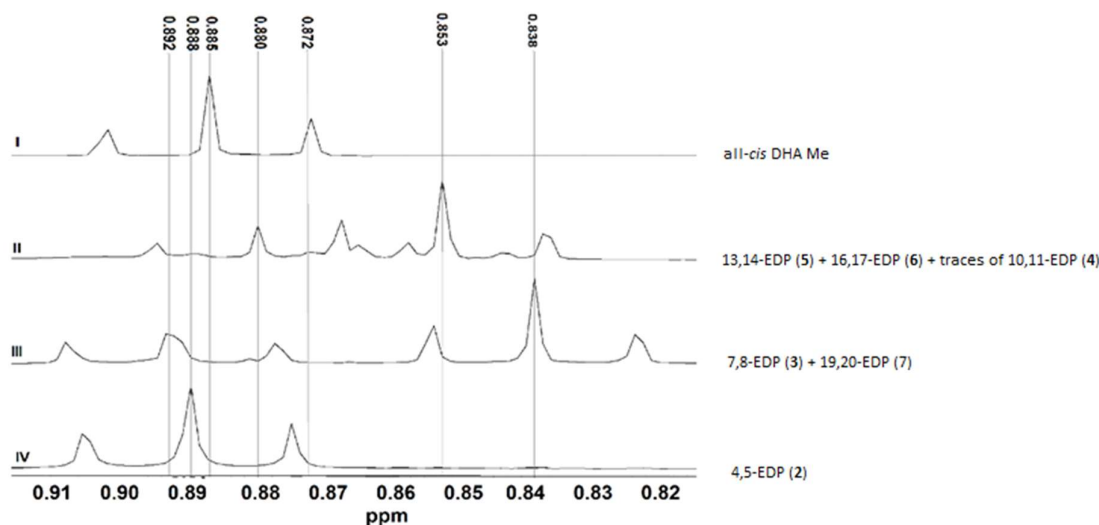


Figure 6.11. Enlargement of the ^1H NMR region related to the terminal methyl group (C-22) of EDP regioisomers. The triplet is centered at different ppm depending on the position of the epoxide along the fatty acid chain; (trace I) all-*cis* DHA-Me; (trace II) mixture of 13,14-EDP (5), 16,17-EDP (6) with traces of 10,11-EDP (4); (trace III) mixture of 7,8-EDP (3) and 19,20-EDP (7); (IV) 4,5-EDP (2).

In the ^{13}C NMR spectrum, the carbon atom resonance of the methyl ester group appears at 50.65 ppm in all EDP isomers. Using the assigned resonances of DHA methyl ester, it is also possible to assign the structures of the five mono-epoxides.

In fact, for the 16,17-EDP two peaks at 55.79 and 55.65 ppm are assigned to the carbon atoms of the epoxide function, since at the same time in the spectrum are absent the chemical shifts of the ethylenic carbon atoms assigned at this C16-C17 double bond in DHA-Me (128.50 and 127.91 ppm, respectively).

The 13,14-EDP has two peaks at 55.66 and 55.65 ppm assigned to the epoxide function, whereas the C13-C14 double bond resonances of DHA-Me at 128.22 and 128.11 ppm, are not present.

The 19,20-EDP has the epoxide carbon atoms at 57.38 and 55.75 ppm, and correspondently the chemical shifts at 131.78 and 127.11 ppm (C19-C20 of DHA-Me) are absent. In the 19,20-EDP regioisomer it is also worth mentioning the chemical shift of the C-22 shifted at 10.45 ppm (instead of the range 14.08 – 14.00 ppm for all the other EDP regioisomers), indicating an upfield shift due to a different electronic distribution influencing the end of the carbon atom chain.

7,8-EDP showed the chemical shifts of the epoxy carbon atom at 55.65 and 55.63 ppm, corresponding to the absence of the resonances at 128.15 and 128.11 ppm (corresponding to the C7-C8 in the DHA-Me).

Finally, 4,5-EDP was individuated by the chemical shifts at 56.07 and 55.32 ppm corresponding to the absence of the peaks at 129.08 and 128.06 ppm (C4-C5 of DHA-Me).

Since the synthetic pathway of mono-epoxides was of crucial importance for the identification of the regioisomers, it was very important to gather further confirmation of such assignments by running specific bidimensional NMR (2D NMR) experiments. Indeed, 2D NMR spectra provide information about a molecule that cannot be obtained by mono-dimensional NMR, and are important to determine the structure of complex molecules.

In this study, heteronuclear single-quantum coherence (HSQC) and heteronuclear multiple bond correlation (HMBC) were applied. HSQC experiment is used to determine proton-carbon single bond correlations, where the protons lie along the observed F2 (X) axis and the carbons are along the F1 (Y) axis. The results obtained by HSQC can be combined with HMBC experiments, that gives correlations between carbons and protons that are separated by two, three, and, sometimes in conjugated systems, four bonds, while direct one-bond correlations are suppressed.

The relevant correlations studied in the 2D NMR experiments for the assignment of the 19,20-EDP are shown in **Appendix 6**.

6.4.4. Isomerization of fish oil

Omega-3 containing oil are important sources of *cis* isomers, therefore the *trans*-isomers of EPA and DHA have been considered by several authors as contaminants after the deodorization or distillation procedures that are used to eliminate the fishy odour (**Chapter 1, Paragraph 1.4.2**).

Since the DHA isomerization in oil has been described to occur by heating procedure and was not yet reported by thiyl radical catalysed process, we performed the isomerization of a DHA-rich fish oil,

commercially available as raw material for nutraceutical formulas. The reaction was carried out as described in the Experimental part.

Figure 6.12 (part a) shows the superimposition of the GC traces of the fish oil isomerization (after transesterification of the triglycerides into the corresponding fatty acid methyl esters) and the appropriate references relative to the *cis* and mono-*trans* DHA isomers as obtained from the previously described dual approach.

In the same **Figure 6.12** (part b) the region of the ^{13}C NMR spectra enlarged at the region corresponding to the C-20 (ethylenic carbon atom) resonance is shown for the DHA-Me (trace I) in comparison with the *cis-trans* DHA-Me mixture (trace II). In the same Figure also the C-20 of the DHA-containing triglycerides of fish oil (trace III) is shown, and it is gratifying to see that the chemical shift are not influenced by the different derivatives (FAME or triglyceride) that contains the DHA residues. Moreover, after fish oil isomerization, also the mixture of *trans*-DHA-containing triglycerides shows similar C-20 resonances for the resulting isomer mixture. In **Appendix 7** and **8** the full ^{13}C NMR spectra of DHA-containing triglycerides before and after isomerization are shown.

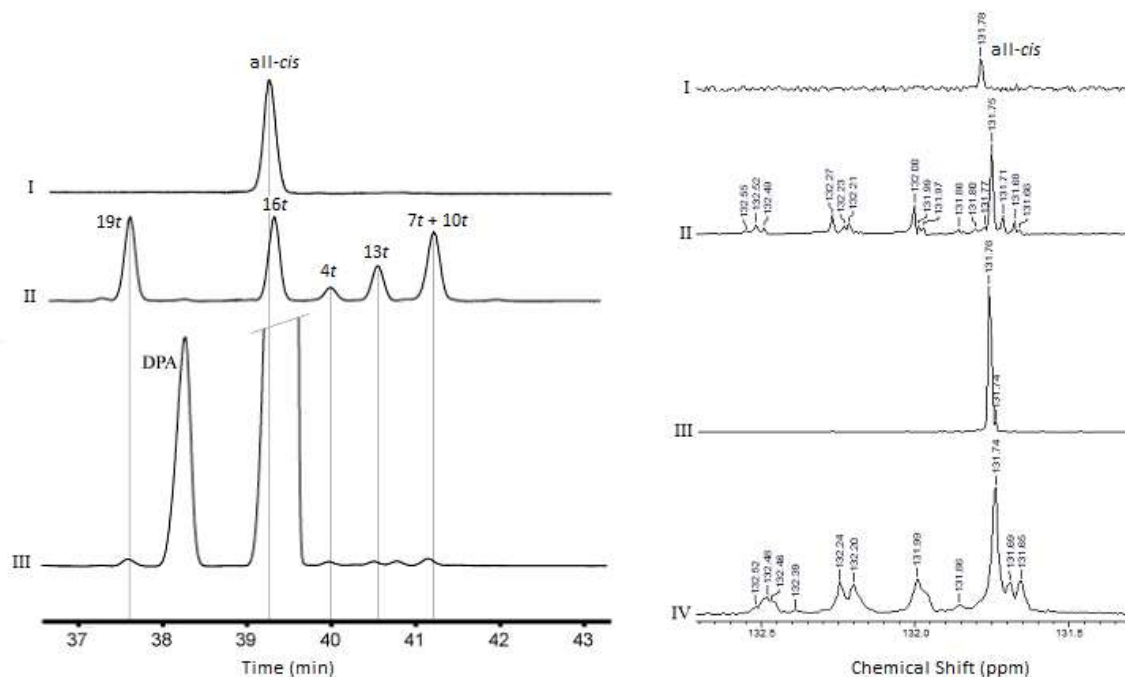


Figura 6.12. a) Partial GC traces of the isomerized fish oil (III) in comparison with all-*cis* DHA-Me (I) and mono-*trans* isomer mixture obtained by photolysis (II). b) Enlargement of the ^{13}C NMR region corresponding to the C-20 ethylenic carbon atom of the *cis* and *trans* triglyceride isomers obtained from fish oil isomerization (IV) in comparison with all-*cis* DHA-Me (I), mono-*trans* DHA-Me isomers in the presence of all-*cis* DHA-Me (II) and fish oil triglycerides prior to isomerization (III).

Therefore, either the GC analysis and the resonance of the C-20 can be of diagnostic value for individuating mono-*trans* DHA isomers as triglycerides and FAMES. It is also worth noting that the region between 131.5 and 132.5 ppm is also a region free of other resonances from biologically important compounds, therefore the DHA isomer assignment presented in our work can be relevant for further development in metabolomics research.

6.4.5. Nutraceutical analysis

Making use of these data, we performed the analysis of the triglyceride fractions contained in nutraceutical and food formulas available on the market in Italy and Spain.

As matter of facts, analytical protocols as quality control of nutraceuticals are important for the interest of producers and consumers, and recently several papers have raised attention on the presence of oxidized and *trans* fatty acids in commercial products of different countries [12,57-60].

Nutraceutical manufacturers are generally concerned with ensuring the absence of heavy metals and other carcinogenic pollutants, such as dioxins and polychlorinated biphenyls, present in the marine habitat [61,62]. However, the current legislation does not yet take into account other pollutants such as those deriving from industrial processes that induce significant transformations of natural oils.

A total of 16 commercially available ω -3 supplements were analysed. Among them, products **1-6** were ω -3 supplements present in the Italian market, of which samples 1-5 made of fish oil and sample 6 by microalgae. Product **7** was a refined and deodorized fish oil based-raw material used for functional foods and product **8** was a milk powder for infants enriched in LC-PUFAs. Products **9-16** were nutraceuticals present in the Spanish market.

A representative chromatogram obtained from nutraceutical products is shown in **Figure 6.13**, while the fatty acid content of the ω -3 supplements analysed for this study is reported in **Table 6.2** and **Table 6.3**.

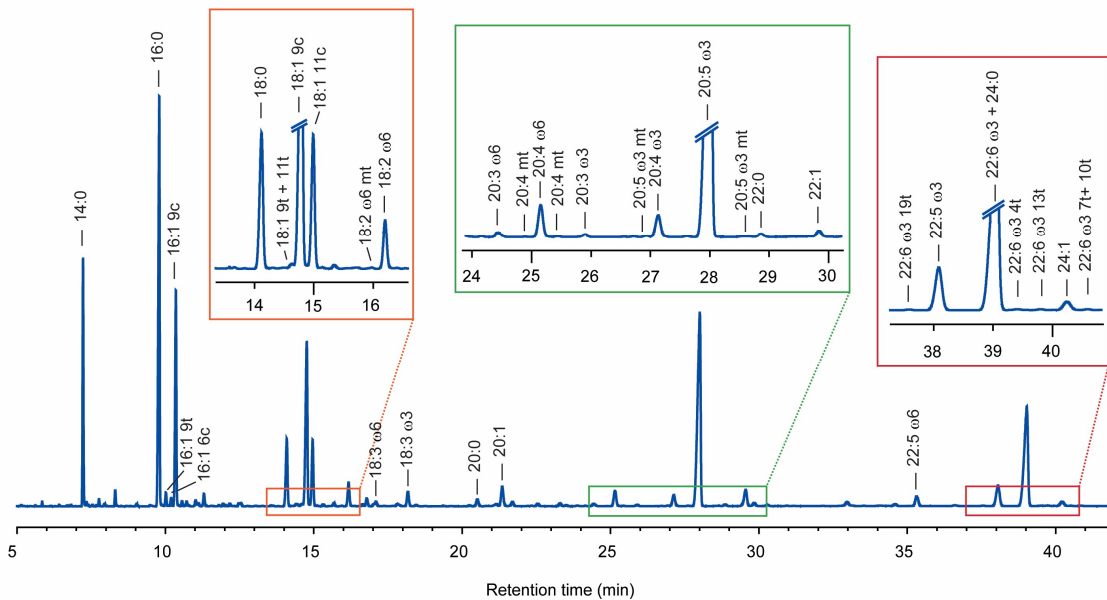


Figure 6.13. GC chromatogram of a representative nutraceutical sample obtained with GC Method A.

Table 6.2. Fatty acids present in nutraceutical products that are commercially available in Italy.

FAME	1	2	3	4	5	6	7	8
14:0	5.75±0.04	0.56±0.01	0.68±0.01	6.11±0.08	6.01±0.05	0.81±0.03	7.58±0.12	3.33±0.06
16:0	12.86±0.01	1.45±0.05	12.94±0.05	22.54±0.15	13.14±0.08	23.48±0.08	19.21±0.14	24.39±0.07
9 <i>t</i> , 16:1	0.34±0.02	0.07±0.01	0.21±0.01	0.64±0.06	0.46±0.00	nd	0.52±0.02	nd
6 <i>c</i> , 16:1	0.16±0.01	0.03±0.00	0.11±0.01	0.26±0.05	0.15±0.01	nd	0.31±0.01	0.04±0.00
9 <i>c</i> , 16:1	6.75±0.05	2.31±0.07	3.96±0.02	9.05±0.03	5.02±0.04	0.44±0.00	9.46±0.06	0.18±0.01
18:0	3.00±0.05	1.44±0.06	16.35±0.13	3.17±0.05	3.86±0.01	1.48±0.12	4.07±0.13	3.59±0.11
9 <i>t</i> , 18:1	0.11±0.03	0.04±0.00	0.31±0.00	0.11±0.00	0.09±0.00	nd	0.13±0.00	0.02±0.00
11 <i>t</i> , 18:1	0.06±0.02	0.01±0.00	0.29±0.14	0.62±0.01	0.02±0.00	nd	0.08±0.00	0.03±0.00
9 <i>c</i> , 18:1	8.41±0.04	10.09±0.10	28.31±0.57	26.70±0.10	6.39±0.13	0.02±0.00	10.43±0.05	44.04±0.19
11 <i>c</i> , 18:1	2.73±0.09	3.59±0.07	10.21±0.15	5.48±0.03	2.41±0.05	0.56±0.04	3.61±0.11	1.25±0.08
LA	1.36±0.05	2.18±0.09	1.26±0.17	1.83±0.04	1.08±0.01	0.14±0.00	1.45±0.01	18.98±0.07
∑ LA mt	nd	0.18±0.02	0.48±0.01	0.09±0.00	0.03±0.00	0.12±0.00	0.04±0.00	0.11±0.00
18:3 ω-6	0.32±0.08	0.29±0.03	0.44±0.03	0.03±0.00	0.43±0.00	nd	0.30±0.02	0.07±0.00
ALA	0.58±0.06	0.98±0.08	0.11±0.01	0.69±0.03	0.49±0.01	nd	0.93±0.11	2.72±0.12
20:0	0.22±0.02	0.13±0.00	2.22±0.06	0.14±0.00	0.37±0.00	0.31±0.01	0.50±0.05	0.31±0.04
20:1	0.98±0.08	1.06±0.04	11.70±0.34	7.75±0.05	1.44±0.12	nd	1.52±0.00	0.28±0.07
20:3 ω-6	0.25±0.09	0.41±0.04	0.43±0.09	0.07±0.00	0.27±0.00	0.21±0.01	0.23±0.04	nd
ARA	1.95±0.07	2.35±0.07	0.14±0.01	0.19±0.01	1.82±0.10	0.13±0.00	1.31±0.11	0.17±0.04
∑ ARA mt	0.08±0.00	0.07±0.00	nd	nd	0.08±0.00	nd	0.07±0.05	nd
20:3 ω-3	0.12±0.00	0.17±0.00	nd	0.12±0.01	0.10±0.01	nd	0.10±0.02	nd
20:4 ω-3	1.08±0.04	2.05±0.06	nd	0.64±0.07	1.14±0.01	0.91±0.01	0.95±0.01	nd
EPA	28.05±0.28	44.34±0.12	0.31±0.01	3.47±0.05	27.40±0.15	0.66±0.01	20.53±0.26	0.07±0.01
∑ EPA mt	0.75±0.02	0.16±0.01	nd	0.03±0.00	0.68±0.02	nd	0.09±0.00	nd
22:0	0.09±0.02	0.08±0.00	1.08±0.03	0.04±0.00	0.13±0.01	0.20±0.01	0.14±0.00	0.21±0.04
22:1	0.12±0.01	0.08±0.00	2.16±0.59	2.06±0.05	0.28±0.06	nd	0.28±0.03	nd
22:5 ω-6	0.70±0.03	0.69±0.00	nd	nd	0.55±0.00	11.91±0.13	nd	nd
DPA	3.67±0.07	4.31±0.02	0.08±0.00	0.77±0.05	3.91±0.18	0.15±0.02	2.44±0.14	nd
24:1	0.34±0.03	0.10±0.00	5.45±0.14	1.30±0.00	0.66±0.01	nd	0.57±0.10	nd
∑ DHA mt	0.65±0.07	0.12±0.01	nd	2.40±0.08	0.62±0.12	1.13±0.03	0.18±0.08	nd
All-<i>cis</i> DHA	18.51±0.10	20.64±0.37	0.75±0.02	3.69±0.04	20.98±0.07	57.35±0.15	12.98±0.15	0.25±0.01
Total SFA	21.92±0.05	3.66±0.10	33.27±0.24	32.00±0.17	23.52±0.14	26.28±0.21	31.49±0.13	31.81±0.16
Total MUFA	19.49±0.20	17.27±0.23	61.91±0.17	52.60±0.14	16.34±0.06	1.03±0.04	26.18±0.03	45.78±0.08
Total PUFA	56.59±0.22	78.41±0.37	3.53±0.11	11.51±0.22	58.16±0.05	71.44±0.27	41.22±0.11	22.25±0.10
ω-6 PUFA	4.58±0.20	5.93±0.16	2.27±0.13	2.12±0.05	4.15±0.09	12.39±0.14	3.29±0.10	19.21±0.09
ω-3 PUFA	52.01±0.31	72.48±0.51	1.26±0.03	9.38±0.18	54.01±0.06	59.06±0.18	37.93±0.15	3.04±0.12
SFA/PUFA	0.39±0.00	0.05±0.00	9.44±0.36	2.78±0.07	0.40±0.00	0.37±0.00	0.76±0.00	1.43±0.01
ω-6/ω-3 ratio	0.09±0.00	0.08±0.00	1.81±0.13	0.23±0.00	0.08±0.00	0.21±0.00	0.09±0.00	6.33±0.25
Total TFA	2.00±0.07	0.66±0.04	1.30±0.16	3.89±0.10	1.98±0.15	1.25±0.02	1.12±0.13	0.15±0.00
ω-3 TFA	1.40±0.10	0.27±0.01	nd	2.43±0.09	1.30±0.14	1.13±0.03	0.27±0.08	nd
% <i>trans</i> / Total DHA	3.40±0.35	0.57±0.04	nd	39.46±0.67	2.87±0.55	1.94±0.05	1.36±0.65	nd

FAMES are expressed as relative percentages of the peak areas detected in the chromatograms (>98% of the total peak areas of the chromatogram). Results are expressed as relative percentages (% rel) ± SD (n=3). nd= not detectable, mt=mono-*trans*.

Table 6.3. Fatty acids present in nutraceutical products that are commercially available in Spain.

FAME	9	10	11	12	13	14	15	16
14:0	0.67±0.01	8.73±0.04	7.28±0.05	0.03±0.00	0.01±0.00	0.01±0.00	10.24±0.19	0.29±0.00
16:0	13.78±0.06	17.72±0.07	17.68±0.13	0.10±0.00	0.06±0.00	0.06±0.00	42.32±0.69	1.02±0.18
9 <i>t</i> , 16:1	0.38±0.03	0.45±0.03	0.52±0.02	nd	nd	nd	0.63±0.03	nd
6 <i>c</i> , 16:1	0.19±0.02	0.21±0.01	0.24±0.02	nd	nd	nd	0.07±0.01	nd
9 <i>c</i> , 16:1	7.21±0.03	11.59±0.05	8.88±0.01	0.09±0.00	0.03±0.00	0.01±0.00	3.73±0.32	0.77±0.03
18:0	3.40±0.09	3.25±0.01	3.91±0.01	0.06±0.00	0.04±0.00	0.03±0.00	1.97±0.17	2.25±0.14
9 <i>t</i> , 18:1	0.25±0.09	0.15±0.03	0.14±0.04	nd	0.01±0.00	nd	0.08±0.02	nd
11 <i>t</i> , 18:1	0.22±0.05	0.03±0.01	0.13±0.02	nd	nd	nd	0.01±0.00	nd
9 <i>c</i> , 18:1	17.78±0.06	8.58±0.01	9.08±0.06	0.24±0.00	0.12±0.00	0.04±0.00	9.04±0.03	nd
11 <i>c</i> , 18:1	6.27±0.04	3.44±0.04	3.15±0.06	0.03±0.00	0.16±0.00	0.01±0.00	5.53±0.02	nd
LA	3.40±0.05	1.53±0.02	4.94±0.02	0.05±0.01	0.13±0.00	0.05±0.01	2.07±0.08	5.61±0.21
∑ LA mt	0.81±0.07	0.19±0.02	0.24±0.03	nd	0.01±0.00	nd	0.04±0.00	nd
18:3 ω-6	0.56±0.06	0.35±0.04	2.14±0.07	0.03±0.00	nd	nd	0.14±0.02	nd
ALA	1.53±0.02	0.81±0.02	0.81±0.02	0.02±0.00	nd	nd	0.85±0.14	nd
20:0	0.24±0.03	0.31±0.01	0.48±0.03	0.04±0.00	nd	nd	0.08±0.01	0.30±0.01
20:1	0.91±0.03	0.64±0.04	1.81±0.04	0.08±0.00	0.02±0.00	nd	0.56±0.05	0.35±0.11
20:3 ω-6	0.21±0.01	0.23±0.03	0.19±0.04	0.03±0.00	0.01±0.00	nd	0.07±0.02	0.23±0.00
ARA	1.49±0.03	1.73±0.01	1.22±0.01	0.12±0.00	0.72±0.00	0.02±0.01	0.28±0.01	0.48±0.01
∑ ARA mt	0.010±0.09	0.05±0.01	0.03±0.00	nd	0.04±0.00	nd	0.03±0.00	nd
20:3 ω-3	0.13±0.01	0.07±0.02	0.11±0.01	0.02±0.00	nd	nd	0.09±0.00	nd
20:4 ω-3	0.86±0.03	0.80±0.02	0.92±0.02	0.09±0.00	0.06±0.00	0.09±0.01	0.33±0.01	nd
EPA	21.87±0.19	21.41±0.11	19.60±0.19	2.29±0.00	3.24±0.01	5.59±0.01	13.48±0.34	2.35±0.03
∑ EPA mt	0.25±0.03	0.16±0.02	0.14±0.01	0.07±0.00	0.08±0.01	0.15±0.01	0.06±0.00	nd
22:0	0.08±0.01	0.11±0.01	0.15±0.01	0.06±0.00	0.02±0.01	nd	0.07±0.01	0.55±0.08
22:1	0.16±0.02	0.09±0.01	0.44±0.02	0.15±0.00	nd	nd	0.45±0.01	nd
22:5 ω-6	nd	nd	nd	1.97±0.00	6.24±0.01	0.52±0.03	nd	3.92±0.80
DPA	2.10±0.03	2.18±0.01	1.98±0.00	9.94±0.32	1.17±0.02	13.32±0.04	0.38±0.02	2.09±0.33
24:1	0.24±0.01	0.31±0.02	0.54±0.03	0.14±0.03	nd	nd	0.04±0.00	0.34±0.14
∑ DHA mt	0.32±0.02	0.18±0.05	0.16±0.04	0.66±0.10	1.64±0.08	1.32±0.09	0.08±0.01	2.71±0.39
All-cis DHA	14.60±0.15	14.71±0.05	13.11±0.06	83.68±0.17	86.19±0.11	78.78±0.11	7.16±0.31	76.75±0.41
Total SFA	18.17±0.12	30.12±0.09	29.50±0.17	0.30±0.00	0.13±0.01	0.10±0.01	54.74±0.82	4.40±0.22
Total MUFA	32.75±0.04	24.86±0.05	24.12±0.15	0.73±0.03	0.33±0.01	0.06±0.01	19.45±0.25	1.47±0.19
Total PUFA	46.75±0.31	43.83±0.06	45.02±0.11	98.24±0.14	97.76±0.10	98.37±0.09	24.87±0.62	91.43±0.56
ω-6 PUFA	5.66±0.07	3.84±0.08	8.49±0.14	2.19±0.01	7.10±0.01	0.59±0.04	2.57±0.13	10.25±0.90
ω-3 PUFA	41.09±0.36	39.99±0.13	36.53±0.23	96.05±0.14	90.66±0.10	97.78±0.11	22.30±0.74	81.18±0.61
SFA/PUFA	0.39±0.00	0.69±0.00	0.66±0.00	0.00±0.00	0.00±0.00	0.00±0.00	2.20±0.09	0.05±0.00
ω-6/ω-3 ratio	0.14±0.00	0.10±0.00	0.23±0.01	0.02±0.00	0.08±0.00	0.01±0.00	0.12±0.01	0.13±0.01
Total TFA	2.33±0.26	1.19±0.08	1.36±0.14	0.72±0.10	1.78±0.08	1.47±0.09	0.93±0.04	2.71±0.39
ω-3 TFA	0.57±0.04	0.34±0.06	0.30±0.05	0.72±0.10	1.72±0.08	1.47±0.09	0.14±0.01	2.71±0.39
% trans / Total DHA	2.13±0.12	1.21±0.30	1.20±0.31	0.78±0.11	1.87±0.09	1.65±0.11	1.05±0.08	3.40±0.48

Fatty acid methyl esters (FAMEs) are expressed as relative percentages of the peak areas detected in the chromatograms (>98% of the total peak areas of the chromatogram). Results are expressed as relative percentages (% rel) ± SD (n=3). nd= not detectable; mt=mono-*trans*.

The GC analyses showed that these products markedly differed one from the other. This was somehow expected since some products declared their lipid content in the labels.

Although all products claimed to contain fish or algal oil, in some of them PUFAs were not the most abundant lipid family. It is known that PUFA content is strongly conditioned by the fish species used, the type of food and the environmental conditions of breeding [63,64]. For example, fish living in

cold waters generally have a high ω -3 PUFA content, which guarantees the fish survival in very cold water by maintaining membrane fluidity.

For example, Product 15 was found to contain more than 50% of SFAs (54.74 ± 0.82) and less than 25% (22.30 ± 0.74) of ω -3 PUFAs, corresponding to a SFA/PUFA ratio of 2.20 ± 0.09 .

Only two samples, i.e. Product 12 and 14, were constituted almost exclusively ($>95\%$) by ω -3 PUFAs (96.05 ± 0.14 and 97.78 ± 0.11 , respectively). Products of this quality are usually obtained by subjecting the raw materials to the winterization process.

Winterization is a technique of fractional crystallization that requires slow cooling, which allows the separation of based on their melting temperature. In this way, waxes and saturated fats, that are characterized by high melting temperatures, can be solidified and separated by the liquid oily bulk by slowly decreasing the preparation temperature.

Unfortunately, also in these samples, TFA derivatives were detected, corresponding to 0.72 ± 0.10 and 1.47 ± 0.09 of the total fatty acids, of which 0.66 ± 0.10 and 1.32 ± 0.09 corresponded to *trans*-DHA, respectively. Considering the high quantity of DHA in the capsules (83.68 ± 0.17 in Product 12 and 78.78 ± 0.11 in Product 14), the percentage of *trans*-DHA referred to the total DHA was lower than 1% in Product 12 (0.78 ± 0.11), while in Product 14 1.65% of DHA in the capsule was in the form of its *trans* geometrical isomer.

These data provide important information regarding the quality of the starting raw materials used for supplement preparation. However, considering the amount of PUFAs over the total fatty acids, it is not sufficient to establish the quality of the product under investigation. Indeed, focusing on DHA, all the samples analyzed, with the exception of Product 3 and Product 8, contained mono-*trans* isomers of DHA, in percentages ranging from 0.12 ± 0.01 up to 2.71 ± 0.39 of the total fatty acid content.

An excess of mono-*trans* isomers of DHA, corresponding to a relative percentage of 2.40 ± 0.08 , was detected in Product 4. It was astonishing to notice that the percentage of *trans*-DHA over the total DHA present in the sample was almost 40% (39.46 ± 0.67). Considering the total TFAs, and not only *trans*-isomers of DHA, the total *trans* content of Product 4 was 3.89 ± 0.10 , i.e. almost 4% of fatty acids in the capsule were *trans* geometrical isomers of natural lipids.

On the other hand, Product 3 and Product 8, that do not contain *trans*-isomers of DHA, contained only traces of all-*cis* DHA, the lipid which originates *trans*-isomers (0.75 ± 0.02 in Product 3 and 0.25 ± 0.01 in Product 8 respectively). More specifically, in Product 3 the most abundant lipid family is represented by MUFAs (61.91 ± 0.17 percent of total lipids), followed by SFAs (33.27 ± 0.24

percent). MUFAs were the major source of TFAs, whose percentage (1.30 ± 0.16) was higher than that of total ω -3 PUFAs in the supplement (1.26 ± 0.03). In Product 8, a powdered milk for infants claimed to be enriched in long-chain PUFAs (> 18 carbons), EPA and DHA are contained only in traces (0.07 ± 0.01 of EPA and 0.25 ± 0.01 of DHA), whereas oleic ($9c$, 18:1) and linoleic (LA, $9c, 12c$, 18:2) acids are more abundant (44.04 ± 0.19 and 18.98 ± 0.07 respectively). Despite these fatty acids are normally present in milk lipid composition, such percentages are reached by vegetable oil addition, and this makes it difficult to understand whether the *trans*-isomers detected in this product (0.15% of the total lipids) is due to the industrial manipulation (oil addition) or to the natural biohydrogenation process occurring in ruminants (**Chapter 1, Paragraph 1.4.4**). In any case, although the percentage of TFAs in this product may be negligible, its nutritional value is questionable, owing to the extremely low content in ω -3 FAs.

Apart from DHA mono-*trans* FAs, other *trans*-fatty acid derivatives were identified using *trans* reference libraries synthesized by our group. In particular, mono-*trans* isomers of palmitoleic ($9c, 16:1$), oleic ($9c$, 18:1), vaccenic ($11c$, 18:1) and arachidonic (20:4 ω -6) acids were individuated. A significant percentage on mono-*trans* isomers of EPA (20:5 ω -3) was detected, especially in some of those samples that contain more than 20% of EPA, such as product 1 (EPA content of 28.05 ± 0.28) and product 5 (EPA content of 27.40 ± 0.02) that were found to have 0.75 ± 0.02 and $0.68\pm 0.02\%$ of mono-*trans* isomers of EPA, respectively.

In the GC area corresponding to the elution of all-*cis* and mono-*trans* DHA-Me, using helium as carrier gas, the presence of other three fatty acid methyl esters, namely all-*cis* 7,10,13,16,19 docosapentaenoic acid (DPA, 22:5 ω -3), 24:0 and $15c$, 24:1, was detected. Among them, the elution time of 24:0 corresponded to the elution time of all-*cis* DHA-Me. Although the overlap did not affect the mono-*trans* isomers of DHA-Me, which are the main focus of this study, a second GC method, described in details in the Experimental part and named *Method B*, was applied. Hydrogen as carrier gas, and variations in the oven program, led to shifts in the time and the elution order of some long-chain fatty acids. With GC *Method B*, 24:0 and 24:1 fatty acids were strongly retained by the stationary phase, avoiding misleading FAME assignments (data not shown).

However, it was important to reconsider at this step the characterization of mono-*trans* isomers of DHA-Me carried out by GC-MS. By comparing the elution profile and the fragmentation pattern of *trans*-containing nutraceutical samples with the data collected from mono-*trans* isomers produced by photolysis, the identity of the peaks was confirmed. Indeed, the match with the mass-to-charge ratio (m/z) of ω -3 PUFAs allowed to exclude false positives such as saturated or mono-unsaturated FAMES eluting in the same region, as well as excessive background noise. These analyses demonstrate that

the synthetic library of mono-*trans* isomers of DHA used as standard reference in gas chromatography constitutes a reliable analytical tool for the identification of these byproducts in commercially available ω -3 supplements. Additionally, since almost all the analyzed samples contained detectable amounts of *trans* lipids, this research underline the importance of the full *trans*-isomers characterization of the most common polyunsaturated fatty acids.

6.5. Conclusions

In this study we report the first separation and identification of mono-*trans* isomers of DHA, obtained by a dual synthetic approach consisting of: i) the direct radical-catalysed isomerization of *cis*-DHA, and ii) mono-epoxide formation from DHA, separated and identified by bidimensional nuclear magnetic resonance experiments, followed by elimination to obtain the corresponding mono-*trans* alkenes.

The full characterization of mono-*trans* derivative of DHA was used as reference library to set up a gas chromatography protocol in order to identify *trans* isomers from a representative fish oil isomerization reaction and from commercially available ω -3-containing supplements.

The GC analyses run on ω -3 enriched supplements showed the presence of mono-*trans* isomers of DHA and other mono-*trans* isomers (including *trans*-palmitoleic, *trans*-oleic, *trans*-vaccenic, *trans*-ARA and *trans*-EPA derivatives), that were identified using previously established synthetic procedures. Some nutraceuticals were found to contain more than 95% of ω -3 PUFAs with SFA/PUFA ratio approximated to zero and only one of them was found to have less that 1% of *trans*-DHA over the total DHA in the preparation, thus suggesting winterization as a valid refining technique for the oils that have nutritional applications, to be used in alternative to deodorization.

Our results underlined that the quality of the final commercially available ω -3 supplements is conditioned by the quality of the raw materials and the type of industrial processes employed. The synthetic library of mono-*trans* isomers of DHA could be a useful tool for the detection and quantification of these geometrical artifacts in ω -3 supplements that can find application in food and nutraceutical studies.

6.6. References

1. Sanders, T.A. DHA status of vegetarians. Prostaglandins Leukot. *Essent. Fatty Acids* **2009**, *81*(2-3), 137-141
2. Tetens, I. Scientific Opinion of the Panel on Dietetic Products, Nutrition and Allergies on a request from the: Question No EFSA-Q-2008-269, **2008**
3. Wesdorp, L.H; Melnikov, S.M.; Gaudier, E.A. Trans fats replacement solutions in Europe. In *Trans Fats Replacement Solutions*, 1st ed.: AOCS Press, Urbana, IL, **2014**, pp. 287-312)
4. Ferreri, C.; Faraone Mennella, M.R.; Formisano, C.; Landi, L.; Chatgililoglu, C. Arachidonate geometrical isomers generated by thiyl radicals: the relationship with trans lipids detected in biological samples, *Free Rad. Bio & Med.* **2002**, *33*(11), 1516-1526
5. Zambonin, L.; Ferreri, C.; Cabrini, L.; Prata, C.; Chatgililoglu, C.; Landi L. Occurrence of trans fatty acids in rats fed a trans-free diet: a free radical-mediated formation? *Free Radic. Biol. Med.* **2006**, *40*(9), 1549-1556
6. Ferreri, C.; Kratzsch, S.; Brede, O.; Marciniak, B.; Chatgililoglu C. Trans lipid formation induced by thiols in human monocytic leukemia cells. *Free Radic. Biol. Med.* **2005**, *38*(1),1180-1187
7. Souabni, H.; Thoma, V.; Bizouarn, T.; Chatgililoglu, C.; Sifaka-Kapadai, A.; Baciou, L.; Ferreri, C.; Houée-Lévin, C.; Ostuni, M.A. *trans* arachidonic acid isomers inhibits NADPH-oxidase activity by direct interaction with enzyme components, *BBA Biomembranes*, **2012**, *1818*(9), 2314-2324
8. Aoun, M; Feillet-Coudray, C.; Fouret, G.; Chabi, B. Crouzier, D.; Ferreri, C.; Chatgililoglu, C.; Cabello, C.; Cristol, J. P.; Carbonneau, M.-A.; Coudray, C. Rat liver mitochondrial membrane characteristics and mitochondrial functions are more profoundly altered by dietary lipid quantity than by dietary lipid quality: effect of different nutritional lipid patterns. *Br. J. Nutr.* **2012**, *107*(5), 647-59
9. Grandgirard, A.; Piconneaux, A.; Sébédio, J.L.; O’Keefe, S.F.; Semon, E.; LeQuere, J.L. Occurrence of geometrical isomers of eicosapentaenoic and docosahexaenoic acids in liver lipids of rats fed heated linseed oil. *Lipids* **1989**, *24*(9), 799-804
10. Vendel Nielsen, L.; Krogager, T.P.; Young, C.; Ferreri, C.; Chatgililoglu, C.; Nørregaard Jensen, O.; Enghild. J.J. Effects of elaidic acid on HepG2 lipid metabolism, investigated by an integrated approach of lipidomics, transcriptomics and proteomics. *Plos One*, **2013**, *8*(9), e74283
11. Ferreri, C.; Samadi, A.; Sassatelli, F.; Landi, L.; Chatgililoglu, C. Regioselective cis-trans isomerization of arachidonic double bonds by thiyl radicals: the influence of phospholipid supramolecular organization, *J. Am. Chem. Soc.*, **2004**, *126*(4), 1063-1072
12. Ferreri, C.; Grabovskiy, S.; Aoun, M.; Melchiorre, M.; Kabal’nova, N.; Feillet-Coudray, C.; Fouret, G.; Coudray, C.; Chatgililoglu, C. Mono-trans eicosapentaenoic acid isomer library: a dual synthetic strategy and follow-up of rats fed deodorized fish oil diets. *Chem. Res. Toxicol.* **2012**, *25*(3), 687–694

13. Vatele, J.M.; Doan, H.D.; Chardigny, J.M.; Grandgirard, A. Synthesis of methyl (5Z, 8Z, 11Z, 14Z, 17E)-eicosapentaenoate and methyl (4Z, 7Z, 10Z, 13Z, 16Z, 19E)-docosahexaenoate. *Chem. Phys. Lipids* **1994**, *74*(2), 185-193
14. Mjøs, S.A. Properties of trans isomers of eicosapentaenoic acid and docosahexaenoic acid methyl esters on cyanopropyl stationary phases. *J. Chromatogr. A* **2005**, *1100*(2), 185-192
15. Mjøs, S.A.; Solvang, M. Geometrical isomerization of eicosapentaenoic acid and docosahexaenoic acid at high temperatures. *Eur. J. Lipid Sci. Technol.* **2006**, *108*, 589-597
16. VanRollins, M.; Frade, P.D.; Carretero, O.A. Synthesis of epoxide and vicinal diol regioisomers from docosahexaenoate methyl esters. *J. Lipid Res.* **1989**, *30*(2), 275-286
17. Jakobsen, M.G.; Vik, A.; Hansen, T.V. Concise syntheses of three ω -3 polyunsaturated fatty acids. *Tetrahedron Lett.* **2012**, *53*(44), 5837-5839
18. Flock, S.; Lundquist, M.; Skattebol, L. Syntheses of some polyunsaturated sulfur-and oxygen-containing fatty acids related to eicosapentaenoic and docosahexaenoic acids. *Acta Chemica Scandinavica* **1999**, *53*(6), 436-445
19. Stillwell, W.; Wassall, S.R. Docosahexaenoic acid: membrane properties of a unique fatty acid, *Chem. Phys. Lipids*, **2003**, *126*(1), 1-27
20. Qiu, X.; Hong, H.; MacKenzie, S.L. Identification of a Delta 4 fatty acid desaturase from *Thraustochytrium* sp. involved in the biosynthesis of docosahexanoic acid by heterologous expression in *Saccharomyces cerevisiae* and *Brassica juncea*. *J. Biol. Chem.* **2001**, *276*(34), 31561-31566
21. Martinez, M.; Ichaso, N.; Setien, F.; Durany, N.; Qiu, X.; Roesler, W. The Δ 4-desaturation pathway for DHA biosynthesis is operative in the human species: Differences between normal controls and children with the Zellweger syndrome. *Lipids Health Dis.* **2010**, *9*(1), 98
22. Oboh, A.; Kabeya, N.; Carmona-Antoñanzas, G.; Castro, L.F.C.; Dick, J.R.; Tocher, D.R.; Monroig, O. Two alternative pathways for docosahexaenoic acid (DHA, 22: 6n-3) biosynthesis are widespread among teleost fish. *Sci. Rep.* **2017**, *7*(1), 3889
23. Sprecher, H. Biochemistry of essential fatty acids. *Progr. Lipid Res.* **1981**, *20*, 13-22
24. Yamazaki, K.; Fujikawa, M.; Hamazaki, T.; Yano, S.; Shono, T. Comparison of the conversion rates of alpha-linolenic acid (18:3(n - 3)) and stearidonic acid (18:4(n - 3)) to longer polyunsaturated fatty acids in rats. *Biochim Biophys Acta.* **1992**, *1123*(1), 18-26
25. Mahfouz, M. Effect of dietary trans fatty acids on the delta 5, delta 6 and delta 9 desaturases of rat liver microsomes in vivo. *Acta Biol. Med. Ger.* **1981**, *40*(12), 1699-1705
26. Das, U.N. Can essential fatty acids reduce the burden of disease(s)?. *Lipids Health Dis.* **2008**, *7*(1), 9
27. Das U.N. Essential fatty acids - a review. *Curr. Pharm. Biotechnol.* **2006**, *7*(6), 467-482
28. Portolesi, R.; Powell, B.C.; Gibson, R.A. Competition between 24:5n-3 and ALA for Δ 6 desaturase may limit the accumulation of DHA in HepG2 cell membranes. *J Lipid Res.* **2007**, *48*(7), 1592-1598

29. Huang, T.L.; Zandi, P.P.; Tucker, K.L.; Fitzpatrick, A.L.; Kuller, L.H.; Fried, L.P.; Burke, G.L.; Carlson, M.C. Benefits of fatty fish on dementia risk are stronger for those without APOE ϵ 4. *Neurology* **2005**, *65*(9), 1409-1414
30. Harwood, J.L.; Guschina, I.A. The versatility of algae and their lipid metabolism, *Biochimie* **2009**, *91*(6), 679-684
31. Abril, R.; Barclay, W. Production of docosahexaenoic acid-enriched poultry eggs and meat using an algae-based feed ingredient. In *The Return of w3 Fatty Acids into the Food Supply*, Karger Publishers, Basel, Switzerland, **1998**, Vol. 83, pp. 77-88
32. Horrocks, L.A.; Farooqui, A.A. Docosahexaenoic acid in the diet: its importance in maintenance and restoration of neural membrane function, *Prostaglandins Leukot. Essent. Fatty Acids.*, **2004**, *70*(4), 361-372
33. Lauritzen, L.; Hansen, H.S.; Jørgensen, M.H.; Michaelsen, K.F. The essentiality of long chain n-3 fatty acids in relation to development and function of the brain and retina, *Prog. Lipid Res.*, **2001**, *40*(1-2), 1-94
34. Horrocks, L.A.; Yeo, Y.K. Health benefits of docosahexaenoic acid (DHA), *Pharmacol. Res.*, **1999**, *40*(3), 211-225
35. Richardson, A.J.; Puri, B.K. A randomized double-blind, placebo-controlled study of the effects of supplementation with highly unsaturated fatty acids on ADHD-related symptoms in children with specific learning difficulties. *Prog Neuropsychopharmacol Biol Psychiatry*. **2002**, *26*(2), 233-239
36. Sinn, N.; Bryan, J. Effect of supplementation with polyunsaturated fatty acids and micronutrients on learning and behavior problems associated with child ADHD. *J. Dev. Behav. Pediatr.* **2007**, *28*(2), 82-91
37. Logan, A.C. Neurobehavioral aspects of omega-3 fatty acids: possible mechanisms and therapeutic value in major depression. *Altern. Med. Rev.* **2003**, *8*(4), 410-425
38. Ghezzi, A.; Visconti, P.; Abruzzo, P.M.; Bolotta, A.; Ferreri, C.; Gobbi, G.; Malisardi, G.; Manfredini, S.; Marini, M.; Nanetti, L.; Pipitone, E.; Raffaelli, F.; Resca, F.; Vignini, A.; Mazzanti, L. Oxidative Stress and Erythrocyte Membrane Alterations in Children with Autism: Correlation with Clinical Features. *PLoS One* **2013**, *8*(6), e66418
39. Augood, C.; Chakravarthy, U.; Young, I.; Vioque, J.; de Jong, P.T.; Bentham, G.; Rahu, M.; Seland, J.; Soubrane, G.; Tomazzoli, L.; Topouzis, F.; Vingerling, J.R.; Fletcher, A.E. Oily fish consumption, dietary docosahexaenoic acid and eicosapentaenoic acid intakes, and associations with neovascular age-related macular degeneration, *Am. J. Clin. Nutr.* **2008**, *88*(2), 398-406
40. Ollero, M.; Powers, R.D.; Alvarez, J.G. Variation of docosahexaenoic acid content in subsets of human spermatozoa at different stages of maturation: implications for sperm lipoperoxidative damage, *Mol. Reprod. Devel.* **2000**, *55*(3), 326-334
41. Kris-Etherton, P.M.; Harris, W.S.; Appel, L.J. Omega-3 fatty acids and cardiovascular disease: new recommendations from the American Heart Association. *Arterioscler. Thromb. Vasc. Biol.* **2003**, *23*(2), 151-152

42. Kinsella, J.E., Lokesh, B., Stone, R.A. Dietary n-3 polyunsaturated fatty acids and amelioration of cardiovascular disease: possible mechanisms. *Am. J. Clin. Nutr.* **1990**, 52(1), 1-28
43. Kremer, J.M.; Lawrence, D.A.; Jubiz, W.; Digiacomio, R.; Rynes, R.; Bartholomew, L.E.; Sherman, M. Dietary fish oil and olive oil supplementation in patients with Rheumatoid Arthritis clinical and immunologic effects. *Arthritis Rheum.* **1990**, 33(6), 810-820
44. Camuesco, D.; Gálvez, J.; Nieto, A.; Comalada, M.; Rodríguez-Cabezas, M.E.; Concha, A.; Xaus, J.; Zarzuelo, A. Dietary olive oil supplemented with fish oil, rich in EPA and DHA (n-3) polyunsaturated fatty acids, attenuates colonic inflammation in rats with DSS-induced colitis. *J. Nutr.* **2005**, 135(4), 687-694
45. Skender, B.; Vaculova, A.H.; Hofmanova, J. Docosahexaenoic fatty acid (DHA) in the regulation of colon cell growth and cell death: A review, *Biomed. Pap.* **2012**, 156(3), 186-199
46. Shin, S.; Jing, K.; Jeong, S.; Kim, N.; Song, K.S.; Heo, J.Y.; Park, J.H.; Seo, K.S.; Han, J.; Park, J.I.; Kweon, G.R.; Park, S.K.; Wu, T.; Hwang, B.D.; Lim, K. The omega-3 polyunsaturated fatty acid DHA induces simultaneous apoptosis and autophagy via mitochondrial ROS-mediated Akt-mTOR signaling in prostate cancer cells expressing mutant p53, *BioMed. Res. Int.*, **2013**, 568671
47. Merendino, N.; Costantini, L.; Manzi, L.; Molinari, R.; D'Eliseo, D.; Velotti, F. Dietary ω -3 polyunsaturated fatty acid DHA: a potential adjuvant in the treatment of cancer, *BioMed. Res. Int.* **2013**, 310186
48. Sansone, A.; Melchiorre, M.; Chatgililoglu, C.; Ferreri, C. Hexadecenoic fatty acid isomers: a chemical biology approach for human plasma biomarker development, *Chem. Res. Toxicol.*, **2013**, 26(11), 1703-1709
49. Mihaljevic, B.; Tartaro, I.; Ferreri, C.; Chatgililoglu, C. Linoleic acid peroxidation vs. isomerization: a biomimetic model of free radical reactivity in the presence of thiols. *Org. Biomol. Chem.*, **2011**, 9, 3541-3548
50. Mjøs, S.A. Properties of trans isomers of eicosapentaenoic acid and docosahexaenoic acid methyl esters on cyanopropyl stationary phases. *J. Chromatogr. A.* **2005**, 1100(2), 185-92.
51. Zhang, G.; Kodani, S.; Hammock, B.D. Stabilized epoxygenated fatty acids regulate inflammation, pain, angiogenesis and cancer". *Prog. Lipid Res.* **2014**, 53, 108–23
52. Lucas, D.; Goulitquer, S.; Marienhagen, J.; Fer, M.; Dreano, Y.; Schwaneberg, U.; Amet, Y.; Corcos, L. Stereoselective epoxidation of the last double bond of polyunsaturated fatty acids by human cytochromes P450. *J. Lipid Res.* **2010**, 51, 1125-1133
53. Fer, M.; Dreano, Y.; Lucas, D.. Metabolism of eicosapentaenoic and docosahexaenoic acids by recombinant human cytochromes P450. *Arch Biochem Biophys.* **2008**, 471, 116-125
54. Newman, J.W.; Morisseau, C.; Hammock, B.D. Epoxide hydrolases: their roles and interactions with lipid metabolism. *Prog. Lipid Res.* **2005**, 44, 1-51

55. Kato, T.; Ishimatu, T.; Aikawa, A.; Taniguchi, K.; Kurahashi, T.; Nakai, T. Preparation of the enantiomers of 19-epoxy docosahexaenoic acids and their 4-hydroxy derivatives. *Tetrahedron: Asymmetry* **2000**, *11*(4), 851-860.
56. Krishna, U.M.; Reddy, M.M.; Xia, J.; Falck, J.R.; Balazy, M. Stereospecific synthesis of trans-arachidonic acids. *Bioorg. Med. Chem. Lett.* **2001**, *11*, 2415-2418
57. Tatarczyk, T.; Engl, J.; Ciardi, C.; Laimer, M.; Kaser, S.; Salzmann, K.; Lenner, R.; Patsch, J.R.; Ebenbichler, C.F. (2007). Analysis of long-chain ω -3 fatty acid content in fish-oil supplements. *Wien Klin Wochenschr.* **2007**, *119*(13-14), 417-22
58. Jackowski, S.A., Alvi, A.Z., Mirajkar, A., Imani, Z., Gamalevych, Y., Shaikh, N.A., Jackowski, G. (2015). Oxidation levels of North American over-the-counter n-3 (omega-3) supplements and the influence of supplement formulation and delivery form on evaluating oxidative safety. *J. Nutr. Sci.* **2015**, *4*, e30
59. Opperman, M.; Benade, A.S. Analysis of omega-3 fatty acid content of South African fish oil supplements: Cardiovascular topics. *Cardiovasc J Afr.* **2011**, *22*(6), 324-329
60. Fournier, V.; Destailats, F.; Hug, B.; Golay, P. A.; Joffre, F.; Juaneda, P.; Semon, E.; Dionisi, F.; Lambelet, P.; Sebedio, J.L.; Berdeaux, O. Quantification of eicosapentaenoic and docosahexaenoic acid geometrical isomers formed during fish oil deodorization by gas-liquid chromatography. *J. Chromatogr. A* **2007**, *1154*(1-2), 353-359
61. Bourdon, J.A.; Bazinet, T.M.; Arnason, T.T.; Kimpe, L.E.; Blais, J.M.; White, P.A. Polychlorinated biphenyls (PCBs) contamination and aryl hydrocarbon receptor (AhR) agonist activity of omega-3 polyunsaturated fatty acid supplements: implications for daily intake of dioxins and PCBs. *Food Chem Toxicol.* **2010**, *48*(11), 3093-3097
62. Storelli, M.M.; Storelli, A.; Marcotrigiano, G.O. Polychlorinated biphenyls, hexachlorobenzene, hexachlorocyclohexane isomers, and pesticide organochlorine residues in cod-liver oil dietary supplements. *J Food Prot.* **2004**, *67*(8), 1787-1791
63. Passi, S.; Cataudella, S.; Di Marco, P.; De Simone, F.; Rastrelli, L. Fatty acid composition and antioxidant levels in muscle tissue of different mediterranean marine species of fish and shellfish, *J. Agric. Food Chem.*, **2002**, *50*, 7314-7322
64. Alasalvar, C.; Taylor, K.D.A.; Zubcov, E.; Shahidi, F.; Alexis, M. Differentiation of cultured and wild sea bass (*Dicentrarchus labrax*): total lipid content, fatty acid and trace mineral composition, *Food Chem.* **2002**, *79*, 145-150

Chapter 7

Conclusions

The results presented in this PhD thesis concern the role of cell membrane lipid composition, in physiological and pathological conditions.

In the first part (**Chapter 3**), the focus was directed at establishing a membrane-based comprehensive approach to be applied to the study of Autism Spectrum Disorder (ASD). The protocol consisted of erythrocyte membrane lipidomic analysis and erythrocyte characterization using hyperspectral dark-field microscopy (HDFM). The study was performed on 41 children, 21 with ASD and 20 with typical development. We found that children affected by ASD had significantly reduced levels of erythrocyte membrane DHA, pointing the attention to the crucial role of this ω -3 fatty acid in neuronal development and brain functioning. The HDFM analyses led to the creation of a hyperspectral library made of 8 scattering spectra, reflecting the contribution of still unidentified erythrocyte components. The relative contribution of each spectrum was examined for each sample. It was found that spectrum 4 (whose characteristic peaks could be attributed to phospholipids and protoporphyrin IX) was significantly increased in erythrocytes from ASD children. The statistical elaboration of data demonstrated an inverse correlation between DHA content of erythrocyte membranes and relative values of spectrum 4. Further statistical analysis showed that individuals with a spectrum 4 percentage higher than 16.225 (cut-off value) have a 24-times higher probability of having ASD. These preliminary results encourage further studies on a larger scale, aimed at integrating this innovative protocol with other diagnostic and intervention tools for the optimization of personalized membrane-targeted therapies.

In the second part (**Chapter 4**), we investigated the possible membrane fatty acid remodeling induced by two apolipoproteins, apoE3 or apoE4, involved in lipid transport in the brain, on cultured SK-N-SH neuroblastoma cells. Apo E3 and apoE4 are two allelic isoforms of the same lipid transporter protein, where carriers of the apoE4 isoform are notably at risk for Alzheimer's disease (AD). SK-N-SH neuroblastoma cells were incubated in the presence or the absence of either apoE3 or apoE4, then the GC analysis of the extracted cell membrane fatty acids was performed. It emerged that the addition of both apoE isoforms induced fatty acid remodeling, but with different outcomes. SFAs and MUFAs were significantly increased after cell incubation with both apoE3 or apoE4, while ω -6 PUFAs were significantly decreased after incubation with apoE3 but were unchanged after incubation with apoE4. ω -3 PUFAs were significantly decreased in the membrane of cells treated with both apoE forms if compared with untreated samples ($p < 0.0001$), but the decrease was of greater magnitude in the presence of apoE3 ($p < 0.001$). As a consequence of the ω -3 reduction, PUFA balance indicator was also decreased compared to controls ($p < 0.0001$). For what TFAs was concerned, the total *trans* isomers tended to decrease after incubation of the cells with apoE3 but TFA content appeared to increase in the presence of apoE4. Opposite trends were observed with regard to stearic acid and DGLA, apoE3 increasing while apoE4 reducing their levels in neuroblastoma cell membranes. Both apoE isoforms decreased membrane homeostasis indexes such as PUFA balance, unsaturation index and peroxidation index. These results suggest further *in vitro* experiments to better clarify the mechanism of action of apolipoproteins on membrane lipid distribution; it may be envisioned a future use of nutritional strategies in the prevention and treatment of AD in the presence of AD predisposing factors, taking into consideration the possibility of monitoring, by membrane lipidomics, the effects of dietary changes.

In **Chapter 5**, the effects of the *trans* geometry of the double bonds on the properties of liposomal models of cell membrane were studied. In particular, different formulations containing increasing percentages of TFAs were prepared and characterized for their size, ζ -potential and morphology. Additionally, since *trans*-lipids are known to influence membrane permeability reducing its fluidity, the stability over time and possibly the efficiency of encapsulation, the encapsulation of two different dyes and their release profile at 37 °C were studied. The data demonstrated that TFAs affect both liposome size and stability, reducing the mean particle diameter and the aggregation phenomena. The encapsulation efficiency was mainly affected by the liposomal formulation and the encapsulation conditions rather than the lipid geometry. However, the presence of *trans*-containing phospholipids, by reducing liposome permeability, gave slightly slower release compared to their *cis*-analogues. These results suggest further experiments where such effects would be explored in biological membranes, where *trans* lipids can be endogenously formed or introduced by exogenous sources.

Given the possibility to functionalize liposome surface in order to favor their concentration in cancer areas due to specific micro-environmental characteristics, it would be interesting to evaluate the possibility to disturb cell signaling and replication of tumor cells and to produce local cytotoxicity by enhancing the concentration of *trans* lipids in the area.

Finally, in **Chapter 6**, we reported the separation and identification of mono-*trans* isomers of DHA, obtained by a dual synthetic approach consisting of direct photolysis of *cis*-DHA in the presence of thiol and formation of mono-epoxide derivatives that can be separated by TLC and GC and characterized by 2D-NMR. The synthesized molecules were used as reference library to set up a GC protocol for the identification of *trans* isomers of DHA in isomerized fish oil and commercially available ω -3 containing supplements. The GC analyses showed the presence of mono-*trans* isomers of DHA and other mono-*trans* isomers (including *trans*-palmitoleic, *trans*-oleic, *trans*-vaccenic, *trans*-ARA and *trans*-EPA derivatives) in the majority of samples, that were identified using previously established synthetic procedures. The presence of these byproducts could be attributed to industrial processes, like deodorization, that induce the *cis-trans* conversion of double bonds in unsaturated lipids. Other differences in the lipid profile of the analysed products, such as excess of SFAs and MUFAs underlined that the quality of the final commercially available ω -3 supplements is conditioned not only by the type of industrial processes but also by the quality of the raw starting materials employed. These results confirmed that the synthetic library of mono-*trans* isomers of DHA could be a useful tool for the detection and quantification of *trans* geometrical artefacts of DHA in ω -3 supplements that can find application in food and nutraceutical studies. This study brings the attention to the need of globally standardizing the legislation and imposing limitation regarding the TFA content in commercially available products, that have harmful effects for health.

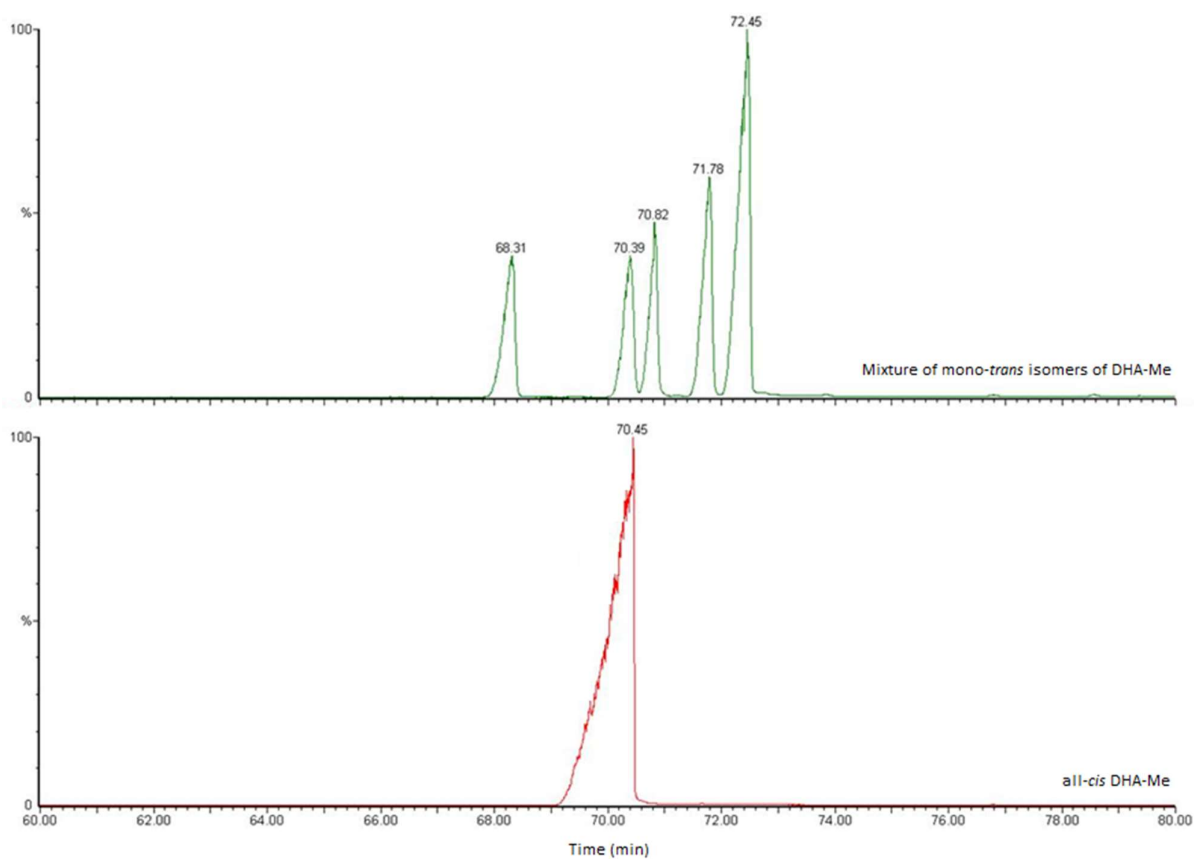
Taken together, these results can better clarify the role of fatty acids in the composition of cellular membranes, which is affected by environmental, nutritional and metabolic conditions, providing also a palette of methodologies for the examination of membrane behaviors, impairments and changes linked with the fatty acid geometry and types.

This PhD thesis encompasses many fields, ranging from the roles of free radicals in medicine, characteristics of membrane composition in different culture conditions, biotechnology of liposomes, lipid analysis and evaluation of nutraceuticals.

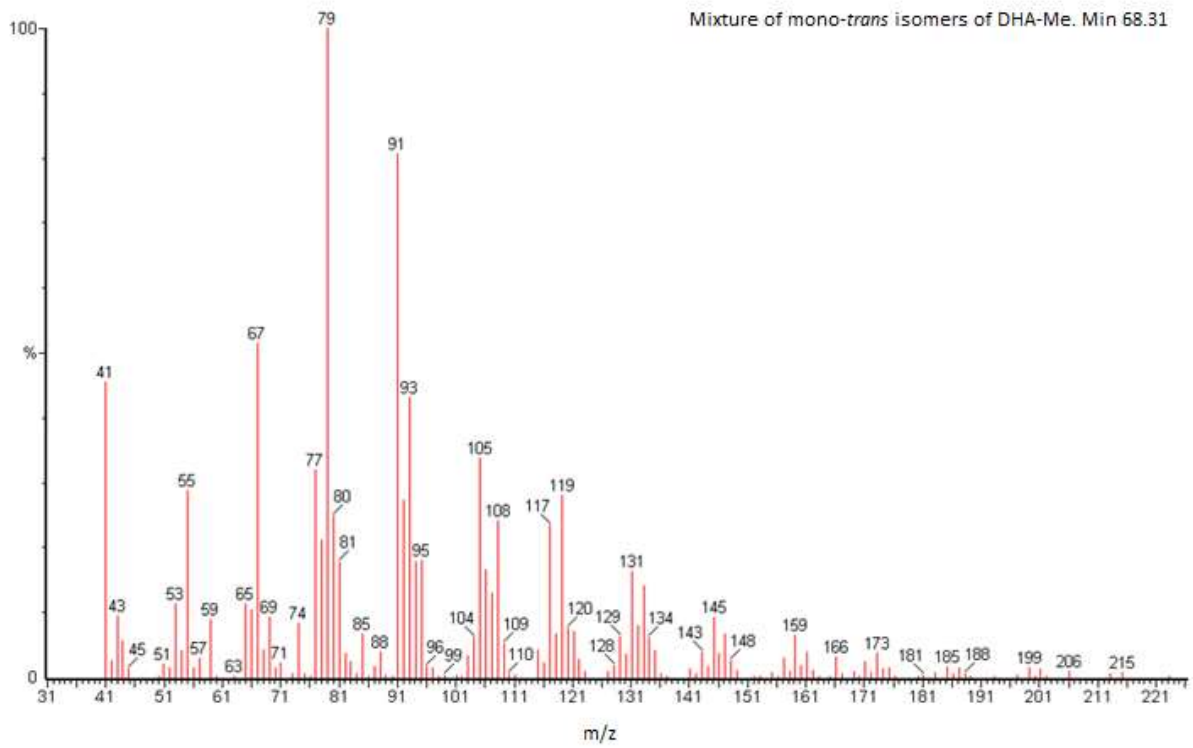
Appendices

Appendix 1. GC-MS characterization of mono-*trans* isomers of DHA-Me.

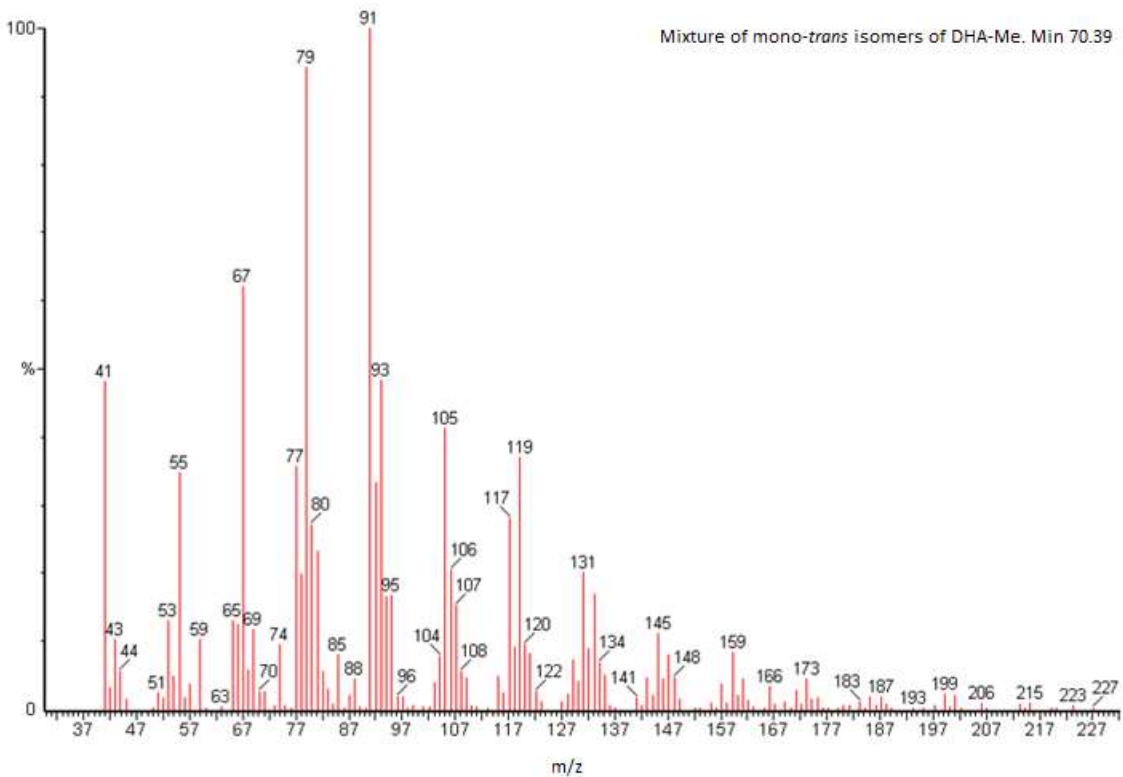
GC-MS separation. Mixture of mono-*trans* isomers of DHA-Me obtained by photolysis, in comparison with all-*cis* DHA-Me.



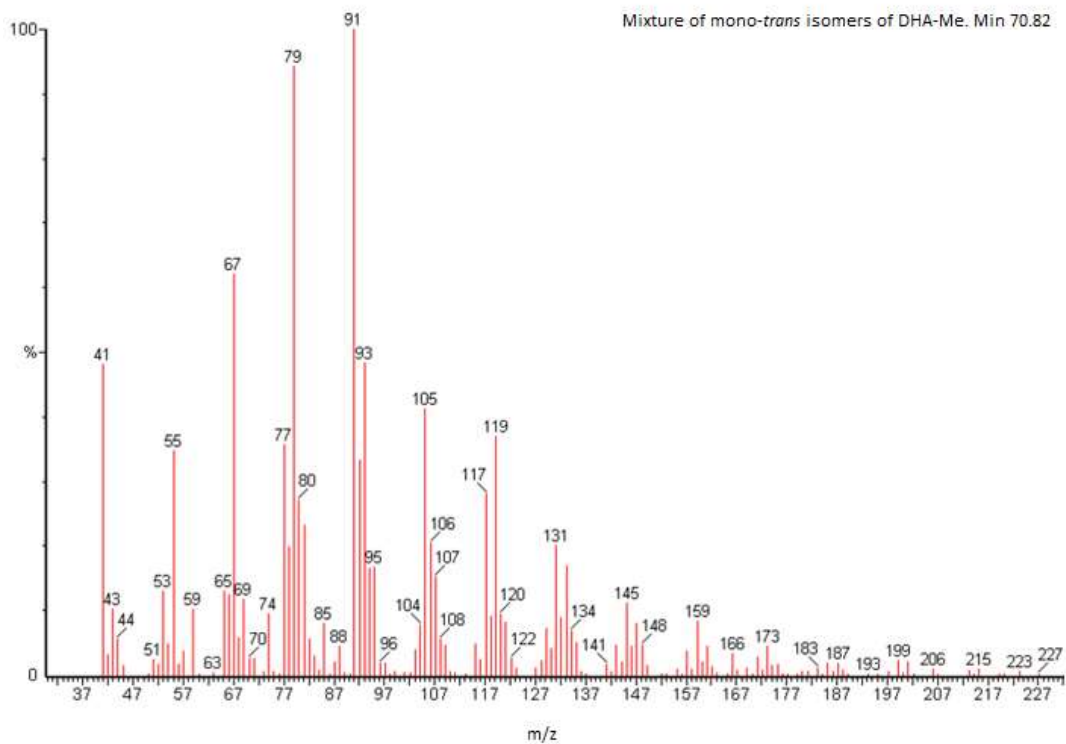
GC-MS separation. Mass fragmentation at 68.31 min (19*t*, DHA-Me).



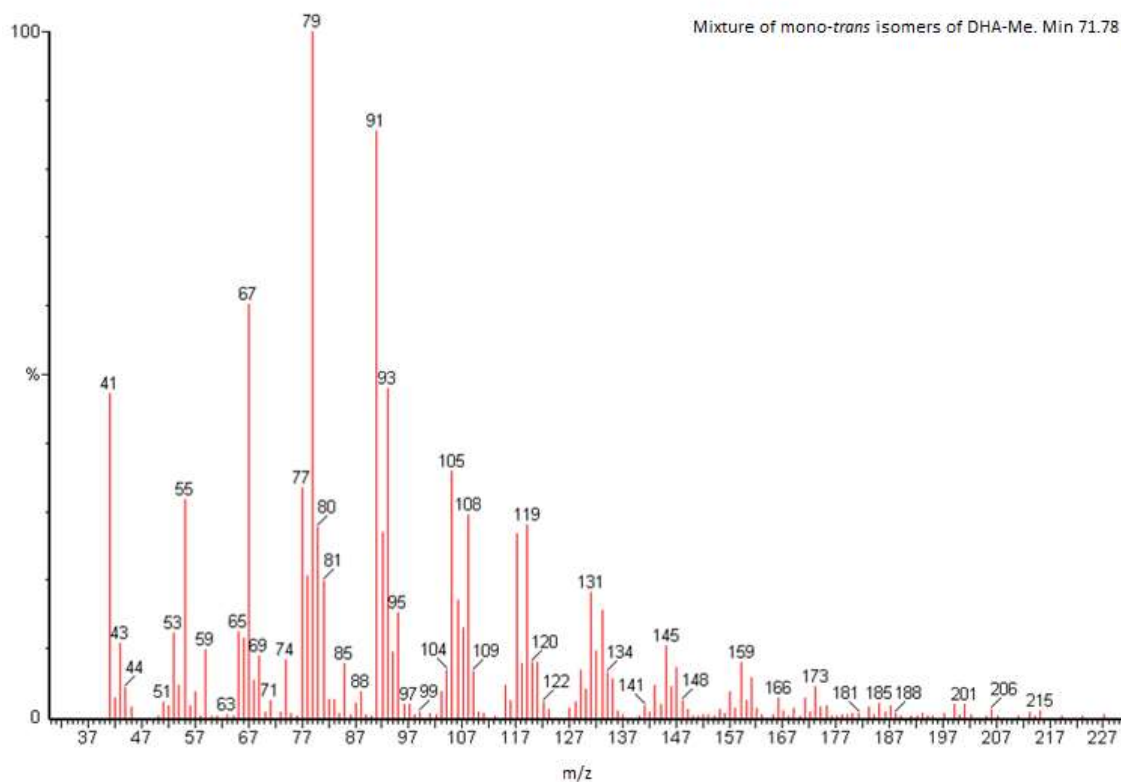
GC-MS separation. Mass fragmentation at 70.39 min (16*t*, DHA-Me).



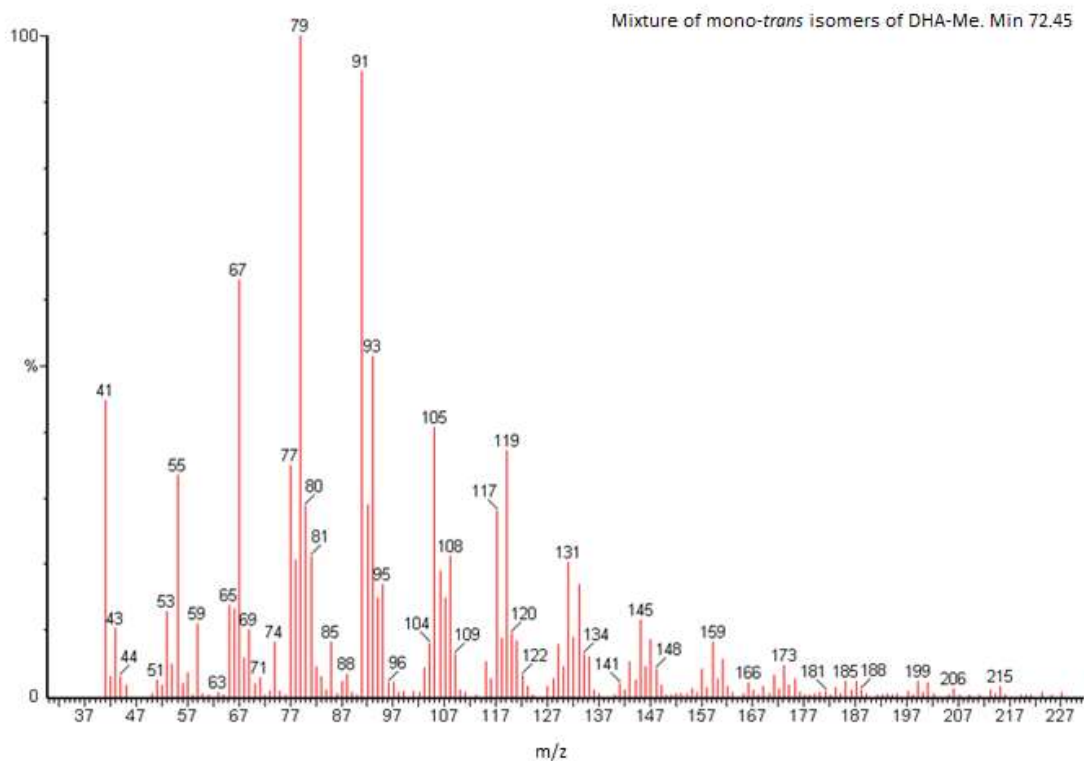
GC-MS separation. Mass fragmentation at 70.82 min (4*t*, DHA-Me).



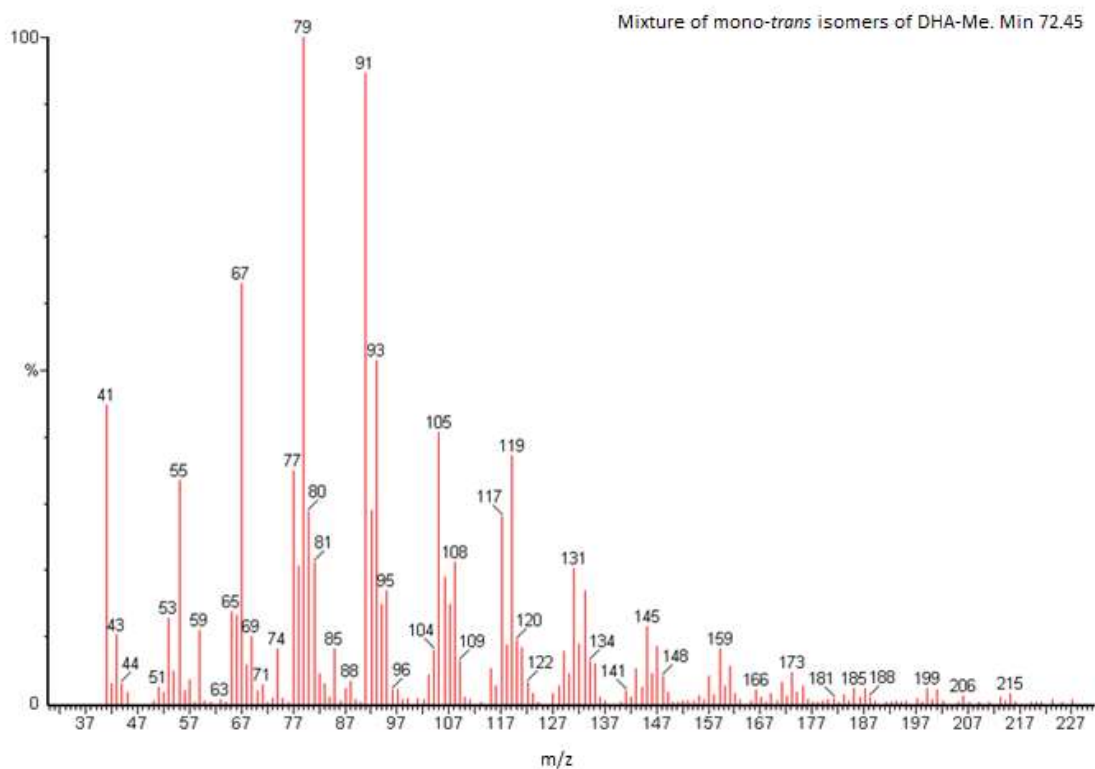
GC-MS separation. Mass fragmentation at 71.78 min (13*t*, DHA-Me).



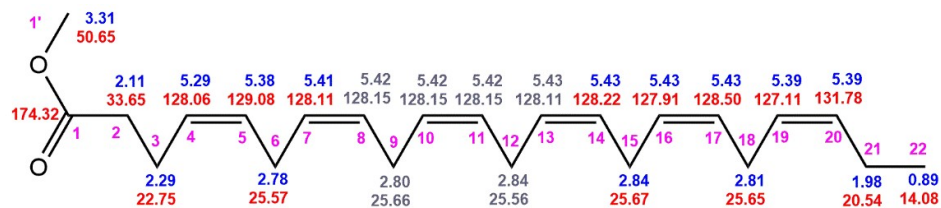
GC-MS separation. Mass fragmentation at 72.45 min (*7t* + *10t*, DHA-Me)



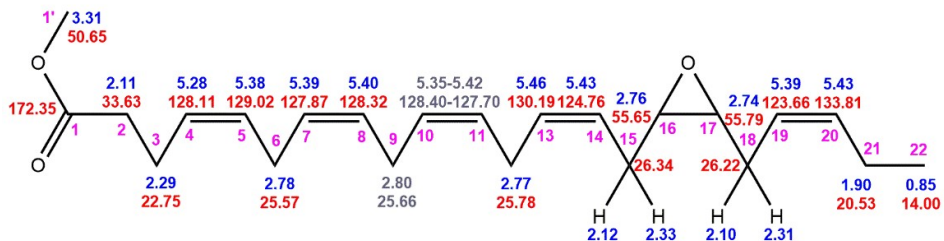
GC-MS separation. Mass fragmentation at 70.45 min (*all-cis* DHA-Me).



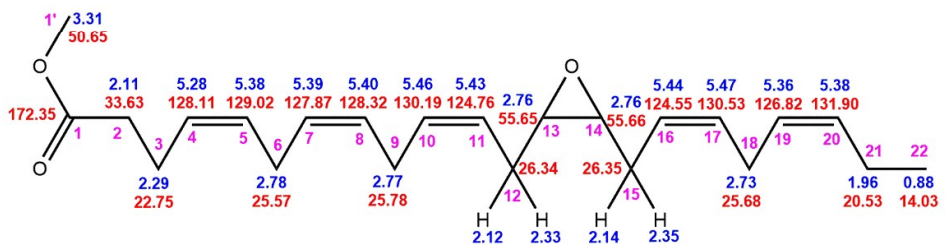
Appendix 2. Summary of the ^1H and ^{13}C resonances assignments for all-*cis* DHA-Me and EDP regioisomers.



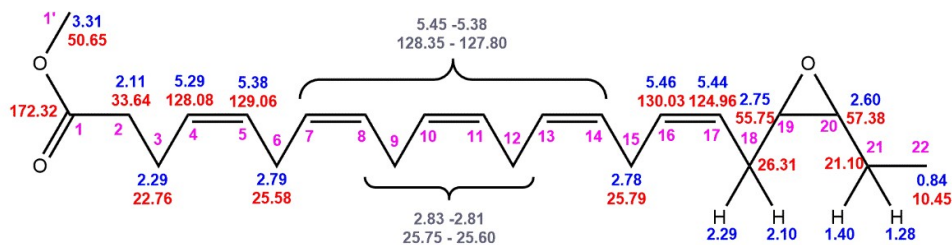
All-*cis* DHA-Me (1)



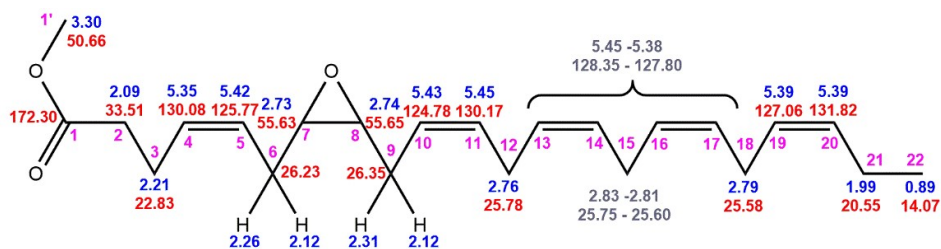
16,17-EDP-Me (6)



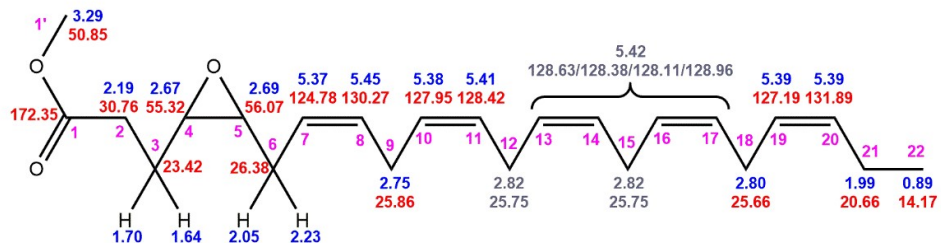
13,14-EDP-Me (5)



19,20-EDP-Me (7)

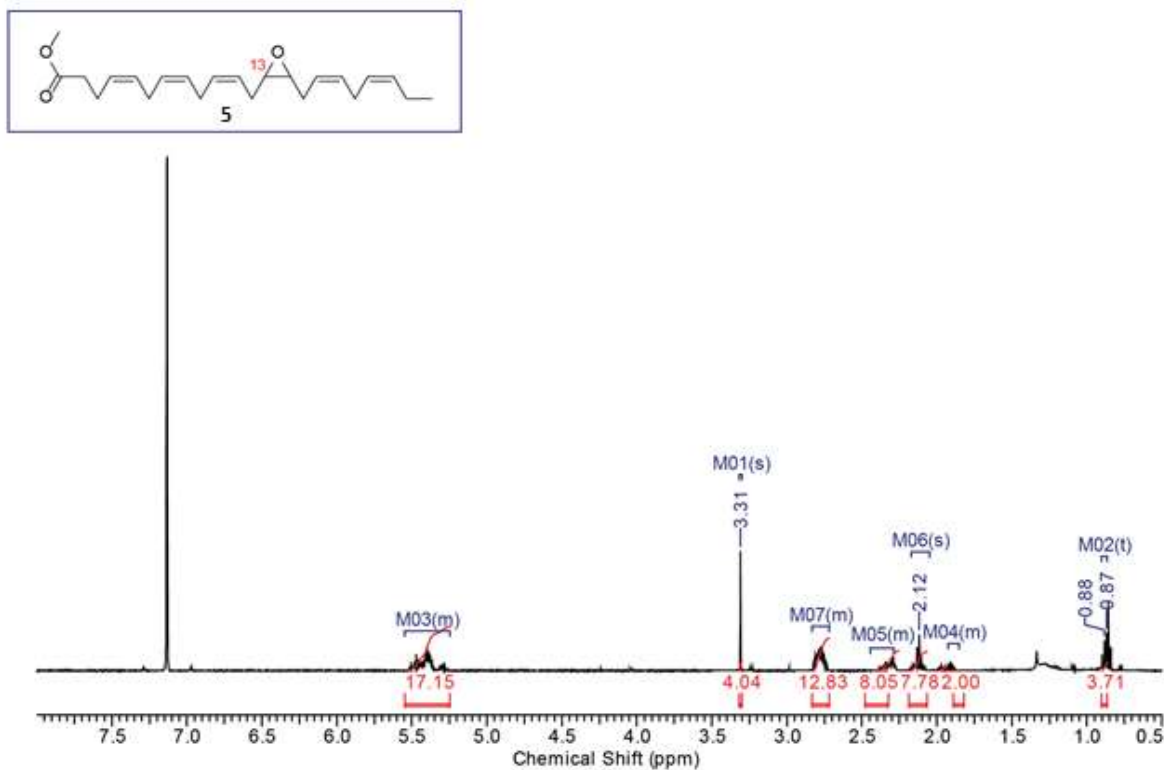
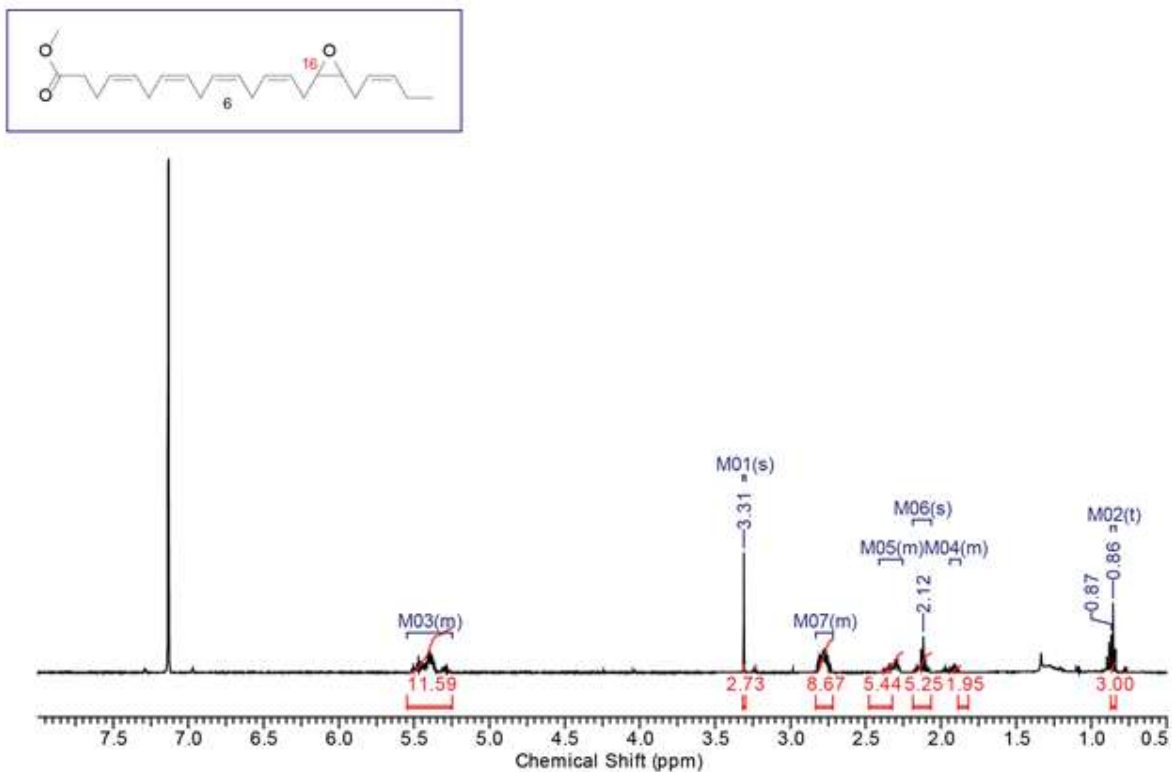


7,8-EDP-Me (3)

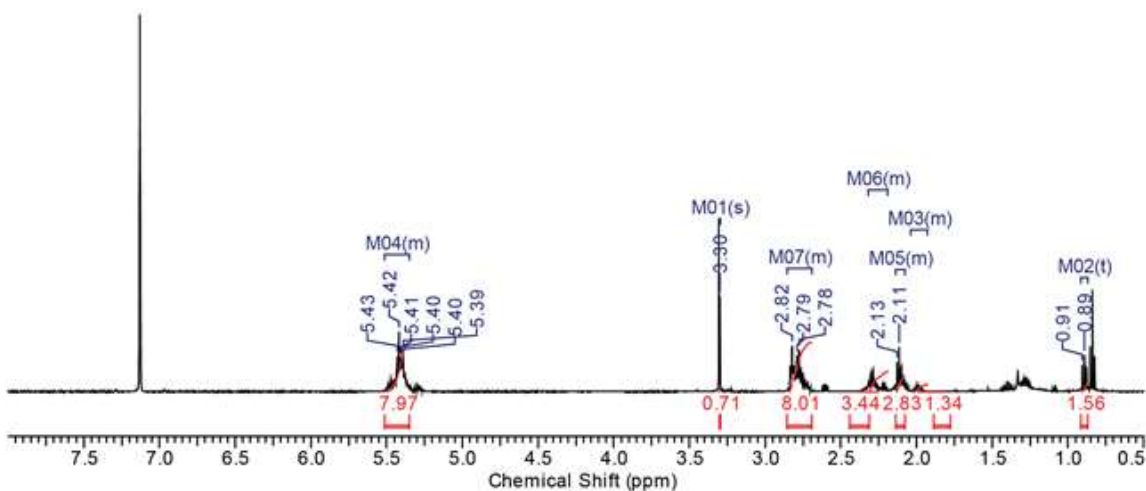
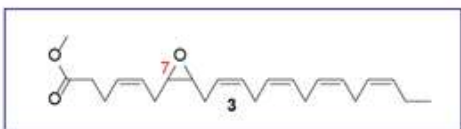
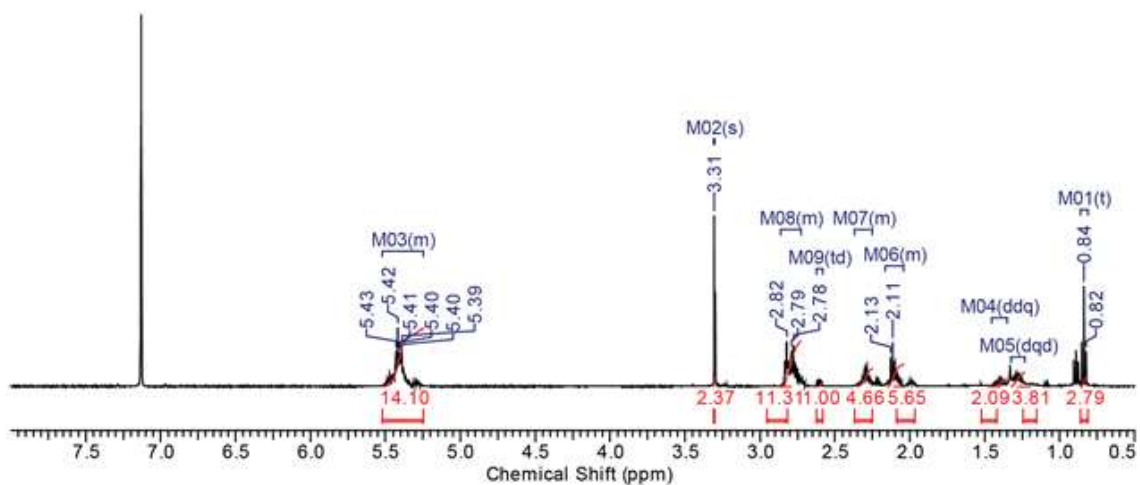


4,5-EDP-Me (2)

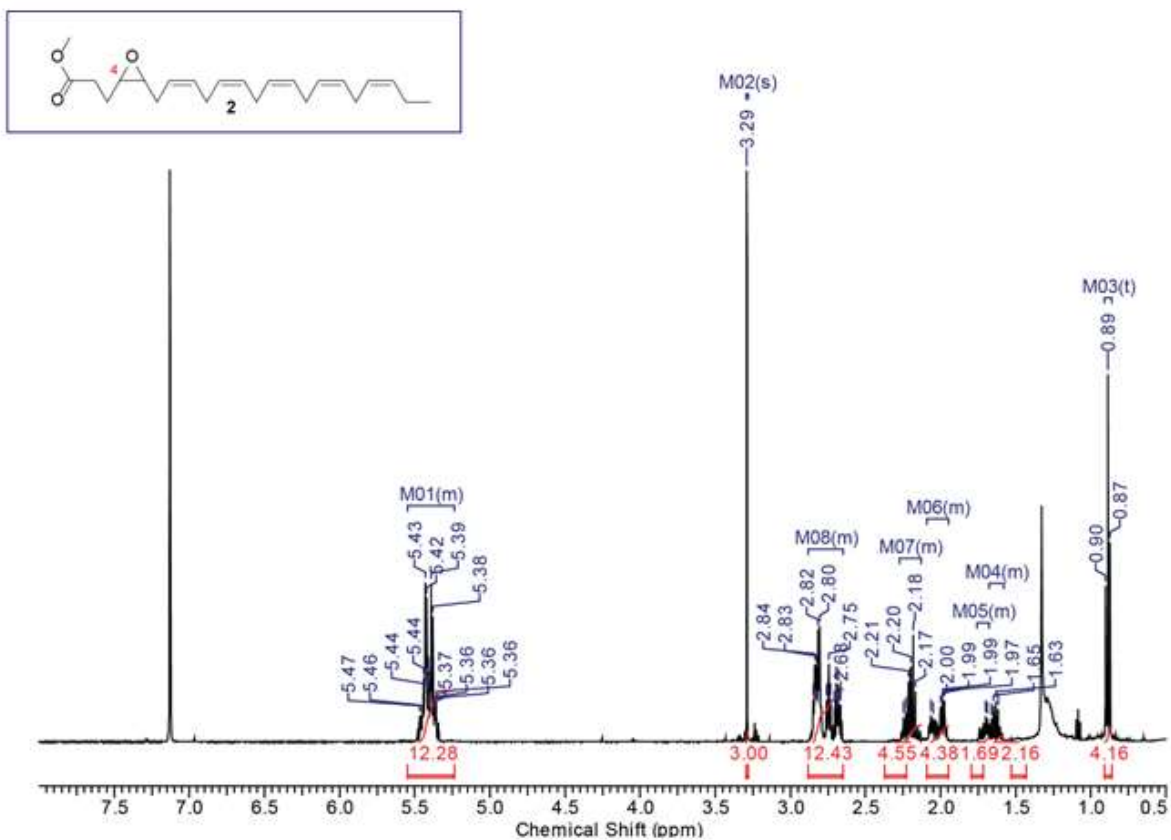
Appendix 3. ^1H NMR spectrum of the first fraction (in C_6D_6) corresponding to 16,17-EDP and 13,14-EDP (**6** and **5** in a ratio 71:29) with traces of all-*cis* DHA-Me and an unknown compound (probably 10,11-EDP) that were not characterized.



Appendix 4. ^1H NMR spectrum of the second fraction (in C_6D_6) corresponding to 19,20-EDP and 7,8-EDP (structures **7** and **3** in a 57:43 ratio).



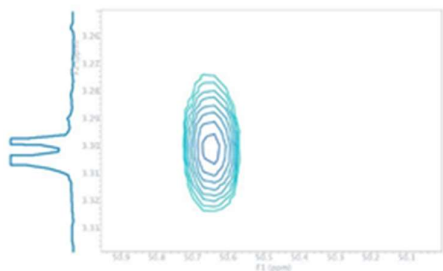
Appendix 5. ^1H NMR spectrum of the third fraction (in C_6D_6), corresponding to pure 4,5-EDP (**2**).



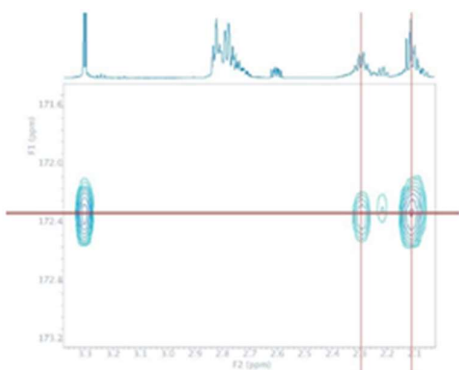
Appendix 6. Relevant correlations in the 2D-NMR (in C₆D₆) for the assignment of 19,20-EDP.

Connections follow the left lane **a-f**, then the right lane **g-o**.

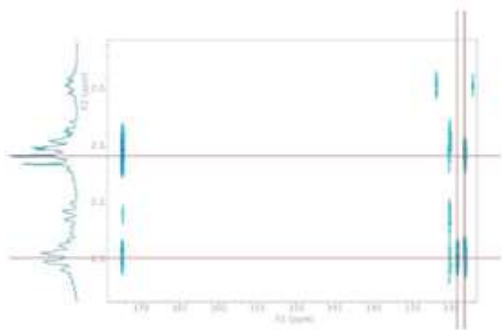
a. The bsgHSQCAD 5-70 showed that H1' (3.31 ppm) corresponds to C1' (50.65 ppm).



b. The gHMBCAD attributed C1 (172.32 ppm) to individual signals (2.11 e 2.29 ppm), corresponding to H2 and H3.

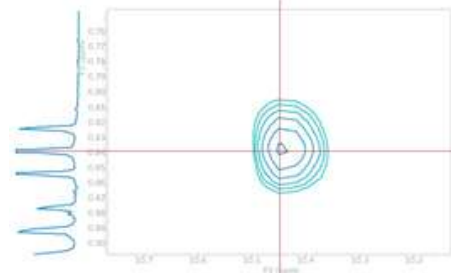


c. The gHMBCAD showed the attribution of H2 (2.11 ppm), H3 (2.29 ppm) to C4 (128.08 ppm) and C5 (129.06 ppm) since H2 interacts only with C1 (170.32 ppm) and C4, while H3 interacts C1, C4 and C5.

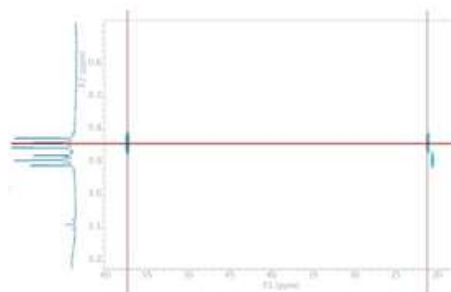


d. The bsgHSQCAD 5-70 showed C2 (33.64 ppm) and C3 (22.76 ppm).

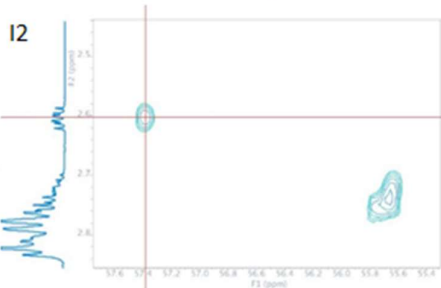
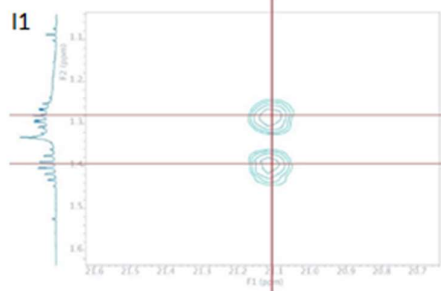
g. The bsgHSQCAD 5-70 showed that H22 (0.84 ppm) corresponds to C22 (10.45 ppm).



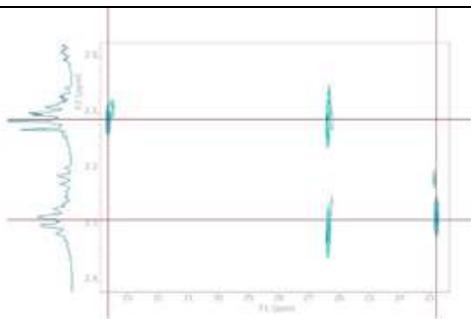
h. In gHMBCAD C21 (21.10 ppm) and C20 (57.38 ppm) are shown.



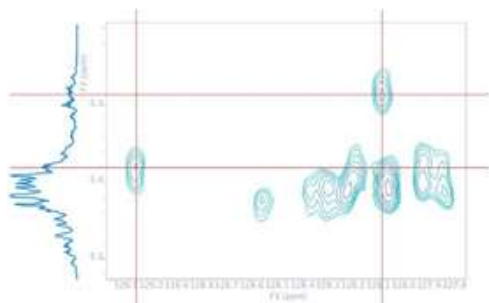
i. The bsgHSQCAD 5-70 confirmed the two diastereotopic protons H21 (1.40-1.28 ppm, I1) and H20 (2.60 ppm; Fig I2)



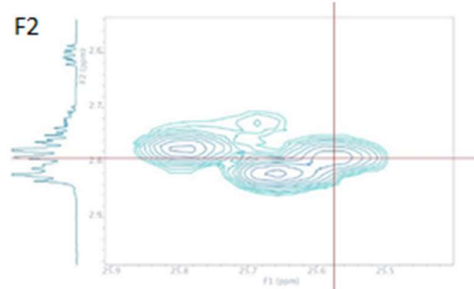
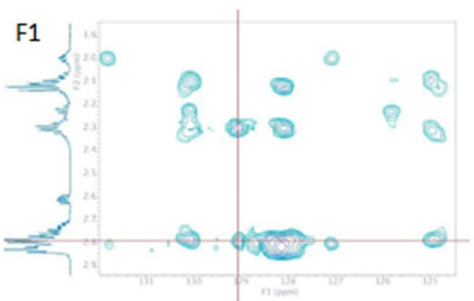
l. The gHMBCAD showed C19 (55.75 ppm, L1) and the bsgHSQCAD 5-70 confirmed H19 (2.75 ppm, L2).



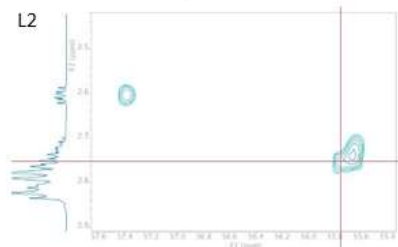
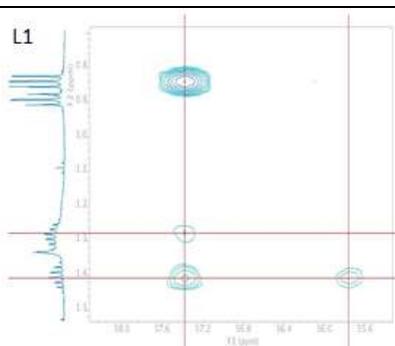
e. In bsgHSQCAD 110-140 the protons H4 (5.29 ppm) and H5 (5.38 ppm) are shown.



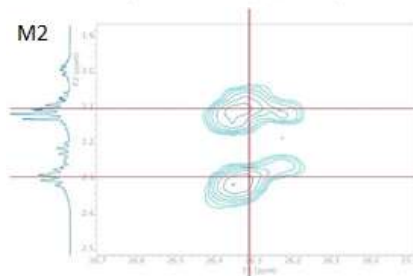
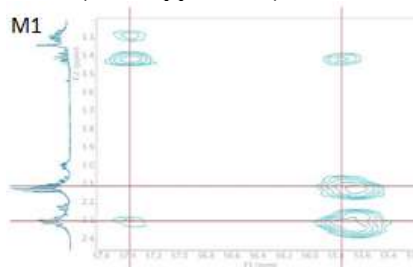
f. gHMBCAD confirmed the interaction of H6 (2.79 ppm) with C4 (129.06 ppm, F1) and from bsgHSQCAD 5-70 C6 (25.58 ppm, F2) is shown.



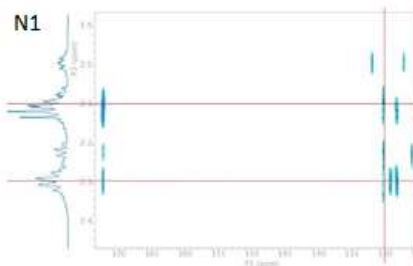
From here, the overlapping of the signals made the attributions difficult, and for this reason we proceeded with the attribution starting from the C22.

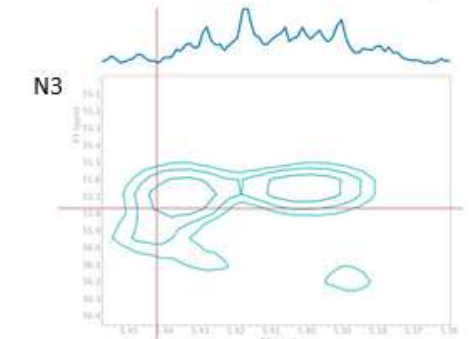
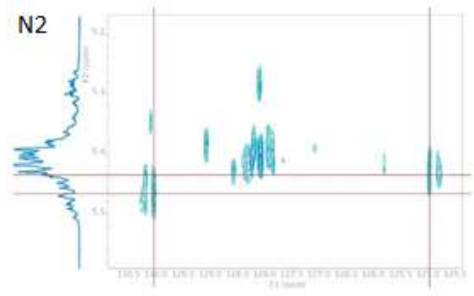


m. From gHMBCAD the two diastereotopic protons H18 are confirmed (2.29-2.10 ppm, M1) and bsgHSQCAD 5-70 showed C18 (26.31 ppm, M2).

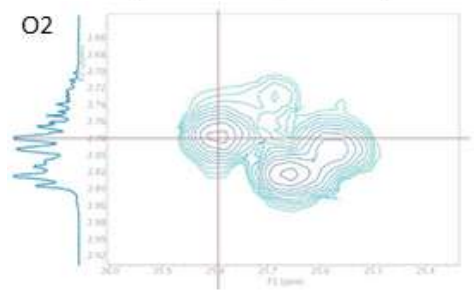
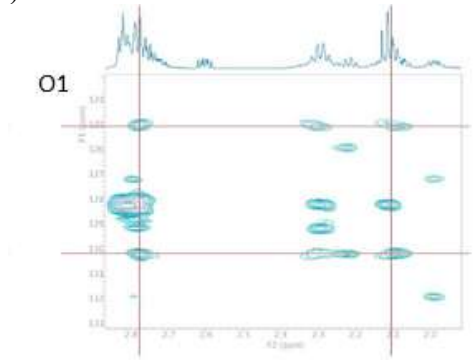


n. From gHMBCAD, C17 and C16 were identified (130.03 and 124.96 ppm, N1), while bsgHSQCAD 110-140 attributed the corresponding protons (130.03/5.46 ppm; 124.96/5.44 ppm, N2). Finally, gHMBCAD showed H17 (5.44 ppm) attached to C19 (N3).

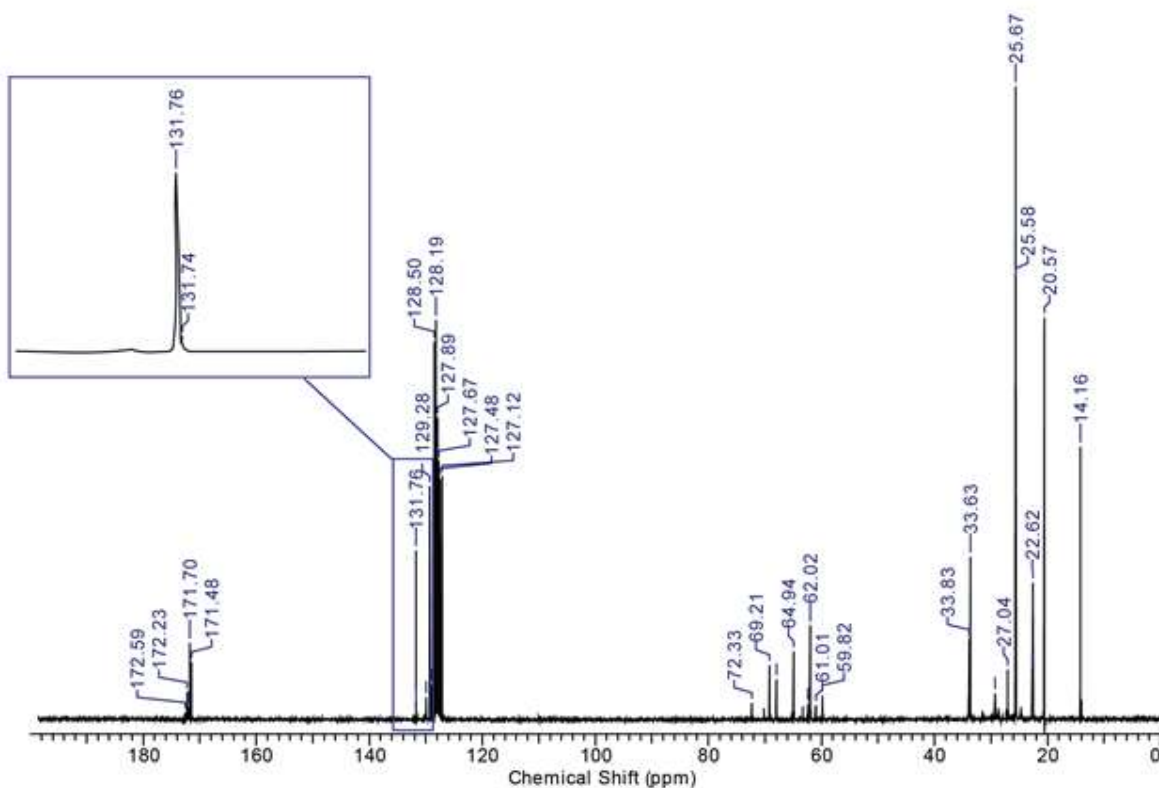




o. Proton H15 was identified (2.78 ppm, O1) by gHMBCAD and bsgHSQCAD 5-70 provided strong evidence that H15 (130.03 ppm) is attached to C15 (5.46 ppm, O2).



Appendix 7. Full ^{13}C NMR spectrum of DHA-containing triglycerides.



Appendix 8. Full ^{13}C NMR spectrum of DHA-containing triglycerides after isomerization.

